Circadian regulation of the vertebrate habenula

A thesis submitted to the University of Manchester for the degree of Doctor of Philosophy in the Faculty of Biology, Medicine and Health

2019

Adriana Basnakova

School of Biological Sciences, Division of Molecular and Cellular Function

Table of Contents

Final word count: 48 928

Abbreviations

AANAT	Aralkylamine N-acetyltransferase
ACh	Acetylcholine
aCSF	Artificial cerebrospinal fluid
AP	Action potential
ARC	Arcuate nucleus of the hypothalamus
AVP	Arginine vasopressin
BMAL	Brain and muscle arnt-like
cAMP	Cyclic adenosine monophosphate
CCGs	Clock-controlled genes
CLZN	Coelenterazine
CNS	Central nervous system
CREB	Cyclic adenosine monophosphate response element-binding
CRY	Cryptochrome
CT	Circadian time
DA	Dopamine
DD	Constant darkness
dpf	days post-fertilisation
DRN	Dorsal raphe nucleus
EGFP	Enhanced green fluorescent protein
ERK	Extracellular signal-regulated kinase
FR	Fasciculus retroflexus
GA	GFP-aequorin
GA-opt	GFP-aequorin codon optimised
GABA	Gamma-aminobutyric acid
GECI	Genetically encoded calcium indicator
GFP	Green fluorescent protein
HCN	Hyperpolarisation-activated cyclic nucleotide-gated
hpf	hours post-fertilisation
Hz	Hertz
IHC	Immunohistochemistry
IPN	Interpeduncular nucleus
IR	Infra-red
KS test	Kolmogorov-Smirnov test
LD	Light-dark
LHb	Lateral habenula

LHbM	Lateral habenula medial portion
LHbL	Lateral habenula lateral portion
MEA	Multi-electrode array
MHb	Medial habenula
mM	Millimolar
MRN	Median raphe nucleus
MUA	Multi-unit activity
NMDAR	N-methyl-D-asparate receptor
OB	Olfactory bulb
OT	Oxytocin
OTR	Oxytocin receptor
PBS	Phosphate buffered saline
PCR	Polymerase chain reaction
PER	Period
pERK	Phosphorylated extracellular signal-regulated kinase
PFA	Paraformaldehyde
PMT	Photomultiplier tube
PTZ	Pentylenetetrazole
PVN	Paraventricular nucleus of the hypothalamus
REM	Rapid eye movement
RHT	Retinohypothalamic tract
RMP	Resting membrane potential
RT	Room temperature
SCN	Suprachiasmatic nucleus
SM	Stria medullaris
SNc	Substantia nigra pars compacta
SON	Supraoptic nucleus
SUA	Single-unit activity
tERK	Total extracellular signal-regulated kinase
TTFL	Transcription-translation feedback loop
TTX	Tetrodotoxin
VTA	Ventral tegmental area
ZT	Zeitgeber time
5-HT	Serotonin
95% CI	95% Confidence interval
ΔCLK	Truncated CLOCK

Abstract

Vertebrate circadian systems, composed of networks of endogenous clocks distributed across tissues and organs and synchronised to one another by one or several 'master' pacemakers, enable organisms to anticipate and exploit favourable conditions for daily activities. The epithalamic habenula has been identified as a component of the extended mammalian circadian system, where through integration of both intrinsic and extrinsic temporal cues, it exhibits circadian rhythms in neuronal activity. In lower vertebrates, such as zebrafish, the habenula contains a molecular clock and responds to changes in blue light via retinal ganglion cells, suggesting a possible effect of circadian effectors on its function. This thesis explores the circadian regulation of this highly conserved epithalamic structure as well as the role of its putative circadian oscillator in the regulation of vertebrate brain and behavioural states.

To determine whether the zebrafish habenula, as in mammals, exhibits daily variations in cellular activity *in vivo*, three distinct approaches – monitoring of bioluminescent calcium (Ca^{2+}) reporter, immunohistochemistry of phosphorylated extracellular signal-regulated kinase (pERK) and two-photon imaging of the Ca^{2+} indicator GCaMP6s – were applied. While the bioluminescent Ca^{2+} indicator failed to report any spontaneous Ca^{2+} events, the two other techniques produced consistent results, demonstrating circadian variation in the putative homologue of the mammalian lateral habenula (LHb), with increased levels of both cytosolic Ca^{2+} and pERK at night. The pERK levels, but not overall Ca^{2+} activity, also showed circadian differences in the putative homologue of the mammalian medial habenula (MHb), but these variations were of opposing polarities and occurred in different subregions of this structure.

Secondly, in order to investigate the functional role of the habenula oscillator in regulation of zebrafish behaviour and brain neurotransmission, a transgenic line, in which the molecular clock was disrupted specifically in the habenula by a dominant-negative strategy, was generated. Circadian rhythms of locomotor activity under constant darkness and arousal-associated sensory responsiveness during the sleep-like state in the transgenic larvae were not affected. In contrast, in adult zebrafish as a result of habenula-specific clock disruption, brain levels of important neurotransmitters – dopamine, serotonin and acetylcholine – were significantly reduced during the day, but not during the night.

Finally, circadian rhythmicity of habenula neuronal activity was monitored in mouse brain slices, by the simultaneous recording of extracellular multi-unit activity from multiple sites within the habenula. Both MHb and LHb exhibited elevated neuronal activity during the night, particularly in the ventral subregion of the MHb and lateral portion of the LHb. In addition, a putative output signal of the suprachiasmatic nucleus (SCN), the neuropeptide arginine vasopressin (AVP), induced excitation in the LHb. However, these results were recapitulated with the related neuropeptide oxytocin (OT) and a specific OT receptor (OTRs) agonist – results implying that the AVP- and OT-induced excitatory effects are likely mediated via OTRs. A more pronounced AVP-induced effect was observed during the day, while OT-induced excitation did not vary between day and night, implying that AVP, but not the OT, could contribute to circadian regulation of the rodent habenula.

In conclusion, this methodologically diverse study contributes to our growing understanding of habenula's function in the processing and transmission of temporal context specific and the role of its circadian oscillator in the daily coordination of brain state and behaviour in vertebrate species.

Declaration

No portion of the work referred to in the thesis has been submitted in support of an application for another degree or qualification of this or any other university or other institute of learning.

A part of the work presented in Chapter 4 was conducted by Dr. David Lyons, University of Bristol. For the specific contribution, please, refer to Chapter 4 results.

Copyright statement

Acknowledgements

Firstly, I gratefully acknowledge the financial support received towards my PhD from the University of Manchester and A*STAR in Singapore, which has made this life-changing experience possible.

I would like to express my sincere gratitude to my supervisors Prof. Hugh Piggins and Prof. Suresh Jesuthasan for their mentorship, continuous guidance, advice and support throughout the course of my PhD and insightful comments on this thesis. I have very much enjoyed our discussions and learned a great deal from both of you.

I am deeply grateful and indebted to Dr. David Lyons for his expertise, invaluable advice and encouragement in the final year of my PhD as well as for the great amount of help with writing this thesis. Thank you for making this difficult time so fun – for the walks, chats, drinks and for always making me laugh.

I would like to express a huge thank you to Dr. Ruey-Kuang Cheng for his help with setting up behavioural assays and for patiently teaching me how to analyse data. Your programming knowledge and expertise have greatly inspired me.

I am also sincerely grateful to Dr. Mahathi Ramaswamy for teaching me numerous techniques and sharing a great amount of knowledge and to Dr. Joanne Chia for the continuous guidance and advice on molecular biology and behavioural assays. A special thanks also goes to Dr. Seetha Krishnan for her expertise in statistical analysis, to Caroline Kibat for her advice and troubleshooting the molecular biology and to Dr. Caroline Wee for her valuable input and help with statistical analysis.

My sincere gratitude goes to Dr. Beatriz Baño-Otálora and Dr. Mino Belle for patiently teaching me how to use the multi-electrode array and for their advice on this project during the first year of my PhD.

I would also like to thank Dr. James Stewart for his assistance with setting up the bioluminescence recording assay.

I am very grateful to many people I had a chance to work with in Manchester, Singapore and Bristol, who have made this journey so enjoyable. In no particular order; thanks to Dr. Adam Watson, Dr. Alun Hughes, Carla Santos, Natasza Klas, Emma Morris, Dr. Rebecca Northeast, Taghreed Almansouri, Dr. Alok Joshi, Rayna Samuels, Cheryl Petit, Matthew Coulthard, Kathleen Cheow Wen Bei, Gadisti Aisha and Dr. Ashleigh Wilcox. A special thanks also goes to the technical team on the E floor of the Biomedical Sciences building at the University of Bristol for the great help with setting up the laboratory.

On a personal level, I would like to acknowledge my closest friends who have greatly supported me throughout the past four years. Thanks to Carla, Emma and Natasza for making my time in Manchester so memorable, for the fun parties and trips and for the sweet messages throughout my time in Singapore; to Joei for the most amazing drawings, post it notes, enthusiasm for lunch

and snacking, awesome time in Berlin and for hosting me during the last few months in Singapore; to Mahathi for being a great listener and for showing me the real Indian food; to Seetha and Caroline for the lunch and coffee times. You have all been so great.

I am eternally grateful to my parents Iveta and Jozef for their care, financial support and constant encouragement throughout many years of my education – without you I would not be where I am today. I am also thankful to my sister Katka for her support and for making my time at home always very fun.

Last but not least, I would like to thank William for being so patient and understanding, for teaching me how to relax and for reminding me the things in life which matter the most.

Chapter 1 Introduction

Circadian rhythms

All living organisms from bacteria and plants to humans exhibit orchestrated 24-h oscillations, referred to as daily or circadian (circadian: *circa*, about; *diem*, a day) rhythms, in physiological processes at molecular, cellular and systemic levels. Indeed, over 40% of all protein-coding genes exhibit circadian rhythms in transcription, which in turn drive oscillations in biological processes, including body temperature, blood pressure and hormone secretion, as well as behavioural outputs, such as feeding and sleep (Wulund and Reddy, 2015).

In nature, rhythmic behaviour is, for instance, exhibited by the Antarctic krill, a small shrimp-like crustacean crucial for the Southern Ocean ecosystem, where it serves as the main consumer of phytoplankton and as the primary food source for many higher predators. This organism migrates vertically in a circadian fashion – a phenomena referred to as diel vertical migration (DVM) – to maximise the food intake in the upper water column during the night when the predator risk is the lowest, and to hide from the predators in the depth of the ocean during the day (Gaten *et al.*, 2008). Contrary to behavioural rhythms driven by predator avoidance, certain predators adapt to the rhythmic activity of their primary prey. For instance, Black harriers exhibit daily rhythms in the provisioning of prey to nestlings – a behaviour highly correlated with activity rhythms of small mammals, the primary prey of this predator (Garcia-Heras *et al.*, 2017). Daily rhythms have evolved as an adaptive mechanism that enables organisms to anticipate regular 24-h changes in environment that could otherwise pose a major threat to their survival (Wulund and Reddy, 2015). These include sudden variations in food availability, predator risk and temperature, amongst others. Central to this anticipatory survival strategy is an endogenous timing mechanism, referred to as the circadian clock, whose timing capabilities persist under constant conditions in the absence of external stimuli. However, under constant conditions the rhythm of the clock free-runs, meaning it gradually drifts from 24-h oscillations in the environment. Therefore, in order to facilitate an enduring and accurate synchronisation with the natural day-night cycle, a crucial characteristic of this clock machinery involves resetting by external environmental signals, including light and temperature (Foulkes *et al.*, 2016).

Circadian clock at molecular level

The first scientific report to propose that daily rhythms are under intrinsic control and are not simply a passive reaction to light and temperature cycles was made by the French astronomer Jean-Jacues d'Ortous de Mairan who, in 1729, discovered that leaves of Mimosa plants fold and unfold with robust 24-h periodicity – a behaviour that persisted under constant darkness (Roenneberg and Merrow, 2005). However, it was not until the 1970-80's that advancements in the mutant screening of the fruit fly, *Drosophila melanogaster*, enabled the discovery of *period* (*per*) gene – an important clock component underpinning animal circadian rhythms (Konopka and

Benzer, 1971; Reddy *et al.*, 1984). Michael Rosbash and Paul Hardin subsequently proposed a hypothesis of how clock genes and their protein products could generate circadian rhythms (Hardin *et al.*, 1990). Based on the observation that *per* RNA levels are reduced following increase in PER protein, this hypothesis described an autoregulating negative feedback loop where clock gene RNA is translated into a protein which, in turn, inhibits its own transcription until the RNA and protein degrade, relaxing feedback inhibition. This paradigm has formed the basis of the current view of the clock mechanism which, since the discovery of other clock genes in flies, plants and vertebrates, has been shown to consist of the interconnected transcription-translation feedback loops (TTFL) of multiple genes and associated proteins (Roenneberg and Merrow, 2005).

Broadly speaking, in a vertebrate circadian system *clock* and *brain and muscle arnt-like (bmal)* genes encode bHLH-PAS (basic helix-loop-helix; *Per-Arnt-Single-Minded*) proteins which serve as positive regulators of the TTFL. Together these proteins form CLOCK:BMAL heterodimers that bind to E-Box enhancer elements (5'-CACGTG-3') in the promoter regions of target genes, and as such initiate their transcription (Buhr and Takahashi, 2013). E-Box elements are present in a variety of genes, including *per* and *cryptochrome* (*cry*), which act as negative regulators of the feedback loop. Upon CLOCK:BMAL-induced transcription of *per* and *cry*, the translated proteins translocate back inside the nucleus where they supress CLOCK:BMAL's ability to activate transcription. As a result, expression of *per* and *cry* is reduced and the inhibition of CLOCK:BMAL is, in turn, released, allowing the onset of another 24-h cycle (Foulkes *et al.*, 2016). An additional stabilising feedback loop, thought to improve the robustness of the former, involves the nuclear orphan receptors REV-ERBα and retinoic acid-related orphan receptor α (RORα) (Duez and Staels, 2009). Herein, CLOCK:BMAL heterodimers activate transcription of *rev-erbα* and *rorα* genes. The REV-ERBα protein supresses *bmal* transcription, resulting in reduced *bmal* RNA levels. In contrast, RORα competes with REV-ERBα for binding to the *bmal* promoter and activates its transcription. Therefore, these two nuclear receptors facilitate an additional regulatory loop, as the occupancy of *bmal* promoter by either RORα or REV-ERBα is essential for proper timing of clock machinery (Duez and Staels, 2009). In addition to the core clock genes, other genes are under direct control of CLOCK:BMAL heterodimers. These are referred to as first-order clock-controlled genes (CCGs) – as they also contain E-Box enhancers (Li *et al.*, 2018). One example of a first-order CCG is the precursor gene for albumin D-site binding protein. This protein is involved in transcriptional regulation of metabolic enzymes (Ando *et al.*, 2005), including cholesterol 7 alpha-hydroxylase, the rate-limiting enzyme for bile acid production and cholesterol excretion from the liver (Bérard *et al.*, 2004). In addition to E-Box-mediated regulation, other CCGs are negatively regulated by REV-ERBα and are consequently in phase with *bmal* expression. In general, the downstream cascading effects of many CCGs drive expression of further gene clusters (Hastings *et al.*, 2003). This extended clock machinery composed of core clock genes, CCGs and their downstream targets, therefore, enables temporal coordination of a wide range of processes including cell signalling pathways, metabolic activities, organelles' function, as well as the tissue-specific functions of differentiated cells (Chaix *et al*., 2016). Figure 1.1 demonstrates a simplified model of molecular circadian clock in vertebrates (adapted from Baño-Otálora and Piggins, 2017).

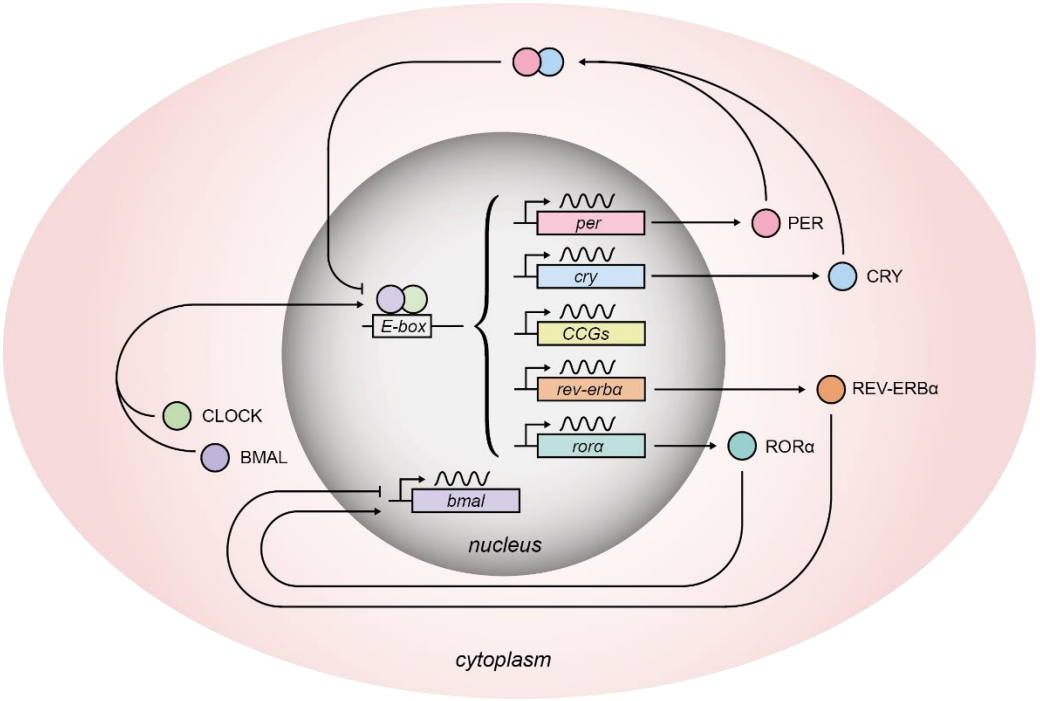

Figure 1.1: Simplified model of vertebrate molecular clock

In comparison to the clock components of *Drosophila*, one of the distinguishing characteristics of the vertebrate molecular clock is the presence of extra clock gene copies. For instance, the single copy of the *bmal* gene in *Drosophila* is represented by *Bmal1* and *Bmal2* in mammals, while the *Drosophila cry* gene corresponds to the *Cry1* and *Cry2* mammalian homologues (Vatine *et al.*, 2011). Van Der Horst *et al.* (1999) further investigated the functional roles of both CRY1 and CRY2 proteins in mice. They found that mice deficient in CRY1 or CRY2 proteins exhibit accelerated and delayed free-running periodicity of locomotor activity, respectively. Only in the absence of both proteins did the animals become completely arrhythmic, suggesting that both proteins are important for maintaining behavioural rhythmicity. Interestingly, zebrafish possess even more extra gene copies than mice – a consequence of a genome duplication event that occurred during the evolution of the teleost lineage. In total, six *cry* genes have been identified in zebrafish, including *cry1a, 1b, 2a*, *2b, 3* and *4* (Vatine *et al.*, 2011). However, only *cry1a, 1b, 2a* and *2b* have a high sequence similarity with mammalian *cry* genes and inhibit CLOCK:BMAL-mediated transcription, whereas *cry3* and *4* more closely resemble *cry* in *Drosophila* (Kobayashi *et al.*, 2000), indicating the divergent functions of these particular genes.

Organisation of the circadian system in vertebrates

In order to ensure the correct synchronisation of the molecular clock to geophysical time, the clock needs to be periodically reset – a process referred to as entrainment – by environmental cues, amongst which the photoperiod is the most prominent synchronising factor or *zeitgeber* (time

giver) (Dibner *et al.*, 2010). All vertebrates perceive light via photoreceptors in the lateral eyes. However, it is now known that non-mammalian species also express photopigments within the brain and peripheral tissues which are critical for entrainment of circadian rhythms and form a basis for the decentralised circadian system found in some vertebrate species (Cassone, 2014; Foulkes *et al.*, 2016). Since mammals detect light exclusively through the retina, they possess a more centralised hierarchical circadian system, where highly specialised pacemakers efficiently integrate and communicate photic information to the rest of the body. This section will therefore discuss the centralised and decentralised circadian systems in vertebrates, focusing on fish and mammalian systems.

Zebrafish circadian oscillators

Identification of the clock location became a principal goal of circadian research in 1960s and 1970s (Roenneberg and Merrow, 2005). One of the first vertebrate circadian centres, or pacemakers, identified was the avian pineal gland. Indeed, avian pineal glands express clock genes and when isolated in culture maintain circadian rhythmicity in biosynthesis of the sleep-promoting hormone, melatonin, this structure's primary output. These rhythms persist for 4-10 days before dampening to arrhythmicity and can be directly entrained by light (Cassone, 2014). The significance of this pacemaker was highlighted in early ablation experiments which demonstrated that surgical removal of this organ abolishes circadian rhythms of locomotor activity and body temperature in house sparrow (*Passer domesticus*) as well as rhythms of migratory restlessness in the white-crowned sparrow (*Zonotrichia albicollis*) (Zimmerman and Menaker, 1979). Furthermore, following its dissection, if the pineal organ is left *in situ*, it retains the ability to regulate activity rhythms and its transplantation successfully restores the host's free-running rhythm, confering the donor's rhythm on the rhythm of the host (Zimmerman and Menaker, 1979). Based on studies of the avian circadian system, which identified a circadian oscillator in the retina as well as the pineal gland, Cahill (1996), inspired by advancement of genetic tools and emerging tractability of the zebrafish, examined whether these two structures also exhibit rhythmicity in this model organism. He showed that when isolated in culture, the zebrafish pineal gland, but not the retina, maintains circadian rhythmicity in melatonin biosynthesis for 5 days under constant darkness and these rhythms can be reset by *in vitro* exposure to light. Indeed, cells exhibiting retinal photoreceptor-like characteristics have been detected in the pineal gland (Bolliet *et al.*, 1997), together with the rhythmic expression of *clock* gene. Furthermore, BMAL:CLOCK heterodimers were found to regulate the circadian expression of *aralkylamine N-acetyltransferase* (*aanat*), a key enzyme for melatonin production (Appelbaum *et al.*, 2005). According to these findings, fish pineal gland exhibits all the features of a complete circadian system, including photoreception, expression of an intrinsic clock oscillator and rhythmic output, and for this reason has been often referred to as master circadian oscillator.

However, in addition to pineal gland, the *clock* gene also rhythmically oscillates in other dissected brain structures, including telencephalon, hindbrain and optic tectum, as well as in the eye, heart, kidney and embryonic zebrafish cell line, PAC-2 (Whitmore *et al.*, 1998). Furthermore, *clock* rhythms in cultured heart, kidney and PAC-2 cell lines are directly entrained by light (Whitmore *et*

al., 2000). Complementary to these findings, monitoring of a bioluminescent *per3-luciferase* reporter line revealed *per3* oscillations in the pineal, retina, heart, spleen and gall bladder (Kaneko *et al.*, 2006) as well as in various brain regions, including teleost equivalent of suprachiasmatic nucleus, telencephalon, multiple hypothalamic nuclei and optic tectum, amongst others (Moore, 2013; Moore and Whitmore, 2014). These oscillations were dampened under constant lighting conditions and recovered after exposure to a new light-dark cycle. Moreover, single-cell analysis of *per4-luciferase* rhythms revealed that individual cells continue to oscillate even after several months under constant darkness. Although, their individual rhythms are markedly desynchronised, which may explain why large populations of cells collectively exhibit dampening of the rhythm under such conditions. Interestingly, a single 15-min light pulse was sufficient to restore the synchrony in cellular oscillators, implying that light serves as the dominant clock synchroniser (Carr and Whitmore, 2005). Therefore, since individual zebrafish cells and tissues possess circadian pacemakers that are directly responsive to light, this organism exhibits a rather decentralised organisation of the circadian system.

Consequently, Ben-Moshe Livne *et al.* (2016) questioned the central role of the pineal oscillator in the zebrafish circadian system, further investigating this problem by genetically blocking clock machinery specifically in melatonin-producing pineal cells using ΔCLK mutation (for explanation of this mutation refer to Chapter 3 Introduction). The authors have reported three major findings, contributing to our understanding of the role of pineal oscillator in circadian regulation of zebrafish physiology and behaviour. First, the specific ΔCLK mutation leads to loss of circadian rhythmicity in melatonin biosynthesis (levels remained relatively high throughout the whole cycle), expression of core clock genes and the majority of CCGs in the pineal gland. Second, consistent with the view of a decentralised circadian system, clock oscillators in peripheral tissues are not affected, implying that peripheral clocks in zebrafish are independent of the pineal gland clock. Third, locomotor activity rhythms – a commonly used measure of circadian clock output – are attenuated, but not completely absent as a result of the pineal-specific ΔCLK mutation, suggesting that the pineal is not the only 'master' regulator of behavioural rhythms in zebrafish, but rather is a part of extended and highly distributed circadian system composed of multiple pacemakers.

In comparison, the mammalian circadian system is more centralised, with the hypothalamic suprachiasmatic nucleus (SCN) acting as a master synchroniser of biological rhythms. A structure anatomically equivalent to mammalian SCN has been identified in zebrafish and this brain area also exhibits rhythmic expression of *per3*, *per2* and *cry1a* clock components (Moore and Whitmore, 2014). Noche and colleagues (2011) further investigated the functional role of this structure in the circadian regulation of the pineal gland. They reported that *cyclops* (*cyc*) mutants that lack ventral brain regions, including the area that gives rise to the SCN, exhibit slightly decreased amplitude of rhythmic *aanat2* expression in the pineal gland and under constant conditions the amplitude of this rhythm decreases more rapidly compared to wild-type fish. This indicates that pineal rhythms in zebrafish are initiated and maintained independently of the SCN, but that this brain structure may be involved in maintaining pineal rhythms particularly in the absence of external time cues.

Photoreception

When considering light detection, or photoreception, thought and discussion naturally focuses upon the visual system, where specialised photoreceptors in the retina facilitate the creation of internal representations of the external world. However, the synchronisation of the biological clock in all vertebrates is mediated by non-visual detection of light – a process mediated by photopigments, or opsins. Currently, the most studied opsin is melanopsin, which is expressed in the retinal ganglion cells and plays a crucial role in circadian clock entrainment and pupillary constriction in mammals. In zebrafish, recent phylogenetic analysis revealed the presence of 42 opsin genes, out of which 32 encode non-visual opsins (Davies *et al.*, 2015). Consistent with the light responsive nature of zebrafish brain and peripheral tissues, multiple non-visual opsins were expressed in all peripheral organs examined, while the brain and retina expressed the majority of the opsin genes. It has been hypothesised that retention of such opsin multiplicity, since it ensures a wide range of spectral sensitivity, is important for survival of a freshwater teleost in a dynamic photic environment. However, to date, the exact function of these photopigments remains unknown (Davies *et al.*, 2015; Frøland Steindal and Whitmore, 2019).

Light-mediated clock entrainment

In zebrafish, photo-entrainment of the circadian clock is primarily mediated by *per2* and *cry1a* genes (Frøland Steindal and Whitmore, 2019). Indeed, light stimulus significantly increases expression of both genes in all examined tissues and cell lines via a light responsive module (LRM) in *per2* and *cry1a* promoters. The *per2* promoter LRM contains both E- and D-box elements, where E-Box facilitates CLOCK:BMAL-mediated regulation and D-box confers light-driven expression. On the other hand, only D-box is present in the LRM of *cry1a* (Mracek *et al.*, 2012). The D-box element mediates light-induced expression through binding of thyrotroph embryonic factor (TEF) that is regulated by light and its knock-down attenuates light-induced *per2* expression (Vatine *et al.*, 2009). It should be noted, however, that due to the clock-feedback mechanism, the light sensitivity of these genes varies across the circadian cycle, as, for instance, light-induced *cry1a* expression at circadian time (CT) 20 is almost twice as high as expression induced at CT8 (Tamai *et al.*, 2007; Frøland Steindal and Whitmore, 2019). The exact mechanisms underlying light-induced expression of these genes have yet to be clarified, although extracellular signal-regulated kinase (ERK) signalling has been implicated in the regulation of D-Box-mediated transcription in wavelength-dependent manner (Mracek *et al.*, 2013).

Development of circadian clock

One of the key advantages of zebrafish as a model organism is that it enables convenient investigation of mechanisms underlying development of the circadian system during embryogenesis – processes generally more difficult to study in mammals due to internal development of the foetus *in utero* (Frøland Steindal and Whitmore, 2019). In general, zebrafish circadian system develops remarkably early and rapidly. During the first 12 hours of development, the endogenous *clock* autonomously initiates *per1* transcription that peaks 27 hours post-fertilisation (hpf) – a process that occurs independently of light. Exposure to the light-dark cycle

is, however, required for the subsequent synchronous oscillations of *per1*, since under constant darkness *per1* expression remains elevated and constant, suggesting that early exposure to an entraining signal is essential for the correct synchronisation of cellular oscillators (Dekens and Whitmore, 2008). In addition to *per1*, bioluminescence monitoring of a *Tg(4xE-Box:luciferase)* reporter line has demonstrated the rhythmic activity of CLOCK:BMAL heterodimers starting from 1 day post-fertilisation (dpf) (Weger *et al.*, 2013). The *per3-luciferase* rhythms, on the other hand, become established 5-6 dpf, suggesting gene specific differences during the onset of clock regulation. Further physiological and behavioural rhythms also appear early during the first hours or days of life. For instance, expression of *aanat2* appears as early as 22 hpf and circadian rhythms in both its transcription and subsequent melatonin production begin 2 dpf. Moreover, rhythms in nocturnal sleep-like behaviour and diurnal locomotor activity become apparent 4-5 dpf. It should be noted, however, that exposure of larvae to light-dark cycles immediately post fertilisation is crucial for establishment of all behavioural, physiological and molecular rhythms (Ben-Moshe *et al.*, 2014).

Master circadian pacemaker in mammals

Similar to the identification of the avian circadian pacemaker, the pineal gland, ablation experiments in rat brains have contributed to the exact localisation of a mammalian pacemaker. These pioneering studies demonstrated that circadian rhythms in locomotor activity, drinking behaviour as well as adrenal corticosterone levels were abolished by lesioning of a bilateral hypothalamic structure located above the optic chiasm, the SCN (Moore and Eichler, 1972; Stephan and Zucker, 1972). Additionally, transplantation of foetal SCN tissue restored circadian rhythms in the locomotor activity of SCN-lesioned hamsters (Lehman *et al.*, 1987), while transplantation of SCN tissue from *Tau* mutants – animals that exhibit accelerated degeneration of PER protein and a correspondingly shortened period – restored rhythms in SCN-lesioned hamsters, which, following the transplantation, acquired periodicity similar to donor mutants (Ralph *et al.*, 1990). Collectively, these findings illustrate the dominant role of the SCN in maintaining mammalian circadian rhythmicity (Dibner *et al.*, 2010).

Integration of environmental parameters in the SCN

The molecular clock in the SCN is synchronised by multiple major input pathways: the retinohypothalamic tract (RHT), geniculohypothalamic tract (GHT) and serotonergic (5-HT) pathways arising from the dorsal raphe nucleus (DRN) and the median raphe nucleus (MRN) (Dibner *et al.*, 2010). Amongst these, the RHT is the most prominent pathway for communicating photic information to the SCN, as lesioning of this pathway abolishes animals' ability to entrain to light-dark cycles (Johnson *et al.*, 1988), while the GHT and raphe nuclei transmit non-photic information. Photic input, as the most dominant *zeitgeber*, is perceived via retinal ganglion cells expressing melanopsin photopigments. These cells project photic information, via the RHT, directly to the ventrolateral SCN, where upon stimulation by light RHT terminals release glutamate and pituitary adenylate-cyclase activating peptide (PACAP), neurotransmitters that activate N-methyl-D-asparate (NMDA) and PAC1 receptors, respectively, on postsynaptic SCN neurons. Activation of these receptors mediates influx of Ca^{2+} into the cell, activating the ERK pathway and

subsequent phosphorylation of cAMP response element-binding (CREB) protein. CREB, in turn, binds to cAMP response elements (CREs) in the promoters of target genes, including amongst others the immediate-early gene *c-Fos*, thereby activating their transcription (Goldsmith and Bell-Pedersen, 2013). Interestingly, CREB also activates transcription of *Per1*, suggesting that the transcription of this gene can occur independently of CLOCK:BMAL. However, CREB-mediated *Per1* transcription is primarily induced by photic stimulation during subjective night and therefore facilitates the resetting of the clock oscillator during adaptation to sudden changes in external illumination (Gau *et al.*, 2002).

Additionally, the RHT also innervates the intergeniculate leaflet (IGL) that, in turn, projects to the SCN via the GHT. Upon stimulation the retinorecipient IGL releases neuropeptide Y (NPY) and gamma-aminobutyric acid (GABA) neurotransmitters from their axon terminals. This additional regulatory pathway has been implicated in the modulation of SCN responses to photic stimulation, as for instance, *npy-/-* mice are significantly slower in shifting their locomotor activity onset in response to altered photoperiods (Kim and Harrington, 2008). However, in addition to RHT innervation, the IGL is also innervated by the DRN, which indicates that regulation of the SCN via the GHT integrates both photic and non-photic stimuli (Dibner *et al.*, 2010).

Serotonergic input from the DRN and MRN represent the third input pathway to the SCN that has been implicated in the modulation of RHT neurotransmission to this structure – effects achieved via the activation of both pre- and post-synaptic 5-HT receptors (Van Esseveldt *et al.*, 2000). Indeed, manipulation of 5-HT systems in the brain alters light-induced phase shifts, as, for instance, administration of the 5-HT receptor agonist 8-OH-DPAT significantly phase-advanced locomotor rhythms in hamsters (Cutrera *et al.*, 1994). Therefore, it is believed that 5-HT transmission mediates non-photic modulation of the SCN.

Time-keeping in the SCN circuit: importance of interneuronal coupling

In general, the SCN is divided into two major subregions, known as the ‘core’ and the ‘shell’ – categorisations based on efferent connectivity and expression of specific neuropeptides, with vasoactive intestinal peptide (VIP) and gastrin releasing peptide (GRP) expressed in the retinorecipient core and arginine vasopressin (AVP) expressed in the shell (Hastings *et al.*, 2018).

Circadian rhythmicity in SCN neurons is primarily mediated by TTFLs that drive daily variations in membrane excitability. Generally, this is achieved by modulating the activity of the various ions channels that determine the intrinsic excitability and computational properties of neurons. For instance, increased activity of persistent Na^+ and Ca^{2+} channels leads to a more depolarised resting membrane potential (RMP), thereby increasing action potential (AP) discharge, whereas increased activity of K^+ channels drives the membrane potential towards more hyperpolarised state (Belle, 2015). During the day SCN neurons are more depolarised and exhibit increased spontaneous firing. The excitatory drive responsible for AP discharge is dominated by persistent Na^+, Ca^{2+} and hyperpolarisation-activated cyclic nucleotide-gated (HCN) currents. However, these currents are relatively constant throughout the circadian cycle, whereas conductances determining AP waveform and consequently discharge frequency, including fast delayed rectifier K^+ currents and subthreshold-activated A-type K^+ currents, are more active during the day and

therefore are likely to contribute to the day-night difference (Colwell, 2011). The daily variation in neuronal excitability is also mediated by increased conductivity of multiple K^+ channels, which drives the SCN neurons into hyperpolarised state at night. The regulation of neuronal excitability enables the SCN neurons to generate daily rhythms in their electrical output (Belle, 2015).

Even when isolated in culture, individual SCN neurons maintain circadian rhythms in spontaneous electrical firing, cytosolic Ca^{2+} concentration and gene expression (Hastings *et al.*, 2003). However, it should be noted that these cell-autonomous rhythms are less coordinated than rhythms in SCN organotypic slices where circuit connectivity is preserved. Herein, neuronal interactions enhance stability and amplitude of TTFLs, synchronising individual neurons and thereby facilitating organised rhythms of gene expression and neuronal activity. This exclusive circuit-level characteristic of the SCN underpins the precise free-running rhythms in physiology and behaviour observed in the absence of temporal cues (Hastings *et al.*, 2018).

A key contributor to SCN synchrony is VIP. This peptide is expressed in approx. 10% of neurons in the SCN's retinorecipient core and mediates SCN synchrony via VIP receptors 2 (VIPR2 also known as VPAC2) located in the adjacent shell. Indeed, mice lacking VPAC2 are incapable of sustaining normal circadian rhythms in rest/activity behaviour (Harmar *et al.*, 2002). Furthermore, *Per2* rhythms in VIP-null mice, measured using a bioluminescent *Per2::Luciferase* (*Per2::Luc*) reporter line, exhibit dampened amplitude and are not synchronised across the circuit. Interestingly, the amplitude and synchrony of the *Per2* rhythms in VIP-null mice were restored when a wild-type SCN was grafted on top of the host VIP-null SCN. This paracrine effect was further confirmed as a 2-kDA cut-off membrane, used to block the VIP diffusion between the graft and host SCN, prevented the synchronisation of the host VIP-null SCN. In addition, grafting of a *Tau* mutant SCN induced shortened *Per2* periodicity in host SCN, recapitulating the *Tau* mutant phenotype (Hastings *et al.*, 2014). The VIP-mediated paracrine effects are potentially facilitated by VIPR2-dependent signalling, involving cytosolic Ca^{2+} and cAMP which regulate TTFLs via CRE in promoters of *Per* genes (Hastings *et al.*, 2018).

Apart from VIP, GABA is expressed in almost all SCN neurons and has been implicated in coupling between the core and shell of this structure (Albus *et al.*, 2005). However, $GABA_A$ receptor-mediated signalling appears to oppose the stabilising and synchronising effects of VIP as inhibition of this transmission by gabazine rescued desynchronised rhythmicity in VIP-deficient SCN slices (Freeman *et al.*, 2013). Contradictory to these results, Liu and Reppert (2000) have demonstrated synchronising influence of $GABA_A$ receptor-mediated signalling on clock cells in the SCN. Furthermore, one of the most recent studies has demonstrated that SCN of foetal mice lacking vesicular GABA transporter ($VGAT^{-/-}$) or GABA synthesising enzyme ($GAD65^{-/-}$ / $67^{-/-}$) exhibit synchronous burst firings associated with large Ca^{2+} spikes throughout a circadian cycle, without affecting *Per2* rhythms (Ono *et al.*, 2019). The authors of this study proposed that GABA neurotransmission is essential for refinement of circadian firing rhythms to ensure noiseless communication with neurons outside SCN, but not for integration of multiple cellular oscillators. Consequently, the mechanism of GABAergic transmission is still a matter of some debate, as controversy exists as to whether it has a synchronising or destabilising influence on cellular rhythms in the SCN.

The last mediator of the interneuronal communication in the SCN to be discussed is AVP. In the SCN, the vasopressinergic neurons form synapses and communicate via AVP receptors V1a and V1b. Signalling within this local AVP circuit has been studied in relation to the SCN's ability to resynchronise its rhythmicity following exposure to experimental jet-lag, where light-dark (LD) cycle is advanced by 8 hours (Yamaguchi, 2018). Generally, a sudden shift in LD cycle leads to dampening and desynchronization of SCN clock oscillations which gradually recover over 10 days. Interestingly, when interneuronal communication between AVP neurons is disrupted by either genetic deletion or SCN-specific blockade of V1a and V1b receptors, rhythms in behaviour, body temperature and clock gene expression re-entrain much more rapidly under the jet-lag condition (Yamaguchi *et al.*, 2013). Furthermore, following pharmacological perturbation of clock gene oscillations by cycloheximide the oscillations in individual neurons in wild-type SCN can be gradually restored by maintaining the original phase order from dorsal to ventral region. However, this was not the case in *V1a*$^{-/-}$ *V1b*$^{-/-}$ mutant SCN where the circadian oscillations in each cell did not recover to the original phase order, suggesting that the mutant SCN is more amenable to external perturbations and therefore can entrain to altered lighting conditions more rapidly (Yamaguchi *et al.*, 2013). According to these findings, vasopressinergic signalling plays a crucial role in the intrinsic resilience of the SCN to external perturbations.

Transmission of SCN-derived circadian cues

In order for the SCN to serve as a pacemaker and synchroniser for brain and peripheral clocks, it needs to communicate time-keeping signals to the rest of the brain and body. The communication of circadian time cues is facilitated by clock-mediated 24-h oscillations in spontaneous neuronal firing that generate rhythmic neuronal signals (Baño-Otálora and Piggins, 2017).

Efferent pathways of the SCN primarily target the hypothalamic subparaventricular zone (sPVZ), preoptic area (POA), dorsomedial hypothalamus (DMH), arcuate nucleus (ARC), paraventricular hypothalamic nucleus (PVN) as well as bed nucleus of stria terminalis (BNST). Extra-hypothalamic structures targeted include the lateral septum (LS) in basal forebrain, paraventricular nucleus of the thalamus (PVT) and, amongst less well established targets the habenula (Hb) (Dibner *et al.*, 2010). Transmitter substances involved in SCN signalling to these targets are less well understood but are believed to include GABA, VIP, AVP and prokineticin 2 (PK2) (Baño-Otálora and Piggins, 2017). Amongst these, PK2 signalling is possibly the most recognised SCN output as, for instance, PK2 receptor messenger RNA (mRNA) has been detected in brain areas including DMH, PVN, PVT, LS and lateral Hb (LHb), suggesting PK2 serves as a signalling substance mediating SCN output into these areas. Additionally, intracerebroventricular administration of PK2 supresses nocturnal wheel-running behaviour in rats, thereby further supporting the hypothesis that SCN-derived PK2 signalling mediates circadian behavioural rhythms (Cheng *et al.*, 2002). Other SCN efferents targeting the neuroendocrine PVN regulate circadian release of cortisol via hypothalamic-pituitary-adrenal axis, while projections into DMH mediate circadian regulation of orexin system that consolidates wakefulness (Hastings *et al.*, 2003).

Furthermore, in mammals the SCN-derived circadian signal is also transmitted to the pineal gland via a multi-synaptic pathway that involves glutamatergic neurons in the PVN projecting to sympathetic preganglionic neurons (SPNs) of intermediolateral nucleus of the spinal cord (IML). When activated, SPNs stimulate, via cholinergic transmission, superior cervical ganglion (SCG) neurons which innervate pineal gland and release norepinephrine, a stimulus necessary for melatonin biosynthesis (Berry, 2012). During the daytime, in the presence of light, a GABAergic input from SCN suppresses melatonin secretion from the pineal gland, by inhibiting PVN glutamatergic transmission to IML, whereas during the night, the SCN-derived inhibition of PVN neurons is absent, thereby allowing melatonin biosynthesis (Berry, 2012). Therefore, in comparison with zebrafish where melatonin synthesis in the pineal gland is directly synchronised by light, in mammals circadian cues are relayed to the pineal gland via a multicomponent circuit orchestrated by the SCN.

Extra-SCN oscillators

The first extra-SCN oscillator discovered in mammals was the retinal circadian clock (Tosini *et al.*, 2008). When cultured, the retina releases melatonin in a circadian fashion. This rhythmic release free-runs in constant darkness and can be directly entrained by light *in vitro*. Furthermore, retinas from hamsters homozygous for *Tau* mutation exhibit a shortened free-running period of melatonin synthesis, suggesting that the mechanism regulating circadian oscillations in the retina is similar to that of the SCN (Tosini and Menaker, 1996). In addition to the retinal circadian pacemaker, monitoring of reporter constructs in which expression of *luciferase* is driven by clock genes enabled the discovery and further investigation of other extra-SCN oscillators in the mammalian brain. For instance, initial examination of *Per1::Luc* in rats has revealed rhythmic *Per1* expression in 14 out of 27 examined brain areas, including the pineal and pituitary glands, olfactory bulb (OB) and ventral hypothalamus where ARC exhibited the most robust rhythm (Abe *et al.*, 2002). In accordance with these findings, cultured OB neurons exhibit near-24 h oscillations in firing rate which are correlated with rhythmic expression of *Per1* (Granados-Fuentes, Saxena, *et al.*, 2004). Interestingly, rendering the SCN arrhythmic, whether by lesions or the housing of rats under constant light, does not abolish *in vivo Per1* rhythms in the OB, suggesting rhythmicity in this structure is independent of the SCN (Granados-Fuentes, Prolo, *et al.*, 2004; Guilding and Piggins, 2007). In addition to the OB, rhythmic PER2::LUC expression has also been detected in isolated hippocampal cultures (Wang *et al.*, 2009). In general, hippocampal excitability and long-term potentiation are under circadian regulation as, for instance, the enhancement of the population spike in long-term potentiation recorded at subjective night is greater than that observed during the subjective day (Chaudhury *et al.*, 2005). Furthermore, mice deficient in *Per2* exhibit abnormal long-term potentiation (Wang *et al.*, 2009), implying that an endogenous circadian oscillator modulates synaptic plasticity in the hippocampus.

Similar to rhythmicity observed in the OB and hippocampus, *Per1*-expressing neurons in ARC exhibit day-night variation in firing rate with increased AP discharge during the night when these neurons receive diminished inhibitory tone. This phenomenon is absent in mice globally lacking *Cry1/2* and in mice with an ARC-specific *Bmal1* mutation, both of which exhibit increased firing

frequency during both day and night, suggesting that the local intact TTFL tightly regulates the bioelectrical properties of ARC neurons (Watson, 2018). The ARC contains critical sensors of metabolic information and accordingly has a key role in regulation of energy homeostasis. This occurs primarily via pro-opiomelanocortin (POMC) and agouti gene-related protein (AgRP)/NPY neurons. The POMC and AgRP/NPY neurons possess antagonistic functions, as the POMC population inhibits, while AgRP/NPY population stimulates food intake (Hirayama *et al.*, 2018). As such, the presence of an endogenous clock in this feeding circuitry may gate responses of ARC neurons, rendering them more responsive to inputs at one time of day versus another (Guilding *et al.*, 2009), suggesting that ARC oscillators have a specialised function in the circadian coordination of feeding behaviour, essential for the preservation of energy homeostasis.

There are two major differences between rhythms detected in the SCN and extra-SCN oscillators: namely strength and phase-resetting properties. For instance, the extra-SCN oscillations exhibit apparent dampening when compared to those detected in the SCN – a structure that robustly oscillates for more than 10 days in culture (Abe *et al.*, 2002). The attenuated robustness of extra-SCN oscillators could be associated with relatively weak interneuronal coupling in these structures, which may lead to gradual desynchronization of individual cellular oscillators (Dibner *et al.*, 2010). Indeed, PER2::LUC rhythms detected in mouse DMH and ARC do not maintain long-term synchrony at the single-cell level, leading to the dampening of oscillations at both the cell and network levels (Guilding *et al.*, 2009). Consequently, it is likely that in the intact animal, the SCN serves as a master synchroniser of weakly coupled or non-coupled cells in other brain oscillators. Furthermore, while the phase of peak PER2 expression in SCN cultures is correlated with ZT, in the case of hypothalamic extra-SCN oscillators the phase is reset by cull or culture preparation and, therefore, is correlated with time of cull, implying these oscillators are generally more sensitive to resetting (Guilding *et al.*, 2009). This characteristic is, however, not shared by all extra-SCN oscillators as other brain explants are either unaffected or completely reset by culture preparation (Guilding *et al*., 2010).

In addition to the extra-SCN oscillators discussed above, autonomous PER2::LUC rhythms, which exhibit slightly faster rates of dampening in comparison to hypothalamic explants, have been detected in the epithalamus, particularly in the structure known as the habenula (Guilding *et al*., 2010). It should be noted, however, that unlike hypothalamic oscillators, phase of rhythmicity in the habenula is correlated to neither ZT, nor time of cull, implying its sensitivity to resetting is differentially modulated in comparison to other circadian pacemakers (Guilding *et al*., 2010). The following sections of this chapter will discuss the neuroanatomy and neuropharmacology underpinning habenula's functional role in the regulation of brain and behavioural states, as well as in circadian timekeeping in vertebrates.

Habenula

The habenula (from the Latin word *habena* meaning, 'little rein') is a bilateral structure located on the most caudal and dorsal edge of the thalamus, adjacent to the third ventricle. Anatomically, its strategic location enables the habenula to act as a relay station, receiving and integrating information from basal forebrain and limbic system, while regulating numerous monoaminergic centres, including the ventral tegmental area (VTA), raphe and interpeduncular nucleus (IPN), through efferent pathways (Baño-Otálora and Piggins, 2017). Therefore, this brain structure has been compared to the 'conductor' of an orchestra modulating behaviour, or to a 'switchboard' selecting different action modes (Mathuru, 2018). In general, the habenula has been implicated in a wide variety of functions, including behavioural responses to fear and negative reward, pain, sleep, circadian regulation and higher cognitive functions (Klemm, 2004). Consequently, its dysfunction has been associated with multiple psychiatric disorders, including depression, schizophrenia and addiction in humans (Mathuru, 2018).

The habenula is present in all vertebrates examined, including those that seemingly lack high-level cognitive functions. Indeed, its circuitry, together with its major afferent and efferent pathways are conserved in lamprey, one of the phylogenetically oldest vertebrates (Stephenson-Jones *et al.*, 2012). The evolutionary conservation of this structure implies that the habenula regulates processes crucial to survival via a basic neuronal circuitry common to all vertebrates. These mechanisms allow animals to predict rewards and punishments and consequently adapt their behaviours to increase their reproductive success and chance of survival. For instance, the habenula, in particular, processes aversive information, such as pain, disappointment and stress, which is important for eliciting an appropriate behavioural response ('flight or fight' or freezing) in the event of danger (Hikosaka, 2010). More recently, this circuitry has been also shown to mediate the transition of brain dynamics during the switch from active to passive stress coping – adaptive behavioural state transition crucial for management of effort expenditure during stress (Andalman *et al.*, 2019). Other factors influencing survival include a fully functional circadian system and sleep, both of which are regulated by the habenula. The circadian system, composed of multiple brain pacemakers, including the habenula, enables animals to appropriately adapt their physiology and behaviour to daily fluctuations in the external environment. For instance, it regulates appropriate amount of sleep which increases behavioural efficiency by minimising energy expenditure when activity is not advantageous (Siegel, 2009; Hikosaka, 2010). Therefore, habenula circuitry reflects the fundamental mechanisms responsible for the regulation of healthy behavioural states.

Suborganisation of habenula in mammals

The mammalian habenula is broadly divided into two major anatomically, biochemically and genetically distinct subregions, the medial (MHb) and the lateral habenula (LHb), both of which are found on each side of the third ventricle. Further cytoarchitecture and immunohistochemical studies in rats and mice have enabled subdivision of LHb and MHb into 9-10 and 5 distinct subnuclei, respectively (Andres *et al.*, 1999; Geisler *et al.*, 2003; Wagner *et al.*, 2014). In addition,

analysis of numerous transcripts from the Allen Brain Atlas support the proposed MHb subdivision as the transcripts appear to obey the subnuclear boundaries. In the LHb, on the other hand, the majority of transcripts are differentially distributed throughout the LHb and not confined to the boundaries of the proposed subnuclear regions. Indeed, although nine distribution patterns were identified, many transcripts could not be assigned to any of these patterns, implying a complex and heterogenous organisation of the LHb (Wagner *et al.*, 2016).

In addition, to differences in molecular nature, the LHb and MHb are divergent in their anatomical connectivity – although both nuclei are known to receive inputs and send efferent projections via the same fibre bundles – the stria medullaris (SM) and fasciculus retroflexus (FR), respectively.

Connectivity of the medial habenula

Initial experiments involving retrograde tracing in rats showed that MHb afferent fibres primarily originate in the posterior parts of the septum, with the septofimbrial nucleus projecting to the rostral MHb and nucleus triangularis projecting to the caudal MHb (Herkenham and Nauta, 1977). In accordance with these findings, more recently conducted tracing experiments in mice have demonstrated major afferent projections to MHb originating in medial septum, nucleus triangularis and nucleus of diagonal band (Qin and Luo, 2009). The minor sources of MHb afferent inputs include nucleus accumbens, median raphe, ventral central grey and dorsolateral tegmental nucleus (Sutherland, 1982).

In addition to MHb afferents, Herkenham and Nauta (1979) were also the first to visualise MHb efferent projections which primarily innervate the IPN in a topographic organisation such that dorsal MHb projects to the lateral IP, medial MHb to the ventral IP and lateral MHb to the dorsal IP. In addition, very sparse MHb fibres were also found in the septum and median raphe. More recently, the principal MHb-IPN pathway has been also confirmed using anterograde tracing (Kim, 2009).

Connectivity of the lateral habenula

The majority of LHb afferents originate in the basal ganglia, particularly in the entopeduncular nucleus, the non-primate homologue of the internal segment of the globus pallidus (GPi). These projections, together with afferent fibres from the lateral preoptic area, as well as lateral hypothalamus, are topographically organised in the LHb as the lateral part of the entopeduncular nucleus projects to the lateral part of the LHb, while the medial aspect of the entopeduncular nucleus projects to the medial LHb (Herkenham and Nauta, 1977). Additional minor sources of LHb afferents include the diagonal band nucleus, lateral septal nucleus, nucleus accumbens, VTA, median raphe (Sutherland, 1982) and locus coeruleus (Jones and Moore, 1977)

Projections originating in the LHb primarily target midbrain areas involved in release of dopamine, *e.g* the substantia nigra pars compacta (SNc) and VTA, and serotonin, *e.g.* the median raphe nucleus (MRN) and dorsal raphe nucleus (DRN) (Hikosaka, 2010). Additionally, the rostromedial tegmental nucleus (RMTg), located on the caudal edge of the VTA, has been identified as a major target of LHb projections (Jhou *et al.*, 2009). This structure, in turn, sends robust GABAergic

projections to the dopaminergic VTA and serotonergic DRN, and therefore facilitates the indirect inhibitory action of the LHb on these structures (Yang, Wang *et al.*, 2018).

Figure 1.2 demonstrates the major afferent and efferent pathways of rodent habenula.

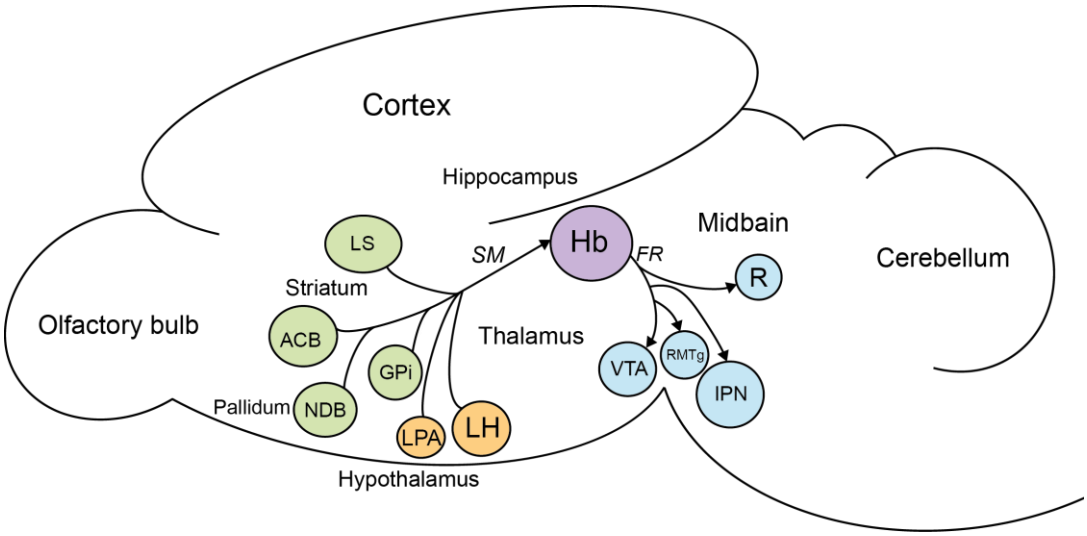

Figure 1.2: Afferent and efferent connectivity of rodent habenula

Sagittal view: Hb – habenula; LS – lateral septal nucleus; ACB – nucleus accumbens; NDB – diagonal band nucleus; GPi – globus pallidus internal segment; LPA – lateral preoptic area; LH – lateral hypothalamus; VTA – ventral tegmental area; RMTg – rostromedial tegmental nucleus; R – raphe; IPN – interpeduncular nucleus; SM – stria medullaris; FR – fasciculus retroflexus. Green colour indicates brain structures in telencephalon; orange – hypothalamic structures; purple – epithalamic structures; blue – midbrain structures. Figure adapted from Aizawa *et al.* (2011).

Human habenula

Morphological and immunohistochemical analysis of the human habenula conducted by Díaz *et al.* (2011) demonstrated that the subnuclear organisation of human MHb resembles that of rats as described by (Andres *et al.*, 1999). However, the shape, relative size and organisation of the LHb appear significantly different as, for example, the contribution of the LHb to the overall size of the habenular complex is about five times larger in humans than in rats. The difference in size between LHb and MHb may reflect the extent of the cortical input through the basal ganglia to the former structure (Aizawa *et al.*, 2011). Moreover, direct projections from the prefrontal cortex to the LHb have been found in rats and primates and therefore there is a possibility that the human LHb receives more enhanced innervation from the basal ganglia and directly from the prefrontal cortex, as this region is significantly more developed in humans. Hence, the enlargement of the LHb in primates and humans may account for a more refined control of the monoaminergic centres in assessing a larger amount of sensory input and eliciting more complex responses. However, in order to support this hypothesis further *in vivo* studies are required to confirm afferent innervations of the LHb as well as to investigate which afferent nuclei primarily contribute to the enlarged LHb in humans (Díaz *et al.*, 2011).

Suborganisation of habenula in zebrafish

Based on cytoarchitectural analysis, fish habenula can be subdivided into dorsal and ventral subregions. Since the dorsal habenula projects to the IPN, it is thus analogous to the mammalian MHb, while the ventral habenula – innervating the raphe – is analogous to mammalian LHb (Amo *et al.*, 2010). Henceforth, in this thesis, the ventral and dorsal habenula are referred to as LHb and MHb, respectively.

A characteristic feature of the fish habenula is bilateral asymmetry, which is reflected in differences in size, projections and neurotransmitter content between left and right habenula (Concha and Wilson, 2001). For instance, in lamprey the habenula in the right hemisphere is larger than the one on the left (Yañez and Anadon, 1994) and this mode of lateralisation is common in the majority of fish species (Bianco and Wilson, 2009). In zebrafish, the development of habenula asymmetry is facilitated by close reciprocal interactions between habenula precursor cells and precursor cells of a pineal complex component, known as the parapineal. Initial lateralisation of habenula precursor cells influences unilateral migration of the parapineal precursor cells from the midline of the diencephalon towards the left side of the epithalamus (Concha *et al.*, 2003). Projections arising from the parapineal subsequently innervate the left dorsomedial neuropil of the habenula, further mediating the development of habenula asymmetry by influencing gene expression (Gamse *et al.*, 2003). As a result, several asymmetric features of the habenula are evident in zebrafish larvae, including enlarged left neuropil and asymmetric expression of numerous molecular markers. The left-right differences in the overall size become more apparent in adult zebrafish where the LHb is generally larger on the left while MHb is larger on the right. Concomitant asymmetries in afferent and efferent connectivity are detected in both larval and adult stages (Bianco and Wilson, 2009).

Habenula connectivity in zebrafish

In order to identify primary afferents to zebrafish habenula, Turner *et al.* (2016) conducted a study applying tract tracing experiments in combination with immunohistochemistry and analysis of multiple transgenic lines. These approaches revealed that in both larval and adult zebrafish habenula afferents primarily originate in the ventral entopeduncular nucleus (vENT), subpallium, nucleus rostrolateralis, preoptic area, posterior tuberculum, posterior hypothalamic lobe and median raphe. Additional asymmetric afferents were also detected from the parapineal to the left habenula and from the OB to the right habenula. Furthermore, injection of a lipophilic tracer into some of these structures demonstrated the distribution of specific terminal fields within the habenula. For instance, OB terminals were found in the right MHb, while terminals from vENT and posterior hypothalamic lobe were primarily detected in the ventral half of the habenula, a structure homologous to mammalian LHb. The vENT innervation of the LHb in zebrafish has been also previously reported by Amo *et al.* (2014). In addition to afferent projections reported by Turner *et al.* (2016) and Amo *et al.* (2014), Cheng and colleagues (2017) identified another source of habenula afferents in larvae – the anterior thalamus – which receives projections from the retina and pineal gland and specifically innervates neuropil of the left MHb. This pathway has been implicated in habenula photo-responsiveness.

In zebrafish, IPN and median raphe are the major targets of MHb and LHb efferent projections, respectively (Amo *et al.*, 2010). While the projections to raphe appear to be symmetric, the innervation of the IPN is asymmetric with the axons from the left MHb predominantly terminating in the dorsal IPN and to a lesser degree in the ventral IPN, while majority of axons from the right MHb terminate in the ventral IPN (Bianco and Wilson, 2009).

Figure 1.3 demonstrates the major afferent and efferent pathways of zebrafish habenula.

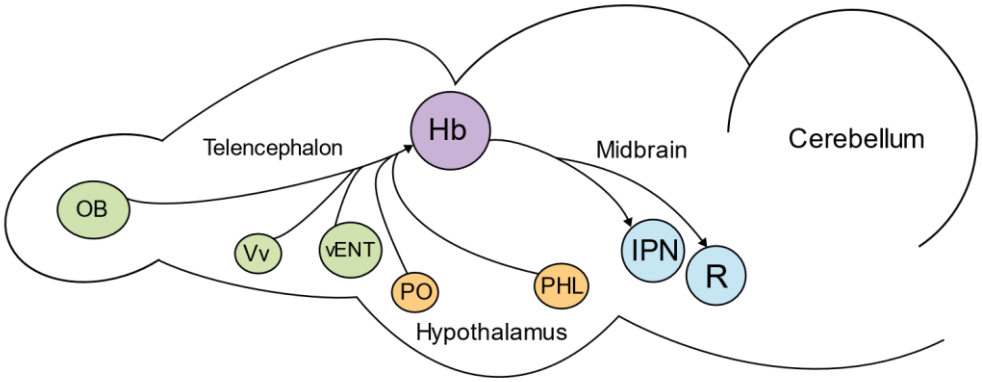

Figure 1.3: Afferent and efferent connectivity of zebrafish habenula

Sagittal view: OB – olfactory bulb; Vv – ventral area of the subpallium; vENT – ventral entopeduncular nucleus; PO – preoptic area; PHL – posterior hypothalamic lobe; IPN – interpeduncular nucleus. Green colour indicates brain structures in telencephalon; orange – hypothalamic structures; purple – epithalamic structures; blue – midbrain structures. Figure adapted from Aizawa *et al.* (2011) and Turner *et al.* (2016).

Neurotransmitter profile of mammalian habenula

Medial habenula

In order to characterise the molecular nature of neuronal subtypes, Aizawa *et al.* (2012) applied immunohistochemistry and *in situ* hybridisation to map the mRNA and protein expression of marker genes for neurotransmitters and their receptors in the rat habenula. According to their findings, all MHb subregions express type 1 and 2 vesicular glutamate transporters (VGLUT1, 2), implying glutamate neurotransmitter is employed throughout the MHb. In addition, choline acetyltransferase (ChAT), the only enzyme responsible for biosynthesis of acetylcholine (ACh), is densely expressed in the ventral MHb. Indeed, cholinergic neurons in the MHb, innervating the IPN, represent the major cholinergic pathway in the central nervous system (CNS) (Lee *et al.*, 2019). Apart from ACh, these neurons also release glutamate as demonstrated by colocalization of the vesicular ACh transporter (VAChT) and VGLUT1 and by optogenetic stimulation in transgenic mice which express a light-gated cation channel Channelrhodopsin-2 (ChR2) in cholinergic neurons (Ren *et al.*, 2011). Activating cholinergic axon terminals by a brief photo-stimulation generated fast excitatory postsynaptic currents that are mediated by ionotropic glutamate receptors, whereas tetanic photo-stimulation produces slow inward currents that are

mediated by nicotinic ACh receptors, implying that the two neurotransmitters activate postsynaptic neurons in the IPN via different transmission modes (Ren *et al.*, 2011).

Apart from cholinergic neurons, other neuronal subtypes in the MHb are either exclusively glutamatergic or both substance P-ergic and glutamatergic. Additionally, the exclusively glutamatergic neurons in the superior MHb co-express a pro-inflammatory cytokine interleukin 18 (IL-18) (Aizawa *et al.*, 2012). In other brain areas, such as hippocampus, IL-18 has been implicated in the regulation of glutamatergic transmission (Alboni *et al.*, 2010). However, the exact function of this cytokine in the circuitry of the MHb is currently unknown.

In addition, neurons in MHb receive glutamatergic projections from the triangular septal nucleus and GABAergic input from the nucleus of diagonal band (Qin and Luo, 2009). Of note, the MHb contains one of the highest concentrations of the $GABA_B$ receptor ($GABA_BR$) in the brain, implying the presence of robust inhibitory inputs (Viswanath *et al.*, 2014). Furthermore, $GABA_A$ receptor ($GABA_AR$) signalling appears to be absent in this part of habenula suggesting that $GABA_BR$-mediated inhibition is involved in balancing neuronal excitation in the MHb (Wang *et al.*, 2006).

Lateral habenula

Neurons in the LHb uniformly express VGLUT2 (Aizawa *et al.*, 2012) and send glutamatergic projections to GABAergic and dopaminergic neurons in the VTA, GABAergic and serotonergic neurons in the DRN and MRN and to GABAergic neurons in the RMTg.

In addition, the LHb receives glutamatergic projections from the medial globus pallidus, lateral hypothalamus and potentially the VTA (Meye *et al.*, 2013). Glutamate released from these afferents predominantly acts on post-synaptic α-amino-3-hydroxy-5-methyl-4-isoxazolepropionic acid receptors (AMPARs). The presence of AMPARs in the LHb was initially shown by immunocytochemical analysis that revealed relatively high expression of GluR1 subunit compared to GluR2 (Spreafico *et al.*, 1994). Generally, GluR2 contains positively charged arginine and confers channel impermeability to Ca^{2+}. Therefore, AMPARs lacking GluR2 are permeable to Ca^{2+} (CP-AMPARs) and exhibit inward rectification due to a voltage-dependent block at positive potentials (Meye *et al.*, 2013). The presence of AMPARs was also confirmed by electrophysiological recordings which demonstrated that LHb neurons exhibit excitatory post-synaptic current (EPSC) mediated primarily through AMPARs and to lesser extent by NMDA receptors (NMDARs) (Li *et al.*, 2011). Furthermore, the AMPAR-mediated component exhibited strong inward rectification implying the glutamatergic input to LHb is mediated by CP-AMPARs (Li *et al.*, 2011; Meye *et al.*, 2013).

Apart from glutamatergic input, GABAergic projections from the entopeduncular nucleus, lateral hypothalamus, lateral preoptic area, nucleus accumbens, substantia innominata and ventral pallidum also innervate the LHb (Araki *et al.*, 1984; Meye *et al.*, 2013). The two receptors implicated in the mediation of this transmission are $GABA_ARs$ and $GABA_BRs$, both of which are expressed in the LHb (Pirker *et al.*, 2000; Geisler *et al.*, 2003). Further evidence suggests that inhibitory $GABA_AR$-mediated signalling takes place in the LHb (Meye *et al.*, 2013) as potassium chloride cotransporter-2 (KCC2) that maintains low intracellular chloride concentration and

thereby ensures $GABA_AR$ signalling is inhibitory, is expressed in the LHb and GABA-induced inhibitory currents are blocked by biccuculine, a selective $GABA_AR$ antagonist (Wang *et al.*, 2006).

The mammalian LHb regulates activity in the dopaminergic VTA and serotonergic raphe and its activity is, in turn, modulated by serotonergic and dopaminergic inputs, reflecting a negative feedback mechanism (Meye *et al.*, 2013). Indeed, serotonin receptor 5-HT2C, as well as the dopamine receptors, D2 and D4 are expressed in the LHb (Aizawa *et al.*, 2012; Good *et al.*, 2013). Activation of 5-HT2C receptors in the LHb using a selective receptor agonist increases firing of glutamatergic LHb neurons, which, in turn, decreases monoamine levels in several brain areas and induces depressive-like behaviour (Han *et al.*, 2015). In addition, dopamine can induce either hyperpolarisation or depolarisation depending on the receptor activated. For instance, when acting through D2 receptors dopamine induces hyperpolarisation, or associated inhibitory outward currents, reducing excitability in a subpopulation of LHb neurons projecting to the VTA and RMTg (Jhou *et al.*, 2013). In contrast, when acting through D4 receptors dopamine induces depolarisation in LHb neurons primarily projecting to RMTg (Good *et al.*, 2013).

Neurotransmitter profile of zebrafish habenula

Medial habenula

All neurons in the larval MHb are glutamatergic, with a proportion of them being either cholinergic or expressing the neuropeptide somatostatin. In addition to these neuronal subtypes, the adult MHb also expresses substance P precursor, *tachykinin 1* (deCarvalho *et al.*, 2014).

Generally, somatostatin acts as a hormone or a neurotransmitter, exerting an inhibitory action on numerous physiological functions as, for instance, it inhibits secretion of growth hormone from the anterior pituitary gland (Lamberts *et al.*, 1997). The transcript expression data from the Allen Brain Atlas indicates the presence of *somatostatin* mRNA in the mouse MHb (Allen Brain Atlas, Allen Institute, http://mouse.brain-map.org/experiment/ivt?id=1001&popup=true) and expression of somatostatin 2 receptor transcript in the MHb is found significantly up-regulated in a rat model of depression (Faron-Górecka *et al.*, 2016). However, to date there is no further evidence supporting the presence of somatostatin signalling in both zebrafish and mammalian MHb.

The cholinergic phenotype of MHb neurons was first reported by Hong *et al.* (2013) who demonstrated asymmetric expression of transcripts for *chat* and *vchat* in larval and adult MHb, with predominant expression in the right nucleus. Investigating the cholinergic transmission in the habenulo-interpeduncular pathway, the authors also found expression of nicotinic ACh receptor subunits α2 and β4 in the IPN. Furthermore, both optogenetic and electrical stimulations of the MHb resulted in a fast glutamatergic postsynaptic current followed by a slow cholinergic current in the IPN. Collectively, these findings reveal the lateralised cholinergic phenotype of MHb neurons in larval and adult zebrafish and support a conserved role for ACh in a major cholinergic pathway of the vertebrate brain (Hong *et al.*, 2013).

Lateral habenula

Neurons in zebrafish LHb generally exhibit a glutamatergic phenotype as shown by expression of *vglut2* in larval and adult brains (deCarvalho *et al.*, 2014). However, in contrast to its mammalian homologue, neurons in zebrafish LHb express the gene encoding the neuropeptide kisspeptin1 (KISS1) (Ogawa *et al.*, 2012). In mammals, the *Kiss1* gene has been implicated in regulation of reproductive functions, in particular, the onset of puberty. Zebrafish, on the other hand, possess two *Kiss1* homologues, *kiss1* and *kiss2*. While *kiss2* is expressed in the hypothalamus and is, therefore, a candidate regulator of the reproductive system, *kiss1*, together with its receptor *kissr1*, is predominantly expressed in the LHb (Ogawa *et al.*, 2012). In addition, LHb *kiss1* neurons are glutamatergic in nature and project to the median raphe, where they have been implicated in serotonergic regulation, potentially via as yet uncharacterised interneurons (Nathan *et al.*, 2015; Ogawa and Parhar, 2018).

Lateralisation

The structure of the habenula exhibits left-right asymmetry in many vertebrate species. However, the extent of lateralisation differs across the classes of vertebrates as more profound asymmetry is found in fish, amphibians and reptiles (Bianco and Wilson, 2009). The mammalian habenula, on the other hand, appears more symmetrical (Concha and Wilson, 2001). It should be noted, however, that lateral asymmetry in the volumes of the LHb was found in albino mice, with the right LHb being larger than left, whereas in albino rats the left MHb is larger than right (Bianco and Wilson, 2009). Therefore, some lateralisation is also present in mammalian species, although the mechanisms underlying this phenomenon remain unknown. Generally, lateralisation may serve to increase neural capacity by specialising structures on the right and left sides for different roles, therefore avoiding the duplication of an equivalent circuits in the two hemispheres (Concha *et al.*, 2012). However, little is known regarding the role of lateralisation in normal brain processing. Investigating this problem in zebrafish, Dreosti *et al.* (2014) found that the left habenula responds to light stimuli whereas neurons on the right respond to odour, suggesting the lateralisation of sensorial processing. Furthermore, loss of this asymmetry results in loss of responsiveness to both visual and olfactory stimuli as well as increased fear and anxiety in zebrafish, implying the importance of lateralisation in normal brain function (Facchin *et al.*, 2015).

Role of habenula in regulation of behaviour

As outlined in previous sections, the habenula, via its afferent and efferent connections, relays information between multiple forebrain and midbrain structures and as such has been implicated in the regulation of multiple brain functions. One such function, which has received a great amount of attention, is the encoding of reward-related information and transmission of associated signals to midbrain dopaminergic and serotonergic systems (Proulx *et al.*, 2014).

Encoding of reward-related information

Dopamine neurons in SNc and VTA generally respond to sensory information that predicts changes in animal's motivational state and thereby facilitate an appropriate behavioural response.

These neurons are naturally excited by larger-than-expected rewards and their predictors, and are inhibited by smaller-than-expected rewards and their predictors (Hikosaka, 2010). It is well established that the dopamine neurons receive reward-related information from the LHb. In a landmark study, Matsumoto and Hikosaka (2007) conducted functional magnetic resonance imaging (fMRI) in rhesus monkeys that had been trained to perform a visually guided saccade task with reward outcomes. Their findings demonstrated that while dopamine neurons in SNc were excited by a reward-predicting target and inhibited by a no-reward-predicting target, exactly opposite response patterns were detected in the LHb. Thus implying that LHb contributes to reinforcement learning through inhibitory action on dopamine neurons (Hikosaka, 2010). The inhibitory effect of the LHb on this dopaminergic circuit was found to be mediated by GABAergic interneurons in RMTg (Jhou *et al.*, 2009). Additional fMRI experiments also demonstrated that the LHb receives reward-related information through afferents from the GPi (Hong and Hikosaka, 2008). Collectively, these results indicate that the GPi-LHb-RMTg-SNc/VTA pathway has an important role in reward-based decision-making (Hikosaka, 2010).

Interestingly, DRN neurons in rhesus monkeys also encode reward-related information, but they do so differently from midbrain dopamine neurons (Nakamura *et al.*, 2008). While dopamine neurons predominantly respond to reward-predicting stimuli, DRN neurons respond to both reward-predicting stimuli and reward itself and in both cases their activity is differentially modulated depending on the size of the predicted or received rewards. Indeed, DRN contains neurons preferring smaller rewards as well as neurons preferring larger rewards and thereby this structure reliably encodes the value of expected and received rewards. Dopamine neurons, on the other hand, respond to reward only when the reward is smaller or larger than expected (Nakamura *et al.*, 2008). Therefore, it appears that DRN neurons encode the expected and received rewards, or 'value state', while the dopamine neurons encode the difference between the two, or 'value change'. Since the LHb projects to the DRN and midbrain dopamine system, it may employ distinct neuronal circuitries to encode both types of reward-related information (Proulx *et al.*, 2014). Indeed, neurons in the LHb are excited by a stimulus predicting a small reward and inhibited by a stimulus predicting a large reward (Matsumoto and Hikosaka, 2007) and these changes in LHb activity are likely to modulate neuronal activity in the DRN (Nakamura *et al.*, 2008). However, to date, this hypothesis has not been supported by any experimental evidence.

Avoidance of danger

Appropriate action selection requires evaluation of each action based on both expected rewards as well as punishments. Therefore, to further investigate if and how the LHb responds to punishments and their predictors, as well as to rewards and their predictors, Matsumoto and Hikosaka (2009) conducted another study where they conditioned monkeys using a Pavlovian procedure. A Pavlovian task was divided into two distinct contexts: an 'appetitive', or rewarding, context where juice was used as an unconditioned stimulus and an 'aversive' context where air puff was used as an unconditioned stimulus. The LHb neurons were most strongly excited by a conditioned stimulus associated with the most unpleasant event in each task: the absence of

reward and the presence of punishment, indicating that the LHb neurons respond to the negative value of a stimulus (Matsumoto and Hikosaka, 2009). By communicating this information to the dopaminergic and serotonergic systems, the habenula contributes to execution of appropriate behaviour in order to avoid the unpleasant stimulus.

Zebrafish LHb also responds with excitation to a conditioned stimulus in a classical fear conditioning task and, in turn, stimulates serotonergic neurons in the MRN (Amo *et al.*, 2014). While inhibition of the synaptic communication within this pathway does not affect the panic behaviour induced by a conditioned stimulus, it does impair the learning ability of fish to actively escape the aversive event. This indicates that the LHb-MRN pathway is essential for learning an adaptive strategy to actively avoid dangerous situations (Amo *et al.*, 2014).

In zebrafish, cholinergic activity in the habenulo-interpeduncular pathway has been implicated in odour-evoked avoidance (Krishnan *et al.*, 2014). Zebrafish larvae are normally attracted to an intermediate concentration of bile salt, a putative social cue, while they avoid high concentrations of this substance. On a circuit level, increasing concentrations of this odour increase neuronal activity in the MHb. Furthermore, blocking nicotinic ACh receptors (nAChRs) as well as lesioning of the MHb both abolish the odour-evoked avoidance, suggesting that cholinergic activity in MHb-IPN pathway facilitates this behavioural phenomenon. Based on these results, Krishnan *et al.* (2014) hypothesised that increased activity in the IPN could lead to increased inhibition of serotonergic raphe, resulting in the negative reward underpinning aversion and avoidance.

Sleep

There are several lines of evidence suggesting the habenula is involved in sleep regulation. For instance, in hibernating squirrels MHb neurons exhibit elevated expression of *Aanat*, implying that similar to pineal gland, the habenula contributes to the initiation and maintenance of hibernation by providing a supplementary site for melatonin biosynthesis (Yu *et al.*, 2002). Furthermore, lesioning of the habenula's major efferent fibre bundle, the FR, as well as the LHb alone reduces the amount of time rats spend in the rapid eye movement (REM) sleep (Valjakka *et al.*, 1998; Aizawa, Yanagihara, *et al.*, 2013). The suppressive effects of the LHb on REM sleep appear to be dependent on intact serotonergic activity in MRN, which indicates that the LHb regulates sleep via serotonergic neurons in MRN (Aizawa, Cui, *et al.*, 2013; Aizawa, Yanagihara, *et al.*, 2013). In contrast, genetic ablation of the dorsal MHb in mice led to sleep fragmentation and overall increase in REM sleep, implying divergent roles of the MHb and LHb in the regulation of this process (Hsu *et al.*, 2017).

In addition to the functions outlined above, the habenula has been implicated in regulation of maternal behaviour, navigation and electromagnetic detection (Hikosaka, 2010). The following section will, however, discuss the evidence supporting habenula's role in circadian regulation of brain and behavioural states.

Habenula as a component of circadian system

Initial evidence of rhythmic clock gene expression in the habenula was provided using sensitive videomicroscopy and photon-counting of a PER2::LUC fusion protein in mice (Guilding *et al.*, 2010). These experiments demonstrated that cultured habenula slices exhibit up to three circadian cycles in PER2::LUC bioluminescence before dampening to apparent arrhythmicity. The PER::LUC rhythms were primarily localised within the medial portion of the LHb, with a less distinctive signal detected in the lateral division of the LHb and occurred autonomously from AP-dependent synaptic communication (Guilding *et al.*, 2010). Complementary to the bioluminescence imaging data, *in vitro* electrophysiological recordings confirmed that neurons in both LHb and MHb exhibit circadian rhythms in electrical activity, with the peak in the activity during the transition between late subjective day and early night, daily variations absent in *Cry1*$^{-/-}$ *Cry2*$^{-/-}$ mice – animals that lack a functional molecular clock (Guilding *et al.*, 2010; Sakhi, Belle, *et al.*, 2014; Sakhi, Wegner, *et al.*, 2014). Collectively, these findings indicate that the habenula contains an intrinsic circadian oscillator that autonomously drives daily rhythms in the neuronal output of this structure and therefore is likely to regulate daily rhythms in habenula-mediated behaviours.

The habenula also exhibits circadian rhythms in neuronal activity *in vivo* (Zhao and Rusak, 2005). However, in an *in vivo* system the afferent projections are intact and the habenula is subjected to various neurochemical signals that could also contribute to circadian regulation of this structure. For instance, AVP-immunopositive fibres are found specifically in the medial subdivision of LHb (Rood and De Vries, 2011; Zhang *et al.*, 2016) and, as demonstrated by retrograde tracing experiments, these fibres primarily originate in the PVN, supraoptic nucleus (SON) and to lesser extent in the SCN (Zhang *et al.*, 2016). This suggests that the SCN may signal time-keeping information into the LHb, either directly or indirectly through other hypothalamic areas (Baño-Otálora and Piggins, 2017). Apart from AVP, PK2 represents another important neurochemical output signal of the SCN and this neuropeptide was found to modulate GABAergic transmission in LHb neurons (Sakhi, Wegner, *et al.*, 2014), which implies that the SCN may employ multiple signalling pathways in the circadian regulation of the habenula. Indirect SCN regulation of the habenula possibly also involves melatonin release from the pineal gland which is under SCN control, since electrophysiological recordings demonstrated that melatonin increases glutamatergic synaptic transmission onto LHb neurons (Evely *et al.*, 2016).

In addition to putative SCN input, early retrograde tracing experiments showed that retinal ganglion cells project to the LHb in rats (Qu *et al.*, 1996), suggesting that photic information may be directly conveyed to the habenula from the retina. Subsequent experiments using lacZ reporter in mice visualised fibres from melanopsin-expressing retinal ganglion cells in the border region adjacent to the dorsal LHb (Hattar *et al.*, 2006). Furthermore, *in vivo* recordings of neuronal activity in rats and mice confirmed that LHb neurons respond, mostly with excitation, to retinal illumination (Zhao and Rusak, 2005; Sakhi, Wegner, *et al.*, 2014). However, since these light-evoked effects were too slow to represent direct responses, photic information is likely to be conveyed to LHb via polysynaptic processes (Sakhi, Wegner, *et al.*, 2014). A recently conducted fMRI study demonstrated that the human habenula is also responsive to light. Although in contrast

to the rodent habenula, changes in illumination leads to deactivation of this structure with the most pronounced effect occurring in the morning, indicating circadian modulation of habenula's hemodynamic response to changes in illumination (Kaiser *et al.*, 2019).

Collectively these findings indicate that in the intact *in vivo* system the habenula oscillator is synchronised by neurochemical signals from the SCN as well as the retina. The importance of photic and SCN-derived signals in entrainment of habenula clocks has been recently assessed by Salaberry *et al.* (2019) who found that rostral and caudal divisions of the habenula both exhibit robust PER2::LUC rhythms that are similar in amplitude and period, and are independent of SCN input and lighting conditions. However, despite their ability to oscillate in a circadian fashion, when animals are kept under constant darkness these two rhythms are largely desynchronised and the desynchrony is even more enhanced in SCN-lesioned animals (Salaberry *et al.*, 2019). Therefore, photic information as well as SCN-derived signals are important for maintaining internal coupling and synchrony between local habenula oscillators.

Circadian regulation of brain state and motivated behaviours

In mammals, glutamatergic neurons in the LHb innervate important monoaminergic brain centres including the dopaminergic VTA and SNc as well as serotonergic raphe nuclei. In addition, the VTA and raphe are also indirectly regulated by the LHb via GABAergic interneurons in the RMTg (Yang, Wang *et al.*, 2018). Therefore, since the habenula exhibits circadian rhythms in neuronal activity it may provide time-keeping signals for these structures. For instance, in an isolated VTA, clock gene expression is not rhythmic (Abe *et al.*, 2002), while *in vivo,* specific clock proteins oscillate (Webb *et al.*, 2009), implying that these rhythms are driven by signals from other areas of the brain (Mendoza, 2017). Dopamine release from the VTA also exhibits circadian rhythmicity, with the highest dopamine levels occurring during the animal's active phase (Hood *et al.*, 2010). Similarly, 5-HT release, which can be directly enhanced by electrical stimulation of the LHb (Kalén *et al.*, 1989), as well as ACh release, the source of which being the habenula itself, both exhibit rhythmic profiles with maximal release during the active phase (Dudley *et al.*, 1998; Hut and Van der Zee, 2011). As a result, behaviours which are dependent on the rhythmic release of these neurotransmitters must be, at least partially, regulated by the habenula clock. To date, the behavioural aspects which are under the control of this oscillator are unknown. Nevertheless, since 5-HT and dopamine mediate reward and motivation, Mendoza (2017) proposed that daily rhythms of motivated behaviours including locomotion, arousal, drug intake and feeding may be regulated by habenula clock. Indeed, wheel-running activity is highly rewarding to rodents and daily rhythms in this behaviour are significantly impaired by lesioning the habenula major output pathway, the FR (Paul *et al.*, 2011). However, to what extent the habenula circadian oscillator contributes to these daily rhythms remains to be clarified and can only be addressed by a local disruption of habenula clock machinery.

Habenula as a circadian pacemaker in zebrafish

In comparison to mammals, the neural components of the zebrafish circadian system are highly decentralised, as demonstrated by the examination of regiospecific brain cultures harvested from

adult *per3-luc* zebrafish – all of which exhibited *per3* rhythms with peak expression at ZT 3-5. These rhythms free-run under DD and can be re-entrained to a new LD cycle, implying the direct responsiveness of the brain tissue to photic stimulation – a phenomenon demonstrated by upregulation of *c-fos* in response to a light stimulus delivered at subjective night (Moore and Whitmore, 2014). Therefore, apart from the previously identified circadian pacemaker in the pineal gland, other parts of the zebrafish brain, including the telencephalon, dienecephalon and optic tectum, contain light-sensitive circadian oscillators which may represent important regulatory components of the zebrafish circadian system (Moore and Whitmore, 2014). A candidate structure to serve as a circadian pacemaker in the zebrafish brain is the habenula which has been previously identified as a component of an extended circadian system in mammals. Indeed, both larval and adult zebrafish habenula express clock gene components and, at least in adults, expression of these genes is rhythmic *in vivo* (Moore, 2013; Weger *et al.*, 2013). Furthermore, the larval habenula responds, primarily with excitation, to photic stimulation – a response largely mediated via the anterior thalamus (Cheng *et al.*, 2017). It should be noted, however, that since enucleation and lesion of the thalamus does not entirely eliminate the habenula response to light, there is a possibility that deep brain photoreceptors are involved in the integration of photic information within this structure, rendering it directly sensitive to light – a principal circadian *zeitgeber* (Cheng *et al.*, 2017). In addition to photic information, the zebrafish habenula indirectly receives circadian cues from other brain pacemakers as, for instance, in adulthood this structure is innervated by hypothalamic projections expressing hypocretin (also known as orexin), a wakefulness-promoting neuropeptide and critical regulator of sleep-wake cycles (Appelbaum *et al.*, 2009).

Finally, the zebrafish habenula has been implicated in several light-dependent behaviours. For instance, sudden changes in illumination can rapidly influence animal behaviours normally under control of the circadian clock – a phenomenon known as masking. In zebrafish larvae, unexpected changes in blue light illumination trigger diel vertical migration. The habenula also responds to blue light and lesioning of this structure impairs the ability of light to mask this circadian response (Lin and Jesuthasan, 2017). In addition, zebrafish larvae start to exhibit circadian rhythms in locomotor activity from 4-5 dpf, when the habenula, although still at a developmental stage, is already spontaneously active and has developed major efferent pathways innervating the IPN and raphe (Aizawa *et al.*, 2005), meaning the development of a functional habenula and the circadian rhythmicity of primary behavioural outputs are temporally correlated. Collectively, these findings indicate that from early developmental stages the clock-expressing zebrafish habenula integrates photic information and facilitates appropriate behavioural responses to changes in external illumination, which in the natural environment fluctuate in a circadian fashion. Therefore, it is highly possible that habenula's time-keeping ability is conserved across vertebrate species.

Thesis aims

This thesis aims to investigate circadian regulation of the habenula in two distinct vertebrate species, zebrafish and mice. These two model organisms offer different methodological advantages allowing investigation of multiple aspects of the habenula's function within the extended vertebrate circadian system. For instance, the zebrafish nervous system develops rapidly, and the transparency of larvae enables non-invasive monitoring of neuronal activity in an intact *in vivo* system. Furthermore, zebrafish reproduce in large numbers, they can be raised at high density at low cost and the availability of numerous genetic tools enables convenient genetic manipulation of this organism. Mice, on the other hand, represent a mammalian organism, in which the habenula's role in circadian physiology has been investigated much more extensively. In addition, due to its relatively large size, the mouse brain is easily dissected, which makes this model organism suitable for *in vitro* preparations, involving high-resolution electrophysiological recordings of neuronal activity where circadian regulation of various aspects of cell physiology and pharmacology can be thoroughly investigated.

The first chapter aims to determine whether there is daily variation in neuronal activity in the habenula of zebrafish larvae *in vivo* by applying three distinct approaches including bioluminescence monitoring, immunohistochemistry and two-photon imaging. As such, this chapter is divided into three parts, each dedicated to an individual approach. This investigation not only aims to demonstrate the circadian profile of the habenula in this diurnal organism, thereby shedding light on the potential effect of chronotype on the circadian regulation of this structure, but it also evaluates the general suitability of the three different techniques for assessing circadian rhythmicity in the oscillators of the vertebrate brain.

The second chapter aims to investigate the role of the habenula molecular clock in circadian regulation of brain neurotransmission and behaviour. In this chapter the tractability of zebrafish is employed to generate a transgenic line in which the habenula's clock is genetically altered by means of a dominant negative strategy. The effect of a habenula-specific clock mutation on behaviour is further analysed using behavioural assays, including monitoring of fish locomotor activity and arousal, while the effect on brain state is analysed by measuring brain content of important neurotransmitters.

The final chapter aims to assess circadian rhythmicity in electrical activity across the habenula neuronal population in mouse brain slices, focusing on the topographic distribution of daily variations within this structure. This investigation therefore involves simultaneous extracellular recording of neuronal activity from multiple sites within the habenula using a multi-electrode array. In addition, taking advantage of the isolated *in vitro* system, this study also aims to investigate role of external neuromodulators, including a putative SCN output signal, AVP, in circadian regulation of this epithalamic structure.

Investigating habenula rhythmicity *in vivo* contributes to our understanding of how this structure functions as a part of an intact circadian system, while *in vitro* studies reveal the clock-regulated intrinsic time-keeping capabilities and neuromodulation involved in circadian regulation of this

structure. This thesis aims to employ multiple approaches not only to improve our understanding of habenula's function as a component of the vertebrate circadian system but also to examine the role of its circadian oscillator in the regulation of the brain and behavioural states.

Chapter 2 Circadian rhythms in the habenula of zebrafish

Introduction

Both *in vivo* and *in vitro* recordings in rats and mice demonstrate that the habenula exhibits circadian rhythmicity in electrical output, with peak activity occurring during the day, or inactive phase (Zhao and Rusak, 2005; Sakhi, Belle, *et al.*, 2014; Sakhi, Wegner, *et al.*, 2014). In contrast, using *c-fos* as a surrogate marker for neuronal activation, the opposing rhythm has been found in mice and hamsters, with the highest levels of *c-fos* levels detected during the night (Tavakoli-Nezhad and Schwartz, 2006). As a consequence of this apparent contradiction, it has been suggested that this structure's intrinsic rhythmicity may be modulated, or overridden, by behavioural state and environmental factors – influences restricted in the *in vivo* recording of anaesthetised animals (Baño-Otálora and Piggins, 2017). Therefore, further work is required to determine the regulatory processes that both establish and refine habenula rhythms.

To date, the majority of studies investigating habenula rhythmicity have been performed using nocturnal rodents, and as such little is known regarding the circadian profile of this structure in diurnal organisms. Furthermore, the potential for chronotype specific differences in the circadian regulation of habenula activity is emphasised by anatomical variation in habenula circuitry observed between diurnal and nocturnal species – with *e.g.* GABAergic interneurons being present in the LHb of diurnal Nile Grass rats but absent in the nocturnal species (Yan *et al.*, 2018). Considering the evolutionary conservation of the habenula in vertebrates, and the experimental tractability of zebrafish, we have therefore selected this diurnal species as a suitable model organism with which to study these phenomena. Accordingly, this chapter will employ genetic, molecular and imaging techniques to investigate circadian rhythmicity in the zebrafish habenula.

Calcium and phosphorylated-ERK rhythms in brain

The hallmark function of brain circadian oscillators is to integrate internal and external signals which drive the daily oscillations in the bioelectrical properties of discrete populations of neurons. The principal intracellular signal linking the molecular clock with the transductional and electrical functioning of the cell membrane is cytosolic Ca^{2+} (Honma and Honma, 2003). Indeed, cytosolic Ca^{2+} levels in SCN neurons oscillate in a circadian fashion, with the peak during subjective day (Enoki *et al.*, 2012; Jones *et al.*, 2018). While endogenous Ca^{2+} rhythms within SCN networks are independent of synaptic transmission, as they occur in the presence of the sodium channel blocker tetrodotoxin (TTX), they do, however, require ryanodine receptor (RyR) dependent Ca^{2+} release from intracellular stores, with levels of RyR mRNA being closely correlated with endogenous rhythms in cytosolic Ca^{2+} (Ikeda *et al.*, 2003). Despite the closeness of this correlation, the pharmacological manipulation of RyRs has no effect on the circadian rhythm of *Per2* expression, implying that RyR activation is a part of the molecular clock output pathway,

via which the clock modulates the cell membrane potential (Aguilar-Roblero *et al.*, 2016). In addition to transmitting clock output signals, intracellular Ca^{2+} also mediates the resetting of the SCN circadian clock via photic inputs transmitted through the RHT. Upon stimulation by light, RHT terminals within the SCN release glutamate, which, upon the activation of NMDARs, facilitates the influx of Ca^{2+} into the post-synaptic neuron. Such elevations in intracellular Ca^{2+} leads to activation of the Ras-Raf pathway and subsequent phosphorylation and recruitment of ERK, also known as mitogen-activated protein kinase (MAPK) (Goldsmith and Bell-Pedersen, 2013). The phosphorylation of ERK is mediated by MAPK/ERK kinase (MEK) and leads to activation of the transcription factors Elk and CREB. This, in turn, induces expression of immediate early genes (IEGs) and clock genes such as *Per1* (Coogan and Piggins, 2003; Tischkau *et al.*, 2003; Antoun *et al.*, 2012) (Fig. 2.1; adapted from Goldsmith and Bell-Pedersen, 2013). Therefore, intracellular Ca^{2+}, whether derived from intra- or extracellular sources, plays an important role in transmitting both the input and output signals of the core molecular clock in the SCN. Consequently, assessment of the intracellular Ca^{2+} and phosphorylated-ERK (pERK) can serve as a valuable measure of circadian rhythmicity in brain oscillators.

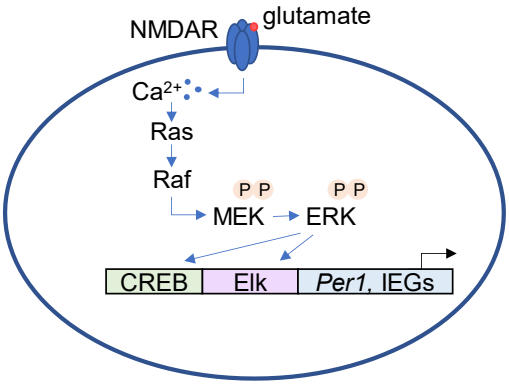

Figure 2.1: Light-induced ERK signalling cascade in the SCN

Calcium and phosphorylated-ERK monitoring in zebrafish

Combining available genetic tools with a suitable model organism, larval zebrafish, has led to several efficient and non-invasive ways to monitor levels of cytosolic Ca^{2+} *in vivo*. The most promising of these techniques enables long-term monitoring of neuronal Ca^{2+} levels in freely behaving zebrafish larvae and was first described by Naumann *et al.* (2010). This type of real time monitoring is achieved using a genetically encoded bioluminescent Ca^{2+} indicator, GFP-aequorin, which can be selectively expressed in distinct neuronal populations. Upon sensing Ca^{2+}, aequorin catalyses oxidation of its substrate coelenterazine (CLZN). Completion of this reaction generates the emission of the blue photons required to excite the GFP, resulting in the enhanced light emission detected (Baubet *et al.*, 2000). The translucency of the zebrafish larvae allows detection of such bioluminescent signals by a large-area photomultiplier tube (PMT). This non-imaging technique does not involve focusing on a single plane, which would normally require the animal being immobilised, but instead simply captures total light emission, allowing the free movement of the larvae during the long recordings required for the circadian assessment of neuronal activity.

Another technique to monitor neuronal Ca^{2+} levels *in vivo* involves the immunohistochemical detection of pERK, an important downstream element in the Ca^{2+}-triggered signalling cascade. In the circadian system, phosphorylation of ERK is required to entrain the molecular clock to environmental cycles (Goldsmith and Bell-Pedersen, 2013). In the rodent SCN, levels of pERK show rhythmicity, peaking during the day as light signals from the retina induces phosphorylation of this substrate and subsequent clock gene expression (Obrietan *et al.*, 1998; Coogan and Piggins, 2003). Similarly, pERK positively regulates light-induced *per2* expression in the zebrafish peripheral cell line Z3, which is directly sensitive to light (Cermakian *et al.*, 2002). Although it should be noted that Mracek and colleagues (2013) have recently demonstrated that the ERK pathway serves as a negative regulator of blue, but not red, light-activated D-box-driven gene transcription. In their discussion, the authors speculate that the contradicting results produced by the two studies might be due to the use of different cell lines, light intensities, light spectral compositions and other methodological aspects. Apart from pERK mediating the photic input to the circadian clock, phosphorylation state of ERK is additionally regulated by the clock itself, as pERK levels in the dorsomedial SCN, a structure known as the shell, exhibit endogenous circadian rhythms which peak during the subjective day (Hughes *et al.*, 2004; Goldsmith and Bell-Pedersen, 2013). Similarly, the activation of ERK-related MAPKs in the fungus *Neurospora crassa* shows rhythmicity under constant conditions and are regulated by the circadian clock (Bennett *et al.*, 2013). Collectively, these findings imply that pERK, as one of the principal elements in the transmission of both the input and output of the molecular clock, constitutes a useful tool for assessing the mechanisms underpinning daily rhythmicity in circadian oscillators.

In comparison with the application of the bioluminescent Ca^{2+} sensor GFP-aequorin, the temporal information provided by the immunohistochemical (IHC) analysis of pERK is limited to the time point of fixation. However, the spatial information gained through imaging is far superior, since the former technique lacks spatial resolution and is limited entirely to the pattern of the GFP-aequorin expression (Randlett *et al.*, 2015).

The final experimental strategy to be discussed employs, currently, the most popular type of genetically encoded Ca^{2+} indicator, GCaMP (Yang, Liu *et al.*, 2018). Originally developed by Nakai *et al.* (2001), GCaMP is composed of a circularly permuted EGFP (cpEGFP) connected to the Ca^{2+}-binding protein calmodulin (CaM) via the *C* terminus and to the M13 fragment of myosin light chain kinase, a target sequence of CaM, via the *N* terminus. Upon the binding of Ca^{2+} to CaM, the Ca^{2+}-CaM-M13 interaction changes the protonation state of the cpEGFP, generating an increase in cpEGFP fluorescence proportional to the change in the intracellular Ca^{2+}. Several updated versions of GCaMP, including GCaMP2 up to the most recent GCaMP7, have been engineered in order to improve signal-to-noise ratio as well as rise and decay kinetics (Akerboom *et al.*, 2012; Ohkura *et al.*, 2012; Chen *et al.*, 2013; Dana *et al.*, 2019). The available sensors differ in their properties and suit various potential applications which require sensors with different dynamics. For instance, GCaMP6s is the most sensitive GCaMP6 Ca^{2+} sensor, generating the largest fluorescent transients in response to a single AP, but exhibiting relatively slow rise and decay kinetics compared to GCaMP6f and 6m. GCaMP6f, on the other hand, exhibits the fastest kinetics and therefore, monitors the temporal dynamics of Ca^{2+} events more reliably but has lower

Ca^{2+} affinity when compared to GCaMP6s (Chen *et al.*, 2013). In zebrafish, GCaMP indicators can be expressed using specific neuronal promoters, which in combination with two-photon microscopy allows *in vivo* monitoring of hundreds of neurons with minimal invasiveness (Leung *et al.*, 2013). In two-photon microscopy, two low-energy photons cooperate to excite a fluorophore within a small precise volume with no illumination of areas above and below the focal plane. This reduces photobleaching and phototoxicity and therefore enables longer imaging of living samples (Svoboda and Yasuda, 2006). Furthermore, the excitation infra-red (IR) wavelengths used in two-photon microscopy do not affect light-sensitive behaviours such as sleep and, therefore, this type of imaging is particularly applicable for studies of circadian phenomena (Appelbaum *et al.*, 2010; Leung *et al.*, 2013).

Aims

The principal aim of this chapter was to use all three approaches discussed above – bioluminescence of GFP-aequorin, IHC of pERK and two-photon imaging of GCaMP6s – in order to monitor circadian changes in the cytosolic Ca^{+} and pERK in the habenula of zebrafish larvae *in vivo*. The chapter is, therefore, split into three parts each dedicated to a single approach and the specific aims are as follows:

The first aim was to monitor circadian variations in the habenula of freely behaving zebrafish larvae using bioluminescence of GFP-aequorin. This was attempted by the generation of a *Tg(gng8:gal4;UAS:GFP-aequorin-opt)* line in which expression of GFP-aequorin is habenula specific. In order to validate the functionality of the recording set-up other *gal4* transgenic lines, particularly those expressing GFP-aequorin in the muscle and/or motoneurons, were used as positive controls.

The second aim was to examine the spatial distribution of daily variations in habenula activity using the IHC detection of pERK. This approach involved day-night comparison of pERK levels in wild-type larvae which were kept either under standard LD conditions or under constant darkness (DD) during the day of fixation.

Since two-photon imaging of GCaMP provides better temporal resolution regarding Ca^{2+} dynamics at the single-cell level, the final objective was to compare Ca^{2+} levels of induvial neurons measured during the day and night using a transgenic line expressing GCaMP6s in the habenula.

This study will not only contribute to our understanding of habenula's function as a circadian oscillator in the intact diurnal organism, but it will also examine the general suitability of these three techniques for assessing circadian rhythms in the oscillators of the vertebrate brain.

Part I: Monitoring circadian variations in the habenula using bioluminescence

Methods

Fish maintenance

All zebrafish (*Danio rerio*) embryos were bleached, raised in E3 embryo medium (5 mM NaCl, 0.17 mM KCl, 0.33 mM CaCl, 0.33 mM $MgSO_4$) at 28ºC under 14-10 h LD cycle, henceforth referred to as standard conditions.

Transgenic line

The *Tg(UAS:GFP-aequorin-opt)* was obtained by outcrossing the *Tg(mnx1:gal4;UAS:GFP-aequorin-opt)*^{icm09} line kindly provided by Dr. Claire Wyart (L'Institut du Cerveau et de la Moelle Épinière, Paris). In this transgenic line, the codon-optimised variant of GFP-aequorin (GA), referred to as GA-opt, was used in order to enhance the protein expression (Knafo, Prendergast, *et al.*, 2017). The *Tg(UAS:GFP-aequorin-opt)* zebrafish were crossed with the *TgBAC(gng8:gal4)*^{c426} line in order to achieve habenula-specific expression of GA-opt. The *TgBAC(gng8:gal4)*^{c426} line was generated as described by Hong *et al.* (2013) and was generously provided by the authors of the study. Larvae expressing GFP fluorescence in the habenula were selected visually using an Olympus MVX10 fluorescence microscope and were grown into adulthood. In addition, the presence of GA-opt was confirmed by the genotyping of adult fish. The genomic DNA was extracted from adult fins using the HotSHOT method (Meeker *et al.*, 2007). The tissue was first incubated in 100 µL of 50 mM sodium hydroxide at 95°C for 20 min, after which 10 µL of 1 M Tris-HCl (pH 7.4) was added to neutralize the alkaline solution. Samples were centrifuged to pellet the debris and the supernatant was analysed by polymerase chain reaction (PCR). Two sets of primers were designed in VectorNTI software to amplify ~68% of the overall length of GA-opt (Table 2.1). The PCR was carried out using Taq DNA Polymerase and 10X Standard Taq Reaction Buffer (New England Biolabs) and the reactions were amplified as follows: 95°C for 3 min, 30 cycles of [95°C for 30 s, 55°C for 30 s, 72°C for 30 s], 72°C for 5 min, 12°C ∞. The PCR amplicons were further examined by gel electrophoresis. Correct sequence of the GA-opt was also validated by the fluorescence-based cycle sequencing of the two PCR amplicons, using BigDye Terminator v3.1 (Applied Biosystems) and the forward primer. The sequences were analysed in Geneious 10.1.3 software.

Table 2.1: Primers for genotyping

Primer 5'→3'	Sequence	Annealing Temperature (°C)	Size (bp)
Forward 1	CAGAAGAACGGAATTAAGG	55	410
Reverse 1	ACGTCGTAAAGGAGCTCT		
Forward 2	GCCGGACTATGCGAGTTT	55	588
Reverse 2	TCTCATGGAACGGCTCCT		

Immunohistochemistry

For immunostaining of extracted brains, the *Tg(gng8:gal4;UAS:GFP-aequorin-opt)* larvae were fixed at 8 dpf in 2% trichloroacetic acid in phosphate-buffered saline (PBS) + 0.25 Triton X-100 (PBST) for 3-4 h at room temperature (RT). Following five washes in PBST, fixed larvae were treated with 1 mg/ml collagenase (Sigma) in PBS for ~25-30 min at RT on a nutator, until the eyes started falling out and the body began disintegrating. The digestion was terminated by transferring the larvae into PBST, in which they were washed five times (Hendricks and Jesuthasan, 2007). The isolated brains were incubated in the blocking solution [1 % Bovine serum albumin (Sigma) + 1 % dimethyl sulfoxide (DMSO) in PBST] for 1 h at RT and in the rabbit anti-GFP primary antibody (Torrey Pines Biolabs Inc., #TP401) at 4°C for 3-4 days. After the incubation, samples were washed five times in PBST and incubated in Alexa Fluor 488 goat anti-rabbit secondary antibody (ThermoFisher and Abcam) for 2 h at RT. Both primary and secondary antibodies were diluted 1:1000 in the blocking solution. Samples were washed at least three times in PBS prior to imaging. All washes in this protocol were performed for 5 min.

For the whole mount IHC, 8 day-old larvae were fixed in ice-cold 4% paraformaldehyde (PFA) in PBS at 4°C for ~22 h. Subsequently, pigmentation was bleached in 3% H_2O_2 + 1% KOH in deionized water for ~7 min at RT, followed by three washes in PBST. Larvae were transferred into the blocking solution with the rest of the procedure as described above.

Imaging

Immunostained brains and whole larvae were mounted in 2% low-melting agarose (LMA) (Bio-Rad Laboratories) in PBS. The brains were imaged using an upright Nikon A1RMP two-photon microscope with a 25X 1.1 NA water immersion objective in order to visualise deeper brain structures. The whole mount larvae were imaged using a Zeiss LSM800 confocal microscope with 10X water immersion objective.

Aequorin reconstruction

Larvae were screened for GFP fluorescence at 3 dpf. The GFP-positive larvae were individually incubated in ~120 µL of E3 with final concentration of 40-60 µM of water soluble coelenterazine-*h* (CLZN-*h*) (Nanolight Technology) for 48 h. The 10 mM stock solutions of CLZN-*h* were kept at -80ºC in order to reduce oxidation. After the incubation, larvae were briefly washed in fresh E3 medium before being transferred into the recording chamber.

Recording neuronal activity with bioluminescence

The bioluminescence recording set-up was assembled with the assistance of Dr. James Stewart as previously described by Naumann *et al.* (2010). Photons were detected by a large-area PMT (H11870-02: Hamamatsu). The PMT was housed in a custom-made light-proof enclosure (Thorlabs), where it was positioned above and in close proximity to a circular dish (inner radius 8.6 mm, depth 6 mm) containing freely-swimming zebrafish larvae in E3 medium. The PMT was connected to a photon counting unit with a USB interface (C8855-01: Hamamatsu) and the

bioluminescent signals were recorded with a gate time of 5 ms using inbuilt sample acquisition software. All data were plotted using Python 2.7.

Recording of pharmacologically evoked neuronal activity

In order to induce evoked activity larvae were exposed to the $GABA_A$ receptor blocker pentylenetetrazole (PTZ, Sigma; final concentration 10 mM in E3 medium). Data acquisition began 30 s after PTZ application, considering a latency of 30 s prior to the onset of epileptic events (Naumann *et al.*, 2010).

Results

GFP-aequorin-opt can be specifically expressed in the habenula

In order to restrict expression of GA-opt to the habenula, the GAL4/Upstream Activating Sequence (UAS) system was employed (Scott, 2009). In the *Tg(gng8:gal4;UAS:GFP-aequorin-opt)* line the GAL4 protein is regulated by the *guanine nucleotide binding protein (G protein), gamma 8* (*gng8*) gene, which is expressed exclusively within the habenula neurons and serves as an enhancer gene for habenula-specific pattern of expression (Hong *et al.*, 2013; deCarvalho *et al.*, 2014). The GAL4 protein in these neurons then targets the UAS sequence, driving the expression of GA-opt in the zebrafish larvae (Fig. 2.2 A, B). Brain extraction followed by the IHC staining of GFP and two-photon imaging enabled visualisation of deeper brain structures. In addition to expression in habenula cell bodies, GA-opt was also detected in habenula output fibres, forming the FR, which innervate the IPN (Fig. 2.2 C). No expression was detected in the muscle fibres within the trunk (Fig. 2.2 D). This is important, as expression of the GA-opt in a single muscle fibre could generate non-specific signals arising from the large changes in intracellular Ca^{2+} concentration that occur during spontaneous tail contractions (Knafo, Fidelin, *et al.*, 2017).

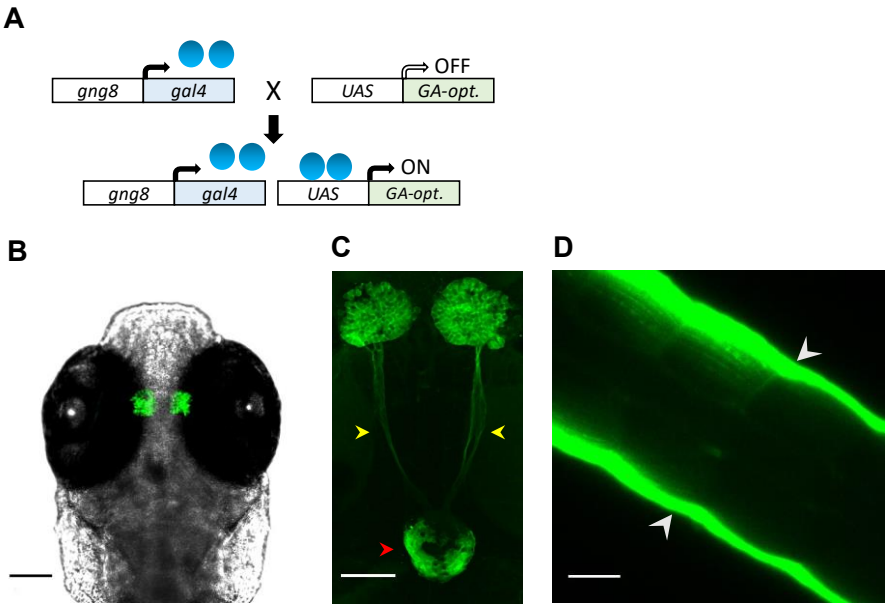

Figure 2.2: Habenula-specific expression of the GA-opt

(A) Schematic diagram demonstrating the application of GAL4/UAS system to induce expression of GA-opt in the habenula. (B) Dorsal view of the habenula-specific expression of GA-opt (green) in a fixed zebrafish larva (8 dpf). Scale bar: 100 µm. (C) Visualisation of GA-opt expression using two-photon imaging. Yellow arrowheads indicate habenula output axons forming the FR. Red arrowhead indicates putative axon terminals in the IPN. Scale bar: 50 µm. (D) Confocal image of a trunk: autofluorescence is present in the skin (indicated by white arrowheads), but no expression is present in the muscle fibres. Scale bar: 50 µm.

GFP-aequorin-opt expressed in the CNS and muscles generates detectable signals

The bioluminescence recording set-up was validated using the *Tg(mnx1:gal4;UAS:GFP-aequorin-opt)*^{icm09} line, in which the GA-opt is expressed specifically in spinal motor neurons. This transgenic line has been previously reported to emit bioluminescent signals of ~ 30 photons/10 ms during escapes and ~ 4 photons/10 ms during slow swimming (Knafo, Fidelin, *et al.*, 2017). In addition, the *Tg(huc:gal4;UAS:GFP-aequorin-opt)* line, which expresses GA-opt throughout the whole CNS and in muscle fibres, was also used. The bioluminescent signals were monitored from pools of 3 spontaneously swimming larvae from the individual transgenic lines. Various signal amplitudes – up to ~160 photons/50 ms from the *Tg(mnx1:gal4;UAS:GFP-aequorin-opt)*^{icm09} line and up to ~24000 photons/50 ms from the *Tg(huc:gal4;UAS:GFP-aequorin-opt)* line – were recorded over the course of 500 s (Fig. 2.3 A, C). The individual signals generally exhibited a rapid time-to-peak of ~5-10 ms and a relatively slower decay, consistent with the previously reported kinetic properties of aequorin and other Ca^{2+} sensors (Naumann *et al.*, 2010) (Fig. 2.3 B, D). These results confirmed the correct methodology applied in this study.

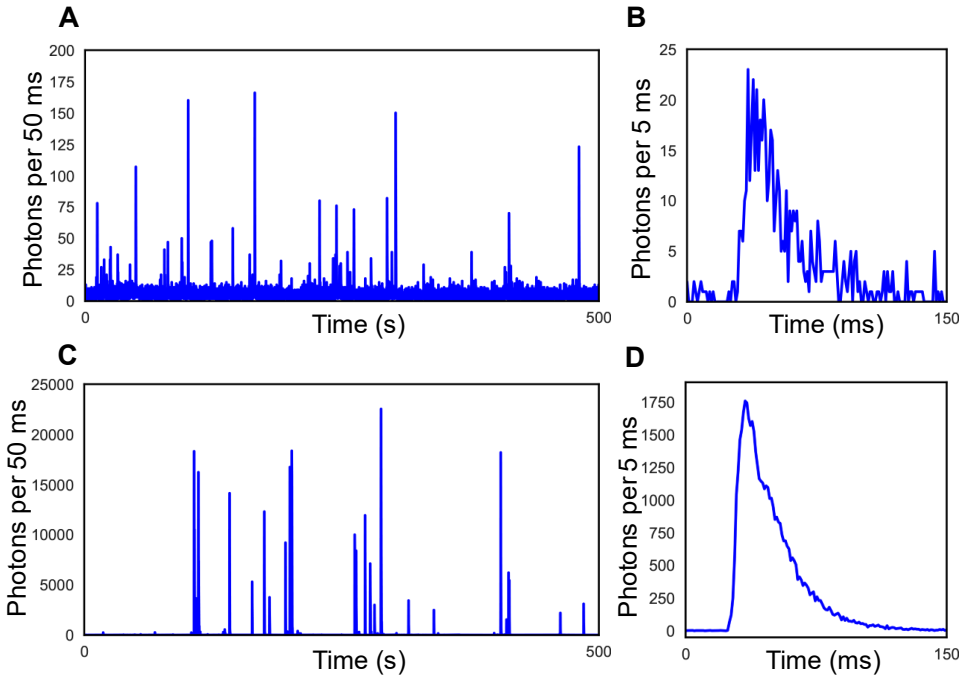

Figure 2.3: Bioluminescent Ca^{2+} events detected from the CNS and muscles during spontaneous swimming

(A) Bioluminescent signals/events recorded from the *Tg(mnx1:gal4;UAS:GFP-aequorin-opt)*^{icm09} line during spontaneous swimming. Pool of 3 larvae; aged 5 dpf. (B) Example of an individual Ca^{2+} event detected from the *Tg(mnx1:gal4;UAS:GFP-aequorin-opt)*^{icm09} line. (C) Bioluminescent signals/events recorded from the *Tg(huc:gal4;UAS:GFP-aequorin-opt)* during spontaneous swimming. Pool of 3 larvae; aged 5 dpf. (D) Example of an individual Ca^{2+} event detected from the *Tg(huc:gal4;UAS:GFP-aequorin-opt)* line.

GFP-aequorin-opt expressed in the habenula failed to generate detectable spontaneous or evoked events

The habenula's spontaneous and evoked Ca^{2+} events were recorded using the *Tg(gng8:gal4;UAS:GFP-aequorin-opt)* line. Overall, no spontaneous bioluminescent events above the baseline noise level were detected from a pool of 5 larvae (Fig. 2.4 A), implying the monitoring of circadian rhythms with this approach would not be possible. In addition, in order to investigate whether any evoked activity could be detected, the $GABA_A$ receptor blocker PTZ was applied to the same pool of larvae. PTZ is known to induce epileptic behaviour in zebrafish accompanied by slow waves of brain activity, which are also detected from the habenula (Naumann *et al.*, 2010; Liu and Baraban, 2019). The PTZ exposure resulted in no overall change in the baseline signal (Fig. 2.4 B).

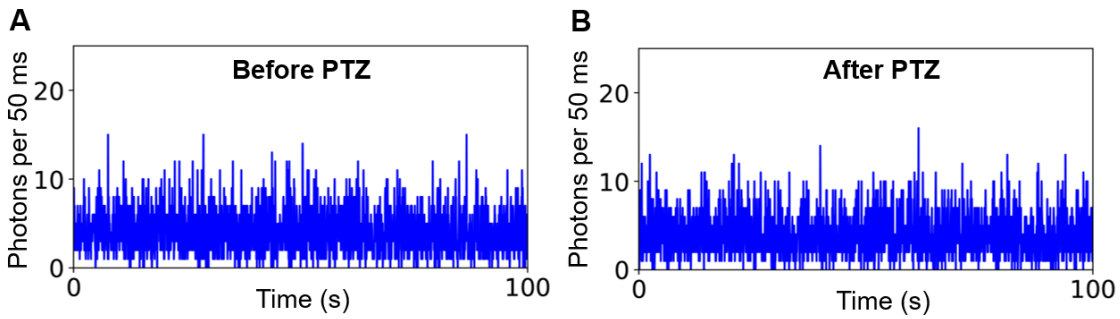

Figure 2.4: No spontaneous or evoked events were detected from the habenula

Bioluminescence was recorded from the *Tg(gng8:gal4;UAS:GFP-aequorin-opt)* line during spontaneous swimming (A) before and (B) 30 s after the application of the PTZ. Pool of 5 larvae; age of 5 dpf.

Discussion

The results have demonstrated that GA-opt can be specifically and exclusively expressed in the zebrafish habenula using the *gng8* enhancer gene, but with the bioluminescent methodology employed no signal could be detected. The correct incubation in CLZN and the functionality of the recording set-up were validated using two other transgenic lines *Tg(mnx1:gal4;UAS:GFP-aequorin-opt)*^{icm09} and *Tg(huc:gal4;UAS:GFP-aequorin-opt)* both of which successfully generated detectable bioluminescent signals during spontaneous swimming with the *Tg(huc:gal4;UAS:GFP-aequorin-opt)* signal being more robust than that produced by *Tg(mnx1:gal4;UAS:GFP-aequorin-opt)*^{icm09} larvae. The primary cause of this apparent difference is most likely a consequence of ectopic expression of GA-opt in the muscle fibres of the *Tg(huc:gal4;UAS:GFP-aequorin-opt)* fish. In muscle cells, rapid increases in cytosolic Ca^{2+} are key determinants of the actin-myosin interaction underpinning muscle contraction (Kuo and Ehrlich, 2015). Upon depolarisation of the muscle cell membrane, Ca^{2+} is released from the intracellular sarcoplasmic reticulum in a highly synchronised manner, resulting in large Ca^{2+} transients (Zoghbi *et al.*, 2000). Recording of bioluminescence from the *Tg(huc:gal4;UAS:GFP-aequorin-opt)* fish, therefore, also demonstrates how the presence of GA-opt in muscle fibres can easily contaminate recording with nonspecific or off-target bioluminescent signals. As a result, if seeking to monitor CNS activity, the GA-opt transgenic lines to be used should be screened with extra care to eliminate the individuals with expression in muscle fibres.

In this study no bioluminescent signals could be detected from *Tg(gng8:gal4;UAS:GFP-aequorin-opt)* fish, despite Naumann *et al.* (2010) having previously demonstrated the successful application of GA for the monitoring of spontaneous activity in a relatively small population of ~20 hypocretin neurons. These cells, which emitted signals as large as ~80 photons/5 ms at the onset of the active phase play a key role in the promotion of wakefulness – effects achieved via their excitatory influence on other arousal centres, in addition to cortical, motor and sympathetic systems (Lee *et al.*, 2005). Hypocretin neurons are thought to represent a relatively homogenous neuronal population, as they share numerous electrophysiological properties, including the capacity high frequency discharge – a firing pattern which may account for the emission of

measurable bioluminescent signals (Li *et al.*, 2002). In this study, *gng8* enhancer gene was used to achieve an habenula-specific pattern of expression. However, unlike the hypocretin neurons, the habenula comprises numerous anatomically, functionally and phenotypically diverse neuronal populations – with the two principal subregions of this structure, the MHb and the LHb, employing different neurotransmitter systems and having distinct neuronal connectivity. For example, specific subregions of the MHb use either glutamate exclusively, or glutamate together with substance-P or ACh. LHb neurons, on the other hand, have been reported almost entirely glutamatergic, although a more recent study has also reported presence of the GABAergic interneurons in the habenula of the rat (Aizawa, 2013; Zhang *et al.*, 2018). Accordingly, subregion-specific circuit properties and the presence of both excitatory and inhibitory transmitters may result in insufficient discharge synchrony for the bioluminescent events originating from individual neurons to be detected with the current recording set-up, in spite of the fact that the zebrafish habenula is spontaneously active (Jetti *et al.*, 2014; Ramaswamy, 2018).

Multiple improvements are therefore required to achieve reliable recording of the habenula's activity using the GA-opt. These should primarily involve improvement of the sensitivity of the recording equipment as well as the application of promoters which induce expression in more homogenous subpopulations of the habenula, such *diamine oxidase (dao)*, which drives expression explicitly in the LHb (Amo *et al.*, 2014).

Part II: Monitoring circadian variations in the habenula using immunohistochemistry of pERK

Methods

Animals

Each experimental run involved wild-type siblings of nacre background at the age of 8 dpf randomly split into 'Day' and 'Night' experimental groups. For the comparison under DD, tanks with the larvae were transferred into a dark box at *zeitgeber* time 14 (ZT14) the day before fixation. All fish were raised at a density of ~0.125 fish/mL and maintained under standard conditions.

Whole mount IHC

Larvae were fixed at ZT3 and ZT15 or CT3 and CT15. These time points were determined according to the previous finding that the peak and trough of *per3* expression in the zebrafish brain occurs at ZT3 and ZT15 respectively (Moore and Whitmore, 2014). Due to the relatively short time course of ERK phosphorylation, immediate and consistent fixation was achieved by pouring the E3 media containing the larvae through a fine sieve which was directly transferred into ice-cold 4% PFA in PBS in which the larvae were incubated at 4ºC for ~22h. Fixations at ZT15, CT3 and CT15 were performed under dim light. Fixed larvae were then stored in 100% methanol at -20ºC for several days. Prior the IHC, larvae were rehydrated by successive 5-min

washes in 70% - 50% - 25% - 0% methanol in PBST. The following steps including blocking and incubation in primary and secondary antibodies were performed as described in the Methods section in Part I of this chapter, with the following alternations: the rabbit anti-pERK (Cell Signalling, #4370) and mouse anti-total-ERK (anti-tERK) (Cell Signalling, #4696) primary antibodies were diluted 1:500. Samples were incubated in the primary antibodies for ~4 days. The secondary antibodies Alexa Fluor 647 goat anti-rabbit (ThermoFisher) and Alexa Fluor 488 goat anti-mouse (ThermoFisher) were diluted 1:500 (Randlett *et al.*, 2015). Controls in which the primary antibody was omitted were used to confirm the specificity of the secondary antibody.

Confocal imaging

Larvae were mounted in 2% LMA in PBS and imaged using a Zeiss LSM800 confocal microscope equipped with a 40X water immersion objective. The imaging settings including laser power, gain and offset were kept consistent through all experiments. In order to improve the image registration, a resolution of 512x512 was used to image the habenula together with parts of the forebrain (pallium and subpallium). The number of frames was set in order to cover the whole depth of habenula and varied across samples, which was later corrected during the registration.

Image registration and data analysis

In order to efficiently compare pERK signal between 'Day' and Night' groups, all confocal stacks were first aligned so that each voxel approximately covered the equivalent physical location in each sample. This was achieved by non-rigid registration of the images to a single reference image using the homogenous anti-tERK staining. The registration was carried out with the Computational Morphometry Toolkit (CMTK, http://www.nitrc.org/projects/cmtk/) and the command string (-awr 010203 -T 4 -X 52 -C 8 -G 80 -R 3 -A '--accuracy 0.4' -W '--accuracy 1.6'). Registered stacks were scaled down to 150/150/30 (x/y/z) resolution and the image noise was reduced with 2D Gaussian filter (sigma = 2) using the 'PrepareStacksForMAPMapping.ijm' macro in FIJI software (http://engertlab.fas.harvard.edu/Z-Brain/, Randlett *et al.*, 2015). Image data was then normalised by calculating pERK/tERK ratio and a pairwise comparison between 'Day' and 'Night' groups was carried out at each pixel as follows: first pseudo groups were randomly generated containing equal number of fish from both groups and Mann-Whitney U statistics Z-score was calculated over 500 iterations, producing a distribution of Z-scores. Assuming the normal distribution, a Z-score value corresponding to the false discovery rate of 0.1% was then used as a threshold so that if the Z-score value of the 'Day' vs 'Night' comparison was higher than the threshold it was considered significant. Application of the false discovery rate of 0.1% as a threshold was justified by a control comparison of randomly created mixed groups. The pixels which were significantly different during the final 'Day'-'Night' comparison were then assigned a colour where green and magenta represented significant increase and decrease respectively in the 'Night' group. Those pixels were also allocated intensity values within the range of 0:65535 according to the size of delta between the median values of the two groups (*i.e.* the lowest and highest intensities indicated the smallest and largest deltas within the range of 0:0.5 correspondingly). The pixels which did not exhibit significant difference were not assigned any

colour. All data were analysed using the 'MakeTheMAPMap.m' script (http://engertlab.fas.harvard.edu/Z-Brain/, Randlett *et al.*, 2015) in Matlab (Mathworks).

Results

ERK expression can be detected in the habenula and other brain areas

In order to visualise expression of tERK and pERK, whole mount IHC was applied. The habenula was imaged together with the pallium and subpallium of the forebrain in order to increase the number of anatomical landmarks, which helped to improve the registration (Fig. 2.5 A). Expression of both tERK and pERK was detected in the cell bodies and neuropil of the MHb (Fig. 2.5 B), LHb (Fig. 2.5 C), as well as in the pallium and subpallium (Fig 2.5 D and E). The expression pattern of tERK was generally more homogenous than that of pERK and was found in the input terminals within the neuropil and in all the cells, specifically within the cellular cytoplasm. In contrast, pERK expression was found in a smaller number of cells, presumably those neurons which had been activated just prior to fixation. Within neurons, the pERK label was found in both nuclei and the cytoplasm, as pERK translocates to the nucleus upon neuronal activation (Plotnikov *et al.*, 2011). Furthermore, relatively strong pERK labelling was detected in the neuropil of both MHb and LHb, where it potentially regulates synaptic plasticity by influencing the trafficking and distribution of local substrates (Mao and Wang, 2016).

The expression of tERK and pERK was also examined in the pineal gland. Since the pineal gland is known to contain an intrinsic circadian oscillator which drives daily rhythms of melatonin production (Ben-Moshe Livne *et al.*, 2016), it could provide a useful control, or example, of circadian rhythms in pERK expression. However, as the tERK antibody failed to clearly distinguish cell bodies within the pineal gland, other anatomical landmarks such as the position of the habenula were used to determine the approximate location of the pineal gland.

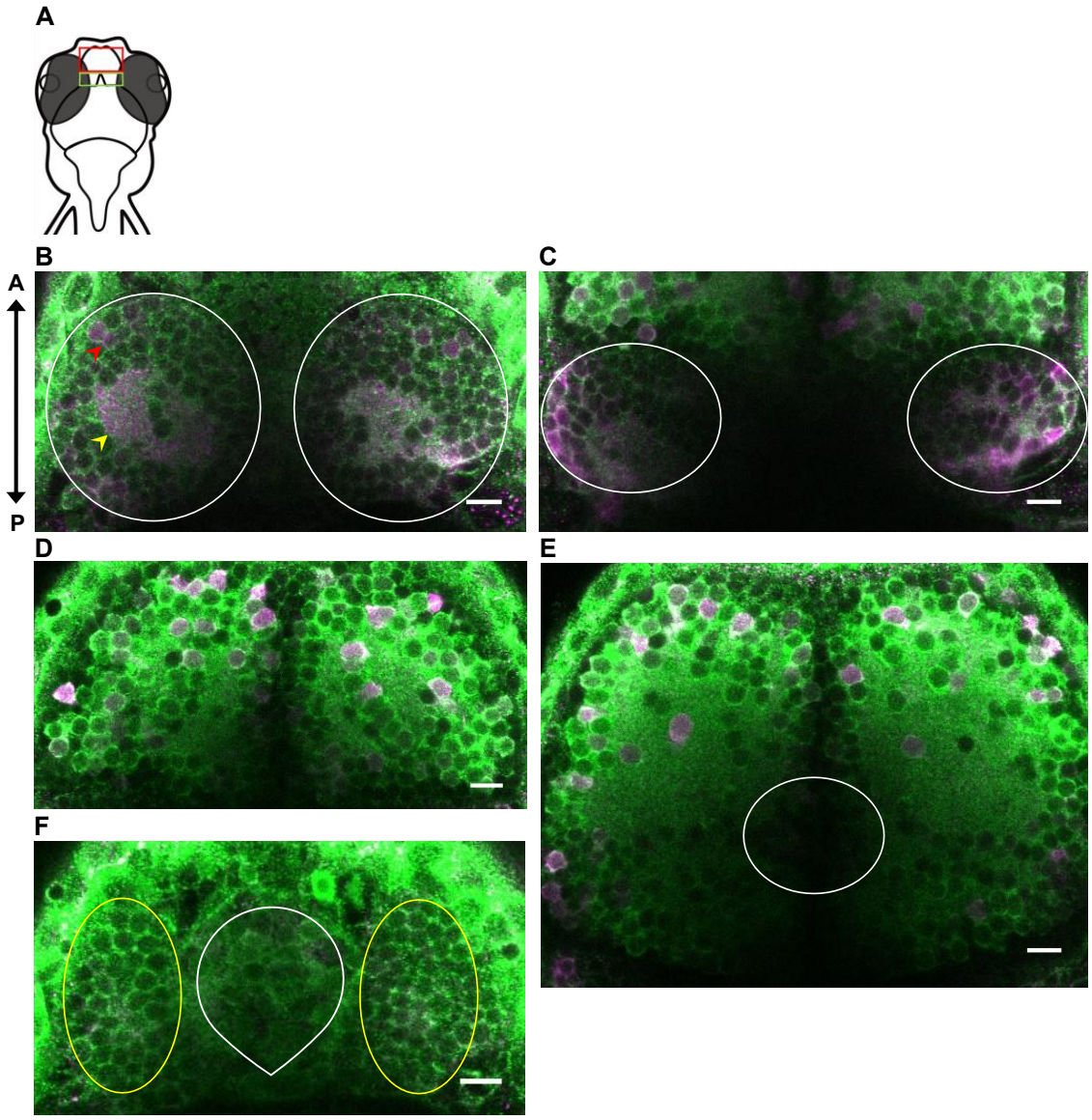

Figure 2.5: Expression of tERK and pERK in the larval brain

Dorsal view of the immunohistochemical detection of tERK (green) and pERK (magenta) in a wild-type zebrafish larva (8 dpf). (A) a schematic diagram of larval brain indicating the imaged areas: pallium indicated by a red rectangle, habenula and pineal gland indicated by the green rectangle; (B) MHb: left and right MHb (l- and r-MHb) located within the white circles; red and yellow arrows point out pERK label in the cell bodies and neuropil respectively; (C) LHb: left and right LHb (l- and r-LHb) located within the white circles; (D) dorsal pallium; (E) ventral pallium and subpallium (subpallium located within the white circle); (F) pineal gland located within the circular area; dorsal l- and r-MHb located within the yellow circles. The approximate anatomic locations of these brain areas were determined using the Z-Brain atlas, developed by Randlett *et al.* (2015) (http://engertlab.fas.harvard.edu/Z-Brain/). A = anterior; P = posterior (same orientation applies for all images); scale bar: 10 µm.

ERK expression in the larval brain exhibits day-night variation under standard light-dark cycle

In order to compare the levels of pERK between day and night, the registered and scaled image data was first normalised by calculating pERK/tERK ratio. (Fig. 2.6 A1-3 and B1-3). Note that the highest pERK/tERK ratio was generally detected in the putative homologue of the mammalian LHb – a structure identified based on the previous characterisation of this nucleus by Amo *et al.* (2014). The normalised image data was then compared between 'Day' (*N* = 130 larvae) and 'Night' (*N* = 102 larvae) groups which were composed of zebrafish larvae fixed at ZT3 and ZT15 time points respectively.

The output of the statistical analysis which involved a pairwise 'Night'-over-'Day' comparison at each pixel, during which the 'Day' group served as a baseline, is demonstrated by Figure 2.6 C1-3. The method, implementing a false discovery rate threshold, identified pixels which were significantly different and those were assigned either green or magenta colour depending on whether the delta between 'Day' and 'Night' group medians was positive or negative, relative to the 'Day' baseline.

Overall, the putative homologue of mammalian MHb exhibited a relative night-time increase in the pERK signal in the cell bodies and neuropil of the right MHb (r-MHb) (Fig. 2.6 C1 and C2). A subregion in the dorsal r-MHb also showed relative decrease in pERK staining (Fig. 2.6 C1). The left MHb (l-MHb) exhibited increase in pERK signal specifically within the lateral subregion and possibly in a small part of the neuropil (Fig. 2.6 C2). However, it remains uncertain whether the pERK increase within this small region definitely occurred in the neuropil of the MHb, since this area borders with cell bodies and the shape of the neuropil varies slightly from fish to fish. Aligning the relative pERK signal map with tERK images taken from different fish produced inconsistent results: in some fish the area of significant pERK increase appeared to align with the neuropil whereas in others it aligned with adjacent cell bodies. In addition to the pERK increase, an anterior part of the l-MHb showed a relative pERK decrease during the night (Fig. 2.6 C1 and C2). The LHb, on the other hand, exclusively exhibited relative night-time increases in the pERK expression, primarily within the l-LHb (Fig. 2.6 C2 and C3). Furthermore, the smaller subregions which lie in the most ventral posterior area in both l-LHb and r-LHb also exhibited a symmetrical night-time increase in pERK. These areas presumably contain the origins of the LHb output fibres forming the FR (Fig. 2.6 C3).

Most of the pallium as well as subpallium showed relative pERK decrease during the night, which was detected in both hemispheres symmetrically (Fig. 2.6 C2 and C3). In contrast, the lateral areas of the cell body rind (Fig. 2.6 C3) and two nuclei symmetrically located in the dorso-medial pallium displayed increased pERK expression during the night (Fig. 2.6 C2).

Finally, the analysis also showed a significant decrease in pERK expression in the dorsal anterior part of the pineal gland (Fig. 2.6 C1).

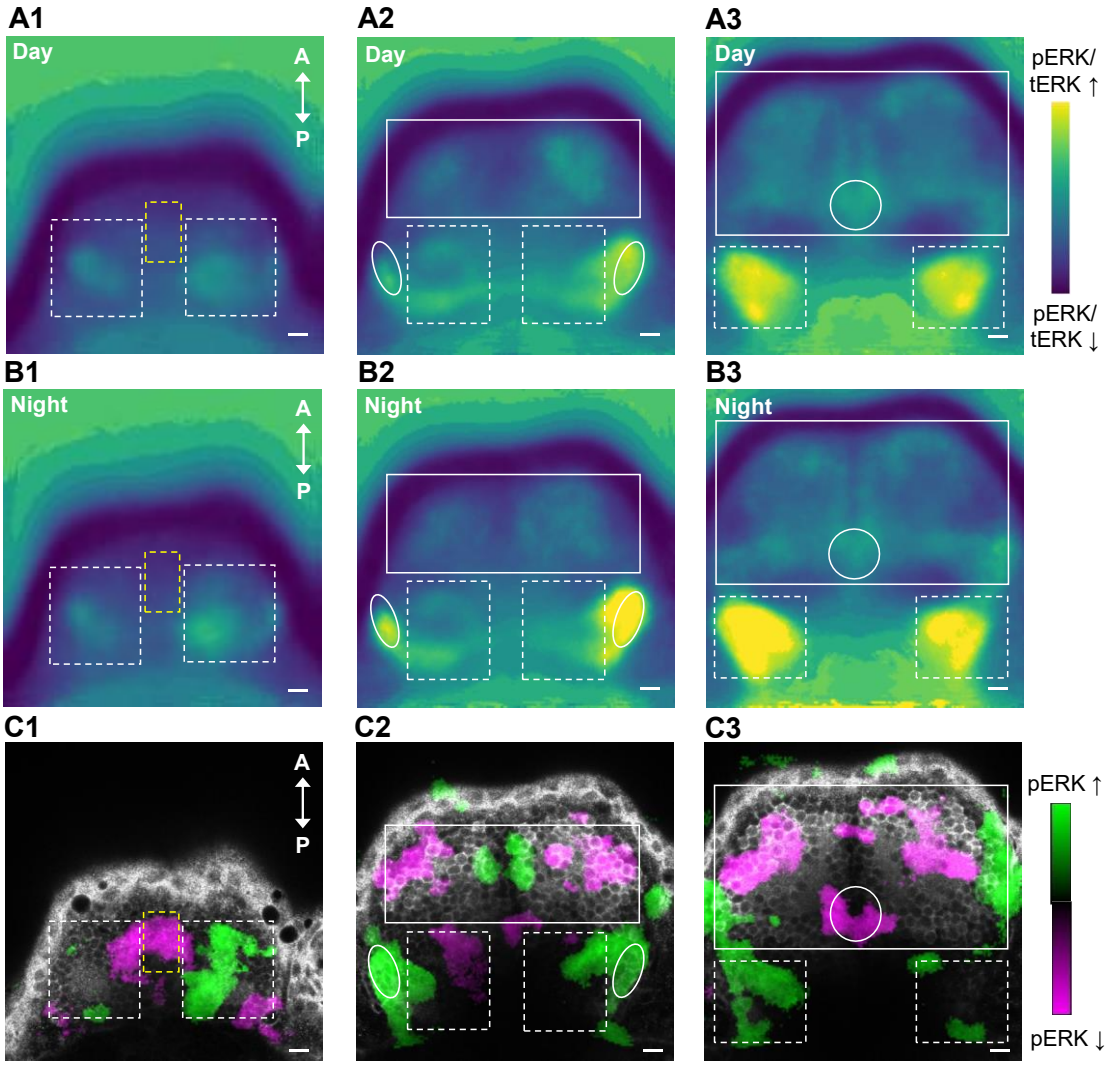

Figure 2.6: Day-night variations in the epithalamus and forebrain under standard LD cycle

(A-B) Raw images were registered, downsampled and smoothed and pERK/tERK ratio was calculated for each pixel. Median pERK/tERK stacks were generated for 'Day' (*N* = 130 larvae) and 'Night' (*N* = 102 larvae) groups. Dark blue and yellow colours indicate lowest and highest median pERK/tERK ratio, respectively. (A1-3) Example planes from 'Day' median pERK/tERK stack with A1 being the most dorsal plane and A3 the most ventral plane. A1 depicts dorsal left and right MHb (dashed white frames) and the pineal gland (dashed yellow frame). A2 depicts dorsal forebrain (solid white frame), MHb (dashed white frame) and dorsal left and right LHb (solid bilateral circles). A3 depicts ventral forebrain (white frame), subpallium (solid white circle) and left and right LHb (dashed white frames). (B1-3) Example planes from 'Night' median pERK/tERK stack with B1 being the most dorsal plane and B3 the most ventral plane. The white and yellow frames demonstrate the same brain structures as demonstrated in A1-3. (C1-3) 'Relative pERK expression' map during the 'Night'-over-'Day' comparison. Z-projections of the 'Relative pERK expression' maps were aligned with the single plane images of tERK staining (grey colour) taken from a representative fish in order to indicate approximate anatomic locations of relative pERK increase (green) and decrease (magenta) within the brain with C1 depicting the most dorsal planes and C3 depicting the most ventral planes. The specific brain structures are indicated by white and yellow frames as in A and B. A = anterior; P = posterior; scale bar: 10 µm.

ERK expression in the larval brain exhibits less day-night variation under the constant darkness

In order to determine whether the day-night variation in the pERK expression remains present under the constant conditions the ‘Day’ (*N* = 104 larvae) and ‘Night’ (*N* = 102 larvae) groups were kept in DD during the day of fixation and were subsequently fixed at CT3 and CT15 respectively. Figure 2.7 (A1-3 and B1-3) depicts the median normalised image data for each group.

The ‘Night’-against-‘Day’ comparison revealed that both l-MHb and r-MHb exhibited almost no day-night variation, as only a small number of pixels were significantly different between the two groups (Fig. 2.7 C1 and C2). Only two small subregions ─ one within the dorsal l-MHb and a second within dorsal r-MHb ─ exhibited significant variation, showing a relative night-time increase and decrease in pERK, respectively (Fig. 2.7 C1). Similarly, the LHb also exhibited less day-night variation under DD, primarily in the r-LHb. However, specific parts of the l-LHb did retain the relative pERK increase during the subjective night (Fig. 2.7 C3).

The pallium exhibited a relative pERK increase during the subjective night, specifically in the lateral and anterior areas of the cell body rind (Fig. 2.7 C2 and C3) and in the subregions of the dorsal neuropil. Only a relatively small area within the pineal gland exhibited pERK increase during the subjective night (Fig. 2.7 C1).

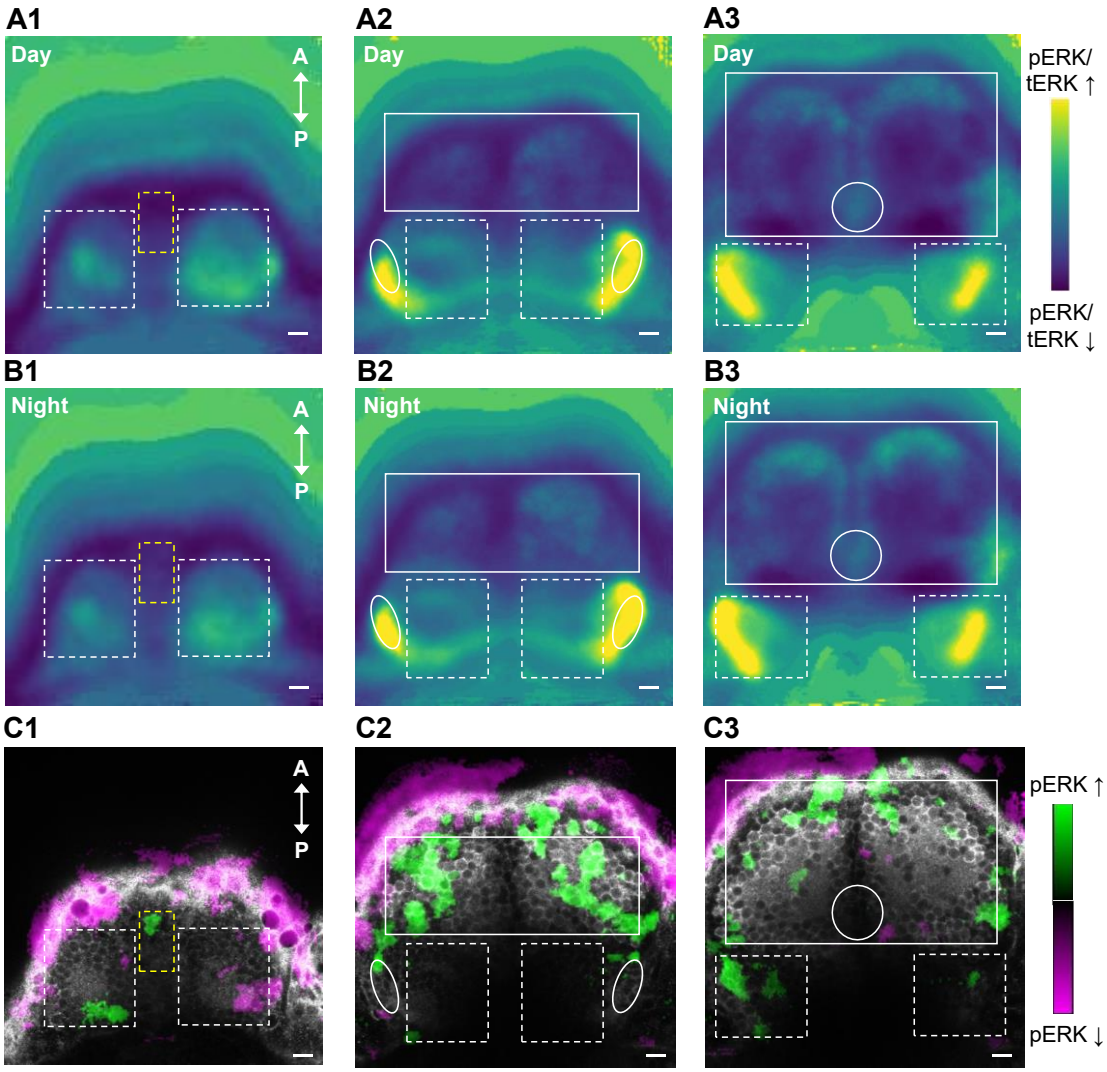

Figure 2.7: Day-night variations in the epithalamus and forebrain under DD conditions

(A-B) Raw images were registered, downsampled and smoothed and pERK/tERK ratio was calculated for each pixel. Median pERK/tERK stacks were generated for 'Day' (*N* = 104 larvae) and 'Night' (*N* = 102 larvae) groups. Dark blue and yellow colours indicate lowest and highest median pERK/tERK ratio respectively. (A1-3) Planes from 'Day' median pERK/tERK stack with A1 being the most dorsal and A3 the most ventral plane. A1 demonstrates dorsal left and right MHb (dashed white frames) and the pineal gland (dashed yellow frame). A2 depicts dorsal forebrain (solid white frame), left and right MHb (dashed white frames) and dorsal left and right LHb (solid bilateral circles). A3 depicts ventral forebrain (solid white frame), subpallium (solid white circle) and left and right LHb (dashed white frames). (B1-3) Planes from 'Night' median pERK/tERK stack with B1 being the most dorsal plane and B3 the most ventral plane. The white and yellow frames demonstrate the same brain structures as in A1-3. (C1-3) 'Relative pERK expression' map during the 'Night'-over-'Day' comparison. Z-projections of the 'Relative pERK expression' maps were aligned with the single plane images of tERK staining (grey colour) taken from a representative fish in order to indicate approximate anatomic locations of relative pERK increase (green) and decrease (magenta) within the brain with C1 demonstrating the most dorsal planes and C3 the most ventral planes. The specific brain structures are indicated by white and yellow frames as in A and B. A = anterior; P = posterior; scale bar: 10 µm.

Discussion

Overall, the results from the immunohistochemical detection of pERK showed that the larval habenula as well as the pallium, subpallium and the pineal gland exhibit day-night variation in pERK expression under the standard LD cycle. This day-night variation in detectable pERK expression appeared to be primarily driven by light as it was no longer present in the examined brain areas under DD conditions.

Since zebrafish pineal gland embodies all characteristics of a complete circadian system, including a photoreceptive pathway, intrinsic circadian clock, and rhythmic output in melatonin production (Ben-Moshe Livne *et al.*, 2016), it could provide a useful positive control for daily rhythms in pERK expression. In general, pineal pERK levels were significantly lower during the night than during the day. This is consistent with previous findings from the photoreceptive zebrafish cell line, Z3, in which pERK and phosphorylated MEK levels increased within 30 min after light stimulation (Hirayama *et al.*, 2009). Although the nature of Ca^{2+} responses in the parapinopsin-expressing cells of the pineal gland was found to be wavelength dependent, as stimulation with light of a wavelength less than 405 nm suppressed intracellular Ca^{2+} levels, whereas the stimulation with a wavelength of 588 nm induced the opposite effect (Wada *et al.*, 2018). Therefore, exposure to light of different spectral compositions could influence the day-time expression of the pERK in the pineal gland.

In the habenula the 'Relative pERK expression' map was found to be asymmetrical between the left and right nuclei of the MHb and LHb. These results are in accordance with previously reported asymmetry in neuronal organisation, gene expression and connectivity previously reported in the zebrafish habenula (Bianco and Wilson, 2009; Aizawa, 2013). The development of asymmetry commences 28 hpf and involves migration of precursor cells of the parapineal organ from the midline within the antero-dorsal epithalamus in the direction of the left habenula, from where axons project towards the medial and dorsal regions of the nucleus (Concha *et al.*, 2003). The parapineal organ, as well as the pineal gland, both contain photoreceptors, express similar neurotransmitters and produce melatonin (Concha *et al.*, 2003) and, therefore, it is likely that both pineal and parapineal organs exhibit similar rhythms of pERK expression. Since the parapineal projections exclusively innervate the left habenula, it is possible that the suppression of pERK levels observed in what appeared to be the l-MHb, might also occur in axon terminals from within the parapineal organ. Another factor which might explain the lower expression of pERK in the l-MHb during the night, is the absence of light-evoked excitation, a phenomena that occurs primarily in the l-MHb (Dreosti *et al.*, 2014; Cheng *et al.*, 2017; Zhang *et al.*, 2017). The light input, coming from the retina and pineal gland, travels via the anterior thalamus and evokes both transient and sustained increases in Ca^{2+} within the neuropil of l-MHb, followed by increases in Ca^{2+} within the cell bodies of the same nucleus (Cheng *et al.*, 2017). The current experiments showed that the relative night-time suppression of pERK in the l-MHb and in the pineal gland was absent in the fish kept in DD, suggesting that the day-night variation in the pERK expression in these areas was primarily driven by the presence of light during the day. Repeating these experiments using fish with enucleated eyes could help to determine whether the night-time suppression of pERK in the l-MHb is primarily mediated by the absence of light signal coming from the retina.

Additionally, considering the link between the asymmetry in the input pathways of the habenula and the pattern of the relative pERK expression map, the pERK increase during the night observed primarily in the r-MHb could possibly be mediated by the input from the OB. Mitral cells, the principal output neurons of the OB, project their axons into the pallium forming two fasciculated bundles, the lateral and medial olfactory tracts, which distribute their branches symmetrically in both pallial hemispheres and interconnect via the anterior commissure (Miyasaka *et al.*, 2009). As demonstrated by genetic labelling and tracing experiments performed in the both larval and adult brains, these fibres project extensively to the r-MHb (Miyasaka *et al.*, 2009; Turner *et al.*, 2016). As a result, odour stimuli – such as dissolved dried food or bile salt, which serve as a social cue – increase Ca^{2+} levels in the right habenula (Dreosti *et al.*, 2014; Krishnan *et al.*, 2014). The OB also expresses *per2* and *per3* genes with a peak and trough at ZT3 and ZT15, respectively. Furthermore, *c-fos* expression in the internal cellular layer of the OB has been reported to be higher at ZT15 as opposed to ZT3, resembling the rhythm in the pERK expression observed in the r-MHb (Moore, 2013).

Generally, pERK levels in the LHb were found to be significantly higher during the night than during the early day, with the day-night variation occurring primarily in the left nucleus. This left-right asymmetry in the relative pERK expression map could, again, be associated with the parapineal's exclusive innervation of the left habenula. Evely and colleagues have previously reported that activation of melatonin receptors in the rat medial LHb increases glutamatergic synaptic transmission via an increase in presynaptic glutamate release (Evely *et al.*, 2016). Hence, the night-time production and release of melatonin from the parapineal organ could enhance glutamatergic transmission in the habenula, leading to increased pERK expression in the l-LHb. Furthermore, the rodent LHb exhibits significantly lower firing rate during the early day as oppose to late day and this increase in discharge frequency appears to endure into early night, although the difference between the early day and early night was not reported significant (Sakhi, Wegner, *et al.*, 2014). The data in this study were acquired using whole-cell patch-clamp recordings in brain slices, which allows high-resolution monitoring of the neuronal activity, but can only be performed on a single cell, one at a time and, therefore, registers limited information regarding network function. This lack of spatial resolution is addressed in the Chapter 4 by the use of a multi-electrode array, apparatus that allows recording from multiple sites within the habenula simultaneously. In their study Sakhi *et al.* (2014) also reported that the daily variation in the firing rate was absent in the *Cry1*$^{-/-}$ *Cry2*$^{-/-}$ mice which lack a functional molecular clock, implying the influence of intrinsic circadian cues on the neuronal state of the LHb. In accordance with this finding, a small area within the zebrafish l-LHb retained the day-night variation in the pERK expression under DD, suggesting a possible influence of a local intrinsic circadian mechanism. Further experiments, involving the selective elimination of the habenula molecular clock would have to be performed to investigate the contribution of the intrinsic circadian clock in driving the day-night differences in this structure's electrical activity.

Additional examination of pERK expression in the pallium and subpallium also revealed day-night differences which occurred symmetrically in both hemispheres. For instance, significant night-time decrease in the pERK expression was found in the area referred to as the anterodorsolateral

pallium (Cheng *et al.*, 2014). This area has been proposed to be a homologue of the mammalian hippocampus as in the adult zebrafish brain it exhibits relatively high spontaneous neuronal activity of fast ripple oscillations which resemble hippocampal sharp waves in rodents (Vargas *et al.*, 2012). In rodent hippocampus, pERK levels also oscillate in circadian fashion with the lowest levels detected during the night. The hippocampal oscillations in the ERK signalling pathway correlate with the ability to consolidate and maintain memory as their pharmacological disruption using MEK1/2 inhibitor impaired the persistence of hippocampus-dependant memory formation (Eckel-Mahan *et al.*, 2008). In contrast, an opposite pERK rhythm was found in the dorsal medial pallium. This area has been proposed to contain a homologue of the mammalian basolateral/lateral amygdala, as local inhibition of this region diminished avoidance fear conditioning (Lal *et al.*, 2018). In rats, the basolateral amygdala and hippocampal dentate gyrus exhibit the same circadian rhythm in the expression of *Per2*, with the increased expression during the day, thus implying the two areas are likely to exhibit similar rhythms in various aspects of their physiology (Lamont *et al.*, 2005). On the other hand, Lamont *et al.* (2005) also report the opposite rhythm in the central nucleus of the amygdala, which in fish is presumably located in the ventral subpallium, a structure that has not been examined in the current experiments (Cheng *et al.*, 2014). Further work is required to investigate the physiological and behavioural significance of the daily rhythms found in these areas.

Finally, the night-time suppression of pERK was detected in a small area within the subpallium which, according to the Z-Brain atlas, contains a cluster of dopaminergic neurons and potentially represents a homologue of the mammalian dorsal striatum (Cheng *et al.*, 2014; Randlett *et al.*, 2015). In rodents, striatal neurons express *Per1, Clock* and *Bmal1,* clock genes which are differentially regulated by the dopamine receptors D1, D2 and D3. For instance, the application of a D1 receptor agonist increases mRNA levels of all clock genes expressed in the striatum, whereas D2 receptor agonism reduces mRNA levels of *Clock* and *Per1* (Korshunov *et al*., 2017). Furthermore, the dopamine content of the adult zebrafish brains, and those of larvae, peaks during the day and is relatively low at night, suggesting dopamine biosynthesis is under circadian regulation. In addition, dopamine levels are significantly reduced during both day and night in the zebrafish mutant for *per1b* gene, results which further indicate that dopaminergic transmission is under the control of the molecular clock (Huang *et al.*, 2015). However, the exact role of the dopamine signalling in the mechanism underlying the pERK rhythm in the zebrafish subpallium remains to be determined.

Overall, the results from the immunohistochemical detection of pERK showed that the day-night variation was absent in the fish kept in DD, specifically in the MHb, pineal gland, subpallium and in various areas of the dorsal pallium. This indicates that the daily rhythms in expression of pERK are primarily mediated by the day-time presence of light. In the adult zebrafish brain daily rhythm in *c-fos* expression persists under constant darkness, even though the rhythm is dampened and shows a significant loss of amplitude by the second day in DD (Moore and Whitmore, 2014). One possible explanation for the absence of the pERK rhythm in larvae kept under the DD could be their early developmental stage, at which they have yet to fully develop robust endogenous rhythms in brain physiology. In addition, it may be the case that any variation in pERK expression

between subjective day and night, manifested at this stage of development, are particularly small and as such beyond the discriminatory capacity of the IHC techniques employed. Nevertheless, the results of these experiments generated detailed topographical information regarding the daily changes in the brain activity occurring in an intact system, data which could provide a valuable insight into the manifestation and control of circadian rhythms in neuronal behaviour and physiology on a brain-wide circuit level.

Part III: Monitoring circadian variation in the habenula using calcium imaging

Methods

Two-photon calcium imaging

Larvae from the *Tg(s1011t:gal4;UAS:GCaMP6s)* line were screened for GFP fluorescence at 3 dpf. At the age of 8 dpf, fish were anaesthetised with mivacurium chloride (Mivacron, GSK) and mounted in 2% LMA in E3 medium at ZT2 and ZT14, one hour prior to imaging at ZT3 and ZT15. For the night experiments the fish were positioned under the microscope immediately after mounting and were kept in the dark prior to imaging. For the day experiments, fish were kept in the dark for 10-15 min prior to imaging, for the purposes of habituation and to avoid capturing evoked response to darkness. The imaging of the habenula's ongoing activity was carried out using the upright Nikon A1RMP two-photon microscope with a 25X 1.1 NA water immersion objective. The laser was set to 920 nm for GCaMP imaging. Single planes of dorsal and ventral habenula as putative homologues of mammalian MHb and LHb, respectively, were imaged, one plane at a time, using the sensitive IRNDD detector for 5 minutes continuously at the rate of 7 frames per second.

Analysis

In order to selectively obtain activity information from individual neurons, circular regions of interest (ROIs) were drawn manually around each cell (Fig. 2.8 A, B) and the mean fluorescence was measured within each ROI, using FIJI software (Fig. 2.8 C). The first 30 seconds (210 frames) of each recording was omitted since some cells exhibited a sudden increase in fluorescence intensity, which appeared to be a response to the initiation of the IR laser. Disregarding this evoked response was necessary as the values during the response abnormally deviated from the overall mean. Subsequently, downward temporal drift of baseline, potentially caused by photo-bleaching or mechanical disturbance, was removed by a detrending method where the best-fit line was subtracted from the raw fluorescence trace (Rahmati *et al.*, 2016) (Fig. 2.8 D). The detrended data were normalised by calculating a Z-score for each cell, using the temporal mean of detrended fluorescence intensity and the standard deviation (Fig. 2.8 E). The calcium events were then extracted from the Z-score traces through a process of deconvolution, using the Online Active Set method to Infer Spikes (OASIS) tool (https://github.com/j-friedrich/OASIS) developed by Friedrich *et al.* (2017). The parameters for deconvolution were implemented consistently for

all traces as follows: Z-score traces were denoised using noise standard deviation of 1 and minimum peak height of 0.1 was used as a threshold for counting peaks as Ca^{2+} events (Fig. 2.8 F). These parameters were set to minimise the detection of the false events from the background noise while not missing physiological information due to excessive stringency. The deconvolved peaks were then detected and counted using a script developed by Marcos Duarte (http://nbviewer.jupyter.org/github/demotu/BMC/blob/master/notebooks/DetectPeaks.ipynb) and the mean rate of Ca^{2+} events was calculated for each cell. The cumulative probability distributions of mean rate of Ca^{2+} events for 'Day' and 'Night' groups were compared using the Kolmogorov-Smirnov (KS) test. The result values were considered statistically significant at $p < 0.05$. This analysis was previously described and implemented by Ramaswamy (2018). All scripts for data processing and plotting were written in Python 2.7 by Dr. Seetha Krishnan.

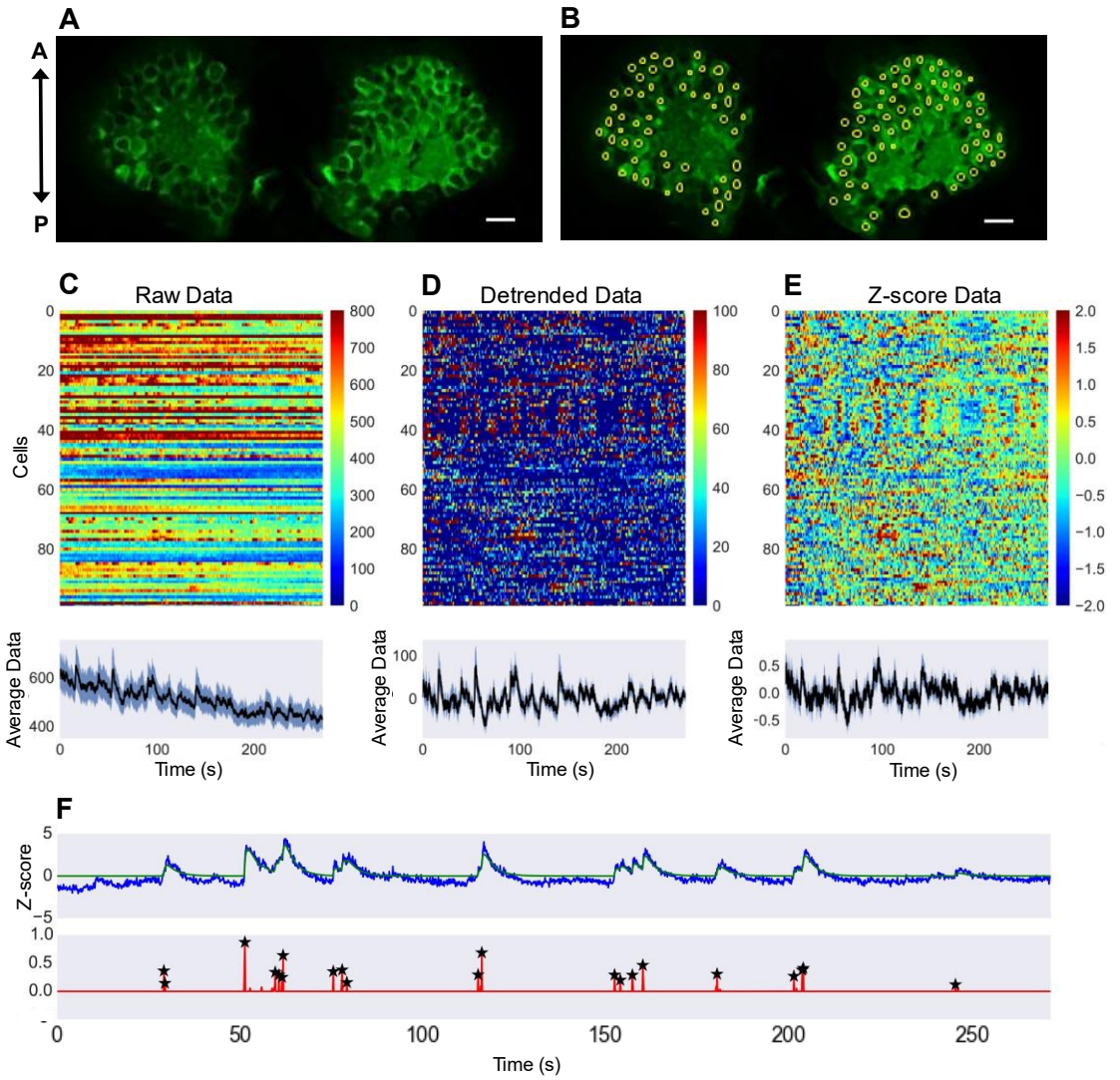

Figure 2.8: Analysis of the Ca^{2+} imaging data

(A) Dorsal view of the GCaMP6s expression in the MHb of a *Tg(s1011t:gal4;UAS:GCaMP6s)* larva at the age of 8 dpf. A = anterior; P = posterior; scale bar: 10 µm. (B) Manually drawn ROIs around each cell are represented by yellow circles. Heatmaps demonstrate temporal activity of all monitored cells from one fish: (C) raw fluorescence activity, (D) activity data after detrending and (E) after Z-score normalisation. Each heatmap row demonstrates fluorescence of one cell during the time course of recording. Different colours represent specific levels of fluorescence as shown by the corresponding colour bars. Average activity of all the cells indicated by a black trace is plotted below each heatmap correspondingly with 95% CI within the shaded area. (F) Example of the deconvolution of discrete Ca^{2+} events from one cell. Top: blue trace indicates temporal activity after Z-score normalisation; green trace indicates denoised Z-score trace. Bottom: red line represents deconvolved events and black stars indicate peaks which were counted as Ca^{2+} events.

Results

The medial habenula does not exhibit day-night variation in overall Ca^{2+} levels

Ongoing Ca^{2+} levels in the MHb of the *Tg(s1011t:gal4;UAS:GCaMP6s)* larvae were monitored during the day and night and the mean rate of Ca^{2+} events was calculated for each cell from the deconvolved Ca^{2+} peaks (Fig. 2.9 A). Similar activity was detected in the whole MHb during both

time points as during the day the overall mean rate was 8.37 Ca^{2+} events per minute (*N* = 8 larvae; 95% CI [7.48, 9.25]) and during the night the overall mean rate was 8.74 Ca^{2+} events per minute (*N* = 8 larvae; 95% CI [8.20, 9.27]). In addition, the distributions of the mean rate of Ca^{2+} events for the 'Day' and 'Night' groups were not significantly different (Fig. 2.9 B; KS test: D = 0.054, p = 0.161).

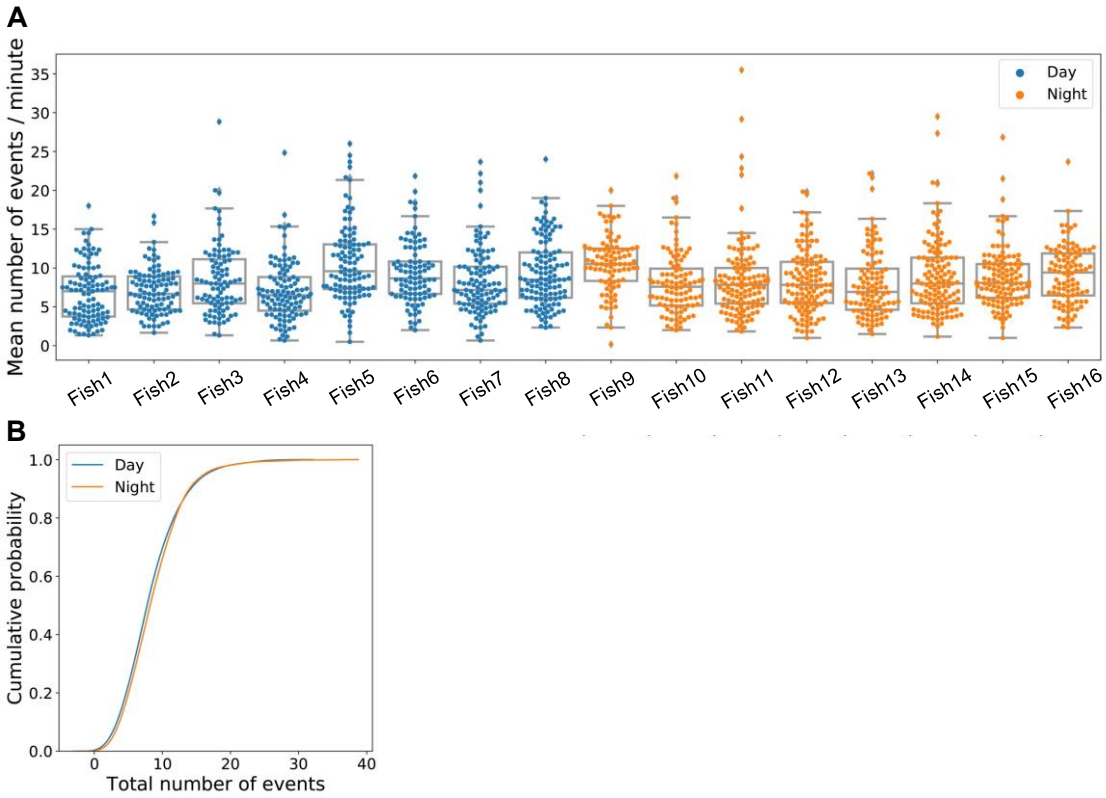

Figure 2.9: MHb exhibits similar Ca^{2+} activity during the day and night

(A) Scatter plots of the mean number of Ca^{2+} events per minute in 'Day' and 'Night' groups (8 larvae in each group). Each dot represents the mean rate of events measured from individual cells. Box plots indicate the distribution of data in four quartiles around the median and demonstrate the outliers. (B) Comparison of the cumulative probability distributions of mean rate of Ca^{2+} events for 'Day' and 'Night' groups: the two distributions were not significantly different.

Left but not right medial habenula exhibits marginally higher Ca^{2+} activity at night

Since the neuronal organisation of the zebrafish habenula exhibits left-right asymmetry, and the daily changes in the pERK expression also differ between the left and right nuclei, the Ca^{2+} activity was compared between the day and night in the left and right MHb nuclei separately. In the l-MHb the mean rate was 7.92 Ca^{2+} events per minute in the 'Day' group (*N* = 8 larvae; 95% CI [6.92, 8.91]) and 8.32 events per minute in the 'Night' group (*N* = 8 larvae; 95% CI [7.70, 8.93]). In the r-MHb nucleus the mean rate was 8.78 Ca^{2+} events per minute during the day (*N* = 8 larvae; 95% CI [7.87,9.70]) and 9.145 events per minute during the night (*N* = 8 larvae; 95% CI [8.56, 9.73]). The mean rate was found to be significantly higher during the night in the l-MHb (Fig. 2.10 A; KS

test: D = 0.111, p = 0.012) whereas the r-MHb exhibited no significant difference between the 'Day' and 'Night' groups (Fig. 2.10 B; KS test: D = 0.048, p = 0.679).

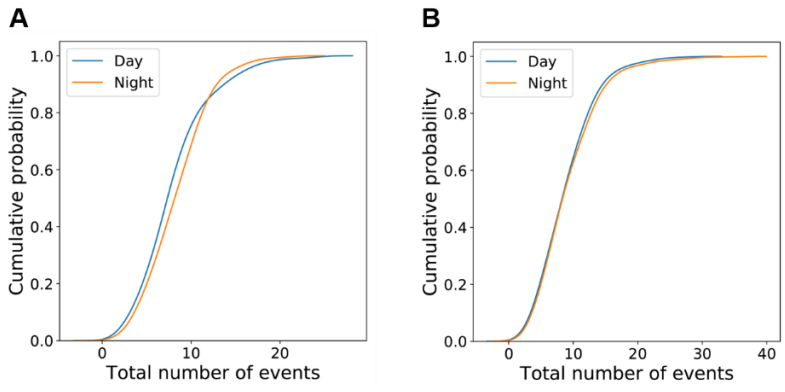

Figure 2.10: Left but not right MHb exhibits marginal increase in Ca^{2+} activity during the night

Comparison of the cumulative probability distributions of mean rate of Ca^{2+} events for 'Day' and 'Night' groups in the l- and r-MHb. (A) L-MHb: the mean rate was marginally significantly higher during the night than during the day. (B) R-MHb: the two distributions were not significantly different.

Lateral habenula exhibits slight increase in Ca^{2+} activity at night

Similar to the MHb, ongoing Ca^{2+} levels were monitored in the LHb of the same *Tg(s1011t:gal4;UAS:GCaMP6s)* larvae at two specific time points during the day and night and the mean rate of Ca^{2+} events was calculated for each cell (Fig. 2.11 A). In this area of the habenula the overall mean rate was 7.34 Ca^{2+} events per minute in the 'Day' group (*N* = 8 larvae; 95% CI [6.78, 7.90]) and 7.82 Ca^{2+} events per minute in the 'Night' group (*N* = 8 larvae; 95% CI [7.42, 8.22]). Further comparison of the distributions of the mean rate of Ca^{2+} events observed in the two groups showed a significant increase in the mean rate during the night (Fig. 2.11 B; KS test: D = 0.099, p = 0.001).

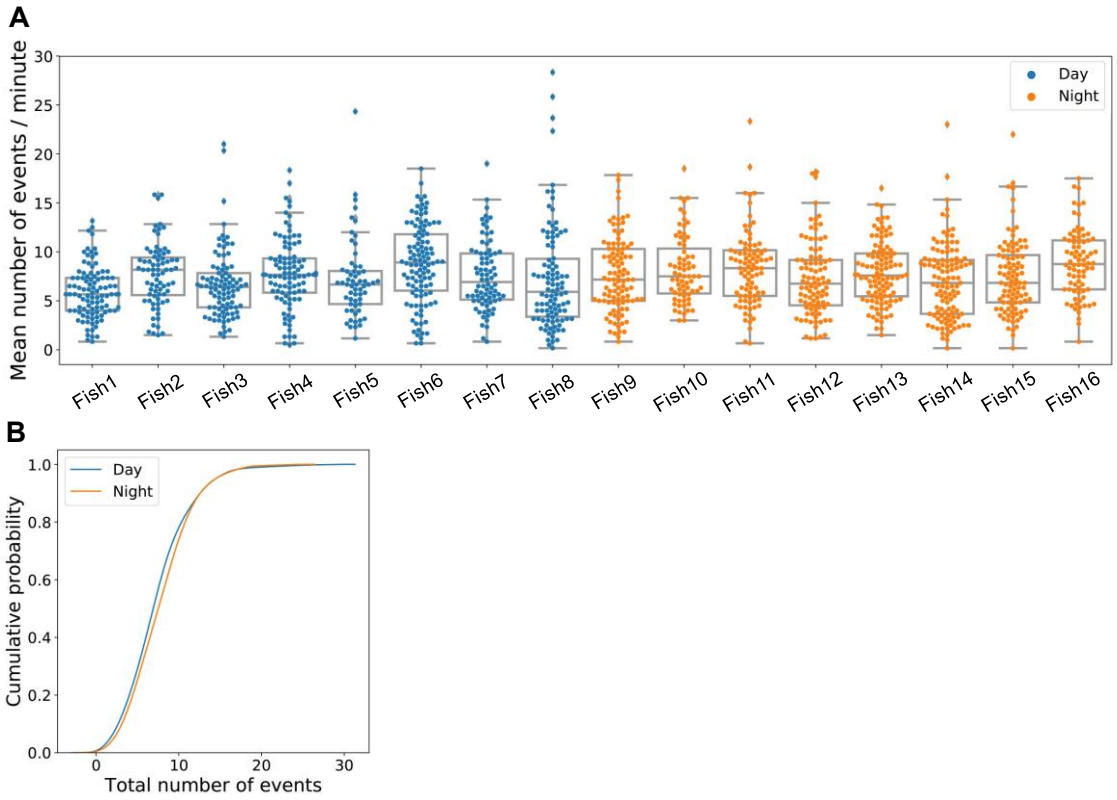

Figure 2.11: LHb exhibits slightly higher Ca^{2+} activity during the night

(A) Scatter plots of the mean rate of Ca^{2+} events in the LHb in 'Day' and 'Night' groups (8 larvae in each group). Each dot represents the mean rate of events measured from individual neurons. Box plots indicate the distribution of data in four quartiles around the median and demonstrate the outliers. (B) Comparison of the cumulative probability distributions of mean rate of Ca^{2+} events for 'Day' and 'Night' groups: the mean rate during the night was significantly higher than during the day.

Left but not right lateral habenula exhibits marginal increase in Ca^{2+} activity at night

Similar to the MHb, day and night Ca^{2+} levels in left and right LHb nuclei were analysed separately in order to investigate the possibility of left-right asymmetry. Overall, the mean rate in the l-LHb was 7.71 Ca^{2+} events per minute in the 'Day' group (*N* = 8 larvae; 95% CI [6.93, 8.50]) and 8.23 events per minute in the 'Night' group (*N* = 8 larvae; 95% CI [7.76, 8.69]). In the r-LHb the mean rate was 6.90 events per minute during the day (*N* = 8 larvae; 95% CI [6.11, 7.69]) and 7.34 events per minute during the night (*N* = 8 larvae; 95% CI [6.83, 7.86]). Comparison of the distributions of the mean rate of Ca^{2+} events in the 'Day' and 'Night' groups showed a significant increase in the mean rate during the night in the l-LHb (Fig. 2.12 A; KS test: D = 0.116, p = 0.007). However, no significant difference between 'Day' and Night' groups was observed in the r-LHb (Fig. 2.12 B; KS test: D = 0.092, p = 0.124).

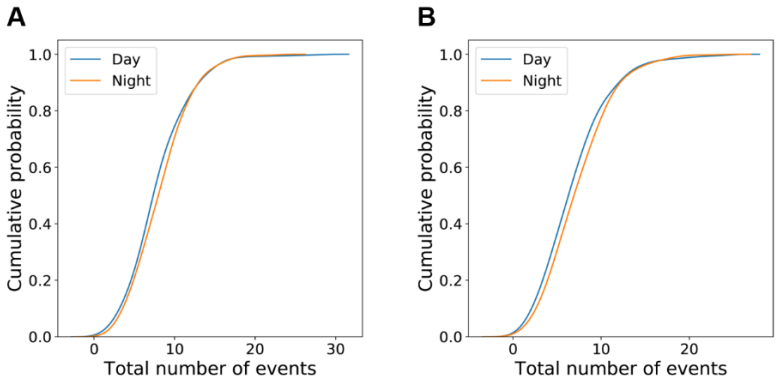

Figure 2.12: Left but not right LHb exhibits slightly higher Ca^{2+} activity during the night

Comparison of the cumulative probability distributions of mean rate of Ca^{2+} events for 'Day' and 'Night' groups in the l- and r-LHb. (A) L-LHb: the mean rate was significantly higher during the night than during the day. (B) R-LHb: the two distributions were not significantly different.

Discussion

The two-photon imaging of GCaMP fluorescence showed that both the MHb and LHb exhibit ongoing Ca^{2+} events during the day as well as during the night. However, a day-night variation in the overall rate of events was observed primarily in the LHb, which exhibited slightly higher activity at night than during the day. Furthermore, the analysis of the left and right LHb revealed that the day-night difference occurs predominantly in the left nucleus. These results are consistent with our IHC data that showed significantly higher levels of pERK at night in the left LHb, where the day-night difference was also present under DD conditions. The MHb, on the other hand, showed both an increase and decrease in the pERK expression in different subareas under normal LD cycle and almost no day-night variation in DD. However, closer examination of Ca^{2+} events in the individual left and right MHb nuclei revealed that only the left MHb exhibited slight increase in frequency during the night.

The inconsistent results from the two-photon imaging and the IHC of pERK could be caused by the alteration of the habenula's spontaneous state by potential stimuli before and at the onset of the two-photon imaging. Studies carried out by Cheng *et al.* (2017) and Ramaswamy (2018) demonstrated that a subpopulation of the MHb neurons are activated by the onset of darkness. This type of stimulus likely originates at the OFF bipolar cells in the retina which are depolarised in the dark (Hack *et al.*, 1999) and relay to the MHb via the retinal ganglion cells and the anterior thalamus (Cheng *et al.*, 2017). Since the day-time imaging was performed in the dark, it is possible that the darkness as a stimulus activated this subset of neurons. Although, the larvae were left to habituate in darkness prior to imaging, this evoked activity could still elicit perturbing effects on measured network activity. Similarly, some habenula cells exhibited an evoked excitatory response to the onset of the IR laser (Ramaswamy, 2018). A study investigating sensitivity of zebrafish to the near-IR light demonstrated that adult fish exhibit positive phototaxis to a light source with wavelengths up to 910 nm (Shcherbakov *et al.*, 2013). This implies that zebrafish are capable of perceiving near-IR light and the wavelength of 920 nm used in this

experiment could still perhaps elicit a slight response on a system level. Nevertheless, the laser-induced response alters the habenula's spontaneous state at both time points and, therefore, remains a concern regarding the application of this technique to zebrafish.

Previous studies of the mouse habenula using *in vitro* whole-cell current-clamp recordings have reported a mean firing rate ranging from approx. 3 – 5 Hz in the LHb and approx. 3 – 8 Hz in the MHb, with the lowest firing rate occurring during early morning and highest during late day and night. Furthermore, neurons in both the LHb and MHb were found to be highly heterogenous with regards to their baseline electrical properties and have accordingly been grouped into the multiple categories. These include: firing, bursting, depolarised low-amplitude membrane oscillators (DLAMO) and those exhibiting hyperpolarised-silent state amongst others (Sakhi, Belle, *et al.*, 2014; Sakhi, Wegner, *et al.*, 2014). The data produced in these studies highlight some of the inherent limitations of Ca^{2+} imaging and demonstrate that the high-resolution electrophysiological recording of membrane potential provides far more detailed information regarding, not only the real AP frequency and discharge patterning of neurons, but also their electrical state. Calcium indicators, on the other hand, are restricted to the registration of neuronal activity during which membrane potential exceeds Ca^{2+} channel's relatively depolarised voltages of activation and even this information is further curtailed by Ca^{2+} indicator's temporal properties and the relatively low sampling rate (*e.g.* 7 frames per second) of the imaging techniques with which they are visualised. As such, phenomena including, high frequency discharge, subthreshold events and the regulation of active and passive conductance ─ function and mechanistic properties which likely exhibit and even drive circadian rhythms ─ cannot be captured. An alternative approach which could overcome some of these deficiencies, whilst retaining the ability to monitor a large population of neurons *in vivo* non-invasively, could involve the use of genetically encoded voltage indicators (GEVIs). GEVIs are fluorescent transmembrane proteins which sense voltage fluctuations via a voltage-sensing domain, linked to a fluorescent protein (FP) or a FRET-FP pair (Kannan *et al.*, 2019). Transgenic zebrafish lines expressing the Accelerated Sensor of Action Potentials 1 (ASAP1) and Quality superior to Arch 2 (QuasAr2) in neurons have been generated (Miyazawa *et al.*, 2018). The QuasAr2 failed to report any neuronal signal whereas the ASAP1 enabled detection of evoked activity in the cerebellum and optic tectum as well as detection of spontaneous activity in the spinal cord neurons with single-cell resolution. However, the application of ASAP1 also has its limitations as, for instance, it was difficult to isolate single-cell responses in the cerebellum. This could be potentially due to the relatively low and dense ASAP1 expression. Since ASAP1 reduces its fluorescence intensity upon depolarisation, it requires sufficient amount of sparsely distributed expression in order to successfully report depolarising events from single cells (Miyazawa *et al.*, 2018). Nevertheless, future improvements in the sensitivity of GEVIs' and their ability to detect the spontaneous voltage dynamics of single cells may enable the *in vivo* monitoring of network bioelectricity and its circadian plasticity in the zebrafish habenula with the required level of spatiotemporal resolution.

Summary and evaluation of the techniques

In this chapter three approaches ─ bioluminescence of GA-opt, IHC of pERK and two-photon imaging of GCaMP6s Ca^{2+} indicator ─ were applied in order to monitor circadian changes in the zebrafish habenula in an intact system. The GA-opt failed to report any spontaneous Ca^{2+} activity, whereas the two other techniques produced consistent results demonstrating circadian variation in the LHb with increased levels of both cytosolic Ca^{2+} and pERK at night. The IHC of pERK also showed circadian differences in the MHb, but since these variations were of opposing polarities and occurred in different subregions of this structure, it is possible that for this reason examination of the whole MHb activity using the two-photon microscopy detected no overall difference. In addition, these changes were dependent on the presence of day-time light, which might explain why they could not be detected using the two-photon imaging as these experiments were performed in dark.

Following the application of all three techniques, Table 2.2 summarizes the pros and cons of each approach in order to evaluate their general suitability for *in vivo* monitoring of brain circadian rhythms.

Table 2.2: Pros and cons of the techniques used in this study

	Pros	Cons
GA-opt	• Enables long-term monitoring in freely behaving fish, therefore is ideal for circadian studies. • Sampling rate is fast, providing the best temporal information. • GA exhibits fast kinetics (6-30 ms rise time) (Naumann *et al.*, 2010).	• Spatial information only depends on the pattern of GA expression. • Nonspecific expression contaminates recording. • No single-cell resolution. • Currently, GA produces insufficient signal to report habenula's activity.
IHC of pERK	• Provides excellent topographic information regarding the whole habenula with single-cell resolution. • ERK phosphorylation can be measured in a large number of fish, providing information about batch-to-batch differences associated with different genetic backgrounds.	• Provides poor temporal information, as it only captures activity at a single time point.
Two-photon Ca^{2+} imaging	• Provides spatial information at single cell resolution. • Provides better temporal information than IHC of pERK.	• Larvae need to be immobilised using anaesthetic which presumably affects the spontaneous state and wears off after some time. • IR laser onset and darkness act as stimuli and affect spontaneous state. • Only allows monitoring of a single larva at a time. • Spatial information is limited to a single plane at a time. • Rate of imaging and kinetics of Ca^{2+} indicators are limited.

Chapter 3 Blocking the clock in the zebrafish habenula

Introduction

The habenula is a weak circadian oscillator that exhibits intrinsic TTX-resistant clock gene rhythms, specifically in the medial portion of the LHb, which have been previously demonstrated using imaging and photon-counting of the Per2::LUC fusion protein in mice (Guilding *et al.*, 2010). Furthermore, the time-keeping ability of the habenula is also present in lower vertebrates, including zebrafish and goldfish in which this brain structure exhibits daily rhythms in *bmal1* and *per1b* gene expression, implying the habenula circadian oscillator has been conserved across vertebrate phylogeny (Weger *et al.*, 2013; Sánchez-Bretaño *et al.*, 2015). However, the function of the habenula clock in regulating brain and behavioural rhythms is unknown.

In order to investigate the physiological and behavioural impact of a circadian oscillator the functional molecular clock within this oscillator can be genetically blocked using the dominant-negative strategy. This technique involves a constructed dominant-negative *clk* (Δ*clk*) gene, which was designed based on a previously identified mutation in the mouse *Clock* gene, leading to exon skipping and deletion of 51 amino acids in the C-terminal transactivation domain (King *et al.*, 1997). The protein product of this mutated gene is a truncated CLOCK protein (ΔCLK) that manifests the dominant effect as it retains the ability to dimerize but can no longer activate transcription of the downstream targets, such as *per1* (Fig. 3.1; Dekens and Whitmore, 2008). Consequently, the ΔCLK competes with the endogenous CLK protein, forming dysfunctional heterodimers with BMAL and disturbing the clock mechanism. Indeed, the dominant-negative mutation in *Drosophila Jrk* gene and zebrafish *clk1*, both of which are homologues of mammalian *Clock*, lead to lower transcriptional activity and decreased levels of PERIOD and TIMELESS proteins in flies and *per1* RNA in fish (Allada *et al*., 1998; Dekens and Whitmore, 2008). On a behavioural level, flies heterozygous for this mutation exhibit lengthened period and half are arrhythmic, while homozygous flies are all arrhythmic in DD (Allada *et al.*, 1998). Similarly, mice homozygous for the *Clock* mutant allele exhibit longer circadian period followed by complete loss of circadian rhythmicity under DD (King *et al.*, 1997).

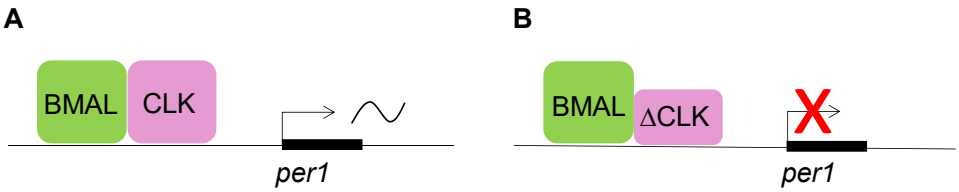

Figure 3.1: Blocking the molecular clock using the dominant-negative strategy

Mechanism underlying dominant-negative strategy. Figure adapted from Dekens and Whitmore (2008). (A) Under normal conditions CLK and BMAL form a heterodimer which induces transcription of *per1* gene. (B) Dominant-negative mutation generates C-terminal truncated protein ΔCLK which forms a heterodimer with BMAL and binds to E-box enhancer but lacks the ability to activate the transcription.

Aims

The first aim of this chapter was to genetically block the habenula clock by generating a transgenic line *Tg(gng8:gal4;UAS:EGFP-ΔCLK)* in which the ΔCLK would be expressed exclusively within the habenula. Generation of this transgenic line would then allow further investigation of how clock disruption in this brain area affects behaviour and brain state.

The habenula tightly regulates the dopaminergic VTA and the serotonergic DRN. Dopamine (DA) and serotonin (5-HT) signalling mediate reward and motivation and their rhythmic release drives circadian rhythms in motivated behaviours such as spontaneous locomotion (Mendoza, 2017). As a consequence of the habenula's influence over these monoaminergic systems, its clock might be contributing to associated behavioural rhythms. To further examine the contribution of the habenula clock to rhythms in motivated behaviours, spontaneous locomotor activity under constant conditions, primarily, was measured in the larvae expressing the ΔCLK in the habenula, referred to as ΔCLK+ larvae, and in their control siblings.

In addition, DA signalling and the LHb have been implicated in the regulation of REM sleep and lesioning of the FR results in REM sleep fragmentation, suggesting the habenula clock may also be involved in the regulation of sleep-wake cycle (Dzirasa *et al.*, 2006; Mendoza, 2017). In zebrafish the sleep-like state is associated with an elevated arousal threshold, which has been measured as attenuated sensory responsiveness to tap stimuli (Rihel *et al.*, 2010; Zhdanova *et al.*, 2001). In order to test whether the habenula clock regulates arousal-associated sensory responsiveness, the night-time responsiveness to auditory stimuli was measured in *Tg(gng8:gal4;UAS:EGFP-ΔCLK)* larvae.

Finally, DA and 5-HT are rhythmically released, with a peak during the active phase *(*Dudley *et al.*, 1998; Hood *et al.*, 2010; Mendoza, 2017). Furthermore, habenula cholinergic neurons innervating the IPN form a major cholinergic pathway in the CNS and, similar to DA and 5-HT, ACh release also peaks during the active phase (Hut and Van der Zee, 2011; Lee *et al.*, 2019). Therefore, it is possible that the habenula clock contributes to daily rhythms in brain neurotransmission by regulating the circadian rhythms in the brain content of DA, 5-HT and ACh.

In order to test this hypothesis, the brain levels of the 5-HT, DA and ACh were measured during the day and night in ΔCLK+ adults and their control siblings.

Collectively, this investigation will provide insight into how the habenula circadian oscillator contributes to the circadian rhythms in brain neurotransmission and behaviour.

Methods

Generation of transgenic line

The *Tg(UAS:EGFP-ΔCLK)* transgenic line was kindly provided by Prof. Yaov Gothilf (Tel Aviv University, Tel Aviv). However, since crossing of the provided fish with the *TgBAC(gng8:gal4)*^{c426} line did not generate sufficient expression in the habenula, the offspring of this cross were additionally injected with the pT2-UAS:EGFP-2A-ΔCLK-5xMyc construct, also provided by Prof. Gothilf. The injections were carried out as follows: the Tol2 Transposase mRNA was first transcribed using the mMESSAGE mMACHINE T3 kit (Life Technologies). A mixture of the Tol2 Transposase mRNA (50 ng/µL) and the pT2-UAS:EGFP-2A-ΔCLK-5xMyc plasmid (50 ng/µL) was injected into the offspring of *Tg(UAS:EGFP-ΔCLK)* crossed with the *TgBAC(gng8:gal4)*^{c426} line (~1 nL per embryo) at single-cell stage. The injected larvae were screened for GFP fluorescence at 3-4 dpf and the positive individuals were grown into adulthood. In order to enhance the expression of EGFP-ΔCLK in the habenula, positive adults from three consecutive generations (F0 – F2) were in-crossed.

Immunohistochemistry and imaging

The *Tg(gng8:gal4;UAS:EGFP-ΔCLK)* larvae at the age of 7 dpf were fixed in 4% PFA at 4ºC for ~22 h. Following multiple washes in PBS, skin covering the brain was manually removed and exposed brains were washed 3 times in PBST. The antigen retrieval was performed by incubating the fish in 150 mM Tris-HCl (pH 9.0) for 5 min at RT in order to equilibrate, and by subsequent heating of the samples at 70ºC for 15 min. Brains were washed 3 times in PBST and the rest of the protocol was followed as described in the Methods section in Part I of Chapter 2. Samples were incubated in the rabbit anti-GFP primary antibody (Torrey Pines Biolabs Inc., #TP401), diluted 1:500, and the mouse anti-Myc antibody (9E10; Santa Cruz Biotechnology), diluted 1:100, at 4ºC for 4 days. The secondary antibodies used were Alexa Fluor 488 goat anti-rabbit (ThermoFisher and Abcam), diluted 1:1000, and Alexa Fluor 647 goat anti-mouse (ThermoFisher), diluted 1:500. The immunostained brains were mounted in 2% LMA in PBS and imaged using a Zeiss LSM800 confocal microscope equipped with 40X water immersion objective.

Screening and selection of larvae used in experiments

All of the *Tg(gng8:gal4;UAS:EGFP-ΔCLK)* fish used in the following experiments were first screened for GFP fluorescence at the age of 3 dpf using Olympus MVX10 fluorescence microscope. Since the expression of EGFP-ΔCLK in the habenula was mosaic, only those

individuals with expression observed in the majority of habenula cells were carefully selected and used for further experiments as ΔCLK-positive (ΔCLK+) fish. Due to in-crossing of three consecutive generations in order to enhance expression of EGFP-ΔCLK, only very few individuals with zero expression could be found. Therefore, those individuals with zero expression as well as larvae exhibiting a minimal number of randomly labelled cells (less than ~15 cells per habenula) were used as the control (CTRL) siblings. Following the behavioural experiments, the larvae were immobilised in tricaine methanesulfonate (MS-222; final concentration of 0.01 mg/ml; Sigma), mounted in 2% LMA in E3 medium and the habenula-specific expression of EGFP was assessed using a Zeiss LSM800 confocal microscope and 40X water immersion objective (Fig. 3.2).

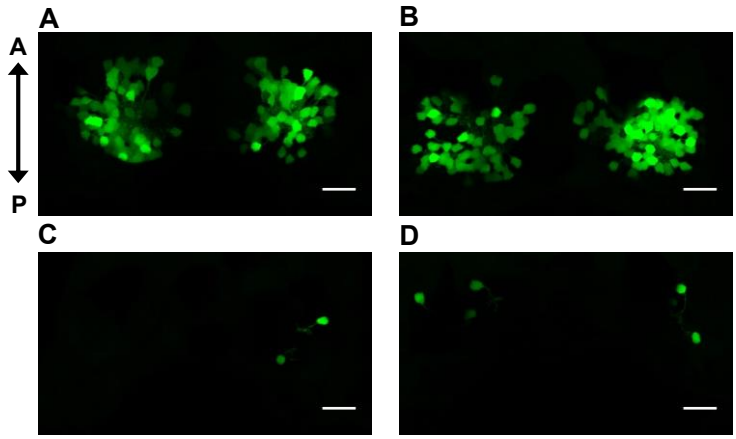

Figure 3.2: Post-experimental screening of EGFP-ΔCLK in the habenula

Dorsal view of the EGFP expression in the habenula of the *Tg(gng8:gal4;UAS:EGFP-ΔCLK)* larvae (7 dpf). (A-B) Examples of two individual larvae exhibiting EGFP-ΔCLK expression in majority of the habenula cells and were assigned to ΔCLK+ group. (C-D) Examples of two individual larvae exhibiting minimal EGFP expression in the habenula cells and were assigned to the CTRL group. A = anterior; P = posterior (same orientation applies for all images); scale bar: 20 µm.

Locomotor activity assay

The *Tg(gng8:gal4;UAS:EGFP-ΔCLK)* larvae from F3 generation were raised under standard conditions. Each experimental run involved animals from the same batch, originating from one pair of parents. The larvae were screened and selected as described in the previous section. At the age of 6 dpf the larvae were placed individually in a 24-well plate filled with 1.5 ml of tank water per well. The plate was then transferred into an incubator equipped with an IR camera (acA2040-90µm USB 3.0: Basler), a white LED box and four IR LED bars (LBS2-00-080-3-IR850-24V, 850 nm: TMS Lite). The camera and the LEDs were connected to a PC via a microcontroller board (Arduino UNO SMD). At the onset of recording (ZT6 – 9), fish were kept under ambient light, which was switched off at ZT14 (10 PM) and was kept off during the next day for the monitoring of activity under DD. A customized script written in Python 2.7, incorporating functions from the OpenCV library was used to control the Arduino microcontroller and simultaneously video-track fish locomotor activity. The video was captured using 576 x 864-pixel resolution at 10

frames per second and the background subtraction method was implemented to extract the 'x' and 'y' coordinates of each fish online.

Arousal assay

Six days-old ΔCLK+ larvae and their CTRL siblings from F3 and F4 generations were randomly placed in a 24-well plate and their locomotor activity was video-tracked as described in the previous section. In order to assess the arousal during sleep, vibration stimuli were applied through a speaker controlled, via the Arduino microcontroller board, by a modified version of the activity-tracking code in Python 2.7. Starting at ZT17, eighteen stimuli of nine different intensities, where 50% of computer audio output represented the highest intensity, were delivered for 200 ms (starting from 0%) in 12-16% increments every minute, first in a descending and then ascending order. The time interval between stimuli was determined based on previous findings that suggest a 30-second inter-stimulus gap is sufficient to avoid behavioural habituation (Burgess and Granato, 2007). The protocol was repeated at the commencement of every hour until ZT22, while the onset by ascending or descending order was altered each time. In total, 12 replicates of each stimulus intensity were generated. A fish was scored as responding if it moved more than 7 pixels (~ 4 mm) following the stimulus delivery and the average percentage of responding fish was calculated for each of the stimulus intensities (Woods *et al.*, 2014). The observed values were corrected for variations in the baseline locomotor activity, by first calculating the background probability of locomotion as a percentage of larvae which moved more than 7 pixels 5 s before the application of each stimulus. The average of 108 measures of the background probability of locomotion was then used to calculate the corrected probability of response at each of the stimulus intensities, implementing the following equation: corrected probability of response = observed value x [(observed value – background offset) / (max observed value – background offset)] (Woods *et al.*, 2014).

Quantification of DA, 5-HT and ACh levels

Three-month old female ΔCLK+ fish and their CTRL siblings from the F3 generation were immobilised on ice and euthanised by decapitation at ZT3 and ZT15. The whole brains, excluding the OB, were extracted in the ice-cold Ringer's solution (116 mM NaCl, 2.9 mM KCl, 1.8 mM $CaCl_2$, 5.0 mM HEPES, pH 7.2), snap-frozen in liquid nitrogen and stored in -80ºC until further analysis. The quantification of DA, 5-HT and ACh neurotransmitters was carried out by liquid chromatography-mass spectrometry (LC/MS) using the following analytical standards: dopamine hydrochloride (D2960000: Sigma-Aldrich), dopamine-1,1,2,2-d_4 hydrochloride (73483: Sigma-Aldrich), serotonin (14927: Sigma-Aldrich), acetylcholine chloride (Y0000002: Sigma-Aldrich). The pre-processing of frozen samples and the analysis by LC/MS was performed by Dr. Chai Yi Hao at the Singapore Phenome Centre (Lee Kong Chian School of Medicine, Singapore).

Data analysis

Data acquired from the quantification of DA, 5-HT and ACh levels were analysed and plotted using Python 2.7.

Data acquired from the online video-tracking of locomotor activity were initially converted to total distance (mm) travelled by each fish per 1 min time interval. The scripts for the data conversion and the analysis of the arousal threshold assay were written by Dr. Ruey-Kuang Cheng in Excel. All data were further analysed and plotted using Python 2.7 and Estimation Statistics (https://www.estimationstats.com/#/, Ho *et al.*, 2018). In order to compare two groups in the locomotor activity assay the Mann-Whitney test was used. Values were considered statistically significant at $p < 0.05$.

Results

EGFP-ΔCLK can be specifically expressed in the habenula

In order to specifically block circadian oscillator in the habenula, the GAL4/UAS system was applied to generate a transgenic line *Tg(gng8:gal4UAS:EGFP-ΔCLK)*. In this line the expression of ΔCLK is under the control of UAS enhancer, which is activated by the GAL4 protein selectively expressed in habenula cells (Fig. 3.3 A). In addition to ΔCLK protein, the *Tg(gng8:gal4;UAS:EGFP-ΔCLK)* line also expresses enhanced green fluorescent protein (EGFP) (Fig. 3.3 B). The EGFP is segregated from ΔCLK by 2A peptide linker for generation of two proteins and its presence enables convenient identification of ΔCLK+ individuals (Ben-Moshe Livne *et al.*, 2016). The expression of ΔCLK in the habenula has been confirmed by IHC of Myc tag that, within the construct, is directly linked to the ΔCLK coding sequence (Fig. 3.3 C).

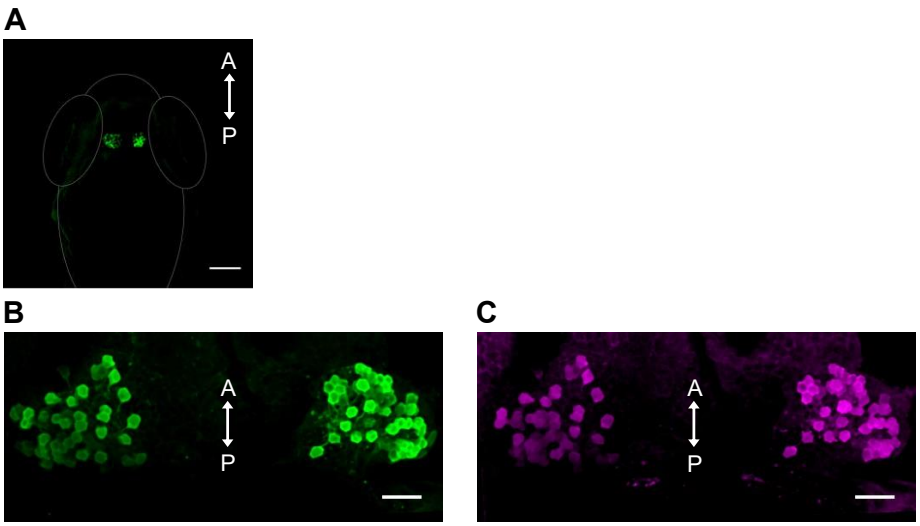

Figure 3.3: Expression of EGFP-ΔCLK in the habenula

(A) Dorsal view of habenula-specific expression of EGFP in *Tg(gng8:gal4;UAS:EGFP-ΔCLK)* larva (7 dpf); Z-projection (depth of ~70 µm); scale bar: 100 µm. B-C: Dorsal view of fixed brain from a *Tg(gng8:gal4;UAS:EGFP-ΔCLK)* larva (7 dpf) following IHC using (B) anti-GFP antibody anti-GFP antibody and (C) anti-Myc antibody; scale bar: 20 µm. A = anterior; P = posterior (same orientation applies for all images).

Blocking habenula's clock does not affect clock-regulated locomotor activity in zebrafish larvae

To investigate whether the habenula clock regulates circadian rhythms of motivated behaviours, the rhythmic locomotor activity of ΔCLK+ zebrafish larvae (*N* = 42) and their control siblings (*N* = 21) was analysed. All larvae were entrained to the standard LD cycle and their locomotor activity was monitored for a few hours during the light-phase, followed by onset of darkness at ZT14 for activity tracking during the night. Subsequently, the fish were monitored for one day under DD, in order to eliminate the masking effects of light and dark on clock-regulated behaviour (Ben-Moshe Livne *et al.*, 2016). Both CTRL and ΔCLK+ larvae generally exhibited increased locomotor activity during the light phase and during the subjective day, while exhibiting quiescent periods of inactivity during 1st and 2nd night of the recording (Fig. 3.4 A, B). The data acquired during the whole recording period were split into 5 timeframes: 1 = light-phase; 2 = 1st night; 3 = early subjective day; 4 = late subjective day; 5 = subjective night (Fig. 3.4 C, D). The difference in the mean locomotor activity between the ΔCLK+ and CTRL groups was calculated for each timeframe separately, as ΔCLK+ groups mean minus CTRL group mean (Fig. 3.4 E). In addition, the 95% CIs of each mean difference was calculated by bootstrap resampling in order to measure the precision and confidence of the estimate. The results of Mann-Whitney test showed no significant difference between the two groups during any of the analysed timeframes as $p > 0.05$ in all 5 comparisons (Table 3.1).

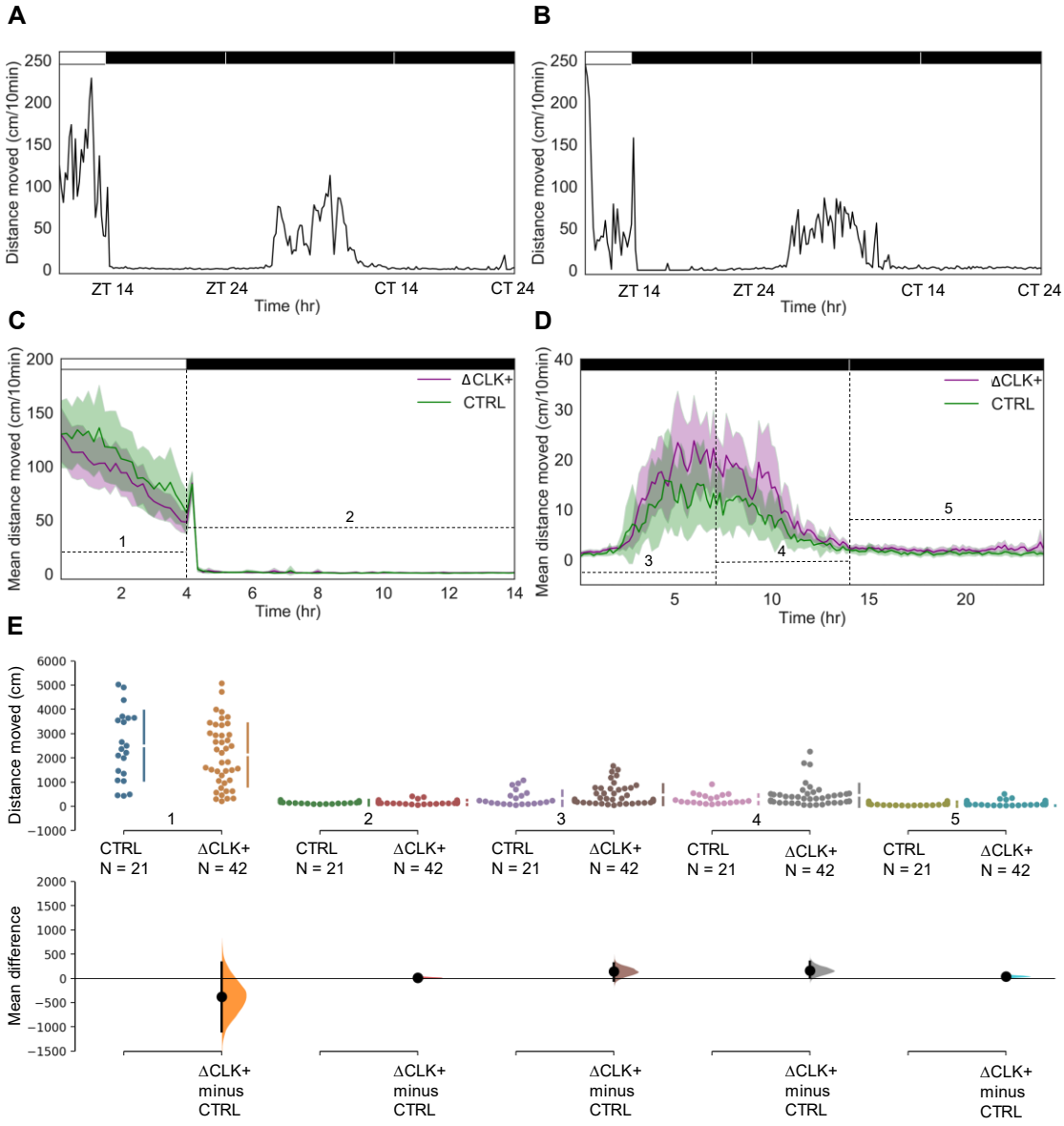

Figure 3.4: Locomotor activity during the light-phase and under DD is not affected by blocking the habenula clock

Analysis of the locomotor activity of the *Tg(gng8:gal4;UAS:EGFP-ΔCLK)* larvae (6-7 dpf) during light-phase and under DD. A-B: Distances moved (cm/10min) by individual larvae from (A) CTRL group and (B) ΔCLK+ group are plotted against time (hr) over the time-course of the whole recording. CT = circadian time. C-D: Mean distances moved (cm/10min) of ΔCLK+ (purple) and CTRL (green) groups are plotted against time (hr) (C) during the first 14 hours of recording, including 4 hours of light-phase and 10 hours in dark during the night and (D) during the subsequent 24 hours of recording under DD. 95% CIs are indicated by the shaded areas; interrupted lines indicate 5 analysed timeframes. Black and white bars represent periods of dark and light, correspondingly. (D) The Cumming estimation plot shows the mean differences for 5 comparisons, corresponding to 5 timeframes of recording. The raw data is plotted on the upper axis, each dot representing the overall distance moved (cm) by a single larva; gapped vertical lines to the right of each group indicate mean ± SD. Each mean difference is plotted on the lower axes as a bootstrap sampling distribution. Mean differences are depicted as black dots and 95% CIs are indicated by the end of vertical error bars.

Table 3.1:

Timeframe	Mean difference	95% CI from resampling	Mann-Whitney *p* value
1	-376.82	[-1096.05, 327.46]	0.35
2	14.56	[-12.59, 45.72]	0.70
3	141.29	[-48.72, 314.34]	0.14
4	162.86	[18.25, 347.66]	0.17
5	42.37	[8.24, 81.62]	0.08

Blocking habenula clock does not affect arousal threshold in zebrafish larvae

Generally, animal arousal states can be characterised by changes in spontaneous locomotor activity and altered responsiveness to sensory or emotional stimuli. The arousal threshold, of zebrafish larvae is under circadian control as it is significantly elevated during the sleep-like state at night. The elevation of the arousal threshold is measured as decreased responsiveness of the larvae to the tap stimuli at night in comparison to the day (Zhdanova *et al.*, 2001; Rihel *et al.*, 2010). In addition, several studies have confirmed that arousal-associated sensory responsiveness is regulated by DA and 5-HT systems in the midbrain (Burgess and Granato, 2007; Chiu and Prober, 2013; Yokogawa *et al.*, 2012). Since the habenula regulates monoaminergic systems, it is possible that its clock may be involved in the regulation of the arousal threshold. In order to investigate, whether the habenula's clock mediates the night-time elevation of the arousal threshold, associated with the decreased responsiveness to sensory stimuli, the *Tg(gng8:gal4;UAS:EGFP-ΔCLK)* larvae were exposed to auditory stimuli of 9 different intensities, delivered between ZT17 and ZT23. The individual larvae responded to stimuli by a sudden change in the locomotor activity and this parameter was used as a measure of their sensory responsiveness (Fig. 3.5 A, B). The robustness of the response generally depended on the intensity of the stimulus (Fig. 3.5 C). A larva was scored as a responder if it moved more than 7 pixels after the stimulus. The average percentage of responders was calculated for each stimulus intensity per group for each experimental run (N = 5 experimental runs). The resulting values were corrected for variations in the baseline locomotor activity. The difference in the mean percentage of responders between the ΔCLK+ and CTRL groups was calculated (ΔCLK+ group mean minus CTRL group mean) as the effect size for each stimulus intensity, together with the 95% CIs of each mean difference acquired from bootstrap resampling. In the case of all the tested intensities a similar percentage of responders was observed in both ΔCLK+ and CTRL groups, as the values from the two groups noticeably overlapped in all 9 comparisons (Fig. 3.5 D). All the mean differences and the bootstrap 95% CIs are listed in Table 3.2.

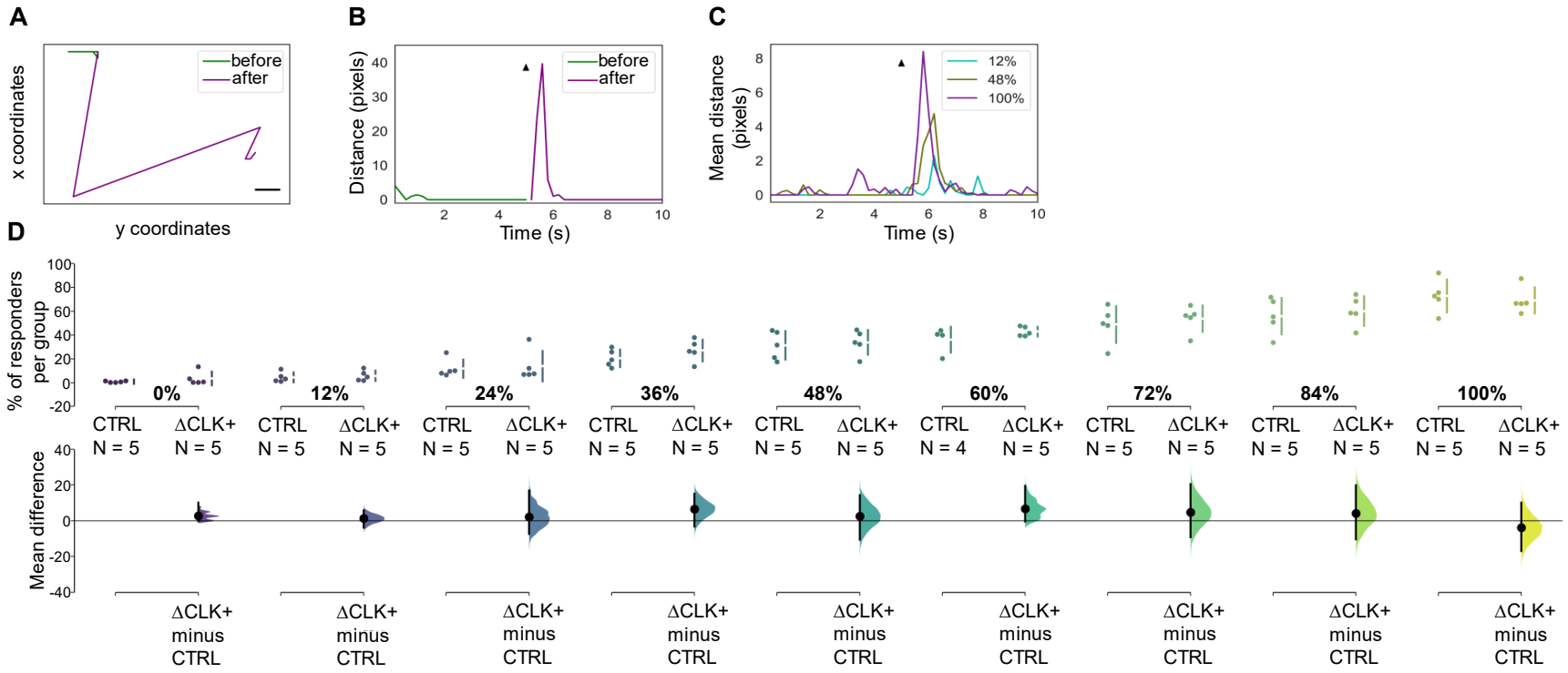

Figure 3.5: Night-time sensory responsiveness is not affected by blocking the habenula clock

Analysis of sensory responsiveness of the *Tg(gng8:gal4;UAS:EGFP-ΔCLK)* larvae (7 dpf) during the delivery of auditory stimuli of 9 different intensities. (A) Movement of an individual CTRL larva 5s before (green) and 5s after (purple) the delivery of a stimulus (100% stimulus intensity); the x and y coordinates of the larva position are plotted on the x and y axes correspondingly, scale bar: 5 pixels. (B) The x and y coordinates from Fig. A are converted to distance in pixels moved 5s before and 5s after the stimulus; black triangle indicates the time of stimulus delivery. (C) Mean distance moved by an individual larva during the delivery of 3 different stimulus intensities (calculated as the average distance moved during the all stimuli of a specific intensity delivered between ZT17 and ZT23). (D) The Cumming estimation plot shows the mean differences for 9 comparisons, corresponding to 9 stimulus intensities (0-100%). The raw data is plotted on the upper axis, each dot representing the percentage of responders per single experimental run; gapped vertical lines to the right of each group indicate mean ± SD. Each mean difference is plotted on the lower axes as a bootstrap sampling distribution. Mean differences are depicted as black dots and 95% CIs are indicated by the end of vertical error bars

Table 3.2:

Stimulus intensity	Mean difference	95% CI from resampling	Mann-Whitney *p* value
0%	2.77	[-0.39, 8.12]	0.53
12%	1.27	[-3.56, 5.81]	0.53
24%	2.11	[-7.71, 15.41]	1.00
36%	6.62	[-2.68, 15.35]	0.30
48%	2.56	[-10.19, 14.28]	0.68
60%	6.76	[-0.83, 18.20]	0.54
72%	4.83	[-9.58, 19.83]	0.68
84%	4.25	[-10.89, 19.57]	0.53
100%	-3.85	[-17.14, 10.04]	0.40

The day-time brain levels of dopamine, serotonin and acetylcholine are reduced in the ∆CLK+ adult fish

In order to investigate whether the habenula clock mediates daily rhythms in brain neurotransmission via the orchestration of rhythms in neuromodulator and neurotransmitter levels, the brain content of DA, 5-HT and ACh was measured in the adult ∆CLK+ fish and their CTRL siblings. In total, six brains from the ∆CLK+ and CTRL adults (3 brains extracted during the day and 3 during the night for each group) were analysed using LC-MS. Since the sample size of each group was too small the normal distribution of the data could not be confirmed. Furthermore, the application of the non-parametric Mann-Whitney test was not appropriate as this test compares the ranks of the values, ignoring how much the values in individual groups differ. In the case of a sample size of three, the Mann-Whitney test has zero power as it will always produce a *p* value greater than 0.05, regardless of how much the groups differ (GraphPad, 2017). Consequently, all result values are listed in Table 3.3 and Figure 3.6 demonstrates that, generally, the CTRL brain contents of DA, 5-HT and ACh were noticeably higher during the day (the active phase) than during the night. These results also show that this daily variation was attenuated in the ∆CLK+ group. Indeed, the levels of all three transmitter substances were lower in the ∆CLK+ group than in the CTRL group during the day, with no overlap between the values from ∆CLK+ and the CTRL groups in the day-time comparison. On the other hand, no apparent difference in the brain content of the examined neuromodulators was observed between the two groups during the night. Additionally, the mean difference was calculated by subtracting the CTRL group mean from the ∆CLK+ group mean, in order to establish how much the neuromodulator levels differed between the groups (Table 3.3). The highest mean difference was observed in case of the ACh, which could be associated with the fact that neurons of the habenula are themselves a prominent source of brain ACh.

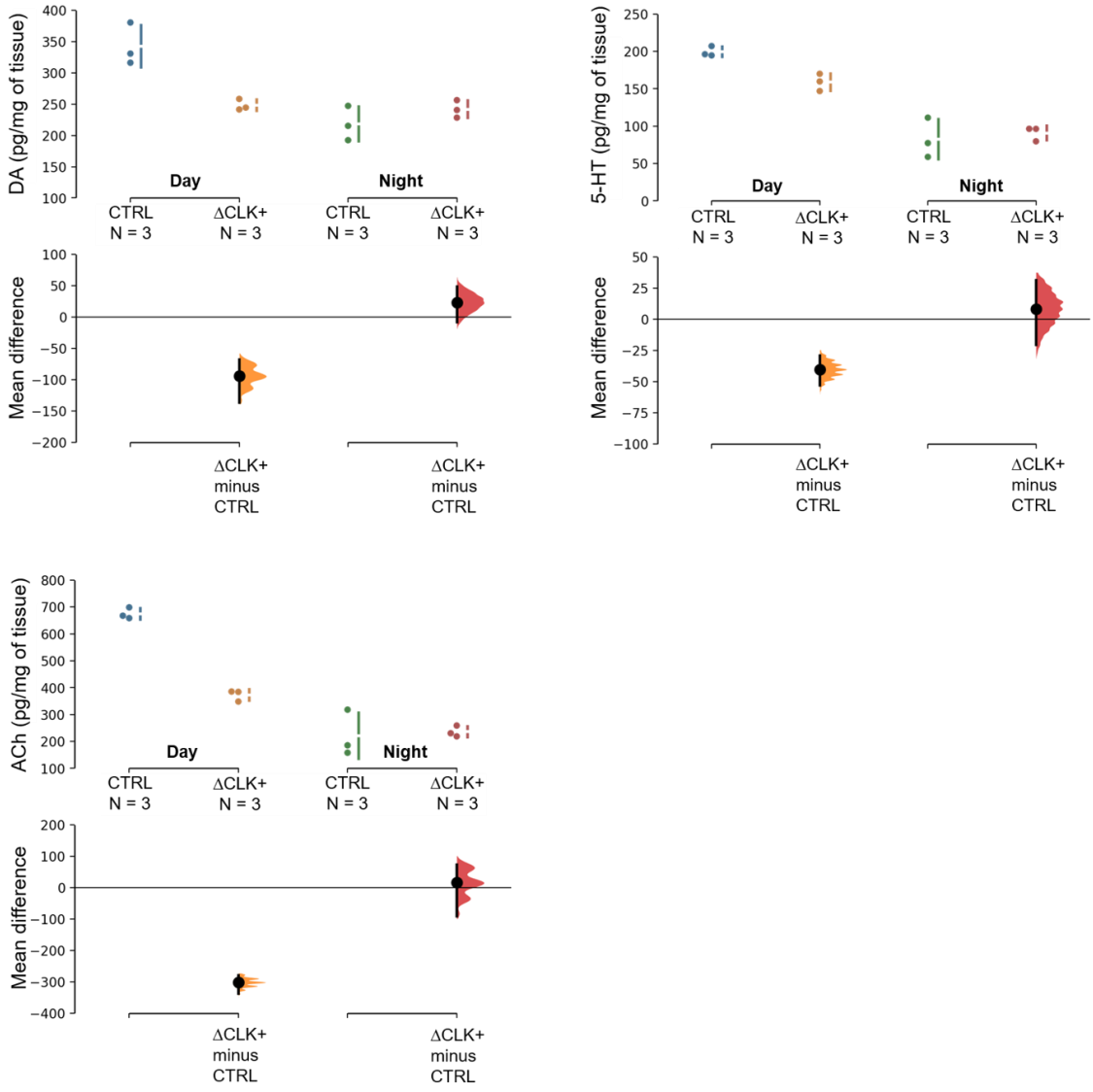

Figure 3.6: Day-time brain neurotransmitter levels are attenuated in ΔCLK+ adults

The Cumming estimation plots show comparisons of brain content of DA, 5-HT and ACh between the ΔCLK+ and CTRLs during day and night. The raw data is plotted on the upper axis, each dot represents a value obtained from a single brain as reported in Table 3.3: blue and orange dots represent values from CTRL and ΔCLK+ groups, correspondingly, during the day and green and red dots represent CTRL and ΔCLK+ groups during the night. Gapped vertical lines to the right of each group indicate mean ± SD. Mean differences are depicted as black dots and bootstrap 95% CIs are indicated by the end of vertical error bars.

Table 3.3:

Dopamine

Group	Sample	DA (pg/mg of tissue)	Mean	SD	Mean difference
CTRL Day	1	330.61	342.30	33.68	-94.27
	2	316.03			
	3	380.27			
ΔCLK+ Day	1	241.44	248.03	8.96	
	2	244.42			
	3	258.24			
CTRL Night	1	192.40	218.27	27.51	23.45
	2	215.24			
	3	247.16			
ΔCLK+ Night	1	256.26	241.72	14.00	
	2	228.33			
	3	240.58			

Serotonin

Group	Sample	5-HT (pg/mg of tissue)	Mean	SD	Mean difference
CTRL Day	1	207.07	199.25	6.81	-40.36
	2	194.57			
	3	196.12			
ΔCLK+ Day	1	159.74	158.89	11.57	
	2	170.01			
	3	146.91			
CTRL Night	1	58.82	82.47	26.60	8.32
	2	77.32			
	3	111.27			
ΔCLK+ Night	1	96.30	90.79	9.63	
	2	79.67			
	3	96.39			

Acetylcholine

Group	Sample	ACh (pg/mg of tissue)	Mean	SD	Mean difference
CTRL Day	1	667.33	674.69	20.94	-301.96
	2	698.32			
	3	658.42			
ΔCLK+ Day	1	385.55	372.73	21.11	
	2	384.28			
	3	348.36			
CTRL Night	1	158.07	220.58	85.52	15.59
	2	185.63			
	3	318.04			
ΔCLK+ Night	1	259.07	236.17	20.63	
	2	219.01			
	3	230.43			

Discussion

The principal aim of this chapter was to investigate the role of the habenula clock in the regulation of clock-regulated behaviour and brain neurotransmission in zebrafish. In order to do so, the *Tg(gng8:gal4;UAS:EGFP-ΔCLK)* transgenic line, in which the habenula's molecular clock was genetically blocked by means of the dominant-negative strategy, was first generated. Subsequently, the effect of disrupting habenula clock function on motivated behaviours, including clock-regulated spontaneous locomotion and arousal-associated sensory responsiveness, was assessed in larvae. Overall, blocking the habenula clock failed to affect either of these behaviours. Both the ΔCLK+ larvae and their CTRL siblings exhibited similar levels of spontaneous activity during the light phase and under DD. Moreover, they exhibited similar responsiveness to all the intensities of auditory stimuli tested. On the other hand, blocking the clock in this epithalamic structure resulted in decreased brain levels of three important neurotransmitters ─ DA, 5-HT, and ACh ─ during the day, but not during the night, in adult zebrafish ─ results that imply that the brain neurotransmission is affected during the adulthood.

This study has been carried out under assumption that the larval and adult zebrafish habenula contains a functional molecular oscillator. The oscillating expression of molecular clock components in the zebrafish habenula has been previously shown using *in situ* hybridisation (ISH) of *bmal1*, *per1b, per3* and *luciferase* genes in adult zebrafish (Moore, 2013; Weger *et al.*, 2013). Weger and colleagues (2013) also performed IHC against *luciferase* in larvae from *Tg(4xE-Box:Luc)* transgenic line at different time points during the circadian cycle. These results indicate a day-night variation in clock activity within the brain region containing the habenula, but since the resolution of the images is very low, it is rather difficult to conclude definitively whether the larval habenula contains the oscillating clock. Better evidence has been produced by Moore (2013) who performed whole-mount ISH against *per3* and showed that the entire brain of 4 day-old larvae exhibited a higher *per3* expression during the day than during the night. More importantly, further analysis of larval brain sections using chromogenic ISH revealed unambiguous *per3* expression in the habenula of zebrafish larvae, although this detailed examination was only performed at ZT3. However, in contrast to this ISH data, bioluminescence imaging of *per3-luc* in larvae only showed circadian rhythmicity of *per3* to be restricted to the olfactory bulb and nowhere else in the brain. In the discussion, the author proposed that the failure to detect the bioluminescent signal elsewhere within the brain could have been associated with the lack of penetration of the luciferin throughout the larvae. Contrary to this statement, Weger *et al*. (2013) generated a *Tg(4xE-Box:Luc)* transgenic line which successfully reports circadian clock core feedback loop activity in real time at early stages of development, implying the penetration of luciferin was not a problem. Although, the bioluminescent signals reported in this study were produced by the whole larvae and no evidence was provided regarding bioluminescence emitted specifically from the brain. Therefore, whether this reporter line generates detectable bioluminescent signal from specific brain oscillators remains to be determined. This could be tested further with the application of high-sensitivity videomicroscopy of the *Tg(4xE-Box:Luc)* brain at the larval stage and, if successful, this transgenic line could be used to monitor clock activity specifically in the habenula. The advantage of the *Tg(4xE-Box:Luc)* line, compared to

detection of specific circadian genes, is that it reduces the risk of reporting gene specific effects which are unrelated to core clock oscillations. Bioluminescence imaging of the *Tg(4xE-Box:Luc)* transgenic line could, therefore, constitute a useful tool to study the habenula core clock activity during the course of development and how oscillations in this activity are entrained to different circadian *zeitgebers* in real time *in vivo*. In addition, dissecting the habenula from adult *Tg(4xE-Box:Luc)* fish could help to determine whether the habenula clock exhibits intrinsic circadian rhythms which are independent from synaptic communication and how robust these rhythms are compared to rodent habenula or other more established zebrafish brain oscillators, such as pineal gland.

Another assumption made during this study was that the expression of ΔCLK in the habenula successfully disrupts this structure's clock machinery. It has been previously shown that the microinjection of Δ*clk* RNA into zygotes led to a four-fold reduction in *per1* RNA at the end of 1 dpf, as well as the dampening of *per1* RNA rhythm induced by light exposure during the first day of development ─ results that suggest the presence of ΔCLK interferes with the initiation of rhythmic *per1* transcription (Dekens and Whitmore, 2008). Furthermore, specific expression of ΔCLK in the pineal gland in *Tg(aanat2:EGFP-Δ**CLK**)* fish resulted in the loss of circadian rhythmicity in many clock-controlled genes, as shown by the mRNA-seq analysis of circadian oscillations in the pineal transcriptome. The core clock genes maintained their rhythmic profile, although the amplitudes of these rhythms were reduced, and, interestingly, a set of 11 genes acquired circadian rhythmicity in ΔCLK+ samples (Ben-Moshe Livne *et al.*, 2016). Together these findings provide the evidence that the expression of ΔCLK interferes with the clock machinery in zebrafish. However, in this study GAL4/UAS system was used for the first time to induce the ΔCLK expression in the habenula and it is currently unknown whether this system generated sufficient amount of ΔCLK to outcompete the endogenous CLK protein, a scenario required for the successful disruption of the clock function. As such, the mRNA-seq analysis of the habenula transcriptome would have to be carried out in the *Tg(gng8:gal4;UAS:EGFP-Δ**CLK**)* line in order to confirm the extent of ΔCLK interference and to determine the specific circadian genes affected. Additionally, if the *Tg(4xE-Box:Luc)* reporter line was found to successfully report habenula clock activity, it could be crossed with *Tg(gng8:gal4;UAS:EGFP-Δ**CLK**)* fish in order to validate the effects of the ΔCLK on the activity of the core clock feedback loop.

The application of the UAS:EGFP-ΔCLK construct, combined with the habenula-specific *gng8* promoter, generated relatively sparse EGFP-ΔCLK expression, when compared to other transgenic lines using the same GAL4 promoter, such as *Tg(gng8:gal4;UAS:GFP-aequorin-opt)*, in which noticeably more habenula cells were labelled. The failure to achieve the EGFP-ΔCLK expression throughout the habenula may be associated with transgene silencing, a phenomena known to occur as a result of UAS methylation, particularly in subsequent generations (Goll *et al*., 2009). The expression of EGFP-ΔCLK in *Tg(gng8:gal4;UAS:EGFP-Δ**CLK**)* fish was mosaic and differed between individuals, and as such could represent a major source of variability in behavioural assays. In order to maximise the ΔCLK expression, the fish with the best EGFP-ΔCLK expression were in-crossed and as a result only the few individuals with no expression could be selected as CTRL siblings. Therefore, some individuals with minimal EGFP-ΔCLK expression

were used as CTRLs. Using clean non-expressing CTRLs which would not be direct siblings of the ΔCLK+ fish tested in these experiments could introduce variations associated with difference in genetic background as opposed to presence of the ΔCLK. However, consequently, there is a small possibility that the ΔCLK could be interfering with the molecular clock in a small number of cells in the CTRL fish, creating a limitation of this experimental design.

Zebrafish larvae, if exposed to at least three light-dark cycles post-fertilisation, develop circadian rhythms in the locomotor activity under constant darkness with peak activity occurring during subjective day, suggesting the behavioural rhythms are not just driven by the onset of light and dark, but are also under control of the circadian clock (Hurd and Cahill, 2002). This phenomenon has been widely used to investigate the role of specific clock genes or brain circadian oscillators in the regulation of behavioural rhythms (Ben-Moshe Livne *et al.*, 2016; Huang *et al*., 2015; Hurd *et al*., 1998). For instance, the role of the pineal gland oscillator in the circadian regulation of behaviour was studied by monitoring rhythmic locomotor activity under constant darkness, light and dim-light in larvae expressing ΔCLK in the pineal gland (Ben-Moshe Livne *et al.*, 2016). In this study, activity was monitored over three circadian cycles, allowing the conversion of time-dependent signals into frequency-dependent signals using a Fast Fourier Transform and quantification of the 'G-factor ratio' as a measure of circadian rhythmicity. This type of analysis could not be performed on data acquired from a single circadian cycle. Hence, in order to fully assess the circadian rhythmicity of behaviour in this study, locomotor activity would have to be monitored over at least three circadian cycles. This would require optimising the current custom-made system used for this assay, by improving temperature regulation and introducing an automated food-delivery system.

Arousal-associated sensory responsiveness is a complex behaviour that is regulated by different neuropeptides and different signalling pathways depending on the sensory modalities involved. For instance, induced expression of hypocretin was found to increase responsiveness to dark-flash stimuli, while having no effect on responsiveness to thermal or acoustic stimuli. On the other hand, calcitonin gene-related peptide potentiated responsiveness to several stimulus modalities, while decreasing reaction time to auditory tap stimuli (Woods *et al.*, 2014). These findings imply the existence of complex overlapping regulatory processes underpinning the neuronal regulation of these behaviours, and as such raise the possibility that the habenula may mediate modality-specific responsiveness. Therefore, in order to gain a more complete understanding of the role the habenula clock plays in the regulation of arousal-associated responsiveness, other stimulus modalities, such as visual dark-flash, must also be tested.

In conclusion, this study has demonstrated that genetically blocking the circadian clock of the habenula does not affect clock-regulated behaviours in zebrafish larvae. However, it may have a profound effect on neurophysiological and behavioural states in adulthood since in adult fish the brain content of important neuromodulators was noticeably lower as a result of habenula-specific ΔCLK mutation. This potential difference between early development and adulthood could arise from the fact that in the early developmental stage examined habenula neurons lack their full complement of functional connections. As a consequence of this connectomic deficit the circadian oscillator of this structure may not be fully synchronised as, for instance, hypocretin

neurons, which regulate sleep and wakefulness, have yet to reach the habenula commissure at this stage of development (Appelbaum *et al.*, 2009). This implies that the habenula's role as a circadian oscillator becomes more apparent in adulthood.

Chapter 4 Circadian rhythms and influence of modulators in the mouse habenula

Introduction

Electrical activity in the rodent habenula oscillates in a circadian fashion *in vivo*, with peak activity occurring during the inactive phase (Zhao and Rusak, 2005). This circadian rhythmicity is presumably regulated by both an intrinsic clock, composed of molecular machinery expressed within habenula neurons themselves, as well as by external factors, mediated predominantly by neurotransmitters and neuromodulators released from other brain oscillators. These include SCN-derived AVP, a neuropeptide known to be involved in the signalling of circadian time (Baño-Otálora and Piggins, 2017). As such, the daily profile of habenula neuronal activity is influenced and refined by both external and internal time cues.

The intrinsic aspect of circadian rhythmicity in the electrical output of habenula neurons has been demonstrated in both rat and mouse brain slices. Early work by Zhao and Rusak (2005) reported a higher firing rate during the day in the rat habenula *in vitro*, while subsequent studies further established this structure's peak activity as occurring, more specifically, during the late day and early night (Guilding *et al.*, 2010; Sakhi, Belle, *et al.*, 2014; Sakhi, Wegner, *et al.*, 2014). Assuming potential SCN projections to the habenula were absent in the *in vitro* preparations used, these findings indicate that the observed rhythmicity is mediated by intrinsic clock machinery, which is, indeed, present in the LHb. This was further confirmed as habenula rhythms were absent in *Cry1*$^{-/-}$ *Cry2*$^{-/-}$ double knock-out mice, animals that lack a functional molecular clock (Sakhi, Wegner, *et al.*, 2014).

Vasopressin is a candidate transmitter of circadian cues to habenula

In addition to the intrinsic molecular clock, SCN-derived circadian inputs have been heavily implicated in the regulation of habenula rhythms. One such input is thought to be AVP, a neuromodulator expressed in the dorsomedial SCN whose release is known to drive daily rhythms in other brain areas, including DMH, SON and PVN (Kalsbeek *et al.*, 2010). As a consequence of these circuit specific interactions, AVP influences circadian rhythms in hormonal release, *e.g.* corticosterone, and behavioural outputs, *e.g.* water intake (Kalsbeek *et al.*, 2010; Tsuji *et al.*, 2017). With regards to the habenula, AVP-immunopositive axon terminals are present in the medial portion of the lateral nucleus (Rood and De Vries, 2011; Zhang *et al.*, 2016), suggesting that the SCN communicates circadian information to the LHb via AVP neurotransmission. However, the exact source of the AVP-positive fibres in the LHb remains controversial. De Vries and Buijs (1983) showed that AVP innervation of the LHb was eliminated following the lesion of BNST, implying that the BNST, and not the SCN, is the principal source of this vasopressinergic projection. However, more recent evidence from retrograde tracing experiments showed that the AVP innervation in the LHb originates primarily in the PVN and SON, although some retrogradely labelled AVP-immunopositive cells were also found in the SCN (Zhang *et al.*, 2016). This indicates

that SCN-derived circadian signals into the LHb may be transmitted both directly and indirectly via other hypothalamic nuclei. Additionally, Zhang and colleagues (2016) proposed that the AVP-positive terminals activate, via glutamatergic transmission, a unique microcircuit of GABAergic interneurons within the LHb. As a result, physiological upregulation of this AVP-containing pathway by water deprivation led to suppression of LHb output, a response correlated with active stress coping. However, further electrophysiological examination is required to confirm the presence of these GABAergic interneurons, the AVP-induced activation of this microcircuit and consequently the pre- or post-synaptic nature of AVP modulation in the LHb.

Mechanism of AVP brain modulation

Vasopressin is a peptide composed of nine amino acids which is synthesised primarily in the PVN and SON and acts both as a hormone and neuromodulator. As a hormone, AVP targets peripheral organs including kidney, blood vessels, liver and anterior pituitary, where it functions to regulate body water retention, blood pressure and adaptation of the hypothalamic-pituitary-adrenal axis during stress (Boone and Deen, 2008; Raggenbass, 2008). In the periphery, AVP binds to V1a, V1b and V2 receptors. Activation of V1a and V1b receptors expressed in smooth muscle, liver platelets and the anterior pituitary stimulates phospholipase Cβ (PLCβ) and the mobilisation of Ca^{2+} from intracellular stores (Raggenbass, 2008). Emptying of Ca^{2+} stores, in turn, may activate transient receptor potential (TRP) channels (Birnbaumer, 2000), a family of mixed cationic channels that pass positively charged Na^{+}, Ca^{+} and K^{+} ions with varying degrees of selectivity (Lyons, no date). As a consequence of the resultant depolarisation and influx of extracellular Ca^{2+}, the activation of TRP channels constitutes a powerful regulator of both electrical and transductional processes (Birnbaumer, 2000).

In the brain, AVP binds primarily to receptors with a pharmacological profile similar to the peripheral V1a receptor (Wrobel *et al.*, 2011), although Young *et al.* (2006) have also demonstrated expression of V1b receptors in mouse, rat and human hippocampus. When binding to the central G protein coupled V1a receptor, AVP is able to influence neuronal activity via a number of distinct mechanisms, both pre- and post-synaptic. Direct, post-synaptic influences are predominantly excitatory and for the most part mediated via either the opening of excitatory TRP channels or the closure of inhibitory K^{+} channels (Lyons, no date; Stoop, 2012). The mechanism of central AVP action has been thoroughly studied in motoneurons of the brain stem and spinal cord in both rats and mice. In facial motoneurons activation of V1 receptors generates an inward current which, being Na^{+}-dependent, voltage gated and resistant to TTX, is redolent of TRP channel activation (Raggenbass *et al.*, 1991). In contrast, spinal motoneurons exhibit an AVP-induced inward current associated with a reduced K^{+} conductance (Oz *et al.*, 2001). As such, the electrogenic mechanism of AVP action varies in different types of motoneurons (Raggenbass, 2008). Furthermore, in addition to the direct excitation of hypoglossal motoneurons – a response dominated by the activation of a mixed cationic conductance – AVP also enhances GABAergic and glycinergic synaptic inputs to these cells. This indirect, network inhibition is mediated via pre-synaptic V1a receptors located on the somatodendritic membrane of GABAergic and glycinergic interneurons, since the AVP-induced inhibition is suppressed by TTX and AVP does not alter the

frequency of miniature inhibitory post-synaptic currents. The activated interneurons subsequently inhibit post-synaptic hypoglossal motoneurons located in the vicinity (Reymond-Marron *et al.*, 2005). Hence, in this neurocircuit, AVP employs two opposing modes of action – direct excitation and indirect inhibition – a compound effect with profound influences on circuit performance that has been additionally observed in other brain structures, including the lateral septum and amygdala (Lu *et al.*, 1997; Raggenbass, 2008).

Vasopressin and oxytocin cross-reactivity

Vasopressin is closely related to oxytocin (OT), with both neuropeptides consisting of nine amino acids, while differing in sequence at only two positions. Similar to AVP, OT is also synthesized in the PVN, SON, and in the "accessory nuclei" located between these two structures, although the expression of OT and AVP occurs in strictly separate neuronal populations (Stoop, 2012). In addition, these two peptides are simultaneously found in other brain areas including hippocampus, amygdala, BNST and lateral septum, where they regulate various social behaviours, such as affiliative, parental and copulatory behaviours (Caldwell, 2017). For instance, administration of both OT and V1a receptor antagonists in the lateral septum blocks mating or AVP-induced pair bond formation in prairie voles, suggesting both types of receptors are involved in pair bond formation (Liu *et al.*, 2001). In general, there is one high affinity receptor for OT (OTR) in the brain (Stoop, 2012). This receptor can be coupled to different G proteins: when coupled to Gq/11 activation of the OTR stimulates PLCβ and mobilisation of Ca^{2+} from intracellular stores, leading to inhibition of inward rectifier K^+ channels (Stoop, 2012). On the other hand, activation of OTR coupled to Gi/o protein has exactly the opposite effect on G protein coupled inwardly rectifying K^+ channels (Gravati *et al.*, 2010). Additionally, activation of OTR can also stimulate adenylyl cyclase, with cyclic adenosine monophosphate production able to activate Na^+-dependent, TTX-resistant inward currents (Alberi *et al.*, 1997). Despite, the existence of their cognate receptors, it should be noted that the physiology and pharmacology of neurohypophyseal hormones is complicated by significant ligand cross-reactivity, with AVP displaying affinity for the OTR only ten times less than that of OT itself. Correspondingly, OT is also capable of interacting with V1 receptors, though with 100 times less affinity than AVP (Kimura *et al.*, 1994; Manning *et al.*, 2012). This cross-reactivity, in conjunction with the well-established phenomena of unwired volume transmission of both neurohypophyseal hormones (Leng and Ludwig, 2008), highlight the potential for OTRs and AVP receptors to influence circuit function in the absence of prominent projections from either OT or AVP expressing neurones. These considerations must be taken into account when ascribing functions to the endogenous peptides, particularly in areas where both OTR and V1 receptors are co-expressed.

Vasopressin and oxytocin receptors in the habenula

To date there is little evidence concerning the presence of V1 and OT receptors in the habenula. The ISH data in the Allen Brain Atlas demonstrates the presence of the V1a receptor transcript primarily at the border between MHb and LHb while the expression of the V1b and OTR appears very low, making substantive expression patterns difficult to determine (Allen Brain Atlas, Allen Institute, http://mouse.brain-map.org/gene/show/33433, http://mouse.brain-

map.org/gene/show/26109, http://mouse.brain-map.org/experiment/show/75081001). The expression of V1a receptor in the LHb has been further established by ISH and IHC assays (Zhang *et al.*, 2016; Zhang *et al.*, 2018). In addition, a detailed examination of OTR distribution in the mouse brain using OTR-lacZ reporter line did not report presence of the OTR in the habenula (Gould and Zingg, 2003). However, ISH analysis carried out by Vaccari *et al.* (1998) revealed expression of the OTR in the rat MHb. Further electrophysiological analysis involving application of selective receptor agonists and antagonists may help to determine the presence of specific receptors in the habenula and given the potential for ligand cross-reactivity their specific contribution to the electrical modulation of this structure by the neurohypophysial hormones AVP and OT.

Aims

Intrinsic circadian rhythms in habenula electrical activity have been demonstrated using both whole-cell patch clamp and extracellular recordings. Both of these techniques are limited to recording from a single cell or site within the habenula, one at a time. Given this lack of spatial resolution, it is difficult to say whether the information generated by such techniques is truly representative of the circadian rhythmicity exhibited across the entire habenula network. Therefore, the first aim of this chapter was to monitor circadian rhythms in habenula activity by simultaneously recording extracellular multi-unit activity from multiple sites in the LHb and MHb using a multi-electrode array. This will enhance our understanding of these structures' network dynamics by demonstrating previously unknown topographic distribution of circadian rhythmicity in the habenula.

The presence of AVP-positive fibres and, potentially, V1 receptors has been previously shown, implying that the AVP nonapeptide may modulate neuronal activity in the habenula. In addition, since part of the AVP input to the LHb originates in the SCN, AVP might act as a transmitter of circadian time cues to synchronise the LHb oscillator. Accordingly, the second aim of this chapter was to determine whether endogenous AVP influences neuronal activity in the LHb *in vitro* and whether its influence differs at two opposing circadian time points.

Finally, since endogenous AVP binds to V1 receptors and OTRs with similar affinity, and pilot data from our laboratory has shown AVP reliably induced responses in the LHb at only relatively high concentrations, we sort to examine whether OT was also capable of influencing LHb electrical activity. Moreover, considering the OT can still bind to V1 receptor – even though with much less affinity – the potential involvement of the OTR itself was investigated using the selective OTR agonist, (Thr^4, Gly^7)-Oxytocin (TGOT).

Methods

Animals

The investigation of the AVP-induced modulation of habenula activity involved male and female *Per1::Venus* mice from C57BL6 genetic background which were bred at the Biological Services Facility at the University of Manchester. The rest of the experiments involved male wild-type mice from C57BL6 background bred at Charles River and the Animal Services Unit at the University of Bristol. Once weaned, all animals were group-housed under 12:12 h LD cycle, with ZT 0 defined as lights on. Food and water were available *ad libitum*. Together, two mice (4 months old) were used for IHC and 45 mice (2 – 5 months old) were used for the *in vitro* extracellular and whole-cell recordings. All experimental procedures were performed according to the guidelines of the UK Animal (Scientific procedures) Act 1986.

Immunohistochemistry

Two adult *Per1::Venus* mice were deeply anesthetised with pentobarbital (20 mg/kg) and perfused transcardially at ZT 8 – 11 with ~ 90 ml of 0.1 M PBS (pH 7.4) with Heparin, followed by 50 – 70 ml of ice-cold 4% PFA in 0.1 M PBS. The brains were removed and post-fixed in the same fixative buffer for 24 h before being stored for 48 h in 30% sucrose at 4ºC. The brains were subsequently flash-frozen in dry ice and cut (30 µm thick) using a freezing sledge microtome (Bright Instruments). Sections containing habenula and hypothalamus, as a positive control, were washed 4 x 30 min in 0.1 M PBS and incubated in 0.1% Triton-X in 0.1 M PBS for 20 min, followed by 3 x 10 min washes in 0.1 M PBS. Nonspecific protein binding was blocked with 5% donkey serum in 0.1 M PBS containing 0.05% Triton-X for 30 min. Sections were then incubated for 48 h at 4ºC in rabbit anti-vasopressin antibody (Millipore), diluted 1:5000 in the blocking solution (5% donkey serum in 0.1 M PBS with 0.05% Triton-X). The incubation was followed by 4 x 30 min washes in 0.1 M PBS, after which sections were incubated in donkey anti-rabbit cy3 secondary antibody (diluted 1:800 in 0.1 M PBS, Jackson Immunoresearch) overnight at 4ºC in a dark environment. Some sections were initially incubated in the blocking solution only (without the primary antibody), followed by incubation in the secondary antibody solution and served as negative controls to visualise any non-specific binding by the secondary antibody. All sections were subsequently washed 4 x 30 min in 0.1 M PBS followed by 2 x 20 min washes with autoclaved water, before being mounted in Vectashield anti-fade mounting medium (Vector Laboratories). Stacks of images were captured in series with Leica SP5 upright laser scanning confocal microscope (Leica Microsystems) at 20 x (~ 20 images per a Z-stack) magnification.

Acute brain slice preparation

Eleven adult *Per1::Venus* mice were used for the experiments investigating AVP modulation. Mice were deeply anaesthetised with isoflurane (Abbott Laboratories) and culled by cervical dislocation followed by decapitation at either ZT 6 - 7 for late day recordings at ZT 9 - 11, or at ZT 11 - 12 for late night recordings at ZT 22 - 23. In addition, 27 male C57BL6 mice were used for investigation of day-night differences in habenula neuronal activity and for investigation of OT and TGOT modulation. These mice were culled by cervical dislocation followed by decapitation at

either ZT 1 for early day recordings at ZT 3 – 5, or at ZT 11 for early night recordings at ZT 15 - 18. All mice, including those used for the night recordings, were strictly culled during the light phase, since culling during the dark phase has been previously found to phase-shift the diurnal rhythm of neuronal firing in the SCN (Gillette, 1986). The brain was quickly removed and immediately immersed in ice-cold (4ºC), oxygenated (95%O_2/5%CO_2) incubation artificial cerebrospinal fluid (aCSF) with low Na^+/Ca^+, high Mg^+ in order to protect the brain tissue from excitotoxicity. The incubation aCSF contained the following components (in mM): 95 NaCl, 1.8 KCl, 1.2 KH_2PO_4, 0.5 $CaCl_2$, 7 $MgSO_4$, 26 $NaHCO_3$, 15 glucose, 50 sucrose, 0.005 mg/L. The cerebellum and a part of the forebrain were removed, and the caudal side of the coronal block was promptly glued on the stage of the vibroslicer (Campden Instruments). Mounted brain was immersed in the ice-cold incubation aCSF and was cut into coronal brain slices (300 µm thick). Habenula-containing sections (distance from bregma ~ -1.7 to -2 mm according to Paxinos and Franklin's mouse brain atlas) were immediately transferred into a chamber containing continuously oxygenated incubation aCSF for at least 30 min. Subsequently, brain slices were transferred into the recording aCSF with the following composition (in mM): 127 NaCl, 1.8 KCl, 1.2 KH_2PO_4, 2.4 $CaCl_2$, 1.3 $MgSO_4$, 26 $NaHCO_3$, 15 glucose.

Extracellular multi-electrode array (MEA) recording

Extracellular MEA recordings were performed according to methodology established by Belle *et al.* (no date) which was also applied by Watson (2018). Acute brain sections containing the habenula were kept at ~25ºC RT in the recording aCSF that was continuously oxygenated (95%O_2/5%CO_2) to allow the acclimatisation to the recording conditions for at least 1 h prior recording. Subsequently a brain section was placed onto the perforated multi-electrode array (pMEA, 60pMEA100/30iR-Ti-gr, Multichannel Systems) equipped with 60 titanium nitride electrodes (diameter of 30 µm). The electrodes in the 60pMEA100/30iR-Ti-gr array are 100 µm apart, arranged in a 6 x 10 layout. This model is generally more suitable for recordings from relatively small brain structures, compared to the other available model 60pMEA200/30iR-Ti-gr, in which the electrodes are 200 µm apart. Inside the array bath chamber, a brain slice was stabilised using a harp grid and was continuously perfused (~ 2ml per min) with gassed recording aCSF. The temperature of aCSF in the bath was maintained within the physiological range at 33ºC and was regulated via temperature controller (TC02, Multichannel Systems) and a heatable perfusion cannula equipped with a temperature sensor. To accurately position the habenula on the electrode array, the brain section was trans-illuminated from below the array with a binocular microscope. Negative pressure (-43.2 mbar) was applied to the tissue through the MEA perforations using a vacuum pump in order to gently pull the slice down which improved the contact between the tissue and the electrodes. The brain slice was then allowed to settle down for at least 10 min prior the start of data acquisition. An external web camera attached to the microscope was used to capture the image of the brain section placed on the array at ~ 4 x magnification. In order to identify the electrodes in contact with the habenula the image of the brain section was merged with the image of 6 x 10 electrode grid taken at the same magnification using Photoshop CS6.

All recordings were sampled at 25 kHz and acquired using MEA2100 amplifier and MC Rack software (Multichannel Systems). For the experiments involving day-night comparison of the habenula activity, spontaneous neuronal activity was first recorded for at least 40 min during early day and early night at ZT 3 – 5 ('Day' group) and at ZT 15 – 17 ('Night' group), correspondingly. These time windows were selected in order to compare the results with the findings from zebrafish habenula. For the experiments investigating neuromodulation of the habenula activity, spontaneous, or baseline, activity was first recorded for at least 20 min minutes prior to ~5-minute bath application of AVP (20 µM, Bachem), OT (500 nm, Tocris) and TGOT (500 nm, Bachem). All drugs were prepared in the recording aCSF. The concentration for the AVP was selected since at this concentration AVP reliably induced detectable responses with each application. The concentrations for OT and TGOT were determined according to previously published data (Maniezzi *et al.*, 2019; Tunstall *et al.*, 2019). At the end of the recording, a voltage-gated Na^+ channel blocker TTX (1 µM, Ascent) was bath applied to inhibit AP discharge and to confirm that the recorded events were APs. All stock solutions were prepared in MilliQ water.

Offline data processing

In the raw acquired data, spikes generated by AP discharge were embedded in the background voltage fluctuations known as local field potential. Therefore, in order to isolate and visualise the spikes, a high-pass filter with a cut-off frequency of 300 Hz was first used to filter low frequency activity (Quiroga, 2012). This way only the fast components of the extracellular spike were retained, while repressing the slower components such as slowly activating or small ionic currents (Molden *et al.*, 2013). Subsequently, a threshold was set for spike detection at -17.5 µV. This was determined taking into account the baseline noise level recorded at each electrode during the TTX application (~ ± 10 µV). The threshold level was set at least 1.5 times the TTX baseline noise level in order to reliably detect spikes representing AP firing, while avoiding noise detection. Data which included detected spikes were exported into Neuroexplorer software in order to calculate mean multi-unit activity (MUA; calculated as spikes detected per second) at each electrode in contact with the habenula. In order to discriminate single units, filtered and thresholded data was imported to Plexon Offline Sorter v3 (Plexon Inc.). Single units were identified manually according to clustering of spikes in principal component space, in order to accurately differentiate single-unit activity.

Additionally, MUA histogram data demonstrating effects of neuromodulators were smoothed in Neuroexplorer using the running average of 10 in order to remove small fluctuations in the raw MUA histogram so that the peaks of the drug responses become more apparent. The mean MUA and the standard deviation (SD) during the 3 min of baseline activity and during the 20 sec of peak response were calculated in Python 2.7. The increase in the MUA rate during the drug application was considered as a response if the delta between the mean firing rate during the peak response and the mean firing rate during the baseline MUA, plus two times its standard deviation, was positive.

Statistical analysis

In order to compare the activity between 'Day' and 'Night' groups, the cumulative probability distributions of the mean MUA and single-unit activity (SUA) were compared using the KS test. This data was analysed and plotted in Python 2.7. Data involving effects of neuromodulators were further analysed using Estimation Statistics (https://www.estimationstats.com/#/, Ho *et al.*, 2018). In order to compare MUA during the baseline and during the drug application, the Wilcoxon paired t-test was used. For the unpaired comparisons between 'Day' and 'Night' groups, the Mann-Whitney test was used. The values were considered statistically significant at $p < 0.05$. All contour plots were produced in Python 2.7.

Whole-Cell recordings

For electrophysiological experiments mice (C57B6/J; *N* = 7) were deeply anaesthetized with sodium pentobarbital and decapitated. The brain was rapidly removed and placed in an ice-cold and oxygenated (95%O_2/5%CO_2) 'slicing' solution containing (in mM) sucrose (214)**,** KCl (2.0), NaH_2PO_4 (1.2), $NaHCO_3$ (26), $MgSO_4$ (1.3), $CaCl_2$ (2.4), D-glucose (10). The meninges were gently removed, and the brain was blocked and glued to a vibratome (Campden Instruments) where 200 µm thick coronal slices of the containing the habenula were prepared. Slices were immediately transferred to aCSF containing (in mM) NaCl (127), KCl (2.0), NaH_2PO_4 (1.2), $NaHCO_3$ (26), $MgCl_2$ (1.3), $CaCl_2$ (2.4), D-glucose (10), in a continuously oxygenated holding chamber at 35ºC for a period of 25 min. Subsequently, slices were allowed to recover in 'recording' solution at RT for a minimum of 1 h before recording. For whole-cell recordings, slices were transferred to a submerged chamber and placed on an elevated grid that allows perfusion both above and below the slice. An Olympus BX51W1 upright microscope (Olympus) was used for IR-differential interference contrast visualisation of cells. Recordings were performed at RT (25ºC) and slices were continuously perfused with oxygenated 'recording' solution (as above) at a rate of ca. 5 ml/min, unless otherwise described. All pharmacological compounds were bath applied.

Whole-cell current- and voltage-clamp recordings were performed with pipettes (3-7 MΩ when filled with intracellular solution) made from borosilicate glass capillaries (World Precision Instruments) pulled on a P-97 Flaming/Brown micropipette puller (Sutter). The intracellular recording solution contained (in mM) K-gluconate (140), KCl (10), HEPES (10), EGTA (1), Na_2ATP (2), pH 7.3 (with KOH). Recordings were performed using a Multiclamp 700B amplifier and pClamp10 software (Molecular Devices). Slow and fast capacitative components were automatically compensated for. Access resistance was monitored throughout the experiments, and neurons in which the series resistance was >25 MΩ or changed >15% were excluded from analysis. Liquid junction potential was 16.4 mV and not compensated. The recorded current was sampled at 10 kHz and filtered at 2 kHz unless otherwise stated.

All whole-cell recordings and analysis of this data were conducted by Dr. David Lyons.

Results

Medial and lateral habenula exhibit elevated multi-unit activity at night

In order to compare habenula network activity during day and night, acute extracellular recordings of MUA were performed at ZT 3-5 ('Day' group) and ZT 15-17 ('Night' group). Coronal brain slices containing the habenula were positioned on a pMEA arranged in a 6 x 10 layout, which allowed simultaneous recording of electrical activity from both MHb and LHb (Fig. 4.1 A, B). The same habenula orientation was used in all recordings in order to measure day-night differences while maintaining comparable topographic resolution and spatial sampling. All recorded sites in the MHb and LHb exhibited different levels of spontaneous multi-unit spiking activity (Fig. 4.1 C). In general, spikes derived from the MHb were more likely to exhibit larger amplitudes than spikes acquired in the adjacent LHb. This could be a result of the fact that the neuronal population in the MHb is much more compact, when compared to the LHb, meaning there is a higher chance of neuronal discharge in close proximity of an electrode. Administration of TTX (1 µM) successfully abolished the detected MUA activity at all recorded sites and, therefore, confirmed that the detected MUA was representative of AP discharge (*N* = 7 mice) (Fig. 4.1 D).

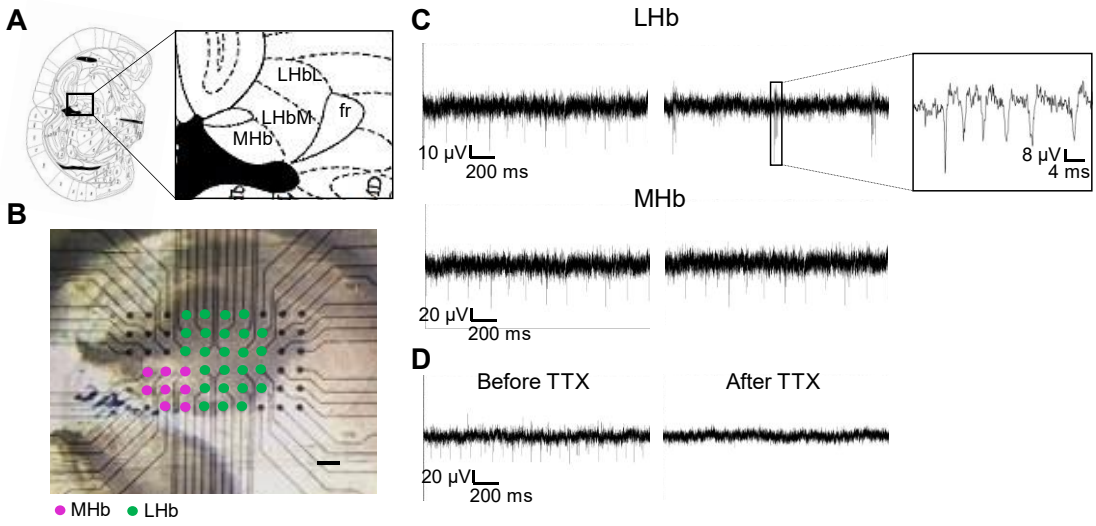

Figure 4.1: Spontaneous AP-derived MUA can be simultaneously recorded from MHb and LHb

(A) A diagrammatic representation of a coronal section containing the habenula (distance from bregma ~ -1.90 mm; taken from the Paxinos and Franklin's mouse brain atlas) was used as approximate reference during brain slice preparation. Schematic indicates the orientation of a brain slice when positioned on a pMEA. MHb: medial habenula; LHbM: lateral habenula, medial part; LHbL: lateral habenula, lateral part; fr: fasciculus retroflexus. (B) Image of an acute brain slice (taken at 4x magnification) positioned on a pMEA with electrodes arranged in 6 x 10 layout. Magenta and green dots indicate electrodes in contact with the MHb and LHb correspondingly. Scale bar: 100 µm. (C) Example traces of spontaneous MUA detected at two different sites in the LHb and MHb. Bursting firing was occasionally detected in the LHb as depicted by the LHb-derived trace on the right. (D) Example trace demonstrating the effect of TTX (1 µM) application on the MUA detected at a single electrode: TTX abolished the spiking MUA activity at the recording site. TTX baseline noise level (~ ± 10 µV) was further used to calculate the threshold for spike detection.

A threshold level was applied to detect spikes from filtered data and to calculate the temporal mean MUA detected at each electrode. For the analysis, 15-min long time windows of the most stable spontaneous MUA were used to compare the mean MUA of 'Day' and 'Night' recordings.

In the MHb, the overall mean MUA was 12.50 Hz in the 'Day' group (*N* = 9 mice; 95% CI [10.26, 14.75]) and 17.94 Hz in the 'Night' group (*N* = 10 mice; 95% CI [14.88, 21.00]) (Fig. 4.2 A). Subsequent comparison of the distributions of the mean MUA in the two groups demonstrated significant increase in the mean MUA during the night (Fig. 4.2 B; KS test: D = 0.298, p = 0.008). However, closer examination of the MUA distribution exhibited by all individuals revealed unusually high mean MUA of ~60 Hz detected at one of the electrodes (Fig. 4.2 A: 'Day' group – Mouse3). Even though, this value was not considered to be a statistical outlier in relation to other values acquired from the same individual, such a high value has not been observed in any other recordings and might be attributed to tissue deterioration or elevated negative pressure applied at this particular site. Excluding this 'physiological outlier' from the comparative analysis of the two distributions produced a similar result – KS test: D = 0.313, p = 0.005 – with slightly more pronounced difference between the two distributions (Fig. 4.2 C).

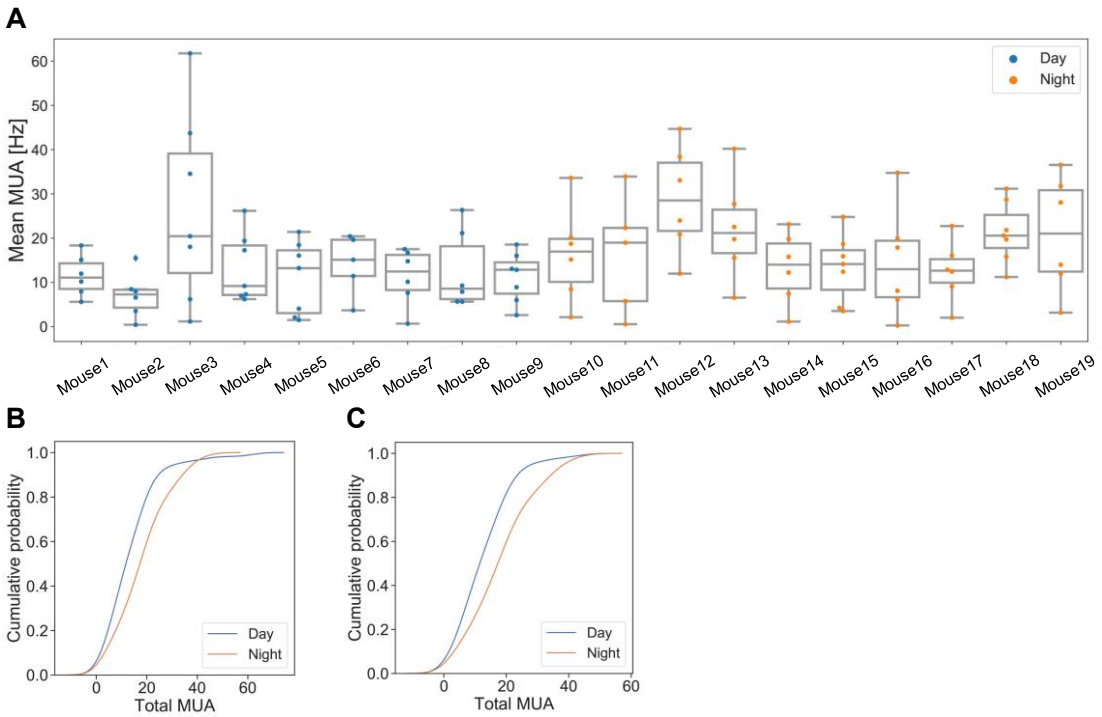

Figure 4.2: Medial habenula exhibits elevated MUA during the night

(A) Scatter plots of the mean MUA in the MHb in 'Day' (9 mice) and 'Night' (10 mice) groups. Each dot represents the mean MUA detected at individual electrodes or sites. Box plots indicate the distribution of data in four quartiles around the median and demonstrate the outliers. (B) Comparison of the cumulative probability distributions of mean MUA for 'Day' and 'Night' groups: the mean MUA during the night was significantly higher than during the day. (C) Comparison of the cumulative probability distributions of mean MUA for 'Day' and 'Night' groups excluding the 'physiological outlier': the mean MUA during the night was significantly higher than during the day, with more apparent difference.

In the LHb, the overall mean MUA was 2.54 Hz in the 'Day' group (*N* = 9 mice; 95% CI [1.34, 3.73]) and 5.31 Hz in the 'Night' group (*N* = 10 mice; 95% CI [2.92, 7.70]) (Fig. 4.3 A). Further comparison of the distributions of the mean MUA exhibited by the two groups showed significant increase in the mean MUA during the night (Fig. 4.3 B; KS test: D = 0.286, p < 0.001). However, similar to the MHb, the individual data distribution around the median, revealed two statistical outliers, which oddly exhibited relatively high MUA (above 40 Hz) in relation to the rest of the values acquired by the same individual (Fig. 4.3 A: 'Night' group – Mouse11). In order to confirm that the difference between the two distributions is not mainly influenced by the presence of the two outliers, the comparative analysis was also performed excluding these two values. The KS test confirmed the mean MUA remained significantly higher during the night, with relatively smaller difference between the two distributions (Fig. 4.3 C; KS test: D = 0.282, p < 0.001).

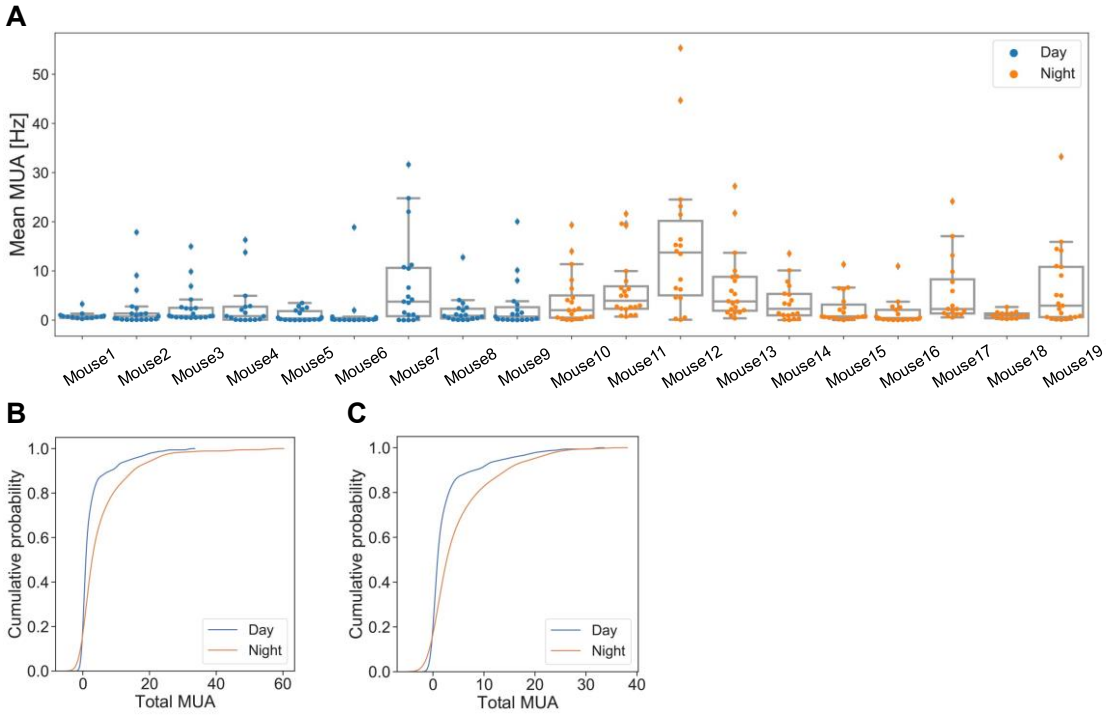

Figure 4.3: Lateral habenula exhibits elevated MUA during the night

(A) Scatter plots of the mean MUA in the LHb in 'Day' (9 mice) and 'Night' (10 mice) groups. Each dot represents the mean MUA detected at individual electrodes. Box plots indicate the distribution of data in four quartiles around the median and demonstrate the outliers. (B) Comparison of the cumulative probability distributions of mean MUA for 'Day' and 'Night' groups: the mean MUA during the night was significantly higher than during the day. (C) Comparison of the cumulative probability distributions of mean MUA for 'Day' and 'Night' groups excluding the outliers: the mean MUA during the night was significantly higher than during the day.

In order to examine the topographic distribution of the day-night differences in habenula MUA, the difference between 'Day' and 'Night' mean MUA, referred to as ΔMUA, was calculated at each recording site, as 'Night' mean MUA – 'Day' mean MUA. Collectively, the night elevation was most apparent in the MHb near the MHb-LHb border, specifically at the electrode 45 (E45), with the mean difference of 7.42 Hz (bootstrap 95% CI [-0.91, 15.4]) (Fig. 4.4). However, the largest elevation of 8.28 Hz (bootstrap 95% CI [1.92, 16.30]) was found in the lateral portion of the LHb

(E51) (Fig. 4.4). A single recording site in the LHb (E83), which appeared close to the FR, exhibited lower mean MUA during the night than during the day, with the mean difference of -3.09 Hz (bootstrap 95% CI [-10.10, 1.07]) (Fig. 4.4). However, the statistical comparison of 'Day' and 'Night' groups using the Mann-Whitney test revealed no statistically significant difference at all three analysed sites (Mann-Whitney test p values: E45: p = 0.131; E51: p = 0.111; E83: p = 1.00).

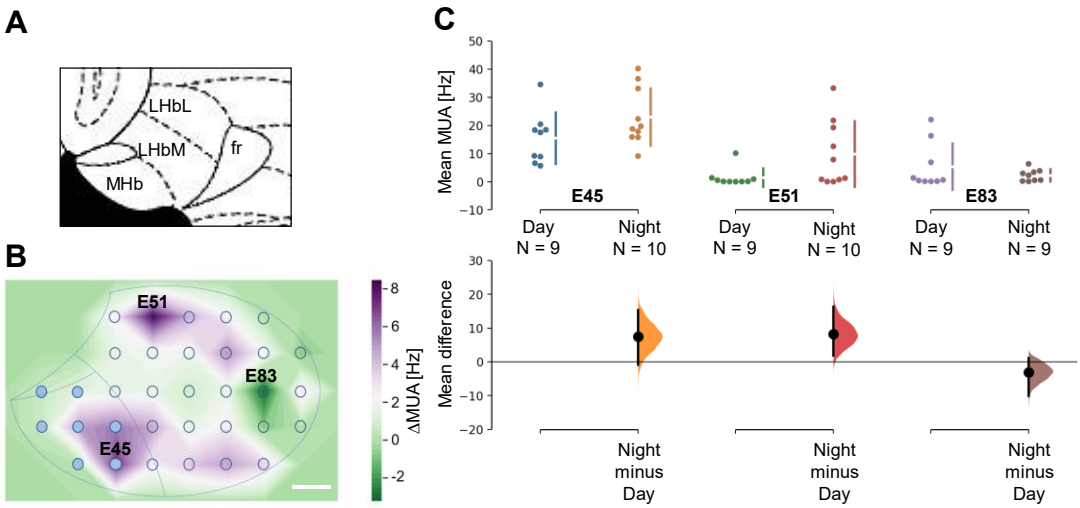

Figure 4.4: Topographic distribution of day-night differences in the habenula MUA

(A) A diagrammatic representation of the habenula (distance from bregma ~ -1.90 mm; taken from the Paxinos and Franklin's mouse brain atlas) was used as a reference to map the day-night MUA differences in specific subregions of the habenula. MHb: medial habenula; LHbM: lateral habenula, medial part; LHbL: lateral habenula, lateral part; fr: fasciculus retroflexus. (B) Contour plot displays the ΔMUA at specific recording sites. Purple/green areas represent regions of increased/decreased MUA when the 'Day' mean is subtracted from the 'Night' mean. Filled and empty circles indicate electrodes in contact with the MHb and LHb, respectively. E45: electrode 45; E51: electrode 51; E83: electrode 83. Scale bar: 100 µm. (C) The mean differences for day-night comparisons at E45, E51 and E83 electrodes are shown in the Cumming estimation plot. The raw data is plotted on the upper axes; each dot representing the mean MUA (per mouse); gapped vertical lines to the right of each group indicate mean ± SD. Each mean difference is plotted on the lower axes as a bootstrap sampling distribution. Mean differences are depicted as black dots; 95% CIs are indicated by the vertical error bars.

Lateral, but not medial, habenula exhibits elevated single-unit activity at night

In order to investigate whether the night elevation in the MUA was a consequence of increased firing of individual neurons or increased number of neurons firing in the vicinity of the recording electrodes, single-unit activity (SUA), representing AP firing of individual neurons, was extracted and analysed from the filtered thresholded data. This was done by principal component analysis (PCA)-based spike sorting: first the detected spikes were aligned at their peak point and the principal components (PCs) of the aligned spikes were obtained via PCA-based feature extraction (Yu *et al.*, 2012). The PCs are orthogonal vectors which capture directions in the data of the largest variation (Adamos *et al.*, 2008). The first two PCs were used to generate low dimensional feature space, into which the aligned spikes were projected. In the feature space, the inherent characteristics of spikes were highlighted and clusters of different data units, corresponding to

individual neurons, were revealed at the recording sites in both MHb (Fig. 4.5 A) and LHb (Fig. 4.5 B). However, it should be noted that in some cases the first two or three PCs failed to clearly reveal the specific clusters (Fig. 4.5 C). This limitation was primarily encountered during the analysis of the MHb and could be associated with the higher neuronal density found in this area.

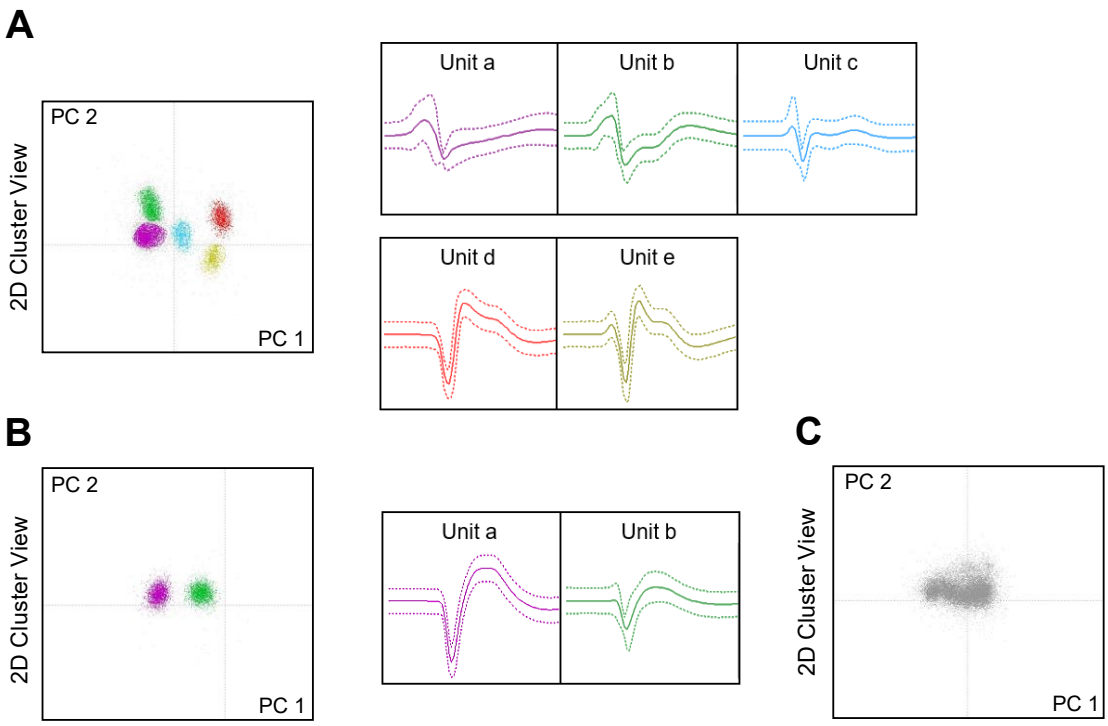

Figure 4.5: Identification of single units

Single units were identified via PCA-based spike sorting. Spikes detected at single electrodes in the (A) MHb and (B) LHb were projected into the feature space generated by the first two PCs where clusters corresponding to individual data units were visualised and isolated. Each cluster was assigned a colour. The diagrams on the right-hand side of the feature space plots demonstrate the average waveforms corresponding to specific clusters according to their colour (dashed lines indicate ± 3 SDs). (A) Five clusters were identified at a representative electrode in the MHb, corresponding to five units of different waveforms. (B) Two clusters were identified at a representative electrode in the LHb, corresponding to two units of different waveforms. (C) Example of spike data from a single electrode in the MHb, projected into the feature space where the clusters could not be clearly identified. PC1: principal component 1; PC 2: principal component 2.

Following the discrimination of the single units, the 15-min time window of the most stable spontaneous activity was used to calculate the temporal mean SUA in order to compare the SUA between day and night recordings and to determine whether the night elevation of the MUA was associated with increased firing of individual data units.

The overall mean rate of SUA in the MHb was 2.83 Hz in the 'Day' group (*N* = 7 mice; 95% CI [2.38, 3.27]) and 4.38 Hz in the 'Night' group (*N* = 6 mice; 95% CI [3.51, 5.25]) (Fig. 4.6 A). Nevertheless, the two distributions of the mean SUA rate were not significantly different (Fig. 4.6 B; KS test: D = 0.143, p = 0.111). This result indicated that the night increase in MUA could be associated with increased number of units contributing to the MUA, rather than with the increased

SUA. In order to address this hypothesis, the number of discriminated single units per electrode was calculated. On average, the number of units per each electrode was 3.37 (*N* = 43 electrodes; 95% CI [13.01, 3.73]) during the day and 3.51 (*N* = 37 electrodes; 95% CI [3.11, 3.91]) during the night. The comparison of the distributions of the two datasets showed no significant difference between day and night (Fig. 4.6 C; KS test: D = 0.095; p = 0.991). One possible explanation for inconsistent results acquired from the SUA analysis could be associated with the inaccurate identification of clusters and potential loss of data as in some cases, projection of spikes into the feature space did not generate evident clusters. Therefore, there is a possibility that the day-night difference in MUA was associated with night elevation in activity of unsorted events.

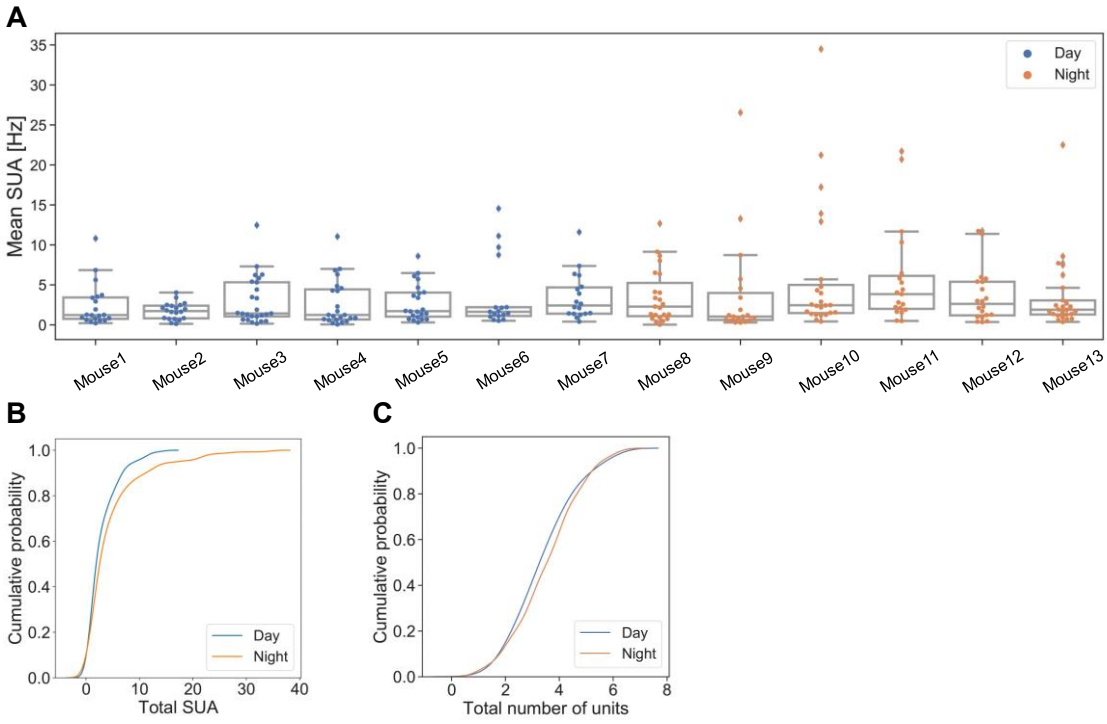

Figure 4.6: Medial habenula exhibits similar levels of SUA during the day and night

(A) Scatter plots of the mean SUA rate in the MHb in 'Day' (7 mice) and 'Night' (6 mice) groups. Each dot represents the temporal mean of SUA. Box plots indicate the distribution of data in four quartiles around the median and demonstrate the outliers. (B) Comparison of the cumulative probability distributions of mean SUA for 'Day' and 'Night' groups: the two distributions were not significantly different. (C) Comparison of the cumulative probability distributions of number of units per electrode for 'Day' and 'Night' groups: the two distributions were not significantly different.

In the LHb, the overall mean rate of SUA was 1.63 Hz during the day (*N* = 7 mice; 95% CI [0.45, 2.81]) and 3.68 Hz during the night (*N* = 6 mice; 95% CI [1.99, 5.37]) (Fig. 4.7 A). Subsequent comparison of the two distributions revealed significant increase in the mean SUA during the night (Fig. 4.7 B; KS test: D = 0.331, p < 0.001). In addition, the two distributions were significantly different after excluding a physiological outlier, detected in the 'Night' group (Fig. 4.7 A: Mouse10) which exhibited unusually high activity of ~ 50 Hz (Fig. 4.7 C; KS test: D = 0.329, p < 0.001). Additionally, in order to determine whether the number of units per electrode was also elevated during the night, the number of discriminated single units was calculated per each electrode in

the LHb. The mean number of units per electrode was 1.48 (*N* = 122 electrodes; 95% CI [1.37, 1.60]) during the day and 1.64 (*N* = 115 electrodes; 95% CI [1.50, 1.77]) during the night. However, the distributions for the two datasets were not significantly different (Fig. 4.7 D; KS test: D = 0.111, p = 0.432). Collectively, these results indicate that the night elevation of the LHb MUA is primarily mediated by the increase in SUA.

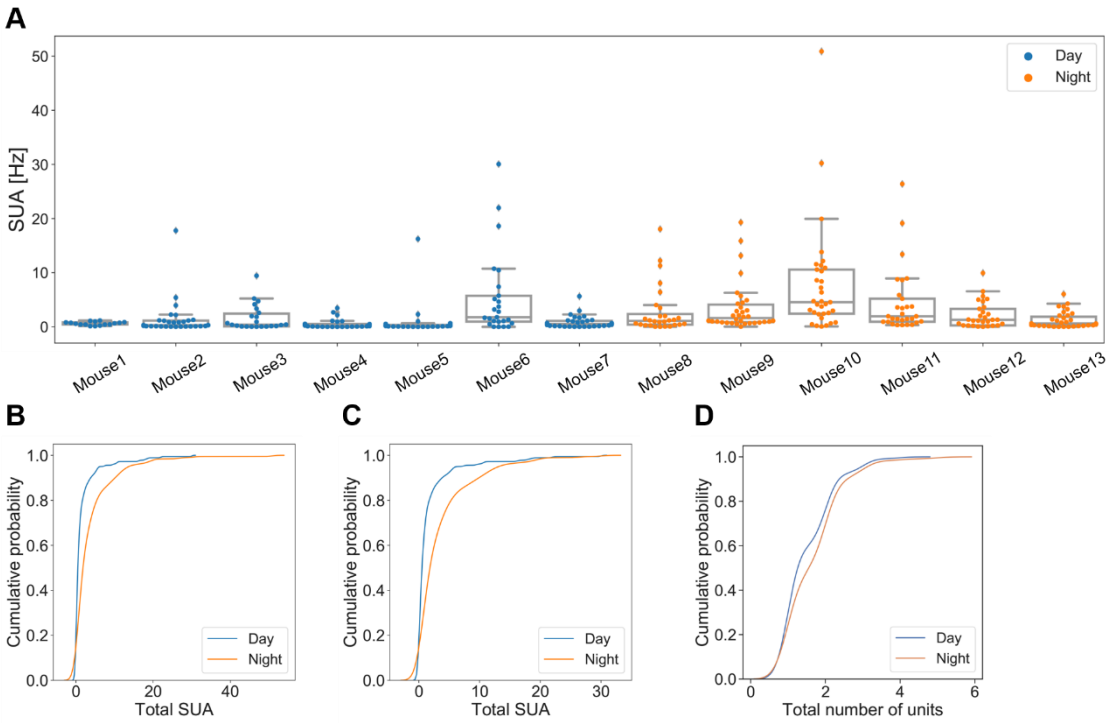

Figure 4.7: Lateral habenula exhibits elevated SUA during the night

(A) Scatter plots of the mean SUA rate in the LHb in 'Day' (7 mice) and 'Night' (6 mice) groups. Each dot represents the temporal mean of SUA. Box plots indicate the distribution of data in four quartiles around the median and demonstrate the outliers. (B) Comparison of the cumulative probability distributions of mean SUA for 'Day' and 'Night' groups: the mean SUA during the night was significantly higher than during the day. (C) Comparison of the cumulative probability distributions of mean SUA for 'Day' and 'Night' groups excluding the outliers: the mean SUA during the night was significantly higher than during the day. (D) Comparison of the cumulative probability distributions of number of units per electrode for 'Day' and 'Night' groups: the two distributions were not significantly different.

Additionally, the topographic distribution of the day-night differences in the habenula SUA was examined. Similar to the analysis of the MUA, the difference between the day and night mean SUA, referred to as ΔSUA, was calculated by subtracting the 'Day' mean SUA from the 'Night' mean SUA for each electrode site. The night elevation remained most prominent in the lateral portion of the LHb (Fig. 4.8).

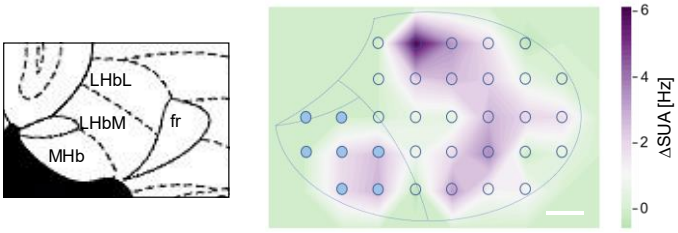

Figure 4.8: Topographic distribution of day-night differences in the habenula SUA

Left: diagrammatic representation of the habenula (distance from bregma ~ -1.90 mm; taken from the Paxinos and Franklin's mouse brain atlas) was used as a reference to allocate the day-night differences to specific subregions of the habenula. LHbM: lateral habenula, medial part; LHbL: lateral habenula, lateral part; fr: fasciculus retroflexus. Right: contour plot depicts topographic distribution of the ΔSUA [Hz]. Purple/green areas represent regions of increased/decreased SUA when the 'Day' mean is subtracted from the 'Night' mean. Filled and empty circles indicate electrodes in contact with the MHb and LHb correspondingly. Scale bar: 100 µm.

In conclusion, these findings showed that the MUA in both MHb and LHb is significantly elevated during the night, while only the LHb exhibits significantly higher SUA at night. In addition, a similar number of units discriminated per each electrode was found during the day and night in both MHb and LHb. Therefore, in the LHb the night elevation in MUA is likely associated with increased activity of single units, while this was not the case in the MHb. Overall, the single-unit analysis in the MHb did not replicate the results from the multi-unit analysis, which might be due to inaccurate discrimination of units specifically in this area. This indicates that it is important to consider findings from both types of analysis when assessing the day-night differences in electrical activity.

Vasopressin fibres innervate lateral habenula

Previous neuroanatomical studies have demonstrated immunostaining for AVP in mouse and rat habenula (Buijs, 1980; Rood and De Vries, 2011; Zhang *et al.*, 2016). In agreement with these studies, AVP-immunoreactive fibres were found throughout rostral to caudal divisions of the mouse habenula, specifically in the medial subdivision of the LHb alongside the border between the LHb and MHb (*N* = 6 brain sections). The innervation was concentrated at the mid- level of the habenula while rostral and caudal levels were innervated to a lesser extent (Fig. 4.9 A2, B2, C2).

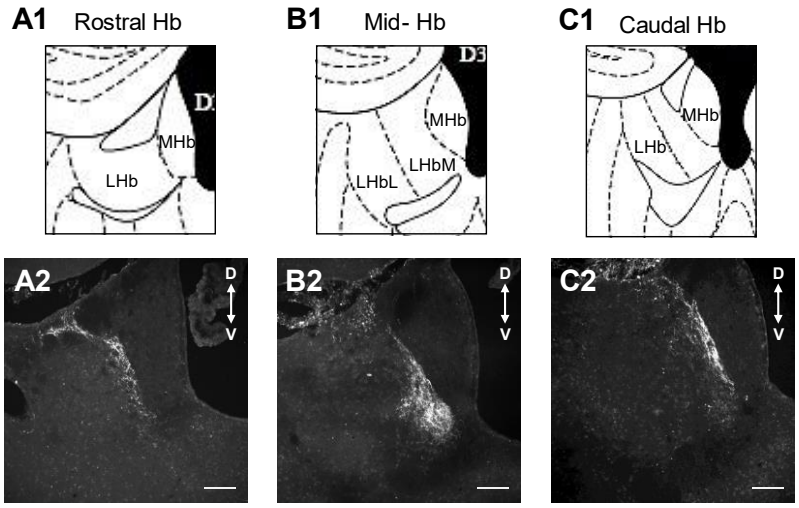

Figure 4.9: Distribution of AVP-immunopositive fibres through the rostro-caudal extent of the mouse habenula

(A1 – C1) Diagrammatic representation of habenula coronal sections (distance from bregma ~ -1.40 mm − -1.90 mm; taken from the Paxinos and Franklin's mouse brain atlas) were used as a reference to allocate the AVP innervation to specific subregions of the habenula. MHb: medial habenula; LHbM: lateral habenula, medial part; LHbL: lateral habenula, lateral part. (A2 – C2) Distribution of the AVP innervation at rostral, mid- and caudal level. Collapsed confocal image stacks take at 20x magnification. D = dorsal; V = ventral. Scale bar: 100 µm.

Vasopressin induces excitation in the lateral habenula

Following identification of AVP immunopositive fibres in the LHb, modulation of LHb electrical activity by this neuropeptide was further investigated using extracellular recordings. These recordings were performed using a perforated MEA (6 x 10 layout) and acute brain slices containing the habenula. Local field potentials were recorded during spontaneous or baseline activity, followed by bath application of AVP (20 µM). Raw data was filtered, and spikes were detected and isolated from the noise using a threshold of -17.5 µV applied at each electrode (Fig. 4.10 A). The MUA was calculated as spikes detected per second, and the data was smoothed in order to eliminate short-term variations in the histogram data and for the peak of the response to become more evident (Fig. 4.10 B). In general, AVP induced elevations in MUA, indicating excitatory action at specific sites in the LHb (Fig. 4.10 B). This could be attributed to elevation of SUA (of the same units which were active during the baseline; Fig. 4.10 C) or to an increase in the number of active units in the vicinity of the electrode. However, it is difficult to interpret such data as a firing neuron, represented by a cluster of spikes in the feature space, can change the shape of AP waveform as a result of AVP modulation. This could generate additional cluster in the feature space, suggesting a new, previously silent, neuron was activated. Therefore, since PCA-based spike-sorting could lead to misinterpretation of the data, the MUA, exclusively, was used for the further analysis.

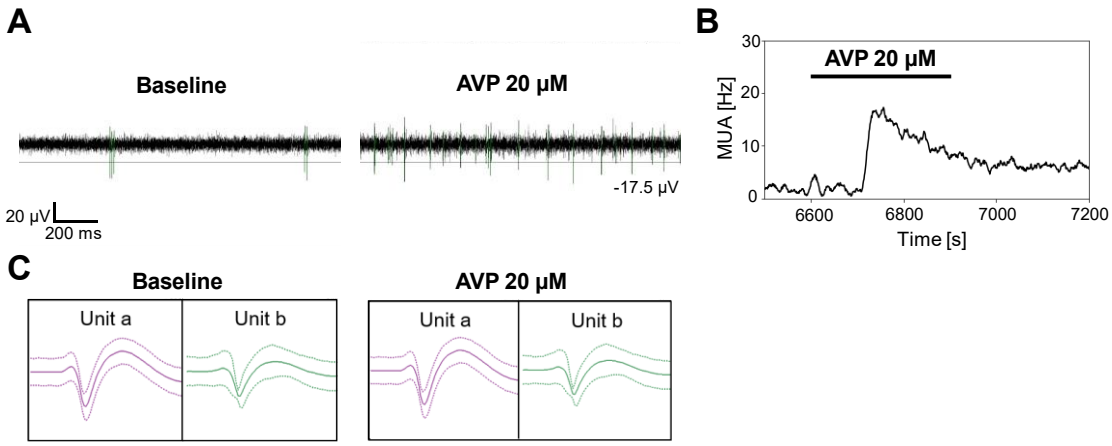

Figure 4.10: Vasopressin induces excitation in the LHb

Excitatory action of AVP neuropeptide was observed as elevation in MUA. (A) Example of filtered data trace detected at a single electrode during the baseline and application of AVP (20 µM). Spikes were detected using the threshold of -17.5 µV. Green colour indicates the detected spikes. (B) Example of smoothed MUA histogram demonstrates variations in MUA before, during and after 5-min long application of AVP (indicated by a black bar) measured at a single electrode in contact with the LHb. (C) Example of PCA-based spike sorting during the baseline and application of AVP at the same electrode as shown in A and B. Two data units were discriminated within ~3-min long time window during the baseline and two units of the same waveform were detected after the application of AVP indicating that at this particular electrode AVP potentially increased firing of the same units which were active during the baseline.

Vasopressin modulation of the lateral habenula vary between day and night

The occurrence of an AVP response at a specific electrode was statistically determined by calculating the temporal mean MUA during 3 minutes of stable baseline activity and during 20 seconds of peak response to AVP application at each electrode. The time window for the baseline was selected in order to capture sufficient information about the activity recorded prior to drug application, including standard deviation. Whereas the time window for the peak response was determined considering the temporal dynamics of AVP responses (longer time windows could capture the decay of the response). If the difference between the mean MUA during the peak response to AVP and mean MUA during the baseline, plus two times its standard deviation, was positive, then an electrode was considered as a 'responder'. Only some sites exhibited a response to AVP within each LHb slice during the day and night and those sites were used to calculate the AVP effect (Fig. 4.11 A, B). Overall, during the day AVP induced a significant increase in MUA by 3.31 Hz (N = 7 slices; bootstrap 95% CI [0.19, 7.77]; Wilcoxon paired t-test: p = 0.018). In addition, during the night AVP induced an increase in MUA by 3.48 Hz (N = 4 slices; bootstrap 95% CI [-4.61, 11.90]), although this difference was not statistically significant (Wilcoxon paired t-test: p = 0.068) (Fig. 4.11 C). In order to determine whether the differences between baseline and AVP MUA were different between day and night, the mean difference between baseline and AVP (∆MUA) was calculated for each slice and 'Day' and 'Night' groups were compared (Fig. 4.11 D). Overall, the ∆MUA in the 'Night' group was higher by 0.17 Hz (bootstrap 95% CI [-3.08, 3.53]). However, a Mann-Whitney test showed the two groups were not significantly different (p = 0.777).

On the other hand, comparison of the % of responders per each LHb showed that during the day the % of LHb responders is significantly higher by 38.9% (bootstrap 95% CI [-51.10, -21.50]; Mann-Whitney test: $p = 0.011$) (Fig. 4.11 E). These results indicate that the AVP exerts similar effect on the MUA during day and night, but at night it may influence smaller and more specific neuronal population within the LHb.

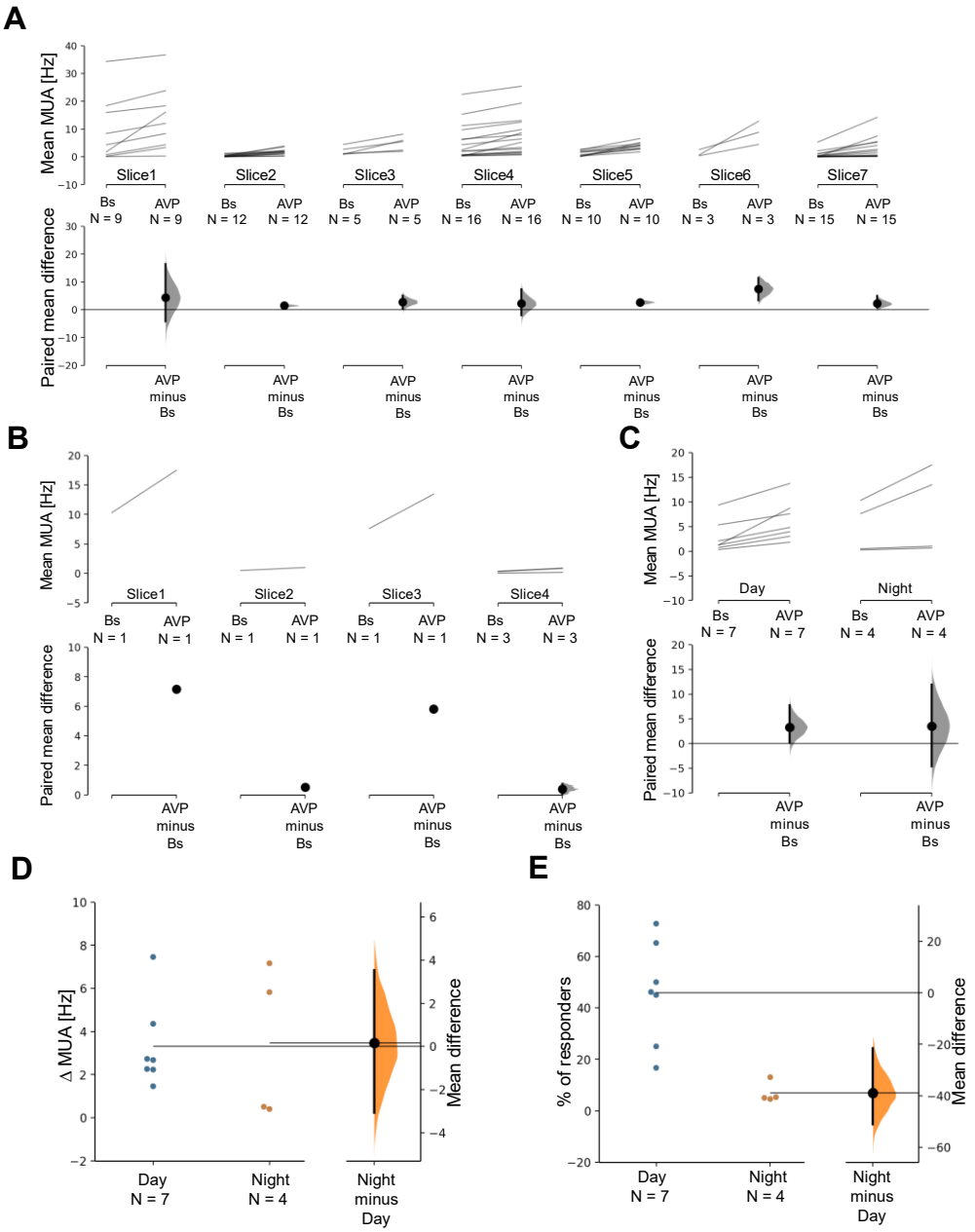

Figure 4.11: Vasopressin induces a similar effect on LHb MUA during day and night but activates smaller number of LHb sites at night

(A-B) The paired mean differences for each slice are shown in the Cumming estimation plot. The raw data is plotted on the upper axes, where N indicates number of responders in each slice. The baseline (Bs) MUA values are paired with corresponding AVP MUA values by a black line. On the lower axes, each paired mean difference is plotted as a bootstrap sampling distribution. Mean differences are depicted as dots; 95% CIs are indicated by the ends of the vertical error bars. (A) Cumming estimation plot demonstrates slices monitored during the day. (B) Cumming estimation plot demonstrates slices monitored during the night. (C) Cumming estimation plot depicts paired mean differences for the day and night recordings: N indicates number of slices for each group. (D-E) The Gardner-Altman estimation plots demonstrate the mean difference between Day and Night groups. The raw data is plotted on the left axis: each dot represents a value obtain from one slice. The mean difference is plotted on the right axis as a bootstrap sampling distribution. Mean difference is depicted as dots; 95% CIs are indicated by the ends of the vertical error bars. (D) The estimation plot demonstrates the mean difference in ΔMUA between day and night. (E) The estimation plot demonstrates the mean difference in % of responders per each LHb slice between day and night.

Topographic distribution of AVP effect in the LHb varies during day and night

In order to determine whether AVP affects the same subregions of the LHb during day and night, the topographic distribution of AVP responses in the LHb was examined for day and night recordings individually. This was done by measuring the magnitude of the excitatory response induced by AVP as the mean ΔMUA (calculated by subtracting the Baseline MUA from the AVP MUA; mean ΔMUA was calculated as an average of all slices) at each electrode site. The analysis revealed that during the day similar excitatory responses were found across the whole LHb, including the medial and lateral subregions. In contrast, during the night the excitatory responses were much more concentrated within the medial subregion of the LHb (LHbM; Fig. 4.12 B). Furthermore, the probability of an AVP response was calculated at each electrode site, revealing that during the day the probability of detecting a response to AVP was evidently higher, particularly in the LHbM. This was not the case during the night, when the probability of AVP response appeared much lower at any recording site (Fig. 4.12 C).

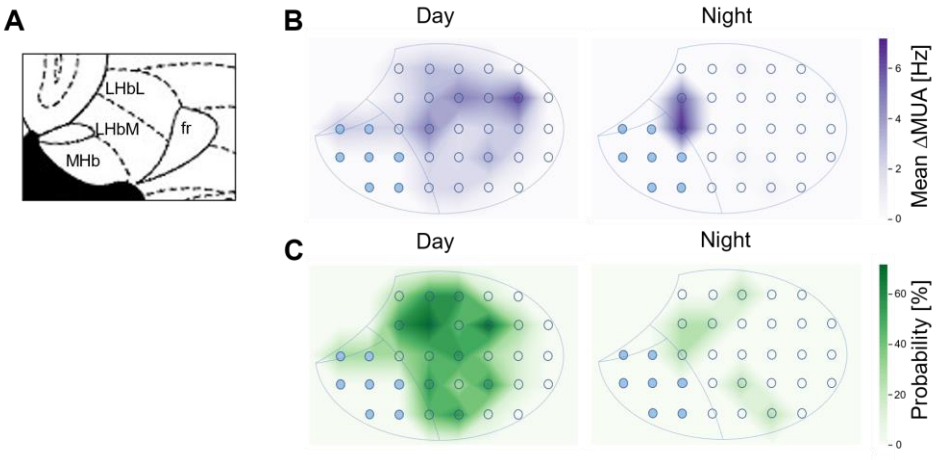

Figure 4.12: Topographic distribution of excitatory responses induced by AVP in the LHb during day and night

(A) A diagrammatic representation of the habenula (distance from bregma ~ -1.90 mm; taken from the Paxinos and Franklin's mouse brain atlas) was used as a reference to allocate AVP responses to specific subregions of the habenula. MHb: medial habenula; LHbM: lateral habenula, medial part; LHbL: lateral habenula, lateral part; fr: fasciculus retroflexus. (B) Contour plot demonstrates the topographic distribution of the mean ΔMUA [Hz] during the day and night. Increasing intensities of purple represent increasing ΔMUA. (C) Contour plot displays the topographic distribution of AVP response probability [%]. Increasing intensities of green represent increasing probability. Filled and empty circles indicate electrodes in contact with the MHb and LHb, correspondingly.

Oxytocin induces excitation in the lateral habenula

The neuropeptide AVP binds to both OTRs and V1a receptors, interacting with the former with significantly less affinity when compared to the latter. Moreover, we observed that AVP reliably induced responses in the LHb only at relatively high concentrations, while the neighbouring subregions of the thalamus – prominent sites of V1a receptor expression – were always excited at lower concentrations. As a consequence of this dose dependency of response and the

pharmacological profile of the receptors involved, we sought to examine a potential role for OTRs in the neuromodulation of the LHb. Similar to AVP, bath application of OT (500 nM) induced an increase in MUA at specific sites within the LHb (Fig. 4.13 A, B). The OT-induced increase in MUA can be associated with an increase in firing of single units or an increase in the number of firing units in the vicinity of an electrode, as demonstrated by Figure 4.13 C. However, as discussed in the previous section, due to the potential risk of misinterpreting SUA data, only MUA was used for further analysis of the OT effect in the LHb.

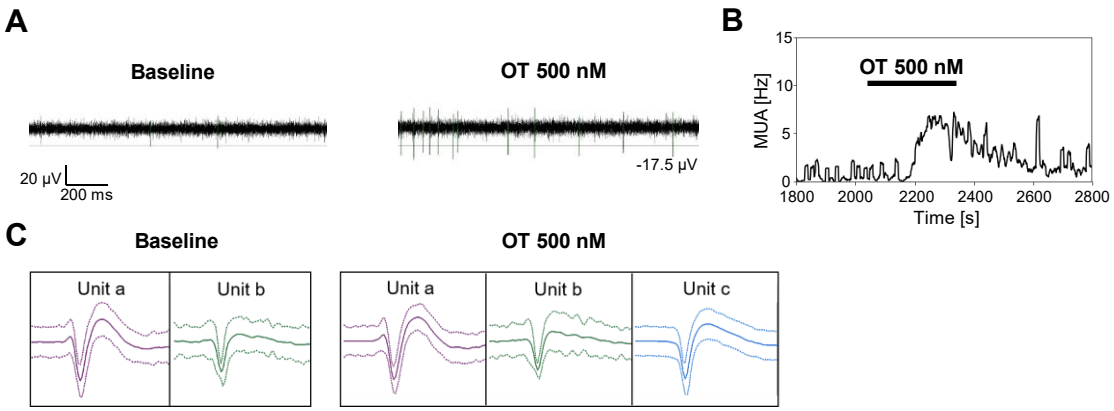

Figure 4.13: Oxytocin induces excitation in the LHb

Oxytocin-induced excitation was observed as an elevation in MUA. (A) Example of filtered data trace detected at a single electrode during the baseline and application of OT (500 nM). Spikes were detected using the threshold of -17.5 µV. Green colour indicates the detected spikes. (B) Example of smoothed MUA histogram demonstrates variations in MUA before, during and after 5-min long application of OT (indicated by a black bar) measured at a single electrode in contact with the LHb. (C) Example of PCA-based spike sorting during the baseline and application of OT at the same electrode as shown in A and B. Two data units were discriminated within ~3-min long time window during the baseline, whereas three units were discriminated after the application of OT.

Oxytocin induces similar excitatory effect in the lateral habenula during day and night

In order to investigate whether OT signalling is involved in the circadian modulation of LHb neuronal activity, the impact of OT on LHb MUA was measured during day and night. The occurrence of OT responses at specific electrode sites in the LHb was first statistically determined at each electrode site using the same method applied for the analysis of AVP responses (a site was determined as a 'responder' if the difference between the mean MUA during the baseline, plus two times its standard deviation, and the mean MUA during the OT application, was positive). The electrode sites classified as responders were further used to calculate the excitatory effect of OT during the day and night. Overall, during the day OT application induced significant increase in MUA by 2.65 Hz (*N* = 6 slices; bootstrap 95% CI [-0.21, 5.14]; Wilcoxon paired t-test: p = 0.028) (Fig. 4.14 A, C). Similarly, OT induced significant increase in MUA by 3.63 Hz (*N* = 6 slices; bootstrap 95% CI [-1.46, 10.10]; Wilcoxon paired t-test: p = 0.028) during the night (Fig. 4.14 B, C). In order to determine whether the excitatory effect of OT varied between the two time points,

the mean ΔMUA was calculated for each slice by subtracting the mean MUA during baseline from the mean MUA during OT application and the 'Day' and 'Night' groups were compared. This comparison showed that the mean ΔMUA was higher by 0.98 Hz during the night (bootstrap 95% CI [-0.82, 4.43]), but the two groups were not significantly different (Mann-Whitney test: $p = 0.936$) (Fig. 4.14 D). However, it should be pointed out that this slight elevation might be attributed to a single ΔMUA value in the 'Night' group which outlies the rest of the value within the same group (this outlier was excluded for the further analysis involving topographic mapping of OT responses within the LHb – see later section). Furthermore, % of responders per each LHb slice was not significantly different between day and night (bootstrap 95% CI [-11.10, 6.78]; Mann-Whitney test: $p = 0.423$) (Fig. 4.14 E).

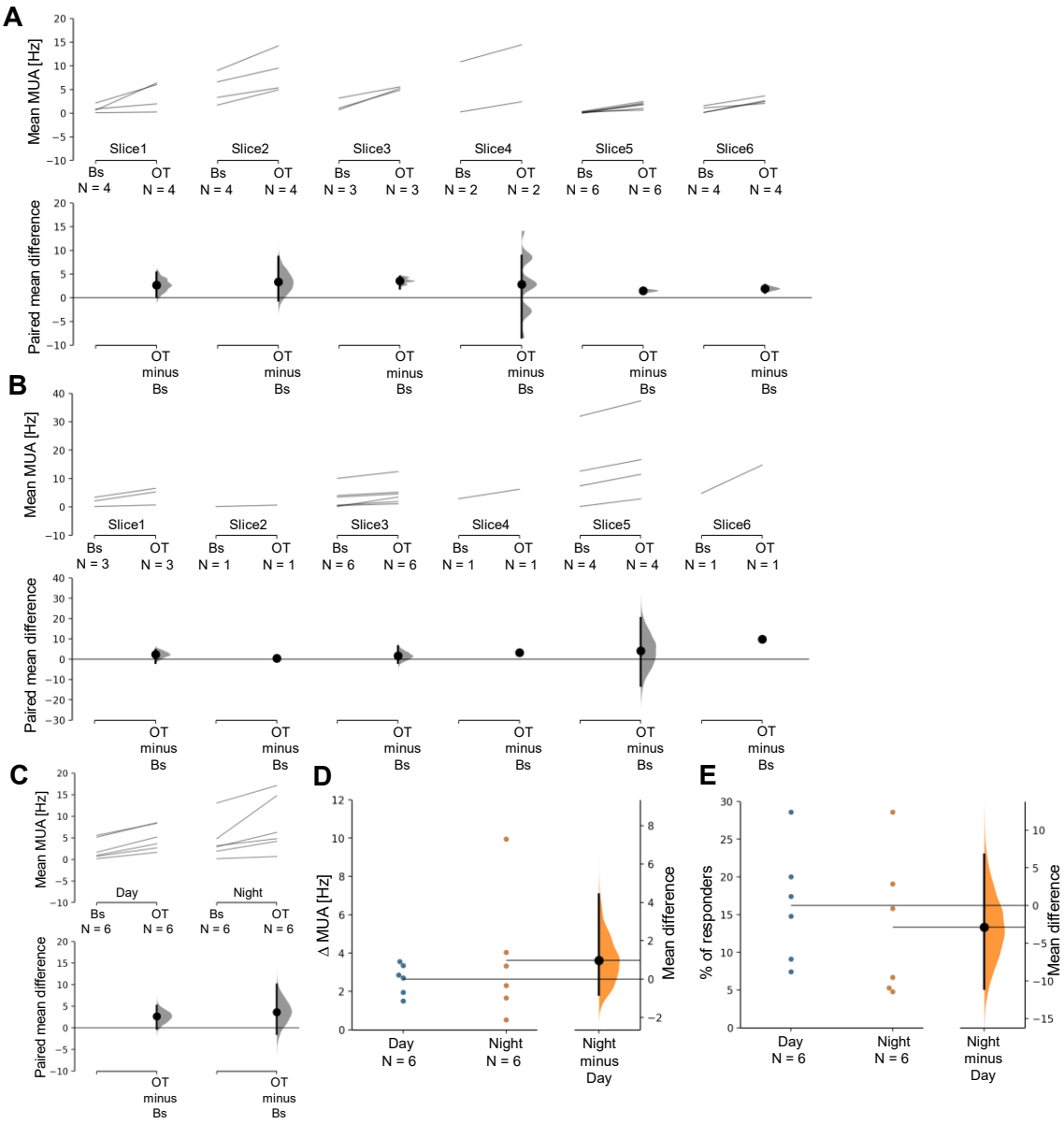

Figure 4.14: Oxytocin induces similar effect on LHb MUA during day and night

(A-B) The paired mean differences for each slice are shown in the Cumming estimation plot. The raw data is plotted on the upper axes, where N indicates number of responders in each slice. The baseline (Bs) MUA values are paired with corresponding OT MUA values by a black line. On the lower axes, each paired mean difference is plotted as a bootstrap sampling distribution. Mean differences are depicted as dots; 95% CIs are indicated by the ends of the vertical error bars. (A) Cumming estimation plot demonstrates slices monitored during the day. (B) Cumming estimation plot demonstrates slices monitored during the night. (C) Cumming estimation plot depicts paired mean differences for the day and night recordings: N indicates number of slices for each group. (D-E) The Gardner- Altman estimation plots demonstrate the mean difference between 'Day' and 'Night' groups. The raw data is plotted on the left axis: each dot represents a value obtain from one slice. The mean difference is plotted on the right axis as a bootstrap sampling distribution. Mean difference is depicted as dots; 95% CIs are indicated by the ends of the vertical error bars. (D) The estimation plot demonstrates the mean difference in ΔMUA between day and night. (E) The estimation plot demonstrates the mean difference in % of responders per each LHb slice between day and night.

Topographic distribution of OT-mediated excitatory responses in the LHb varies between day and night

As shown by the previous results, the magnitude of the OT-induced responses as well as the % of the responding sites in the LHb does not differ between day and night. However, in order to determine whether OT acts within the same subregions of the LHb during day and night, the topographic distribution of OT-mediated responses in the LHb was mapped during the two time points. First, the topographic distribution of the response magnitude was mapped by calculating the mean ΔMUA (ΔMUA = OT MUA – Baseline MUA; mean ΔMUA was calculated as average of all slices) for each electrode site. This analysis showed that during the day the largest OT-induced responses were primarily observed in the LHbM, while at night the largest responses to this neuropeptide occurred mostly within the lateral subregion of the LHb (LHbL) (Fig. 4.15 B). In addition, the probability of the response was calculated at each electrode site. The probability map revealed that the LHbM is more likely to exhibit a response to OT during the day, whereas most responses observed during the night occurred in the LHbL (Fig. 4.15 C). Collectively, these results indicate a possibility that OT affects distinct neuronal populations during day and night.

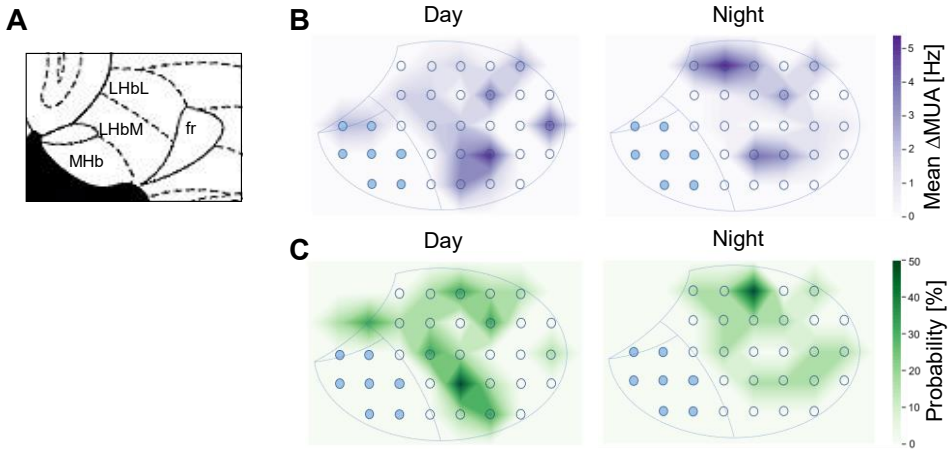

Figure 4.15 Topographic distribution of excitatory responses induced by OT in the LHb during day and night

(A) A diagrammatic representation of the habenula (distance from bregma ~ -1.90 mm; taken from the Paxinos and Franklin's mouse brain atlas) was used as a reference to allocate OT-induced responses to specific subregions of the habenula. MHb: medial habenula; LHbM: lateral habenula, medial part; LHbL: lateral habenula, lateral part; fr: fasciculus retroflexus. (B) Contour plot depicts the topographic distribution of the mean ΔMUA [Hz] difference during the day and night. Increasing intensities of purple represent increasing ΔMUA. (C) Contour plot demonstrates the topographic distribution of the response probability [%]. Increasing intensities of green represent increasing probability. Filled and empty circles indicate electrodes in contact with the MHb and LHb correspondingly.

Lateral habenula exhibits OTR-mediated excitation

Since OT binds to V1 receptors – although with 100 times less affinity than with which it binds to OTRs – the possibility that the excitatory effect was mediated via OTRs, exclusively, was investigated in the LHb. This was achieved by the bath application of the OTR specific agonist

TGOT during day recordings of MUA in the LHb (*N* = 6 slices harvested from 4 mice). Similar to OT, the administration of TGOT (500 nM) induced excitatory responses, observed as elevated MUA at specific sites within the LHb (Fig. 4.16 A). Overall, the application of TGOT significantly increased MUA by 2.05 Hz (*N* = 6 slices; bootstrap 95% CI [-0.31, 4.80]; Wilcoxon paired t-test: p = 0.028; Fig. 4.16 B). However, it should be noted that the topographic patterning of TGOT responses – being more evenly distributed throughout the LHb – lacked apparent spatial restriction of those observed following the application of OT (Fig. 4.16 C, D). Nonetheless, the presence of TGOT-induced excitations indicates that the previously observed excitatory responses evoked by OT and AVP are likely to be mediated via OTRs.

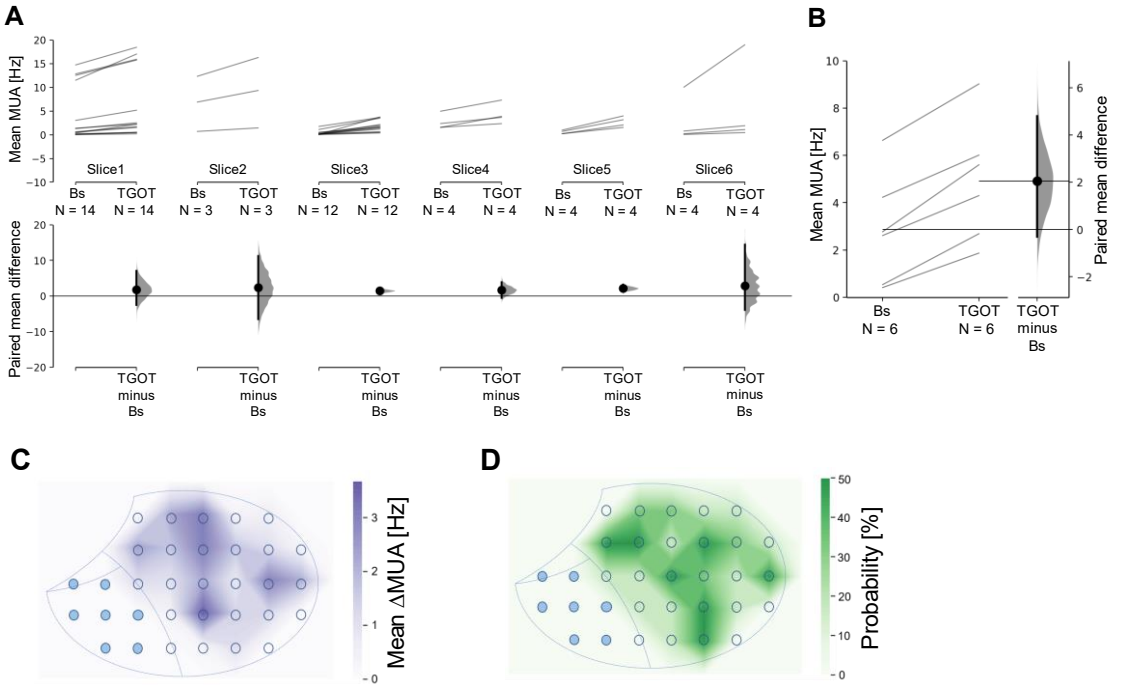

Figure 4.16: Selective OTR agonist TGOT induces excitation in the LHb

(A) Cumming estimation plot demonstrates the paired mean differences between the baseline (Bs) and TGOT MUA for each slice. The raw data is plotted on the upper axes, where N indicates number of responders in each slice. The Bs MUA values are paired with corresponding TGOT MUA values with a black line. On the lower axes, each paired mean difference is plotted as a bootstrap sampling distribution. Mean differences are depicted as dots; 95% CIs are indicated by the ends of the vertical error bars. (B) Gardner-Altman estimation plot shows the paired mean difference between the Bs and TGOT MUA. Paired sets of observations are plotted on the left axis, where N indicates number of slices. The paired mean difference is plotted on the right axis as a bootstrap sampling distribution. The mean difference is depicted as a dot; the 95% CI is indicated by the ends of the vertical error bars. (C) Contour plot demonstrates the topographic distribution of the mean ΔMUA [Hz]. Increasing intensities of purple represent increasing ΔMUA. (C) Topographic distribution of the response probability [%]. Increasing intensities of green represent increasing probability. Filled and empty circles indicate electrodes in contact with the MHb and LHb correspondingly.

To more directly examine their TGOT responsiveness, whole-cell patch clamp recordings of LHb neurons were performed. These data revealed that LHb neurons possess a number of active conductances, including the slowly activating, slowly inactivating, mixed cationic conductance, I_H

(Biel *et al.*, 2009) and the rapidly activating, low voltage activated Ca^{2+} conductance, I_T (Cain and Snutch, 2013) (Fig. 4.17 – figure made by Dr. David Lyons). This combination of electrophysiological conductances is often associated with neuronal populations that exhibit oscillatory behaviour and network rhythmogenesis – with thalamic relay neurons of the dorsal lateral geniculate nucleus being the archetypal example (McCormick and Bal, 1997). Indeed, when in the appropriate voltage range, LHb neurons exhibited membrane potential oscillations and burst firing (Fig. 4.17) – a discharge pattern redolent of that observed with the MEA (Fig. 4.1). In current-clamp mode, TGOT (500nM) was bath to 25 LHb neurons, resulting in a reversible depolarisation in 5 of the neurons tested. The resultant depolarisation was sufficiently strong to shift membrane potential beyond the range required for sequential I_H and I_T activation, terminating membrane potential oscillations and switching discharge pattern from 'bursting' to tonic or 'pacemaking' (Fig. 4.18 – figure made by Dr. David Lyons). These data demonstrate the responsiveness of a subpopulation of LHb neurons to OTR activation. Though further current- and voltage-clamp experiments are requirements to determine the pre- and post-synaptic components of the TGOT-dependent excitatory mechanism.

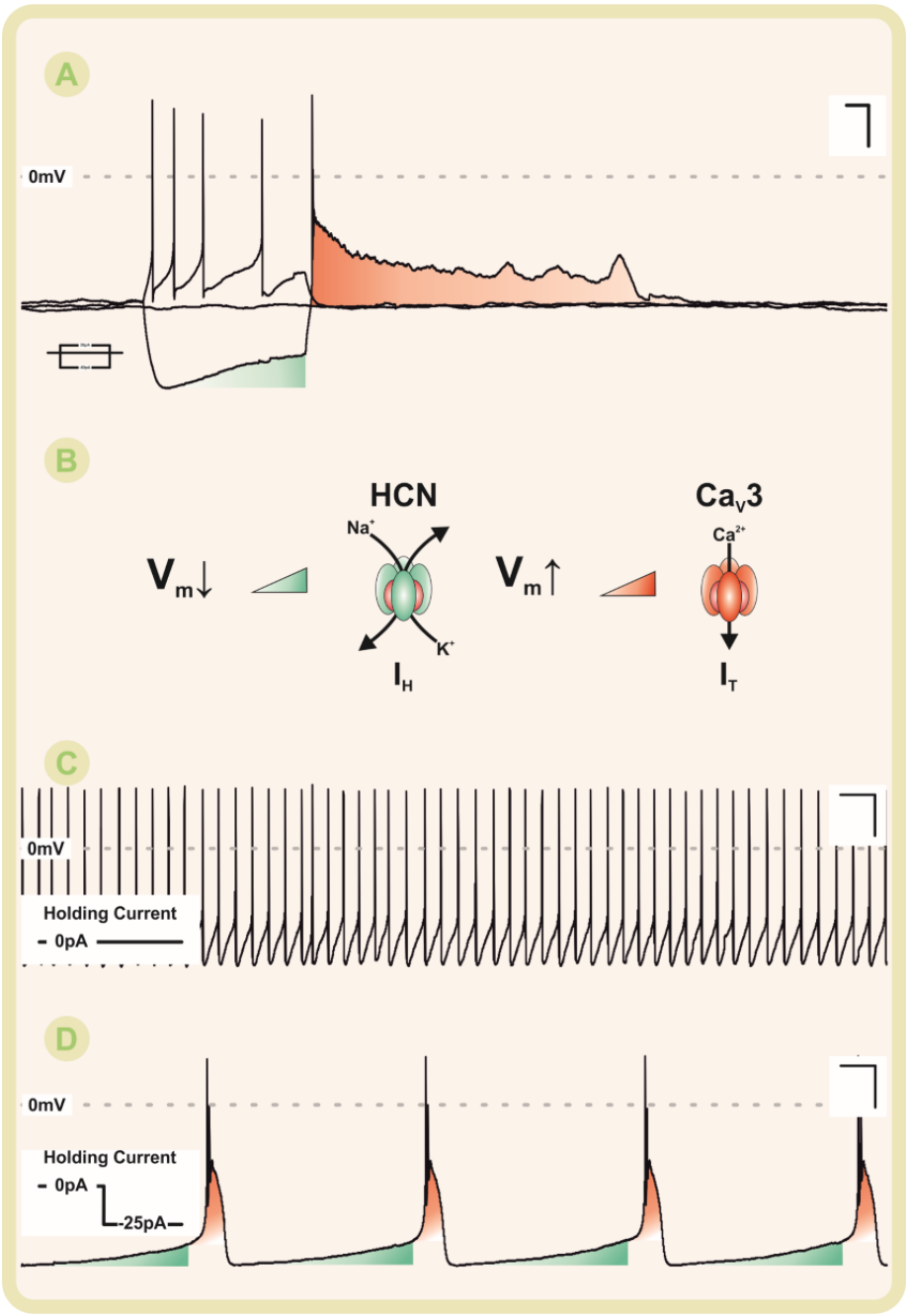

Figure 4.17: LHb neurons possess I_H, I_T and are capable of phasic discharge

(A) Superimposed membrane potential responses of a LHb neuron to negative (-60pA) and positive (+30pA) square form current steps. This current injection protocol reveals these neurons' characteristic voltage dependent conductances: note the depolarising sag underpinned by the slowly activating, slowly inactivating, mixed cationic conductance, I_H (green); and the prominent rebound excitation, driven by the low voltage activated, transient Ca^{2+} conductance, I_T (red). Scale bar inset: 20 mV / 200 msec. (B) Diagrammatic representation of the sequential activation of these conductances underpinning burst firing and rhythmic discharge. Membrane potential hyperpolarisation recruits the slowly inactivating I_H (carried by HCN channels; green) whose enduring activation is sufficient to trigger the low voltage activated I_T (carried by Ca_V3 channels; red), the termination of which permits cycle recommencement. (C) Passive current clamp recording of an LHb neuron displaying a 'pacemaking' pattern of action potential discharge. Scale bar inset: 20 mV / 200 msec. (D) The same neuron depicted in C following the constant injection of -25pA of holding current. The resultant hyperpolarisation draws the LHb neuron into the voltage range required for the sequential activation of voltage dependent I_H (green) and I_T (red), resulting in the observed membrane potential oscillation and phasic pattern of action potential discharge. Scale bar inset: 20 mV / 200 msec. Figure made by Dr. David Lyons.

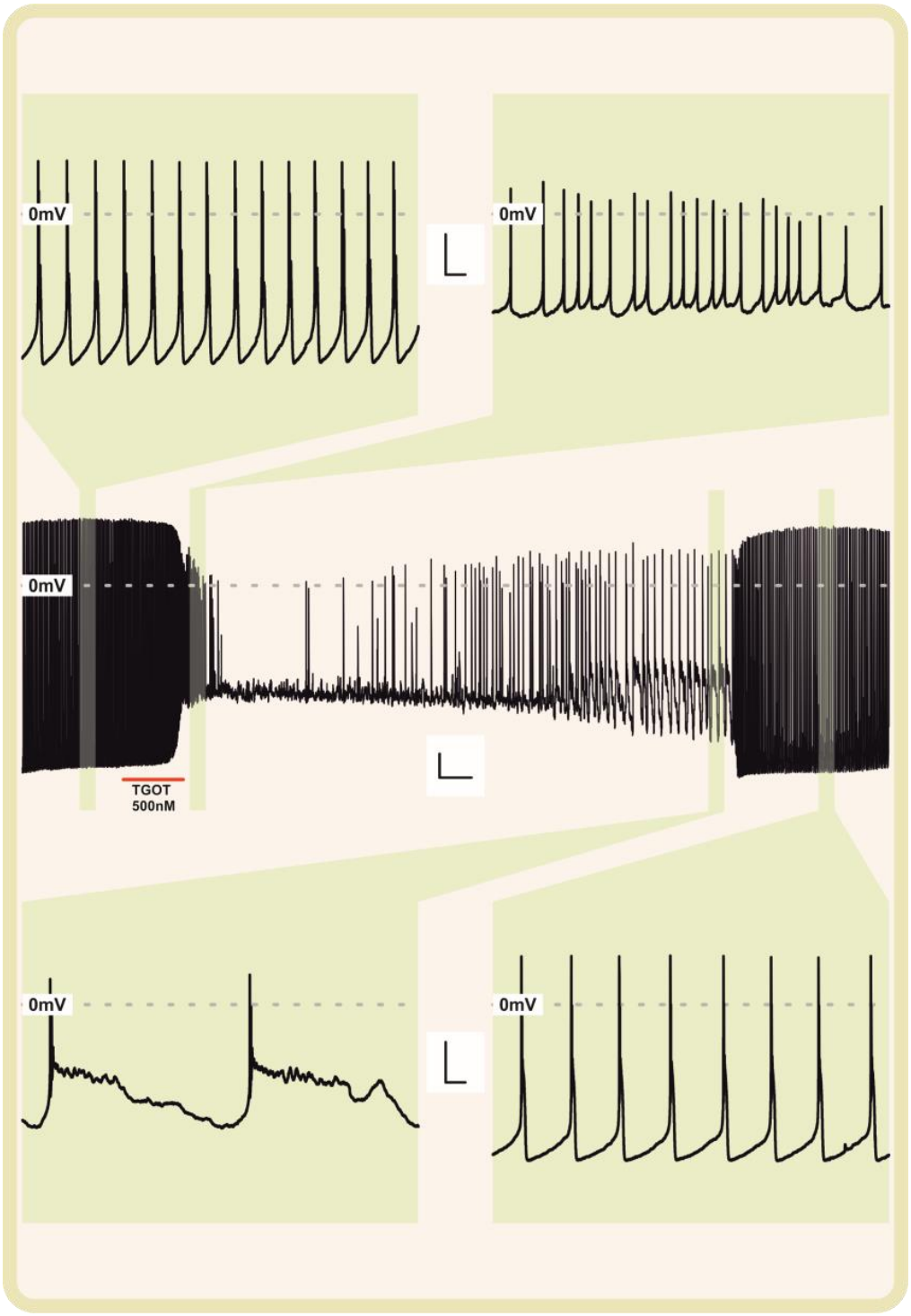

Figure 4.18: The selective OTR agonist TGOT depolarises a subpopulation of LHb neurons

Central panel: current-clamp recording of a LHb neuron following the constant injection of -25pA of holding current to initiate phasic discharge. Scale bar inset: 10 mV / 200 msec. Top Left – Control conditions: note phasic discharge. Scale bar inset: 20mv / 500mSec. Top Right – Peak of TGOT response: TGOT initiates a membrane potential depolarisation sufficient to terminate phasic discharge and briefly initiate pacemaking. Scale bar inset: 20 mV / 500 msec. Bottom Left – Partial recovery of TGOT response: note the altered waveform dynamics of the underlying membrane potential oscillation. Scale bar inset: 20 mV / 500 msec. Bottom Right – Complete recovery of TGOT response: restoration of phasic discharge and underlying membrane potential oscillation with waveform dynamics similar to that observed under control conditions. Scale bar inset: 20 mV / 500 msec. Figure made by Dr. David Lyons.

Discussion

This study demonstrates that both MHb and LHb exhibit significant elevation in MUA during the night, which is in agreement with previous single unit electrophysiological studies that reported a peak in the habenula electrical activity during late day and early night *in vitro* (Guilding *et al.*, 2010; Sakhi, Belle, *et al.*, 2014; Sakhi, Wegner, *et al.*, 2014). Our data adds a spatial dimension to these observations by revealing that the most prominent day-night difference in MUA is to be found in the ventral MHb and in the LHbL. While day-night differences in the LHb are anti-correlated with *Per2* expression – this occurring primarily in the medial aspect of this nucleus – those observed in the MHb coincide with the expression of this clock gene and so are more likely under direct control of the circadian oscillator (Guilding *et al.*, 2010). However, given that *Per2* expression straddles the border between MHb and LHb and the lack of a truly objective approach for electrode allocation, it may be the case that borderline electrodes have been erroneously categorised.

As noted, the most prominent day-night difference in the LHb was found in the dorso-lateral subregion and, therefore, was not correlated with the topographic distribution of the molecular clock, which is primarily located in the medial subregion. This part of the LHb receives extrinsic input from melanopsin-containing retinal ganglion cells, as demonstrated by X-gal staining in *Opn4*$^{tau\text{-}LacZ}$ reporter mice (Hattar *et al.*, 2006). The X-gal-positive fibres were also detected within a region where habenula abuts the central lateral nucleus and lateral nuclear group of the thalamus – an area which exhibits much more rapid visual responses (Sakhi, Wegner, *et al.*, 2014) – indicating that retinal input to the habenula could be transmitted via other thalamic nuclei. Indeed, indirect transmission of photic signals to the habenula via the anterior thalamus has been demonstrated in zebrafish (Cheng *et al.*, 2017). Collectively, these findings indicate a potential connectivity between the LHb and surrounding posterior thalamus in rodents – circuit interactions which could contribute to the regulation of circadian rhythms in the LHb *in vivo*. Furthermore, since the posterior thalamus was present in the coronal brain slices used in our studies, it remains a possibility that the circadian rhythmicity observed in the lateral portion of the LHb is driven *in vitro* by either a local molecular clock or through enduring thalamic plasticity mediated by photic entrainment which could be retained in acute preparations. The potential connectivity between posterior thalamus and LHb could be further examined by local stimulation of the thalamic area while simultaneously recording extracellular activity in the LHb.

In addition to the day-night difference in the MUA, a significant increase in SUA was observed in the LHb, implying the night elevation in MUA was associated with increased firing of individual units, rather than an increase in the number of units. In contrast, the SUA in the MHb as well as the average number of units detected per each electrode were not significantly different between the two time points. This implies a possibility that unsorted events which were not assigned to any single-unit clusters were contributing to the night elevation of the MUA in this subregion. Indeed, in some cases projection of MHb spikes into the feature space revealed merged clusters which could not be easily discriminated, some of which have been excluded from the analysis.

One cause underlying this problem could be associated with relatively high neuronal density found specifically in the MHb and has been demonstrated by Nissl staining of nucleic acid (Allen Brain Atlas, Allen Institute, https://connectivity.brain-map.org/static/ivt?id=100140665&popup=true). In agreement with this neuroanatomical characteristic of the MHb, a relatively high range of 1-6 units could be detected at single electrode sites in MHb, whereas on average only 1-3 units could be discriminated at single electrode sites in the LHb. Consequently, high neuronal density could increase the probability of detecting synchronous firing activity of multiple neurons. Highly synchronous neuronal firing will not only lead to overlapping of spikes, making the cluster isolation difficult, but it can also generate complex compound waveforms giving rise to artificial clusters (Rey *et al.*, 2015). Indeed, some discriminated units in the MHb exhibited waveform shapes with two peaks. However, such waveforms could also represent complex spikes, derived from a single neuron, which consist of fast sodium-dependent action potentials that give rise to slower calcium-dependent spikes. Therefore, in addition to the limited ability to discriminate all clusters contributing to the MHb MUA, there is a possibility that some discriminated clusters, particularly those exhibiting more complex waveforms, could represent highly synchronised spikes originating from either multiple or single neurons.

One extrinsic factor which has been proposed to regulate circadian rhythms in habenula activity is the SCN-derived neuropeptide, AVP. Indeed, the IHC analysis performed in this study confirmed the presence of AVP immunoreactive fibres throughout the rostro-caudal levels of the LHbM, results supported by previous neuroanatomical studies (Buijs, 1980; Rood and De Vries, 2011; Zhang *et al.*, 2016). Complementing the results from IHC analysis, extracellular recordings of the MUA showed that AVP induces excitatory response in multiple sites within the LHb. The direct excitatory effect of AVP has been previously shown in motoneurons, lateral septum and amygdala. However, in addition to direct, cell autonomous excitations, AVP was found to indirectly induce presynaptic inhibition via GABAergic interneurons within the same brain areas. The AVP-mediated indirect inhibition has been also proposed in the LHb as AVP-positive axon terminals were found in contact with dendrites of local GABAergic interneurons (Zhang *et al.*, 2016). However, since the presence of the GABAergic interneurons in the LHb was only confirmed by IHC analysis and the supplementary results from the *in vitro* whole-cell electrophysiological recordings do not provide enough evidence for this phenomenon, the AVP-mediated indirect inhibition via the proposed GABAergic microcircuit remains to be confirmed. In this study, the extracellular recording of MUA from multiple habenula sites was applied to investigate the effect of AVP. This technique enables detection of the drug effect on firing rate of cells in the vicinity of electrodes which are either already active and the drug increases their firing rate or are silent and the drug initiates their firing. The detection of inhibitory effects is more complicated as it requires sufficient spontaneous baseline activity and is not possible at those sites at which cells are quiescent. This limitation can be overcome by pharmacologically induced increase in baseline firing rate via increased extracellular K^+ concentration. This would raise the normally hyperpolarised K^+ reversal potential, reducing the driving force for positively charged K^+ ions to leave the cell, thus resulting in a more depolarised resting membrane potential. Although such an intervention could affect those neurons which are already in a depolarised firing state, as stronger

depolarisation could possibly drive their membrane potential through the firing threshold and paradoxically abolish AP discharge. Furthermore, if AVP induces indirect inhibition in the LHb, the counteraction of presumed direct excitation and indirect inhibition could result in negligible net effect on the MUA, as detected across a neuronal population. Given this possibility, the marked excitatory effects observed at relatively high AVP concentrations may imply that the post-synaptic excitation induced by AVP at such higher doses is sufficiently strong to override any concomitant pre-synaptic inhibitory drive. However, taking into account that AVP binds to OTRs with only 10 times less affinity than it binds to V1 receptors (Manning *et al.*, 2012), another possibility is that the excitatory effect detected at relatively high concentration of AVP could be mediated via OTRs. Indeed, OT, at the much lower concentration of 500 nM, induced excitatory responses within more distinct subregions of the LHb. In addition, similar excitatory responses were induced by the selective OTR agonist TGOT, which indicates that the OT-induced excitation is most likely mediated via OTRs. On the other hand, the excitatory effect of AVP is likely to be mediated by both OT and V1a receptors as the probability of the AVP-induced excitation was generally higher at some LHb sites which exhibited low probability of OT-induced responses and previous data from ISH and IHC analysis demonstrate a presence of V1a receptor in the LHb (Allen Brain Atlas, Allen Institute, http://mouse.brain-map.org/gene/show/33433, Zhang *et al.*, 2016). The V1 receptors are also implicated in AVP-induced excitations by the fact that the day-night difference in the AVP-induced effect was much more pronounced than the day-night difference in the OT-induced effect, as the percentage of responding sites to AVP was significantly lower during the day than during the night while there was no such a difference in the percentage of responding sites to OT. However, the inconsistency of these results could also be associated with the fact that the AVP modulation was examined during the late day and late night while the OT modulation was examined during the early day and early night.

The pronounced day-night difference in AVP-induced excitatory effect implies that the AVP neuropeptide could be involved in circadian regulation of habenula activity. The probability of AVP-induced excitation was significantly elevated during late day compare to late night. This result corresponds with the circadian profile of AVP release from the SCN as the peak of release occurs during mid-day (Watanabe *et al.*, 2000). Moreover, AVP innervation in the LHb originates primarily from the PVN and SON and has been implicated in regulation of fluid homeostasis as thirst-induced upregulation of these pathways resulted in reduced *c-fos* expression in the LHb and mediated active stress coping during behavioural despair (Zhang *et al.*, 2016). Thirst motivates animals to find and consume water and, therefore, is an important regulator of fluid homeostasis, which is also under circadian control (Zimmerman *et al.*, 2017). Indeed, the AVP-containing neurons in the SCN that project to organum vasculosum lamina terminalis (OVLT) – a brain structure intimately involved in fluid homeostasis – are more active during hours preceding sleep. The activation of OVLT neurons by SCN subsequently stimulates thirst leading to water intake (Gizowski *et al.*, 2016), which prevents the decrease in plasma volume that would otherwise occur during sleep. In addition, AVP-positive SCN neurons project to the SON and this projection has been implicated in AVP secretion by the SON, stimulating fluid retention during late sleep (Trudel and Bourque, 2010). This SCN-mediated complementary regulation of fluid homeostasis prevents the dehydration by promoting water retention before and during sleep

(Zimmerman *et al.*, 2017). Since AVP modulation of the LHb exhibits significant day-night difference, the AVP innervation of the LHb which originates in the PVN, SON and SCN could be also involved in regulation of fluid homeostasis. As such, these pathways could mediate thirst-motivated water seeking and water intake which are driven by contextual physiological needs superimposed over circadian rhythms imposed by the circadian clock in the SCN.

Unlike AVP, the OT-induced excitatory effect did not exhibit a day-night difference in the LHb, suggesting this neuropeptide is not involved in the circadian regulation of this structure. Although OT levels exhibit circadian rhythmicity in human plasma (Forsling *et al.*, 1998), to date there is no evidence of circadian rhythms of OT release in rodent brain. Nevertheless, our results provide the first evidence that this neuropeptide alters firing activity in this brain area. Interestingly, the OTergic modulation of the LHb has been implicated in pain regulation, as microinjection of this neuropeptide into the LHb significantly prolonged hind paw withdrawal latency following thermal and mechanical noxious stimuli in rats – suggesting the analgesic effect of OT is mediated, at least in part, through the LHb (Gao *et al.*, 2015). In the discussion, the authors proposed that the analgesic effect of OT injection could be mediated via opioid receptors expressed in this brain area, including μ opioid receptor (MOR). Indeed, OT markedly enhances MOR signalling induced by opioid agonists β-endorphin and morphine (Meguro *et al.*, 2018). In addition, similar to OT, injection of morphine into the LHb also induces analgesia; and selective activation of MORs was found to inhibit a subset of LHb neurons *in vitro* (Margolis and Fields, 2016), suggesting MORs are expressed in the LHb. Therefore, even though our results demonstrate OTR-mediated modulation of the LHb, there remains a possibility that OT affects habenula activity through enhancement of MOR signalling.

Collectively, this study has demonstrated that mouse habenula exhibits day-night difference in extracellular activity in specific subregions of MHb and LHb *in vitro*. Circadian rhythmicity in the LHb is likely to be regulated by the neuropeptide AVP that is, at least, partially derived from the master circadian pacemaker in the SCN. In addition, neuronal activity in the LHb is also modulated by OT via OTRs, and potentially via enhancement of MOR signalling. Further electrophysiological examination on single-cell level is required in order to establish whether the mechanism of AVP and OT-driven excitation in the LHb is pre- or post-synaptic and the potential contribution of OTergic modulation of MOR signalling.

Chapter 5 General discussion

The habenula oscillator and its electrical output

In the conventional model of the mammalian circadian system, endogenous rhythms in behaviour and physiology are mediated by a single dominant circadian clock that resides in the SCN of the hypothalamus. Indeed, lesion of the SCN abolishes hormonal and behavioural rhythms which can be restored by transplantation of foetal SCN tissue (Moore and Eichler, 1972; Stephan and Zucker, 1972; Lehman *et al.*, 1987). Recent findings have, however, demonstrated intrinsic clock oscillations in other areas of the mammalian brain including the OB, habenula, amygdala and several hypothalamic nuclei – observations that challenge the omnipotence of the master circadian pacemaker (Abe *et al.*, 2002; Guilding and Piggins, 2007). In comparison with the SCN, which when isolated in culture exhibits sustained clock rhythmicity for a prolonged period, the cultured extra-SCN oscillators display dampening oscillations as individual neurons drift out of phase. As such, these oscillators are semiautonomous since, despite their ability to generate autonomous rhythms, they appear to require input from the master pacemaker in order to synchronise the independent cellular rhythms into a coherent rhythmic output of the whole neuronal population (Guilding and Piggins, 2007).

The habenula features a semiautonomous circadian oscillator within a subpopulation of neurons that display intrinsic PER2::LUC rhythms dampening to arrhythmicity after three circadian cycles in culture, a period over which isolated SCNs continue to manifest robust oscillations (Guilding *et al.*, 2010). Within the habenula, the clock-containing neurons are predominantly localised in the medial portion of the lateral nucleus – a site coinciding with the night-time increase in MUA we observed in mouse brain slices. On the other hand, in the *in vivo* system, zebrafish habenula exhibits day-night differences of opposing polarities occurring in different subregions of the structure, implying that the rhythmicity of electrical output is more heterogenous when compared to the homogenous oscillations of clock components. It should be noted, however, that in the intact *in vivo* system the oscillations in habenula electrical outputs are, in addition to intrinsic clock activity, modulated by numerous inputs, absent in the reduced *in vitro* preparation, which can be inhibitory or excitatory depending on their neurotransmitter phenotype.

Daily changes in habenula activity in vertebrates

The results from Chapter 2 have demonstrated that the zebrafish habenula, as in mammals, exhibits daily variations in neuronal physiology. Indeed, in the putative homologue of the mammalian LHb, both pERK and Ca^{2+} levels were found to be significantly higher during the night than during the day. On the other hand, in subregions of the putative homologue of the MHb, nocturnal pERK levels either increased or decreased with no overall change in Ca^{2+} levels. The results from IHC analysis of pERK are comparable with previous findings from IHC of *c-fos* in mice and hamsters which demonstrated increased levels of *c-fos* in LHb during the night in

comparison with the day-time (Tavakoli-Nezhad and Schwartz, 2006). Additionally, Chapter 4 has demonstrated that in mice both LHb and MHb exhibit increased neuronal activity during the night when compared to the day. Since these recordings were performed in a reduced slice preparation in which the habenula's afferent input is presumably no longer functional, this suggests that such daily rhythms arise through intrinsic processes in the habenula. Therefore, at least in rodents, circadian rhythmicity of this structure is seemingly regulated by intrinsic clock machinery – a hypothesis that has been supported by findings demonstrating the loss of habenula rhythmicity in *Cry1*$^{-/-}$ *Cry2*$^{-/-}$ mice (Sakhi, Belle, *et al.*, 2014; Sakhi, Wegner, *et al.*, 2014).

A similar circadian profile of LHb neuronal activity was found between diurnal zebrafish and nocturnal rodents, with increased LHb activity during the night – a time that represents the active phase for nocturnal rodents and inactive phase for diurnal zebrafish. The habenula circuitry has been recently implicated to underlie the differences in circadian regulation between diurnal and nocturnal mammalian species, since GABAergic neurons, which are detected in the LHb of diurnal Nile Grass rats, are absent in nocturnal Norway rats (Langel *et al.*, 2018). Collectively, these findings together with our data and results from rodent studies outlined above, indicate that the principal difference between diurnal and nocturnal species may not be reflected in the day-night variations in the overall neuronal activity, but rather in the neurotransmitter phenotype of active LHb neurons and the inhibitory or excitatory effect they may exert on downstream targets of this structure. Therefore, identifying the neurotransmitter profiles of LHb neurons which exhibit circadian rhythmicity in both diurnal and nocturnal species may contribute to our understanding of the chronotype-dependent circadian regulation of this epithalamic structure.

Potential role of rhythmic habenula

Mammalian LHb neurons innervate the dopaminergic VTA either directly or indirectly via GABAergic interneurons in the RMTg. In a well-studied behavioural paradigm, LHb neurons are excited by aversive stimuli or no-reward-predicting targets and, in turn, inhibit DA neurons via the RMTg (Jhou *et al.*, 2009; Hikosaka, 2010). Since the habenula features intrinsic time-keeping properties which mediate its rhythmic electrical output, this structure may provide circadian cues to downstream targets in the VTA. For instance, the spontaneous firing rate in the VTA exhibits circadian rhythmicity *in vivo* (Domínguez-López *et al.*, 2014). However, no such rhythms are detected in an isolated *in vitro* preparations, implying the daily rhythms in VTA's neuronal activity are dependent on inputs from other circadian pacemakers (Mendoza, 2017). As such, circadian variation in the activity of the LHb and its subsequent influence on the VTA could lead to a time specific modulation in the perception of rewarding stimuli (Baño-Otálora and Piggins, 2017). This, in turn, could further influence daily rhythms in motivated behaviours, including administration of drugs of abuse. For example, cocaine-induced place preference in mice is significantly higher when animals are treated during the early day as opposed to late day under the standard LD cycle (Abarca *et al.*, 2002), implying that rewarding properties of this drug vary throughout the circadian cycle. Likewise, apparent day-night differences have been reported in cocaine self-administration or alcohol intake in rats (Salaberry and Mendoza, 2016). However, to date, the

degree to which daily oscillations in the habenula's electrical output contribute to the circadian regulation of such motivated behaviours remains unclear.

In addition to the dopaminergic VTA, LHb also innervates the serotonergic raphe nuclei and, when stimulated, inhibits 5-HT neurons either via local GABAergic interneurons within the raphe itself, or via the RMTg. Since the median raphe projects to multiple areas of the brain, including SCN, lateral preoptic area and hippocampus, the LHb may indirectly regulate numerous cognitive functions in a circadian manner (Baño-Otálora and Piggins, 2017). For instance, the LHb's modulation of the serotonergic system has been implicated in maintaining the hippocampal theta oscillations which are critical for memory formation and are under circadian control (Baño-Otálora and Piggins, 2017). Indeed, LHb activity exhibits phase-locking with theta oscillation cycle in the hippocampus – a cross correlation detected primarily in the medial portion of the LHb, coinciding with expression of habenula clock components (Aizawa, Yanagihara *et al*., 2013). However, whether the phase-locking activity in the habenula is under circadian control yet remains to be determined.

Role of AVP and OT neuromodulators in regulation of the vertebrate habenula

Since the daily rhythm in habenula activity may be modulated by neurochemical signals from other brain oscillators, one of the principal aims of this thesis was to investigate whether the neuropeptide AVP, as a putative output signal of the SCN, influences habenula neuronal activity in a time of day dependent manner. Our results demonstrate that AVP-immunopositive fibres are found in the medial portion of mouse LHb and neurons in this region respond to bath application of this neuropeptide with excitation. Furthermore, the spatial distribution of these responses varied between day and night, suggesting that AVP differentially modulates discrete populations of LHb neurons at specific times of the day. A recently conducted study demonstrated that Per2::LUC rhythms in rostral and caudal habenulas, which are harvested from animals kept under constant darkness, are out of phase and this desynchrony is even more enhanced in SCN-lesioned animals (Salaberry *et al.*, 2019). This suggests that the SCN provides a neurochemical signal that is, at least partially, involved in synchronising rostral and caudal oscillators within the habenula. Since AVP serves as a neurochemical output signal of the SCN and, as shown by our preliminary results, modulates LHb neuronal activity in a circadian fashion, it may contribute to the regulation of clock synchrony in this structure. However, whether the AVP-induced effect observed in this study is mediated via V1 receptors remains to be determined, since AVP also binds to OTRs and our results demonstrate the presence of OTR-mediated signalling in the LHb. Indeed, our data provide the first evidence of OT modulation of LHb activity. The OT-induced excitatory effects detected in this structure did not vary between day and night, implying OT may not be involved in circadian regulation of the habenula and currently its exact function remains to be clarified.

In nonmammalian species, including zebrafish, arginine vasotocin (AVT) represents a homologue of mammalian AVP and has been implicated in regulation of social and reproductive behaviours. In zebrafish, this neuropeptide is expressed in and around the SCN (Noche *et al.*, 2011) and vasotocin receptors are expressed in various parts of larval brain, although at this developmental stage no receptors are found in the habenula (Iwasaki *et al.*, 2013). To date, the role of AVT in circadian regulation of zebrafish is unclear. In Atlantic salmon, AVT brain levels do not exhibit rhythmicity (Gozdowska *et al.*, 2006), whereas AVT plasma levels are rhythmic in flounder fish (Kulczykowska *et al.*, 2001), suggesting that the role of this neuropeptide in circadian regulation of fish might vary in a species dependent manner. Further investigation is, however, required to elucidate the specific function of SCN-derived AVT in zebrafish.

Similarly, OT neural circuits are also well conserved across vertebrates. In fish, the OT orthologue isotocin is primarily expressed in the preoptic hypothalamic area, which is homologous to the PVN, SON and accessory nucleus of hypothalamus in mammals (Wee *et al.*, 2019). This neuropeptide enhances social preference, attenuates fear to predator response (Braida *et al.*, 2012) and recently has been also implicated in regulation of nocifensive behaviour in zebrafish larvae. Indeed, hypothalamic OT-expressing neurons respond robustly to noxious stimuli, with some neurons encoding sensory information while others correlate more strongly with defensive swimming behaviour (Wee *et al.*, 2019). Interestingly, OT-immunopositive cells have been also detected in larval habenula (Herget *et al.*, 2017), a structure that also responds with excitation to noxious stimuli such as electric shock (Duboué *et al.*, 2017). However, the exact function of OT innervation in the habenula of zebrafish remains to be clarified. Together these results indicate that zebrafish represents a suitable model organism to further investigate the role of this highly conserved circuitry.

Role of habenula oscillator in circadian regulation of brain neurotransmission and behaviour

In this study, a zebrafish transgenic line *Tg(gng8:gal4;UAS:EGFP-ΔCLK)*, in which the molecular clock of the habenula was genetically altered, was generated. Our preliminary results demonstrate that the habenula-specific clock manipulation has no overall effect on clock regulated behaviours such as locomotor activity or arousal threshold in zebrafish larvae. On the other hand, in adult zebrafish the disruption of habenula clock machinery significantly attenuated day-time brain levels of important neurotransmitters, including DA, 5-HT and ACh, with ACh levels exhibiting the most pronounced reduction. Collectively, these results suggest that the habenula clock play a more important role in the circadian regulation of brain and behaviour in adulthood, rather than during the development. However, this is necessarily speculative, since only two behavioural assays were conducted in larvae, while at this developmental stage habenula clock might still regulate other behavioural aspects which are under circadian control, such as feeding or place preference in a vertical column. Likewise, further investigation is required to determine whether the reduction in neurotransmitter levels correlates with specific behavioural phenotypes in adults.

The marked day-time reduction of transmitter content, particularly that of ACh, implies that that habenula clock tightly regulates rhythmicity in cholinergic transmission. In mammals, markers of cholinergic signalling are significantly down-regulated in a rat model of depression and knock-down of CHAT specifically in the rat habenula is sufficient to induce anhedonia-like behaviour (Han *et al.*, 2017). Furthermore, activation of habenula cholinergic neurons stimulates DA neurons in the VTA and reduces 5-HT immunoreactivity in the raphe, implying that cholinergic transmission itself regulates dopaminergic and serotonergic systems (Han *et al.*, 2017). It is currently unknown whether disruption of the habenula clock could also lead to reductions in cholinergic transmission and associated symptoms of depression in mammals. Nevertheless, the transgenic zebrafish line presented in this study provides a tool to further investigate the potential mechanisms underpinning impaired circadian regulation in pathophysiology of depression.

Future work

Chapter 2

This study demonstrates circadian rhythmicity in zebrafish habenula *in vivo*, it does not, however, answer the question whether the zebrafish habenula, like its mammalian homologue, represents a self-sustained circadian oscillator. This problem can be addressed by bioluminescence monitoring of clock rhythms in cultured dissected habenula from *Tg(4xE-Box:luciferase)* or *Tg(per3:luciferase)* reporter lines using photon-counting and/or sensitive videomicroscopy. Since zebrafish habenula are relatively small even in adult zebrafish and cannot be easily identified based on their morphology, these experiments would have to be performed using transgenic fish which also express a habenula-specific fluorescent marker in order to guide the dissection with the help of fluorescent microscopy. Complementary to these experiments, Ca^{2+} activity in the adult dissected habenula could be monitored *in vitro* using *Tg(gng8:Gal4;UAS:GCaMP6s)* transgenic line in order to determine whether putative clock gene rhythms correlate with rhythmic output in neuronal activity.

The rhythmicity of the habenula oscillator could be also investigated during larval development *in vivo*, assuming the *Tg(4xE-Box:luciferase)* line is able to report clock activity in the larval brain. This could be achieved either using sensitive videomicroscopy where larvae would be mounted in agarose or photon-counting in freely swimming fish expressing a clock reporter specifically in the habenula. These experiments could shed light on how different *zeitgebers*, including light-dark schedules and food availability, entrain brain oscillators during development.

Chapter 3

In Chapter 3, the dominant negative strategy had been applied to block the habenula molecular clock machinery by overexpressing ΔCLK protein specifically in this structure. However, whether the overexpression of ΔCLK affected specific clock genes has not been confirmed. This could be further investigated by crossing the *Tg(gng8:gal4;UAS:EGFP-ΔCLK)* line with *Tg(4xE-Box:luciferase)* or *Tg(per3:luciferase)* reporter lines, assuming they would be able to report clock

activity in the habenula in adult or larval stages. Furthermore, the effect on peripheral clocks could also be examined using *Tg(per1b:luciferase)* as this has been previously employed as a reporter for peripheral clock gene rhythms (Ben-Moshe Livne *et al.*, 2016). It should be noted, however, that monitoring the activity of specific promoters such as *per1b* or *per3* may not be representative of the entire array of rhythmic genes. Possibly, the best approach to address this question would involve analysis of the whole habenula transcriptome using RNA seq, which would highlight all genes affected by this mutation. Alternatively, a cheaper method could also involve measurement of mRNA levels using quantitative real-time PCR (qRT-PCR), although this analysis would be limited to a certain number of clock genes.

In order to further investigate the role of habenula oscillators in the circadian regulation of behaviour in both adult and larval zebrafish, the effect of habenula-specific ΔCLK expression on additional aspects of behaviour would need to be tested. For instance, zebrafish larvae tend to swim in the top third of the water column during the day, while descending to the bottom upon loss of illumination where they remain during sleep (Ben-Moshe Livne *et al.*, 2016). Masking of this circadian behaviour by light is partially regulated by the habenula (Lin and Jesuthasan, 2017). Therefore, to test whether habenula clock regulates circadian rhythmicity in place preference, the movement of *Tg(gng8:gal4;UAS:EGFP-ΔCLK)* larvae within a vertical column could be monitored over a 24-h circadian cycle under both LD and DD conditions. In addition, to further investigate the role of habenula oscillators in the circadian regulation of motivated behaviours, feeding behaviour of *Tg(gng8:gal4;UAS:EGFP-ΔCLK)* larvae could also be examined by using fluorescently-labelled paramecia (paramecia is a commonly used food source for developing zebrafish larvae). Following the feeding, the gut fluorescence signal could be used to quantitatively measure paramecia intake.

Since expression of ΔCLK in the adult habenula results in day-time reductions in the brain content of important neuromodulators, their locomotor activity could be affected particularly during the day. Therefore, day-time locomotor activity could also be monitored in adult *Tg(gng8:gal4;UAS:EGFP-ΔCLK)* zebrafish, measuring both the velocity as well as place preference within the tank. The place preference response, in particular, appears to be regulated by DA neurotransmission, as mutant zebrafish that lack the DA transporter tend to swim at the bottom of the tank and exhibit ‘digging-like’ behaviour. Since DA brain content is significantly attenuated in our transgenic line, these fish may well display a similar behavioural phenomenon.

In addition, the day-time reduction in these neuromodulators could possibly lead to altered anxiety of *Tg(gng8:gal4;UAS:EGFP-ΔCLK)* fish. In general, anxiety increases the valence of perceived threats and is reflected in changes in mobility of zebrafish under stressful conditions. Such conditions can be, for instance, induced by alternating periods of light and darkness (Peng *et al.*, 2016). In general, dark stimuli are aversive to zebrafish larvae which in a light-dark choice assay prefer to swim in an illuminated compartment while avoiding the dark part of the swimming arena (Cheng *et al.*, 2016). Therefore, the anxiety level of *Tg(gng8:gal4;UAS:EGFP-ΔCLK)* fish could be examined using a visual motor assay where multiple light-dark cycles are applied and locomotor response to sudden changes in illumination are quantitatively measured (Peng *et al.*, 2016). Likewise, anxiety levels could also be investigated using the light-dark choice assay. The

light-dark preference behaviour itself reflects anxiety, as drugs which reduce anxiety, such as diazepam, increase entry into regions that are normally avoided (Cheng *et al.*, 2016).

In addition to avoidance of darkness, zebrafish larvae also display avoidance of aversive olfactory stimuli such as high concentrations of bile salt. This behavioural response is mediated by cholinergic transmission in the habenulo-interpeduncular pathway, as blocking nicotinic ACh receptors abolishes avoidance (Krishnan *et al.*, 2014). Since brain levels of ACh are significantly reduced in *Tg(gng8:gal4;UAS:EGFP-ΔCLK)* zebrafish, there is a possibility that this avoidance behaviour is attenuated as a result of habenula-specific ΔCLK expression. Therefore, this transgenic line could also be examined using an odour avoidance assay where location of fish within a swimming arena is monitored as an indicator of odour preference.

In adult zebrafish, anxiety-related behaviour could also be examined using a novel tank diving assay which is similar to a rodent open field test. Generally, anxiety in this test is reflected in reduced exploration, which is displayed as increased bottom dwelling with fewer entries to the top part of the tank, together with elevated erratic movements and freezing (Stewart *et al.*, 2012). Therefore, vertical movement of adult *Tg(gng8:gal4;UAS:EGFP-ΔCLK)* zebrafish could be monitored within a novel tank, where place preference together with velocity of locomotor activity could be used as indicators of anxiety-like behaviour. In addition, anxiety in zebrafish is also reflected in their social behaviours (Stewart *et al.*, 2012). This could be examined using a social preference paradigm where one individual is separated by transparent plexiglass from its conspecifics, while its place preference within a two-armed behavioural arena is continuously monitored (Dreosti *et al.*, 2015). Normally, adult zebrafish strongly prefer to remain in a compartment where they can view conspecifics and since the social preference is attenuated by pharmacological manipulation with a D1 receptor antagonist (Scerbina *et al.*, 2012), this behaviour may also be affected by reduced DA levels as a consequence of habenula-specific ΔCLK expression.

Chapter 4

This chapter has demonstrated that AVP and OT neuromodulators influence neuronal activity in mouse LHb. However, while the presence of OTR-signalling in this structure has been confirmed, the V1 receptor-mediated effect of AVP remains to be determined. This could be further investigated in extracellular recordings of MUA where AVP would be co-applied with V1a and V1b receptor antagonists. In addition, the pre- and post-synaptic mechanisms of the individual neuropeptides could be further determined using single-cell voltage-clamp recordings of the miniature EPSC (mEPSC) before and after the drug application. The frequency and amplitudes of mEPSCs would be subsequently analysed, since drug-induced change in the mEPSC frequency reflects changes in presynaptic release probability, whereas variation in the amplitude of mEPSC indicates changes in post-synaptic responsiveness. Complementary to electrophysiological analysis, the mRNA expression of individual V1a, V1b and OT receptors could also be examined using *in situ* hybridisation and mRNA levels could be quantitatively measured at different time points during the circadian cycle using qRT-PCR in order to further clarify the role of individual receptors in circadian regulation of the habenula. Furthermore, the

role of AVP neuromodulation in synchronisation of regional circadian oscillators could be examined by investigating the effect of AVP and/or V1a, b receptor antagonists on the phase of Per2::LUC rhythms in cultured rostral and caudal habenula oscillators.

Evaluation of mouse and zebrafish animal models for investigation of brain oscillators

This thesis explored circadian regulation of the habenula using two different model organisms, mouse and zebrafish, both of which offer their own methodological benefits enabling the use of multiple tools for the study of circadian oscillators in the vertebrate brain. Table 5.1 highlights the major advantages and disadvantages of both model organisms, pros and cons which should be considered when selecting an appropriate animal model for investigation of neuronal structures in circadian regulation.

Table 5.1:

	Advantages	Disadvantages
Zebrafish	• Transparency of larvae enables non-invasive *in vivo* imaging of the whole brain. Advancement in bioluminescent Ca^{2+}/voltage and clock reporters would allow monitoring in freely moving animals. • Allows investigation of brain oscillators during the development. • Reproduce in large numbers and breeding is relatively cheap. • Relatively easy and fast generation of transgenic/mutant lines. • Represents a diurnal model organism.	• Zebrafish brain expresses numerous opsins and their function is poorly understood. Consequently, *in vivo* as well as *in vitro* imaging of brain oscillators may be problematic, since the opsins might be sensitive to various wavelengths, including IR light. The perception of IR light may also influence zebrafish behaviour during the video-tracking of locomotion using IR camera system. • Brain is relatively small and specific regions are not easily dissected. • High-resolution recording of neuronal activity using single-cell patch clamp is currently not a well-established technique for zebrafish.
Mouse	• Represents a model of mammalian circadian system. • Brain circadian oscillators are better understood. • Brain is comparatively large and specific regions can be easily dissected and isolated for *in vitro* preparations. • Brain oscillators can be easily isolated from light input. • Techniques for high-resolution monitoring of neuronal activity are well established.	• Breeding is relatively slow and expensive. • Generation of transgenic and mutant lines is relatively slow. • Monitoring of neuronal activity *in vivo* is more complex and invasive. • Represents a nocturnal model organism, meaning some aspects of circadian regulation in mice might not relate to diurnal humans.

Implications of habenula research

The strategic position of the habenula, together with its regulation of monoaminergic midbrain centres, indicate that dysfunction of this important brain circuitry may underpin pathogenesis of neurological disorders such as depression (Aizawa, Cui, *et al.*, 2013). Animal models of depression exhibit a higher metabolic rate in the LHb as well as increased presynaptic tone onto VTA projecting LHb neurons, a phenomena which correlates with symptoms of depression (Li *et al.*, 2011; Aizawa, Cui, *et al.*, 2013). Likewise, during the transitions from active to passive stress coping – adaptive behavioural state transitions that can become maladaptive in depression – zebrafish LHb neurons are progressively activated, suppressing downstream serotonergic raphe, which eventually leads to behavioural passivity (Andalman *et al.*, 2019). Furthermore, increased neural activity has been detected in the habenula of volunteer patients under tryptophan-depletion treatment, experiencing depressive-like symptoms (Morris *et al.*, 1999).

One treatment for clinical depression involves deep brain stimulation (DBS) where repeated electrical activation of LHb afferents depletes transmitter release onto LHb neurons (Li *et al.*, 2011). Indeed, application of DBS in the LHb over the course of 28 days significantly improved depressive-like symptoms and elevated monoamine levels in blood serum and brain tissue in a rat model of depression (Meng *et al.*, 2011). Similarly, Sartorius and colleagues (2010) reported the first successful treatment of a severe treatment-resistant major depression using bilateral DBS of the afferent bundle stria medullaris of the LHb in a human subject. Therefore, this evidence indicates that the modulation of LHb activity is a powerful tool to treat the most severe symptoms of depression. However, although DBS provides a potential intervention for patients for whom no other treatments are available, it is important to highlight the adverse effects which may be associated with this invasive neurosurgical procedure. These may include infection, haemorrhage, headache and seizures (Delaloye and Holtzheimer, 2014). Consequently, there is a need for further research of habenula physiology which will provide alternative less invasive means to modulate hyperactive LHb circuitry in patients suffering from this debilitating disorder.

In general, depression is associated with impaired circadian rhythmicity as, for instance, a microarray study revealed a dysregulated expression of clock genes in post-mortem brain tissue of depressed patients (Bunney *et al.*, 2015). However, to date it remains to be clarified whether altered LHb activity in depression is a cause or consequence of this disturbed rhythmicity. To address this problem, Bunney *et al.* (2015) hypothesised that antidepressant effects of sleep deprivation therapy may be due to its capability to reset abnormal clock gene expression in depression and subsequently restore normal circadian rhythmicity. However, this begs a number of questions as to whether intrinsic molecular oscillators are dysregulated in the LHb in depression and, if so, whether restoration of the LHb molecular clock could improve dysregulated activity within this structure and consequently ameliorate the depressive-like symptoms. Therefore, circadian regulation of the habenula is an important aspect of the habenula physiology and its further investigation will not only lead to a better understanding of how this circuitry operates, but also lead to development of more efficient therapeutic interventions.

References

Abarca, C., Albrecht, U., & Spanagel, R. (2002). Cocaine sensitization and reward are under the influence of circadian genes and rhythm. *Proceedings of the National Academy of Sciences of the United States of America*, *99*(13), 9026–9030. https://doi.org/10.1073/pnas.142039099

Abe, M., Herzog, E. D., Yamazaki, S., Straume, M., Tei, H., Sakaki, Y., … Block, G. D. (2002). Circadian Rhythms in Isolated Brain Regions. *The Journal of Neuroscience*, *22*(1), 350–356. https://doi.org/10.1523/JNEUROSCI.22-01-00350.2002

Adamos, D. A., Kosmidis, E. K., & Theophilidis, G. (2008). Performance evaluation of PCA-based spike sorting algorithms. *Computer Methods and Programs in Biomedicine*, *91*(3), 232–244. https://doi.org/10.1016/J.CMPB.2008.04.011

Aguilar-Roblero, R., Quinto, D., Báez-Ruíz, A., Chávez, J. L., Belin, A. C., Díaz-Muñoz, M., … Lundkvist, G. (2016). Ryanodine-sensitive intracellular Ca2+ channels are involved in the output from the SCN circadian clock. *The European Journal of Neuroscience*, *44*(7), 2504–2514. https://doi.org/10.1111/ejn.13368

Aizawa, H. (2013). Habenula and the asymmetric development of the vertebrate brain. *Anatomical Science International*, *88*(1), 1–9. https://doi.org/10.1007/s12565-012-0158-6

Aizawa, H., Amo, R., & Okamoto, H. (2011). Phylogeny and ontogeny of the habenular structure. *Frontiers in Neuroscience*, *5.* https://doi.org/10.3389/fnins.2011.00138

Aizawa, H., Bianco, I. H., Hamaoka, T., Miyashita, T., Uemura, O., Concha, M. L., … Okamoto, H. (2005). Laterotopic representation of left-right information onto the dorso-ventral axis of a zebrafish midbrain target nucleus. *Current Biology*, *15*(3), 238–243. https://doi.org/10.1016/j.cub.2005.01.014

Aizawa, H., Cui, W., Tanaka, K., & Okamoto, H. (2013). Hyperactivation of the habenula as a link between depression and sleep disturbance. *Frontiers in Human Neuroscience*, *7*. https://doi.org/10.3389/fnhum.2013.00826

Aizawa, H., Kobayashi, M., Tanaka, S., Fukai, T., & Okamoto, H. (2012). Molecular characterization of the subnuclei in rat habenula. *Journal of Comparative Neurology*, *520*(18), 4051–4066. https://doi.org/10.1002/cne.23167

Aizawa, H., Yanagihara, S., Kobayashi, M., Niisato, K., Takekawa, T., Harukuni, R., … Okamoto, H. (2013). The synchronous activity of lateral habenular neurons is essential for regulating hippocampal theta oscillation. *Journal of Neuroscience*, *33*(20), 8909–8921. https://doi.org/10.1523/JNEUROSCI.4369-12.2013

Akerboom, J., Chen, T.-W., Wardill, T. J., Tian, L., Marvin, J. S., Mutlu, S., … Looger, L. L. (2012). Optimization of a GCaMP Calcium Indicator for Neural Activity Imaging. *Journal of Neuroscience*, *32*(40), 13819–13840. https://doi.org/10.1523/JNEUROSCI.2601-12.2012

Alberi, S., Dreifuss, J. J., & Raggenbass, M. (1997). The Oxytocin-induced Inward Current in Vagal Neurons of the Rat is Mediated by G Protein Activation but not by an Increase in the Intracellular Calcium Concentration. *European Journal of Neuroscience*, *9*(12), 2605–2612. https://doi.org/10.1111/j.1460-9568.1997.tb01690.x

Alboni, S., Cervia, D., Sugama, S., & Conti, B. (2010, January 29). Interleukin 18 in the CNS. *Journal of Neuroinflammation*. https://doi.org/10.1186/1742-2094-7-9

Albus, H., Bonnefont, X., Chaves, I., Yasui, A., Doczy, J., van der Horst, G. T., & Meijer, J. H. (2002). Cryptochrome-Deficient Mice Lack Circadian Electrical Activity in the

Suprachiasmatic Nuclei. *Current Biology*, *12*(13), 1130–1133. https://doi.org/10.1016/S0960-9822(02)00923-5

Albus, H., Vansteensel, M. J., Michel, S., Block, G. D., & Meijer, J. H. (2005). A GABAergic mechanism is necessary for coupling dissociable ventral and dorsal regional oscillators within the circadian clock. *Current Biology*, *15*(10), 886–893. https://doi.org/10.1016/j.cub.2005.03.051

Allada, R., White, N. E., So, W. V., Hall, J. C., & Rosbash, M. (1998). A Mutant Drosophila Homolog of Mammalian Clock Disrupts Circadian Rhythms and Transcription of period and timeless. *Cell*, *93*(5), 791–804. https://doi.org/10.1016/S0092-8674(00)81440-3

Amo, R., Aizawa, H., Takahoko, M., Kobayashi, M., Takahashi, R., Aoki, T., & Okamoto, H. (2010). Identification of the zebrafish ventral habenula as a homolog of the mammalian lateral habenula. *Journal of Neuroscience*, *30*(4), 1566–1574. https://doi.org/10.1523/JNEUROSCI.3690-09.2010

Amo, R., Fredes, F., Kinoshita, M., Aoki, R., Aizawa, H., Agetsuma, M., … Okamoto, H. (2014). The Habenulo-Raphe Serotonergic Circuit Encodes an Aversive Expectation Value Essential for Adaptive Active Avoidance of Danger. *Neuron*, *84*(5), 1034–1048. https://doi.org/10.1016/J.NEURON.2014.10.035

Andalman, A. S., Burns, V. M., Lovett-Barron, M., Broxton, M., Poole, B., Yang, S. J., … Deisseroth, K. (2019). Neuronal Dynamics Regulating Brain and Behavioral State Transitions. *Cell*, *177*(4), 970-985.e20. https://doi.org/10.1016/j.cell.2019.02.037

Ando, H., Yanagihara, H., Hayashi, Y., Obi, Y., Tsuruoka, S., Takamura, T., … Fujimura, A. (2005). Rhythmic messenger ribonucleic acid expression of clock genes and adipocytokines in mouse visceral adipose tissue. *Endocrinology*, *146*(12), 5631–5636. https://doi.org/10.1210/en.2005-0771

Andres, K. H., von Düring, M., & Veh, R. W. (1999). Subnuclear organization of the rat habenular complexes. *The Journal of Comparative Neurology*, *407*(1), 130–150. https://doi.org/10.1002/(SICI)1096-9861(19990428)407:1<130::AID-CNE10>3.0.CO;2-8

Antoun, G., Bouchard-Cannon, P., Cannon, P. B., & Cheng, H.-Y. M. (2012). Regulation of MAPK/ERK signaling and photic entrainment of the suprachiasmatic nucleus circadian clock by Raf kinase inhibitor protein. *The Journal of Neuroscience: The Official Journal of the Society for Neuroscience*, *32*(14), 4867–4877. https://doi.org/10.1523/JNEUROSCI.5650-11.2012

Appelbaum, L., Anzulovich, A., Baler, R., & Gothilf, Y. (2005). Homeobox-clock protein interaction in zebrafish: A shared mechanism for pineal-specific and circadian gene expression. *Journal of Biological Chemistry*, *280*(12), 11544–11551. https://doi.org/10.1074/jbc.M412935200

Appelbaum, L., Wang, G. X., Maro, G. S., Mori, R., Tovin, A., Marin, W., … Mourrain, P. (2009). Sleep-wake regulation and hypocretin-melatonin interaction in zebrafish. *Proceedings of the National Academy of Sciences of the United States of America*, *106*(51), 21942–21947. https://doi.org/10.1073/pnas.906637106

Appelbaum, L., Wang, G., Yokogawa, T., Skariah, G. M., Smith, S. J., Mourrain, P., & Mignot, E. (2010). Circadian and homeostatic regulation of structural synaptic plasticity in hypocretin neurons. *Neuron*, *68*(1), 87–98. https://doi.org/10.1016/j.neuron.2010.09.006

Araki, M., McGeer, P. L., & McGeer, E. G. (1984). Retrograde HRP tracing combined with a pharmacohistochemical method for GABA transaminase for the identification of presumptive GABAergic projections to the habenula. *Brain Research*, *304*(2), 271–277. https://doi.org/10.1016/0006-8993(84)90330-5

Baño-Otálora, B., & Piggins, H. D. (2017). Contributions of the lateral habenula to circadian timekeeping. *Pharmacology Biochemistry and Behavior*, *162*, 46–54. https://doi.org/10.1016/J.PBB.2017.06.007

Baubet, V., Le Mouellic, H., Campbell, A. K., Lucas-Meunier, E., Fossier, P., & Brúlet, P. (2000). Chimeric green fluorescent protein-aequorin as bioluminescent Ca2+ reporters at the single-cell level. *Proceedings of the National Academy of Sciences of the United States of America*, *97*(13), 7260–7265. https://doi.org/10.1073/pnas.97.13.7260

Belle, M. D. C. (2015). Circadian Tick-Talking Across the Neuroendocrine System and Suprachiasmatic Nuclei Circuits: The Enigmatic Communication Between the Molecular and Electrical Membrane Clocks. *Journal of Neuroendocrinology*, *27*(7), 567–576. https://doi.org/10.1111/jne.12279

Belle, M. D. C., Baño-Otálora, B., & Piggins, H. D. (n.d.). Perforated Multi-Electrode Array recording.

Ben-Moshe Livne, Z., Alon, S., Vallone, D., Bayleyen, Y., Tovin, A., Shainer, I., … Gothilf, Y. (2016). Genetically Blocking the Zebrafish Pineal Clock Affects Circadian Behavior. *PloS Genet 12*(11), e1006445. https://doi.org/10.1371/journal.pgen.1006445

Ben-Moshe, Z., Foulkes, N. S., & Gothilf, Y. (2014). Functional development of the circadian clock in the zebrafish pineal gland. *BioMed Research International*. https://doi.org/10.1155/2014/235781

Bennett, L. D., Beremand, P., Thomas, T. L., & Bell-Pedersen, D. (2013). Circadian activation of the mitogen-activated protein kinase MAK-1 facilitates rhythms in clock-controlled genes in Neurospora crassa. *Eukaryotic Cell*, *12*(1), 59–69. https://doi.org/10.1128/EC.00207-12

Bérard, A. M., Dumon, M.-F., & Darmon, M. (2004). Dietary fish oil up-regulates cholesterol 7alpha-hydroxylase mRNA in mouse liver leading to an increase in bile acid and cholesterol excretion. *FEBS Letters*, *559*(1–3), 125–128. https://doi.org/10.1016/S0014-5793(04)00049-3

Berry, R. B. (2012). Circadian Rhythm Sleep Disorders. In *Fundamentals of Sleep Medicine* (pp. 515–543). Elsevier. https://doi.org/10.1016/B978-1-4377-0326-9.00026-9

Bianco, I. H., & Wilson, S. W. (2009). The habenular nuclei: a conserved asymmetric relay station in the vertebrate brain. *Philosophical Transactions of the Royal Society of London. Series B, Biological Sciences*, *364*(1519), 1005–1020. https://doi.org/10.1098/rstb.2008.0213

Biel, M., Wahl-Schott, C., Michalakis, S., & Zong, X. (2009). Hyperpolarization-Activated Cation Channels: From Genes to Function. *Physiological Reviews*, *89*(3), 847–885. https://doi.org/10.1152/physrev.00029.2008

Birnbaumer, M. (2000). Vasopressin Receptors. *Trends in Endocrinology & Metabolism*, *11*(10), 406–410. https://doi.org/10.1016/S1043-2760(00)00304-0

Bolliet, V., Bégay, V., Taragnat, C., Ravault, J. P., Collin, J. P., & Falcón, J. (1997). Photoreceptor cells of the pike pineal organ as cellular circadian oscillators. *The European Journal of Neuroscience*, *9*(4), 643–653. https://doi.org/10.1111/j.1460-9568.1997.tb01413.x

Boone, M., & Deen, P. M. T. (2008). Physiology and pathophysiology of the vasopressin-regulated renal water reabsorption. *Pflugers Archiv: European Journal of Physiology*, *456*(6), 1005–1024. https://doi.org/10.1007/s00424-008-0498-1

Braida, D., Donzelli, A., Martucci, R., Capurro, V., Busnelli, M., Chini, B., & Sala, M. (2012). Neurohypophyseal hormones manipulation modulate social and anxiety-related behavior in zebrafish. *Psychopharmacology*, *220*(2), 319–330. https://doi.org/10.1007/s00213-011-2482-2

Buhr, E. D., & Takahashi, J. S. (2013). Molecular Components of the Mammalian Circadian Clock (pp. 3–27). https://doi.org/10.1007/978-3-642-25950-0_1

Buijs, R. M. (1980). Immunocytochemical demonstration of vasopressin and oxytocin in the rat brain by light and electron microscopy. *Journal of Histochemistry & Cytochemistry*, *28*(4), 357–360. https://doi.org/10.1177/28.4.6989899

Bunney, B. G., Li, J. Z., Walsh, D. M., Stein, R., Vawter, M. P., Cartagena, P., … Bunney, W. E. (2015). Circadian dysregulation of clock genes: clues to rapid treatments in major depressive disorder. *Molecular Psychiatry*, *20*(1), 48–55. https://doi.org/10.1038/mp.2014.138

Burgess, H. A., & Granato, M. (2007). Sensorimotor Gating in Larval Zebrafish. *Journal of Neuroscience*, *27*(18), 4984–4994. https://doi.org/10.1523/JNEUROSCI.0615-07.2007

Cahill, G. M. (1996). Circadian regulation of melatonin production in cultured zebrafish pineal and retina. *Brain Research*, *708*(1–2), 177–181. https://doi.org/10.1016/0006-8993(95)01365-2

Cain, S. M., & Snutch, T. P. (2013). T-type calcium channels in burst-firing, network synchrony, and epilepsy. *Biochimica et Biophysica Acta (BBA) - Biomembranes*, *1828*(7), 1572–1578. https://doi.org/10.1016/j.bbamem.2012.07.028

Caldwell, H. K. (2017). Oxytocin and Vasopressin: Powerful Regulators of Social Behavior. *The Neuroscientist*, *23*(5), 517–528. https://doi.org/10.1177/1073858417708284

Carr, A. J. F., & Whitmore, D. (2005). Imaging of single light-responsive clock cells reveals fluctuating free-running periods. *Nature Cell Biology*, *7*(3), 319–321. https://doi.org/10.1038/ncb1232

Cassone, V. M. (2014, January). Avian circadian organization: A chorus of clocks. *Frontiers in Neuroendocrinology*. https://doi.org/10.1016/j.yfrne.2013.10.002

Cermakian, N., Pando, M. P., Thompson, C. L., Pinchak, A. B., Selby, C. P., Gutierrez, L., … Sassone-Corsi, P. (2002). Light Induction of a Vertebrate Clock Gene Involves Signaling through Blue-Light Receptors and MAP Kinases. *Current Biology*, *12*(10), 844–848. https://doi.org/10.1016/S0960-9822(02)00835-7

Chaix, A., Zarrinpar, A., & Panda, S. (2016). The circadian coordination of cell biology. *Journal of Cell Biology*. Rockefeller University Press. https://doi.org/10.1083/jcb.201603076

Chaudhury, D., Wang, L. M., & Colwell, C. S. (2005). Circadian regulation of hippocampal long-term potentiation. *Journal of Biological Rhythms*, *20*(3), 225–236. https://doi.org/10.1177/0748730405276352

Chen, T.-W., Wardill, T. J., Sun, Y., Pulver, S. R., Renninger, S. L., Baohan, A., … Kim, D. S. (2013). Ultrasensitive fluorescent proteins for imaging neuronal activity. *Nature*, *499*(7458), 295–300. https://doi.org/10.1038/nature12354

Cheng, M. Y., Bullock, C. M., Li, C., Lee, A. G., Bermak, J. C., Belluzzi, J., … Zhou, Q. Y. (2002). Prokineticin 2 transmits the behavioural circadian rhythm of the suprachiasmatic nucleus. *Nature*, *417*(6887), 405–410. https://doi.org/10.1038/417405a

Cheng, R. K., Krishnan, S., & Jesuthasan, S. (2016). Activation and inhibition of tph2 serotonergic neurons operate in tandem to influence larval zebrafish preference for light over darkness. *Scientific Reports*, *6*. https://doi.org/10.1038/srep20788

Cheng, R.-K., Jesuthasan, S. J., & Penney, T. B. (2014). Zebrafish forebrain and temporal conditioning. *Philosophical Transactions of the Royal Society of London. Series B, Biological Sciences*, *369*(1637), 20120462. https://doi.org/10.1098/rstb.2012.0462

Cheng, R.-K., Krishnan, S., Lin, Q., Kibat, C., & Jesuthasan, S. (2017). Characterization of a thalamic nucleus mediating habenula responses to changes in ambient illumination. *BMC Biology*, *15*(1), 104. https://doi.org/10.1186/s12915-017-0431-1

Chiu, C. N., & Prober, D. A. (2013). Regulation of zebrafish sleep and arousal states: current and prospective approaches. *Frontiers in Neural Circuits*, *7*, 58. https://doi.org/10.3389/fncir.2013.00058

Colwell, C. S. (2011, October). Linking neural activity and molecular oscillations in the SCN. *Nature Reviews Neuroscience*. https://doi.org/10.1038/nrn3086

Concha, M. L., Bianco, I. H., & Wilson, S. W. (2012, December). Encoding asymmetry within neural circuits. *Nature Reviews Neuroscience*. https://doi.org/10.1038/nrn3371

Concha, M. L., Russell, C., Regan, J. C., Tawk, M., Sidi, S., Gilmour, D. T., … Wilson, S. W. (2003). Local Tissue Interactions across the Dorsal Midline of the Forebrain Establish CNS Laterality. *Neuron*, *39*(3), 423–438. https://doi.org/10.1016/S0896-6273(03)00437-9

Concha, M. L., & Wilson, S. W. (2001). *Asymmetry in the epithalamus of vertebrates*. *J. Anat* (Vol. 199).

Coogan, A. N., & Piggins, H. D. (2003). Circadian and photic regulation of phosphorylation of ERK1/2 and Elk-1 in the suprachiasmatic nuclei of the Syrian hamster. *The Journal of Neuroscience: The Official Journal of the Society for Neuroscience*, *23*(7), 3085–3093. https://doi.org/10.1523/JNEUROSCI.23-07-03085.2003

Cutrera, R. A., Ouarour, A., & Pévet, P. (1994). Effects of the 5-HT1a receptor agonist 8-OH-DPAT and other non-photic stimuli on the circadian rhythm of wheel-running activity in hamsters under different constant conditions. *Neuroscience Letters*, *172*(1–2), 27–30. https://doi.org/10.1016/0304-3940(94)90654-8

Dana, H., Sun, Y., Mohar, B., Hulse, B. K., Kerlin, A. M., Hasseman, J. P., … Kim, D. S. (2019). High-performance calcium sensors for imaging activity in neuronal populations and microcompartments. *Nature Methods*, *16*(7), 649–657. https://doi.org/10.1038/s41592-019-0435-6

Davies, W. I. L., Tamai, T. K., Zheng, L., Fu, J. K., Rihel, J., Foster, R. G., … Hankins, M. W. (2015). An extended family of novel vertebrate photopigments is widely expressed and displays a diversity of function. *Genome Research*, *25*(11), 1666–1679. https://doi.org/10.1101/gr.189886.115

de Vries, G. J., & Buijs, R. M. (1983). The origin of the vasopressinergic and oxytocinergic innervation of the rat brain with special reference to the lateral septum. *Brain Research*, *273*(2), 307–317. https://doi.org/10.1016/0006-8993(83)90855-7

deCarvalho, T. N., Subedi, A., Rock, J., Harfe, B. D., Thisse, C., Thisse, B., … Hong, E. (2014). Neurotransmitter map of the asymmetric dorsal habenular nuclei of zebrafish. *Genesis (New York, N.Y.: 2000)*, *52*(6), 636–655. https://doi.org/10.1002/dvg.22785

Dekens, M. P. S., & Whitmore, D. (2008). Autonomous onset of the circadian clock in the zebrafish embryo. *The EMBO Journal*, *27*(20), 2757. https://doi.org/10.1038/EMBOJ.2008.183

Delaloye, S., & Holtzheimer, P. E. (2014). Deep brain stimulation in the treatment of depression. *Dialogues in Clinical Neuroscience*, *16*(1), 83–91. Retrieved from http://www.ncbi.nlm.nih.gov/pubmed/24733973

Díaz, E., Bravo, D., Rojas, X., & Concha, M. L. (2011). Morphologic and immunohistochemical organization of the human habenular complex. *The Journal of Comparative Neurology*, *519*(18), 3727–3747. https://doi.org/10.1002/cne.22687

Dibner, C., Schibler, U., & Albrecht, U. (2010). The Mammalian Circadian Timing System: Organization and Coordination of Central and Peripheral Clocks. *Annual Review of Physiology*, *72*(1), 517–549. https://doi.org/10.1146/annurev-physiol-021909-135821

Domínguez-López, S., Howell, R. D., López-Canúl, M. G., Leyton, M., & Gobbi, G. (2014). Electrophysiological characterization of dopamine neuronal activity in the ventral tegmental area across the light-dark cycle. *Synapse*, *68*(10), 454–467. https://doi.org/10.1002/syn.21757

Dreosti, E., Lopes, G., Kampff, A. R., & Wilson, S. W. (2015). Development of social behavior in young zebrafish. *Frontiers in Neural Circuits*, *9*(AUGUST). https://doi.org/10.3389/fncir.2015.00039

Dreosti, E., Vendrell Llopis, N., Carl, M., Yaksi, E., & Wilson, S. W. (2014). Left-right asymmetry is required for the habenulae to respond to both visual and olfactory stimuli. *Current Biology: CB*, *24*(4), 440–445. https://doi.org/10.1016/j.cub.2014.01.016

Duboué, E. R., Hong, E., Eldred, K. C., & Halpern, M. E. (2017). Left Habenular Activity Attenuates Fear Responses in Larval Zebrafish. *Current Biology*, *27*(14), 2154-2162.e3. https://doi.org/10.1016/j.cub.2017.06.017

Dudley, T. E., DiNardo, L. A., & Glass, J. D. (1998). Endogenous Regulation of Serotonin Release in the Hamster Suprachiasmatic Nucleus. *Journal of Neuroscience*, *18*(13), 5045–5052. https://doi.org/10.1523/JNEUROSCI.18-13-05045.1998

Duez, H., & Staels, B. (2009, December). Rev-erb-α: An integrator of circadian rhythms and metabolism. *Journal of Applied Physiology*. https://doi.org/10.1152/japplphysiol.00570.2009

Dzirasa, K., Ribeiro, S., Costa, R., Santos, L. M., Lin, S.-C., Grosmark, A., … Nicolelis, M. A. L. (2006). Dopaminergic Control of Sleep-Wake States. *Journal of Neuroscience*, *26*(41), 10577–10589. https://doi.org/10.1523/JNEUROSCI.1767-06.2006

Eckel-Mahan, K. L., Phan, T., Han, S., Wang, H., Chan, G. C. K., Scheiner, Z. S., & Storm, D. R. (2008). Circadian oscillation of hippocampal MAPK activity and cAmp: implications for memory persistence. *Nature Neuroscience*, *11*(9), 1074–1082. Retrieved from http://www.ncbi.nlm.nih.gov/pubmed/19160506

Enoki, R., Kuroda, S., Ono, D., Hasan, M. T., Ueda, T., Honma, S., & Honma, K. (2012). Topological specificity and hierarchical network of the circadian calcium rhythm in the suprachiasmatic nucleus. *Proceedings of the National Academy of Sciences of the United States of America*, *109*(52), 21498–21503. https://doi.org/10.1073/pnas.1214415110

Evely, K. M., Hudson, R. L., Dubocovich, M. L., & Haj-Dahmane, S. (2016). Melatonin Receptor Activation Increases Glutamatergic Synaptic Transmission in the Rat Medial Lateral Habenula. *Synapse*, *70*, 181–186. https://doi.org/10.1002/syn.21892

Facchin, L., Duboué, E. R., & Halpern, M. E. (2015). Disruption of Epithalamic Left-Right Asymmetry Increases Anxiety in Zebrafish. *The Journal of Neuroscience: The Official Journal of the Society for Neuroscience*, *35*(48), 15847–15859. https://doi.org/10.1523/JNEUROSCI.2593-15.2015

Faron-Górecka, A., Kušmider, M., Kolasa, M., Zurawek, D., Szafran-Pilch, K., Gruca, P., … Dziedzicka-Wasylewska, M. (2016). Chronic mild stress alters the somatostatin receptors in the rat brain. *Psychopharmacology*, *233*(2), 255–266. https://doi.org/10.1007/s00213-015-4103-y

Fore, S., Ilyas Cosacak, M., Diaz Verdugo, C., Kizil, C., & Yaksi, E. (n.d.). Functional properties of habenular neurons are determined by developmental stage and sequential neurogenesis. https://doi.org/10.1101/722462

Forsling, M. L., Montgomeryt, H., Halpintt, D., Windle, R. J., & Treachert, D. F. (1998). *DAILY PATTERNS OF SECRETION OF NEUROHYPOPHYSIAL HORMONES IN MAN: EFFECT OF AGE*. *Experimental Physiology* (Vol. 83). Retrieved from https://physoc.onlinelibrary.wiley.com/doi/pdf/10.1113/expphysiol.1998.sp004124

Foulkes, N. S., Whitmore, D., Vallone, D., & Bertolucci, C. (2016). Studying the Evolution of the Vertebrate Circadian Clock: The Power of Fish as Comparative Models. *Advances in Genetics*, *95*, 1–30. https://doi.org/10.1016/bs.adgen.2016.05.002

Freeman, G. M., Krock, R. M., Aton, S. J., Thaben, P., & Herzog, E. D. (2013). GABA networks destabilize genetic oscillations in the circadian pacemaker. *Neuron*, *78*(5), 799–806. https://doi.org/10.1016/j.neuron.2013.04.003

Friedrich, J., Zhou, P., & Paninski, L. (2017). Fast online deconvolution of calcium imaging data. *PLOS Computational Biology*, *13*(3), e1005423. https://doi.org/10.1371/journal.pcbi.1005423

Frøland Steindal, I. A., & Whitmore, D. (2019). Circadian Clocks in Fish-What Have We Learned so far? *Biology*, *8*(1). https://doi.org/10.3390/biology8010017

Gamse, J. T., Thisse, C., Thisse, B., & Halpern, M. E. (2003). The parapineal mediates left-right asymmetry in the zebrafish diencephalon. *Development (Cambridge, England)*, *130*(6), 1059–1068. https://doi.org/10.1242/dev.00270

Gao, Q., Li, D., Liu, W., Xu, X., Li, H., Fu, L., & Wang, Y. (2015). The participation of oxytocin in the abirritation of lateral habenular nucleus on normal adult rats. *Brain Research*, *1602*, 106–110. https://doi.org/10.1016/J.BRAINRES.2014.12.006

Garcia-Heras, M. S., Mougeot, F., Simmons, R. E., & Arroyo, B. (2017). Regional and temporal variation in diet and provisioning rates suggest weather limits prey availability for an endangered raptor. *Ibis*, *159*(3), 567–579. https://doi.org/10.1111/ibi.12478

GarphPad. (2017). The power of nonparametric tests. Retrieved July 15, 2019, from https://www.graphpad.com/guides/prism/7/statistics/index.htm?stat_the_power_of_nonparametric_tes.htm

Gaten, E., Tarling, G., Dowse, H., Kyriacou, C., & Rosato, E. (2008). Is vertical migration in Antarctic krill (Euphausia superba) influenced by an underlying circadian rhythm? *Journal of Genetics*, *87*(5), 473–483. Retrieved from http://www.ncbi.nlm.nih.gov/pubmed/19147936

Gau, D., Lemberger, T., Von Gall, C., Kretz, O., Le Minh, N., Gass, P., … Schütz, G. (2002). Phosphorylation of CREB Ser142 regulates light-induced phase shifts of the circadian clock. *Neuron*, *34*(2), 245–253. https://doi.org/10.1016/S0896-6273(02)00656-6

Geisler, S., Andres, K. H., & Veh, R. W. (2003). Morphologic and cytochemical criteria for the identification and delineation of individual subnuclei within the lateral habenular complex of the rat. *The Journal of Comparative Neurology*, *458*(1), 78–97. https://doi.org/10.1002/cne.10566

Gillette, M. U. (1986). The suprachiasmatic nuclei: circadian phase-shifts induced at the time of hypothalamic slice preparation are preserved in vitro. *Brain Research*, *379*(1), 176–181. https://doi.org/10.1016/0006-8993(86)90273-8

Gizowski, C., Zaelzer, C., & Bourque, C. W. (2016). Clock-driven vasopressin neurotransmission mediates anticipatory thirst prior to sleep. *Nature*, *537*(7622), 685–688. https://doi.org/10.1038/nature19756

Goldsmith, C. S., & Bell-Pedersen, D. (2013). Diverse roles for MAPK signalling in circadian clocks. *Advances in Genetics*, *84*, 1–39. https://doi.org/10.1016/B978-0-12-407703-4.00001-3

Goll, M. G., Anderson, R., Stainier, D. Y. R., Spradling, A. C., & Halpern, M. E. (2009). Transcriptional Silencing and Reactivation in Transgenic Zebrafish. *Genetics*, *182*(3), 747. https://doi.org/10.1534/GENETICS.109.102079

Good, C. H., Wang, H., Chen, Y. H., Mejias-Aponte, C. A., Hoffman, A. F., & Lupica, C. R. (2013). Dopamine D4 receptor excitation of lateral habenula neurons via multiple cellular mechanisms. *Journal of Neuroscience*, *33*(43), 16853–16864. https://doi.org/10.1523/JNEUROSCI.1844-13.2013

Gould, B., & Zingg, H. (2003). Mapping oxytocin receptor gene expression in the mouse brain and mammary gland using an oxytocin receptor–LacZ reporter mouse. *Neuroscience*, *122*(1), 155–167. https://doi.org/10.1016/S0306-4522(03)00283-5

Gozdowska, M., Kleszczyńska, A., Sokołowska, E., & Kulczykowska, E. (2006). Arginine vasotocin (AVT) and isotocin (IT) in fish brain: Diurnal and seasonal variations. *Comparative Biochemistry and Physiology - B Biochemistry and Molecular Biology*, *143*(3), 330–334. https://doi.org/10.1016/j.cbpb.2005.12.004

Granados-Fuentes, D., Prolo, L. M., Abraham, U., & Herzog, E. D. (2004). The Suprachiasmatic Nucleus Entrains, but Does Not Sustain, Circadian Rhythmicity in the Olfactory Bulb. *Journal of Neuroscience*, *24*(3), 615–619. https://doi.org/10.1523/JNEUROSCI.4002-03.2004

Granados-Fuentes, D., Saxena, M. T., Prolo, L. M., Aton, S. J., & Herzog, E. D. (2004). Olfactory bulb neurons express functional, entrainable circadian rhythms. *European Journal of Neuroscience*, *19*(4), 898–906. https://doi.org/10.1111/j.0953-816X.2004.03117.x

Gravati, M., Busnelli, M., Bulgheroni, E., Reversi, A., Spaiardi, P., Parenti, M., … Chini, B. (2010). Dual modulation of inward rectifier potassium currents in olfactory neuronal cells by promiscuous G protein coupling of the oxytocin receptor. *Journal of Neurochemistry*, *114*(5), no-no. https://doi.org/10.1111/j.1471-4159.2010.06861.x

Guilding, C., Hughes, A. T. L., & Piggins, H. D. (2010). Circadian oscillators in the epithalamus. *Neuroscience*, *169*(4), 1630–1639. https://doi.org/10.1016/j.neuroscience.2010.06.015

Guilding, C., Hughes, A. T., Brown, T. M., Namvar, S., & Piggins, H. D. (2009). A riot of rhythms: Neuronal and glial circadian oscillators in the mediobasal hypothalamus. *Molecular Brain*, *2*(1). https://doi.org/10.1186/1756-6606-2-28

Guilding, C., & Piggins, H. D. (2007). Challenging the omnipotence of the suprachiasmatic timekeeper: are circadian oscillators present throughout the mammalian brain? *European Journal of Neuroscience*, *25*(11), 3195–3216. https://doi.org/10.1111/j.1460-9568.2007.05581.x

Hack, I., Peichl, L., & Brandstätter, J. H. (1999). An alternative pathway for rod signals in the rodent retina: rod photoreceptors, cone bipolar cells, and the localization of glutamate receptors. *Proceedings of the National Academy of Sciences of the United States of America*, *96*(24), 14130–14135. https://doi.org/10.1073/PNAS.96.24.14130

Han, L.-N., Zhang, L., Li, L.-B., Sun, Y.-N., Wang, Y., Chen, L., … Liu, J. (2015). Activation of serotonin(2C) receptors in the lateral habenular nucleus increases the expression of depression-related behaviors in the hemiparkinsonian rat. *Neuropharmacology*, *93*, 68–79. https://doi.org/10.1016/j.neuropharm.2015.01.024

Han, S., Yang, S. H., Kim, J. Y., Mo, S., Yang, E., Song, K. M., … Kim, H. (2017). Down-regulation of cholinergic signaling in the habenula induces anhedonia-like behavior. *Scientific Reports*, *7*(1). https://doi.org/10.1038/s41598-017-01088-6

Hardin, P. E., Hall, J. C., & Rosbash, M. (1990). Feedback of the Drosophila period gene product on circadian cycling of its messenger RNA levels. *Nature*, *343*(6258), 536–540. https://doi.org/10.1038/343536a0

Harmar, A. J., Marston, H. M., Shen, S., Spratt, C., West, K. M., Sheward, W. J., … Hastings, M. H. (2002). The VPAC2 receptor is essential for circadian function in the mouse suprachiasmatic nuclei. *Cell*, *109*(4), 497–508. https://doi.org/10.1016/S0092-8674(02)00736-5

Hastings, M. H., Brancaccio, M., & Maywood, E. S. (2014, January). Circadian pacemaking in cells and circuits of the suprachiasmatic nucleus. *Journal of Neuroendocrinology*. https://doi.org/10.1111/jne.12125

Hastings, M. H., Maywood, E. S., & Brancaccio, M. (2018, August 1). Generation of circadian rhythms in the suprachiasmatic nucleus. *Nature Reviews Neuroscience*. Nature Publishing Group. https://doi.org/10.1038/s41583-018-0026-z

Hastings, M. H., Reddy, A. B., & Maywood, E. S. (2003). A clockwork web: Circadian timing in brain and periphery, in health and disease. *Nature Reviews Neuroscience*, *4*(8), 649–661. https://doi.org/10.1038/nrn1177

Hattar, S., Kumar, M., Park, A., Tong, P., Tung, J., Yau, K.-W., & Berson, D. M. (2006). Central projections of melanopsin-expressing retinal ganglion cells in the mouse. *The Journal of Comparative Neurology*, *497*(3), 326–349. https://doi.org/10.1002/cne.20970

Hendricks, M., & Jesuthasan, S. (2007). Electroporation-based methods for in vivo, whole mount and primary culture analysis of zebrafish brain development. *Neural Development*, *2*, 6. https://doi.org/10.1186/1749-8104-2-6

Herget, U., Gutierrez-Triana, J. A., Thula, O. S., Knerr, B., & Ryu, S. (2017). Single-cell reconstruction of oxytocinergic neurons reveals separate hypophysiotropic and encephalotropic subtypes in larval zebrafish. *ENeuro*, *4*(1). https://doi.org/10.1523/ENEURO.0278-16.2016

Herkenham, M., & Nauta, W. J. (1979). Efferent connections of the habenular nuclei in the rat. *The Journal of Comparative Neurology*, *187*(1), 19–47. https://doi.org/10.1002/cne.901870103

Herkenham, M., & Nauta, W. J. (1977). Afferent connections of the habenular nuclei in the rat. A horseradish peroxidase study, with a note on the fiber-of-passage problem. *The Journal of Comparative Neurology*, *173*(1), 123–146. https://doi.org/10.1002/cne.901730107

Hikosaka, O. (2010, April). The habenula: From stress evasion to value-based decision-making. *Nature Reviews Neuroscience*. https://doi.org/10.1038/nrn2866

Hirayama, J., Miyamura, N., Uchida, Y., Asaoka, Y., Honda, R., Sawanobori, K., … Nishina, H. (2009). Common light signaling pathways controlling DNA repair and circadian clock entrainment in zebrafish. *Cell Cycle*, *8*(17), 2794–2801. https://doi.org/10.4161/cc.8.17.9447

Hirayama, M., Mure, L. S., & Panda, S. (2018, October 1). Circadian regulation of energy intake in mammals. *Current Opinion in Physiology*. Elsevier Ltd. https://doi.org/10.1016/j.cophys.2018.11.002

Ho, J., Tumkaya, T., Aryal, S., Choi, H., & Claridge-Chang, A. (2018). Moving beyond P values: Everyday data analysis with estimation plots. *BioRxiv*, 377978. https://doi.org/10.1101/377978

Hong, E., Santhakumar, K., Akitake, C. A., Ahn, S. J., Thisse, C., Thisse, B., … Halpern, M. E. (2013). Cholinergic left-right asymmetry in the habenulo-interpeduncular pathway.

Proceedings of the National Academy of Sciences of the United States of America, *110*(52). https://doi.org/10.1073/pnas.1319566110

Hong, S., & Hikosaka, O. (2008). The Globus Pallidus Sends Reward-Related Signals to the Lateral Habenula. *Neuron*, *60*(4), 720–729. https://doi.org/10.1016/j.neuron.2008.09.035

Honma, S., & Honma, K. ichi. (2003). The biological clock: Ca2+ links the pendulum to the hands. *Trends in Neurosciences*, *26*(12), 650–653. https://doi.org/10.1016/J.TINS.2003.09.012

Hood, S., Cassidy, P., Cossette, M.-P., Weigl, Y., Verwey, M., Robinson, B., … Amir, S. (2010). Endogenous Dopamine Regulates the Rhythm of Expression of the Clock Protein PER2 in the Rat Dorsal Striatum via Daily Activation of D2 Dopamine Receptors. *Journal of Neuroscience*, *30*(42), 14046–14058. https://doi.org/10.1523/JNEUROSCI.2128-10.2010

Hsu, Y. W. A., Gile, J. J., Perez, J. G., Morton, G., Ben-Hamo, M., Turner, E. E., & de la Iglesia, H. O. (2017). The Dorsal Medial Habenula Minimally Impacts Circadian Regulation of Locomotor Activity and Sleep. *Journal of Biological Rhythms*, *32*(5), 444–455. https://doi.org/10.1177/0748730417730169

Huang, J., Zhong, Z., Wang, M., Chen, X., Tan, Y., Zhang, S., … Wang, H. (2015). Circadian modulation of dopamine levels and dopaminergic neuron development contributes to attention deficiency and hyperactive behaviour. *35*(6). https://doi.org/10.1523/JNEUROSCI.2551-14.2015

Hughes, A. T., Fahey, B., Cutler, D. J., Coogan, A. N., & Piggins, H. D. (2004). Aberrant Gating of Photic Input to the Suprachiasmatic Circadian Pacemaker of Mice Lacking the VPAC2 Receptor. *Journal of Neuroscience*, *24*(14), 3522–3526. https://doi.org/10.1523/JNEUROSCI.5345-03.2004

Hurd, M. W., Debruyne, J., Straume, M., & Cahill, G. M. (1998). Circadian Rhythms of Locomotor Activity in Zebrafish. *Physiology & Behavior*, *65*(3), 465–472. https://doi.org/10.1016/S0031-9384(98)00183-8

Hurd, M. W., & Cahill, G. M. (2002). *Entraining Signals Initiate Behavioral Circadian Rhythmicity in Larval Zebrafish*. Retrieved from https://journals.sagepub.com/doi/pdf/10.1177/074873002129002618

Hut, R. A., & Van der Zee, E. A. (2011). The cholinergic system, circadian rhythmicity, and time memory. *Behavioural Brain Research*, *221*(2), 466–480. https://doi.org/10.1016/J.BBR.2010.11.039

Ikeda, M., Sugiyama, T., Wallace, C. S., Gompf, H. S., Yoshioka, T., Miyawaki, A., & Allen, C. N. (2003). Circadian dynamics of cytosolic and nuclear Ca2+ in single suprachiasmatic nucleus neurons. *Neuron*, *38*(2), 253–263. https://doi.org/10.1016/S0896-6273(03)00164-8

Iwasaki, K., Taguchi, M., Bonkowsky, J. L., & Kuwada, J. Y. (2013). Expression of arginine vasotocin receptors in the developing zebrafish CNS. *Gene Expression Patterns*, *13*(8), 335–342. https://doi.org/10.1016/j.gep.2013.06.005

Jetti, S. K., Vendrell-Llopis, N., & Yaksi, E. (2014). Spontaneous Activity Governs Olfactory Representations in Spatially Organized Habenular Microcircuits. *Current Biology*, *24*(4), 434–439. https://doi.org/10.1016/J.CUB.2014.01.015

Jhou, T. C., Geisler, S., Marinelli, M., Degarmo, B. A., & Zahm, D. S. (2009). The mesopontine rostromedial tegmental nucleus: A structure targeted by the lateral habenula that projects to the ventral tegmental area of Tsai and substantia nigra compacta. *The Journal of Comparative Neurology*, *513*(6), 566–596. https://doi.org/10.1002/cne.21891

Jhou, T. C., Good, C. H., Rowley, C. S., Xu, S.-P., Wang, H., Burnham, N. W., … Ikemoto, S. (2013). Cocaine drives aversive conditioning via delayed activation of dopamine-responsive

habenular and midbrain pathways. *The Journal of Neuroscience: The Official Journal of the Society for Neuroscience*, *33*(17), 7501–7512. https://doi.org/10.1523/JNEUROSCI.3634-12.2013

Johnson, R. F., Moore, R. Y., & Morin, L. P. (1988). Loss of entrainment and anatomical plasticity after lesions of the hamster retinohypothalamic tract. *Brain Research*, *460*(2), 297–313. https://doi.org/10.1016/0006-8993(88)90374-5

Jones, B. E., & Moore, R. Y. (1977). Ascending projections of the locus coeruleus in the rat. II. Autoradiographic study. *Brain Research*, *127*(1), 23–53. https://doi.org/10.1016/0006-8993(77)90378-X

Jones, J. R., Simon, T., Lones, L., & Herzog, E. D. (2018). SCN VIP Neurons Are Essential for Normal Light-Mediated Resetting of the Circadian System. *The Journal of Neuroscience*, *38*(37), 7986–7995. https://doi.org/10.1523/JNEUROSCI.1322-18.2018

Kaiser, C., Kaufmann, C., Leutritz, T., Arnold, Y. L., Speck, O., & Ullsperger, M. (2019). The human habenula is responsive to changes in luminance and circadian rhythm. *NeuroImage*, *189*, 581–588. https://doi.org/10.1016/j.neuroimage.2019.01.064

Kalén, P., Strecker, R. E., Rosengren, E., & Björklund, A. (1989). Regulation of striatal serotonin release by the lateral habenula-dorsal raphe pathway in the rat as demonstrated by in vivo microdialysis: role of excitatory amino acids and GABA. *Brain Research*, *492*(1–2), 187–202. https://doi.org/10.1016/0006-8993(89)90901-3

Kalsbeek, A., Fliers, E., Hofman, M. A., Swaab, D. F., & Buijs, R. M. (2010). Vasopressin and the Output of the Hypothalamic Biological Clock. *Journal of Neuroendocrinology*, *22*(5), 362–372. https://doi.org/10.1111/j.1365-2826.2010.01956.x

Kaneko, M., Hernandez-Borsetti, N., & Cahill, G. M. (2006). Diversity of zebrafish peripheral oscillators revealed by luciferase reporting. *Proceedings of the National Academy of Sciences of the United States of America*, *103*(39), 14614–14619. https://doi.org/10.1073/pnas.0606563103

Kannan, M., Vasan, G., & Pieribone, V. A. (2019). Optimizing Strategies for Developing Genetically Encoded Voltage Indicators. *Frontiers in Cellular Neuroscience*, *13*, 53. https://doi.org/10.3389/fncel.2019.00053

Kim, H. J., & Harrington, M. E. (2008). Neuropeptide Y-deficient mice show altered circadian response to simulated natural photoperiod. *Brain Research*, *1246*, 96–100. https://doi.org/10.1016/j.brainres.2008.09.040

Kim, U. (2009). Topographic commissural and descending projections of the habenula in the rat. *The Journal of Comparative Neurology*, *513*(2), 173–187. https://doi.org/10.1002/cne.21951

Kimura, T., Makino, Y., Saji, F., Takemura, M., Inoue, T., Kikuchi, T., … Tokugawa, Y. (1994). Molecular characterization of a cloned human oxytocin receptor. *European Journal of Endocrinology*, *131*(4), 385–390. Retrieved from http://www.ncbi.nlm.nih.gov/pubmed/7921228

King, D. P., Zhao, Y., Sangoram, A. M., Wilsbacher, L. D., Tanaka, M., Antoch, M. P., … Takahashi, J. S. (1997). Positional cloning of the mouse circadian clock gene. *Cell*, *89*(4), 641–653. Retrieved from http://www.ncbi.nlm.nih.gov/pubmed/9160755

Klemm, W. R. (2004). Habenular and interpeduncularis nuclei: shared components in multiple-function networks. *Medical Science Monitor: International Medical Journal of Experimental and Clinical Research*, *10*(11), RA261-73. Retrieved from http://www.ncbi.nlm.nih.gov/pubmed/15507867

Knafo, S., Fidelin, K., Prendergast, A., Tseng, P.-E. B., Parrin, A., Dickey, C., … Wyart, C. (2017). Mechanosensory neurons control the timing of spinal microcircuit selection during locomotion. *ELife*, *6*. https://doi.org/10.7554/eLife.25260

Knafo, S., Prendergast, A., Thouvenin, O., Figueiredo, S. N., & Wyart, C. (2017). Bioluminescence Monitoring of Neuronal Activity in Freely Moving Zebrafish Larvae. *Bio-Protocol*, *7*(18), e2550. https://doi.org/10.21769/BioProtoc.2550

Kobayashi, Y., Ishikawa, T., Hirayama, J., Daiyasu, H., Kanai, S., Toh, H., … Todo, T. (2000). Molecular analysis of zebrafish photolyase/cryptochrome family: Two types of cryptochromes present in zebrafish. *Genes to Cells*, *5*(9), 725–738. https://doi.org/10.1046/j.1365-2443.2000.00364.x

Konopka, R. J., & Benzer, S. (1971). Clock mutants of Drosophila melanogaster. *Proceedings of the National Academy of Sciences of the United States of America*, *68*(9), 2112–2116. https://doi.org/10.1073/pnas.68.9.2112

Korshunov, K. S., Blakemore, L. J., & Trombley, P. Q. (2017). Dopamine: A Modulator of Circadian Rhythms in the Central Nervous System. *Frontiers in Cellular Neuroscience*, *11*, 91. https://doi.org/10.3389/fncel.2017.00091

Krishnan, S., Mathuru, A. S., Kibat, C., Rahman, M., Lupton, C. E., Stewart, J., … Jesuthasan, S. (2014). The Right Dorsal Habenula Limits Attraction to an Odor in Zebrafish. *Current Biology*, *24*(11), 1167–1175. https://doi.org/10.1016/J.CUB.2014.03.073

Kulczykowska, E., Warne, J. M., & Balment, R. J. (2001). Day-night variations in plasma melatonin and arginine vasotocin concentrations in chronically cannulated flounder (Platichthys flesus). *Comparative Biochemistry and Physiology. Part A, Molecular & Integrative Physiology*, *130*(4), 827–834. Retrieved from http://www.ncbi.nlm.nih.gov/pubmed/11691618

Kuo, I. Y., & Ehrlich, B. E. (2015). Signaling in muscle contraction. *Cold Spring Harbor Perspectives in Biology*, *7*(2), a006023. https://doi.org/10.1101/cshperspect.a006023

Lal, P., Tanabe, H., Suster, M. L., Ailani, D., Kotani, Y., Muto, A., … Kawakami, K. (2018). Identification of a neuronal population in the telencephalon essential for fear conditioning in zebrafish. *BMC Biology*, *16*(1), 45. https://doi.org/10.1186/s12915-018-0502-y

Lamberts, S. W. J., Reubi, J. C., & Krenning, E. P. (1997). Chapter 17 Somatostatin. In *Principles of Medical Biology* (Vol. 10, pp. 403–419). Elsevier Inc. https://doi.org/10.1016/S1569-2582(97)80162-6

Lamont, E. W., Robinson, B., Stewart, J., & Amir, S. (2005). The central and basolateral nuclei of the amygdala exhibit opposite diurnal rhythms of expression of the clock protein Period2. *Proceedings of the National Academy of Sciences of the United States of America*, *102*(11), 4180–4184. https://doi.org/10.1073/pnas.0500901102

Langel, J., Ikeno, T., Yan, L., Nunez, A. A., & Smale, L. (2018). Distributions of GABAergic and glutamatergic neurons in the brains of a diurnal and nocturnal rodent. *Brain Research*, *1700*, 152–159. https://doi.org/10.1016/j.brainres.2018.08.019

Lee, H. W., Yang, S. H., Kim, J. Y., & Kim, H. (2019). The Role of the Medial Habenula Cholinergic System in Addiction and Emotion-Associated Behaviors. *Frontiers in Psychiatry*, *10*(FEB), 100. https://doi.org/10.3389/fpsyt.2019.00100

Lee, M. G., Hassani, O. K., & Jones, B. E. (2005). Discharge of Identified Orexin/Hypocretin Neurons across the Sleep-Waking Cycle. *Journal of Neuroscience*, *25*(28), 6716–6720. https://doi.org/10.1523/JNEUROSCI.1887-05.2005

Lehman, M., Silver, R., Gladstone, W., Kahn, R., Gibson, M., & Bittman, E. (1987). Circadian rhythmicity restored by neural transplant. Immunocytochemical characterization of the graft and its integration with the host brain. *The Journal of Neuroscience*, *7*(6), 1626–1638. https://doi.org/10.1523/JNEUROSCI.07-06-01626.1987

Leng, G., & Ludwig, M. (2008). Neurotransmitters and peptides: whispered secrets and public announcements. *The Journal of Physiology*, *586*(Pt 23), 5625. https://doi.org/10.1113/JPHYSIOL.2008.159103

Leung, L. C., Wang, G. X., & Mourrain, P. (2013). Imaging zebrafish neural circuitry from whole brain to synapse. *Frontiers in Neural Circuits*, *7*, 76. https://doi.org/10.3389/fncir.2013.00076

Li, B., Piriz, J., Mirrione, M., Chung, C., Proulx, C. D., Schulz, D., … Malinow, R. (2011). Synaptic potentiation onto habenula neurons in the learned helplessness model of depression. *Nature*, *470*(7335), 535–541. https://doi.org/10.1038/nature09742

Li, X., Zhang, C., & Zhou, Q.-Y. (2018). Overexpression of Prokineticin 2 in Transgenic Mice Leads to Reduced Circadian Behavioral Rhythmicity and Altered Molecular Rhythms in the Suprachiasmatic Clock. *Journal of Circadian Rhythms*, *16*(1). https://doi.org/10.5334/jcr.170

Li, Y., Gao, X.-B., Sakurai, T., & van den Pol, A. N. (2002). Hypocretin/Orexin Excites Hypocretin Neurons via a Local Glutamate Neuron—A Potential Mechanism for Orchestrating the Hypothalamic Arousal System. *Neuron*, *36*(6), 1169–1181. https://doi.org/10.1016/S0896-6273(02)01132-7

Lin, Q., & Jesuthasan, S. (2017). Masking of a circadian behavior in larval zebrafish involves the thalamo-habenula pathway. *Scientific Reports*, *7*(1). https://doi.org/10.1038/s41598-017-04205-7

Liu, C., & Reppert, S. M. (2000). GABA synchronizes clock cells within the suprachiasmatic circadian clock. *Neuron*, *25*(1), 123–128. https://doi.org/10.1016/S0896-6273(00)80876-4

Liu, J., & Baraban, S. C. (2019). Network Properties Revealed during Multi-Scale Calcium Imaging of Seizure Activity in Zebrafish. *ENeuro*, *6*(1), ENEURO.0041-19.2019. https://doi.org/10.1523/ENEURO.0041-19.2019

Liu, Y., Curtis, J. T., & Wang, Z. (2001). Vasopressin in the lateral septum regulates pair bond formation in male prairie voles (Microtus ochrogaster). *Behavioral Neuroscience*, *115*(4), 910–919. https://doi.org/10.1037/0735-7044.115.4.910

Lu, Y.-F., Moriwaki, A., Tomizawa, K., Onuma, H., Cai, X.-H., & Matsui, H. (1997). Effects of vasopressin and involvement of receptor subtypes in the rat central amygdaloid nucleus in vitro. *Brain Research*, *768*(1–2), 266–272. https://doi.org/10.1016/S0006-8993(97)00655-0

Lyons, D. (n.d.). Hormones and the Regulation of Neuronal Voltage-Sensing Ion Channels. In *Hormonal Signalling in Biology and Medicine*.

Maniezzi, C., Talpo, F., Spaiardi, P., Toselli, M., & Biella, G. (2019). Oxytocin Increases Phasic and Tonic GABAergic Transmission in CA1 Region of Mouse Hippocampus. *Frontiers in Cellular Neuroscience*, *13*, 178. https://doi.org/10.3389/fncel.2019.00178

Manning, M., Misicka, A., Olma, A., Bankowski, K., Stoev, S., Chini, B., … Guillon, G. (2012). Oxytocin and vasopressin agonists and antagonists as research tools and potential therapeutics. *Journal of Neuroendocrinology*, *24*(4), 609–628. https://doi.org/10.1111/j.1365-2826.2012.02303.x

Mao, L.-M., & Wang, J. Q. (2016). Synaptically Localized Mitogen-Activated Protein Kinases: Local Substrates and Regulation. *Molecular Neurobiology*, *53*(9), 6309–6315. https://doi.org/10.1007/s12035-015-9535-1

Margolis, E. B., & Fields, H. L. (2016). Mu Opioid Receptor Actions in the Lateral Habenula. *PloS One*, *11*(7), e0159097. https://doi.org/10.1371/journal.pone.0159097

Mathuru, A. S. (2018, June 1). A little rein on addiction. *Seminars in Cell and Developmental Biology*. Elsevier Ltd. https://doi.org/10.1016/j.semcdb.2017.09.030

Matsumoto, M., & Hikosaka, O. (2009). Representation of negative motivational value in the primate lateral habenula. *Nature Neuroscience*, *12*(1), 77–84. https://doi.org/10.1038/nn.2233

Matsumoto, M., & Hikosaka, O. (2007). Lateral habenula as a source of negative reward signals in dopamine neurons. *Nature*, *447*(7148), 1111–1115. https://doi.org/10.1038/nature05860

McCormick, D. A., & Bal, T. (1997). SLEEP AND AROUSAL: Thalamocortical Mechanisms. *Annual Review of Neuroscience*, *20*(1), 185–215. https://doi.org/10.1146/annurev.neuro.20.1.185

Meeker, N. D., Hutchinson, S. A., Ho, L., & Trede, N. S. (2007). Method for isolation of PCR-ready genomic DNA from zebrafish tissues. *BioTechniques*, *43*(5), 610–614. https://doi.org/10.2144/000112619

Meguro, Y., Miyano, K., Hirayama, S., Yoshida, Y., Ishibashi, N., Ogino, T., … Uezono, Y. (2018). Neuropeptide oxytocin enhances μ opioid receptor signaling as a positive allosteric modulator. *Journal of Pharmacological Sciences*, *137*(1), 67–75. https://doi.org/10.1016/J.JPHS.2018.04.002

Mendoza, J. (2017). Circadian neurons in the lateral habenula: Clocking motivated behaviors. *Pharmacology Biochemistry and Behavior*, *162*, 55–61. https://doi.org/10.1016/j.pbb.2017.06.013

Meng, H., Wang, Y., Huang, M., Lin, W., Wang, S., & Zhang, B. (2011). Chronic deep brain stimulation of the lateral habenula nucleus in a rat model of depression. *Brain Research*, *1422*, 32–38. https://doi.org/10.1016/j.brainres.2011.08.041

Meye, F. J., Lecca, S., Valentinova, K., & Mameli, M. (2013, December 16). Synaptic and cellular profile of neurons in the lateral habenula. *Frontiers in Human Neuroscience*. Frontiers Media S. A. https://doi.org/10.3389/fnhum.2013.00860

Miyasaka, N., Morimoto, K., Tsubokawa, T., Higashijima, S. -i., Okamoto, H., & Yoshihara, Y. (2009). From the Olfactory Bulb to Higher Brain Centers: Genetic Visualization of Secondary Olfactory Pathways in Zebrafish. *Journal of Neuroscience*, *29*(15), 4756–4767. https://doi.org/10.1523/JNEUROSCI.0118-09.2009

Miyazawa, H., Okumura, K., Hiyoshi, K., Maruyama, K., Kakinuma, H., Amo, R., … Tsuda, S. (2018). Optical interrogation of neuronal circuitry in zebrafish using genetically encoded voltage indicators. *Scientific Reports*, *8*(1), 6048. https://doi.org/10.1038/s41598-018-23906-1

Molden, S., Moldestad, O., & Storm, J. F. (2013). Estimating Extracellular Spike Waveforms from CA1 Pyramidal Cells with Multichannel Electrodes. *PLoS ONE*, *8*(12), e82141. https://doi.org/10.1371/journal.pone.0082141

Moore, H. A. (2013). *Circadian rhythmicity and light sensitivity of the zebrafish brain*.

Moore, H. A., & Whitmore, D. (2014). Circadian rhythmicity and light sensitivity of the zebrafish brain. *PloS one*. Public Library of Science. https://doi.org/10.1371/journal.pone.0086176

Moore, R. Y., & Eichler, V. B. (1972). Loss of a circadian adrenal corticosterone rhythm following suprachiasmatic lesions in the rat. *Brain Research*, *42*(1), 201–206. https://doi.org/10.1016/0006-8993(72)90054-6

Morris, J. S., Smith, K. A., Cowen, P. J., Friston, K. J., & Dolan, R. J. (1999). Covariation of Activity in Habenula and Dorsal Raphé Nuclei Following Tryptophan Depletion. *NeuroImage*, *10*(2), 163–172. https://doi.org/10.1006/nimg.1999.0455

Mracek, P., Pagano, C., Fröhlich, N., Idda, M. L., Cuesta, I. H., Lopez-Olmeda, J. F., … Foulkes, N. S. (2013). ERK Signaling Regulates Light-Induced Gene Expression via D-Box Enhancers in a Differential, Wavelength-Dependent Manner. *PloS One*, *8*(6), e67858. https://doi.org/10.1371/journal.pone.0067858

Mracek, P., Santoriello, C., Idda, M. L., Pagano, C., Ben-Moshe, Z., Gothilf, Y., … Foulkes, N. S. (2012). Regulation of per and cry Genes Reveals a Central Role for the D-Box Enhancer in Light-Dependent Gene Expression. *PLoS ONE*, *7*(12). https://doi.org/10.1371/journal.pone.0051278

Nakai, J., Ohkura, M., & Imoto, K. (2001). A high signal-to-noise Ca2+ probe composed of a single green fluorescent protein. *Nature Biotechnology*, *19*(2), 137–141. https://doi.org/10.1038/84397

Nakamura, K., Matsumoto, M., & Hikosaka, O. (2008). Reward-dependent modulation of neuronal activity in the primate dorsal raphe nucleus. *Journal of Neuroscience*, *28*(20), 5331–5343. https://doi.org/10.1523/JNEUROSCI.0021-08.2008

Nathan, F. M., Ogawa, S., & Parhar, I. S. (2015). Neuronal connectivity between habenular glutamate-kisspeptin1 co-expressing neurons and the raphe 5-HT system. *Journal of Neurochemistry*, *135*(4), 814–829. https://doi.org/10.1111/jnc.13273

Naumann, E. A., Kampff, A. R., Prober, D. A., Schier, A. F., & Engert, F. (2010). Monitoring neural activity with bioluminescence during natural behavior. *Nature Neuroscience*, *13*(4), 513–520. https://doi.org/10.1038/nn.2518

Noche, R. R., Lu, P. N., Goldstein-Kral, L., Glasgow, E., & Liang, J. O. (2011). Circadian rhythms in the pineal organ persist in zebrafish larvae that lack ventral brain. *BMC Neuroscience*, *12*. https://doi.org/10.1186/1471-2202-12-7

Obrietan, K., Impey, S., & Storm, D. R. (1998). Light and circadian rhythmicity regulate MAP kinase activation in the suprachiasmatic nuclei. *Nature Neuroscience*, *1*(8), 693–700. https://doi.org/10.1038/3695

Ogawa, S., Ng, K. W., Ramadasan, P. N., Nathan, F. M., & Parhar, I. S. (2012). Habenular Kiss1 neurons modulate the serotonergic system in the brain of zebrafish. *Endocrinology*, *153*(5), 2398–2407. https://doi.org/10.1210/en.2012-1062

Ogawa, S., & Parhar, I. S. (2018, May 7). Biological significance of kisspeptin-Kiss 1 receptor signaling in the habenula of teleost species. *Frontiers in Endocrinology*. Frontiers Media S.A. https://doi.org/10.3389/fendo.2018.00222

Ohkura, M., Sasaki, T., Sadakari, J., Gengyo-Ando, K., Kagawa-Nagamura, Y., Kobayashi, C., … Nakai, J. (2012). Genetically encoded green fluorescent Ca2+ indicators with improved detectability for neuronal Ca2+ signals. *PloS One*, *7*(12), e51286. https://doi.org/10.1371/journal.pone.0051286

Ono, D., Honma, K., Yanagawa, Y., Yamanaka, A., & Honma, S. (2019). GABA in the suprachiasmatic nucleus refines circadian output rhythms in mice. *Communications Biology*, *2*(1). https://doi.org/10.1038/s42003-019-0483-6

Oz, M., Kolaj, M., & Renaud, L. P. (2001). Electrophysiological Evidence for Vasopressin V_1 Receptors on Neonatal Motoneurons, Premotor and Other Ventral Horn Neurons. *Journal of Neurophysiology*, *86*(3), 1202–1210. https://doi.org/10.1152/jn.2001.86.3.1202

Paul, M. J., Indic, P., & Schwartz, W. J. (2011). A role for the habenula in the regulation of locomotor activity cycles. *European Journal of Neuroscience*, *34*(3), 478–488. https://doi.org/10.1111/j.1460-9568.2011.07762.x

Peng, X., Lin, J., Zhu, Y., Liu, X., Zhang, Y., Ji, Y., … Li, Q. (2016). Anxiety-related behavioral responses of pentylenetetrazole-treated zebrafish larvae to light-dark transitions. *Pharmacology Biochemistry and Behavior*, *145*, 55–65. https://doi.org/10.1016/j.pbb.2016.03.010

Pirker, S., Schwarzer, C., Wieselthaler, A., Sieghart, W., & Sperk, G. (2000). GABA(A) receptors: Immunocytochemical distribution of 13 subunits in the adult rat brain. *Neuroscience*, *101*(4), 815–850. https://doi.org/10.1016/S0306-4522(00)00442-5

Plotnikov, A., Zehorai, E., Procaccia, S., & Seger, R. (2011). The MAPK cascades: Signaling components, nuclear roles and mechanisms of nuclear translocation. *Biochimica et Biophysica Acta (BBA) - Molecular Cell Research*, *1813*(9), 1619–1633. https://doi.org/10.1016/J.BBAMCR.2010.12.012

Proulx, C. D., Hikosaka, O., & Malinow, R. (2014). Reward processing by the lateral habenula in normal and depressive behaviors. *Nature Neuroscience*. Nature Publishing Group. https://doi.org/10.1038/nn.3779

Qin, C., & Luo, M. (2009). Neurochemical phenotypes of the afferent and efferent projections of the mouse medial habenula. *Neuroscience*, *161*(3), 827–837. https://doi.org/10.1016/j.neuroscience.2009.03.085

Qu, T., Dong, K., Sugioka, K., & Yamadori, T. (1996). Demonstration of direct input from the retina to the lateral habenular nucleus in the albino rat. *Brain Research*, *709*(2), 251–258. https://doi.org/10.1016/0006-8993(95)01306-7

Quiroga, R. Q. (2012). Spike sorting. *Current Biology*, *22*(2), R45–R46. https://doi.org/10.1016/J.CUB.2011.11.005

Raggenbass, M. (2008). Overview of cellular electrophysiological actions of vasopressin. *European Journal of Pharmacology*, *583*(2–3), 243–254. https://doi.org/10.1016/J.EJPHAR.2007.11.074

Raggenbass, M., Goumaz, M., Sermasi, E., Tribollet, E., & Dreifuss, J. J. (1991). *Vasopressin Generates a Persistent Voltage-dependent Sodium Current in a Mammalian Motoneuron*. *The Journal of Neuroscience* (Vol. 1). Retrieved from https://www.jneurosci.org/content/jneuro/11/6/1609.full.pdf

Rahmati, V., Kirmse, K., Marković, D., Holthoff, K., & Kiebel, S. J. (2016). Inferring Neuronal Dynamics from Calcium Imaging Data Using Biophysical Models and Bayesian Inference. *PLoS Computational Biology*, *12*(2), e1004736. https://doi.org/10.1371/journal.pcbi.1004736

Ralph, M. R., Foster, R. G., Davis, F. C., & Menaker, M. (1990). Transplanted suprachiasmatic nucleus determines circadian period. *Science*, *247*(4945), 975–978. https://doi.org/10.1126/science.2305266

Ramaswamy, M. (2018). *An Optical Study of Ongoing Activity in the Zebrafish Habenula*. Retrieved from http://scholarbank.nus.edu.sg/handle/10635/142743

Randlett, O., Wee, C. L., Naumann, E. A., Nnaemeka, O., Schoppik, D., Fitzgerald, J. E., … Schier, A. F. (2015). Whole-brain activity mapping onto a zebrafish brain atlas. *Nature Methods*, *12*(11), 1039–1046. https://doi.org/10.1038/nmeth.3581

Reddy, P., Zehring, W. A., Wheeler, D. A., Pirrotta, V., Hadfield, C., Hall, J. C., & Rosbash, M. (1984). Molecular analysis of the period locus in Drosophila melanogaster and identification

of a transcript involved in biological rhythms. *Cell*, *38*(3), 701–710. https://doi.org/10.1016/0092-8674(84)90265-4

Ren, J., Qin, C., Hu, F., Tan, J., Qiu, L., Zhao, S., … Luo, M. (2011). Habenula "Cholinergic" Neurons Corelease Glutamate and Acetylcholine and Activate Postsynaptic Neurons via Distinct Transmission Modes. *Neuron*, *69*(3), 445–452. https://doi.org/10.1016/j.neuron.2010.12.038

Rey, H. G., Pedreira, C., & Quian Quiroga, R. (2015). Past, present and future of spike sorting techniques. *Brain Research Bulletin*, *119*(Pt B), 106–117. https://doi.org/10.1016/j.brainresbull.2015.04.007

Reymond-Marron, I., Raggenbass, M., & Zaninetti, M. (2005). Vasopressin facilitates glycinergic and GABAergic synaptic transmission in developing hypoglossal motoneurons. *European Journal of Neuroscience*, *21*(6), 1601–1609. https://doi.org/10.1111/j.1460-9568.2005.03996.x

Rihel, J., Prober, D. A., & Schier, A. F. (2010). Monitoring Sleep and Arousal in Zebrafish. *Methods in Cell Biology*, *100*, 281–294. https://doi.org/10.1016/B978-0-12-384892-5.00011-6

Roenneberg, T., & Merrow, M. (2005, December). Circadian clocks - The fall and rise of physiology. *Nature Reviews Molecular Cell Biology*. https://doi.org/10.1038/nrm1766

Rood, B. D., & De Vries, G. J. (2011). Vasopressin innervation of the mouse (Mus musculus) brain and spinal cord. *The Journal of Comparative Neurology*, *519*(12), 2434–2474. https://doi.org/10.1002/cne.22635

Sakhi, K., Belle, M. D. C., Gossan, N., Delagrange, P., & Piggins, H. D. (2014). Daily variation in the electrophysiological activity of mouse medial habenula neurones. *The Journal of Physiology*, *592*(4), 587–603. https://doi.org/10.1113/jphysiol.2013.263319

Sakhi, K., Wegner, S., Belle, M. D. C., Howarth, M., Delagrange, P., Brown, T. M., & Piggins, H. D. (2014). Intrinsic and extrinsic cues regulate the daily profile of mouse lateral habenula neuronal activity. *The Journal of Physiology*, *592*(22), 5025–5045. https://doi.org/10.1113/jphysiol.2014.280065

Salaberry, N. L., Hamm, H., Felder-Schmittbuhl, M.-P., & Mendoza, J. (2019). A suprachiasmatic-independent circadian clock(s) in the habenula is affected by Per gene mutations and housing light conditions in mice. *Brain Structure & Function*, *224*(1), 19–31. https://doi.org/10.1007/s00429-018-1756-4

Salaberry, N. L., & Mendoza, J. (2016). Insights into the role of the habenular circadian clock in addiction. *Frontiers in Psychiatry*. Frontiers Media S.A. https://doi.org/10.3389/fpsyt.2015.00179

Sánchez-Bretaño, A., Gueguen, M.-M., Cano-Nicolau, J., Kah, O., Alonso-Gómez, Á. L., Delgado, M. J., & Isorna, E. (2015). Anatomical distribution and daily profile of *gper1b* gene expression in brain and peripheral structures of goldfish (*Carassius auratus*). *Chronobiology International*, *32*(7), 889–902. https://doi.org/10.3109/07420528.2015.1049615

Sartorius, A., Kiening, K. L., Kirsch, P., von Gall, C. C., Haberkorn, U., Unterberg, A. W., … Meyer-Lindenberg, A. (2010). Remission of Major Depression Under Deep Brain Stimulation of the Lateral Habenula in a Therapy-Refractory Patient. *Biological Psychiatry*, *67*(2), e9–e11. https://doi.org/10.1016/J.BIOPSYCH.2009.08.027

Scerbina, T., Chatterjee, D., & Gerlai, R. (2012). Dopamine receptor antagonism disrupts social preference in zebrafish: A strain comparison study. *Amino Acids*, *43*(5), 2059–2072. https://doi.org/10.1007/s00726-012-1284-0

Scott, E. K. (2009). The Gal4/UAS toolbox in zebrafish: new approaches for defining behavioral circuits. *Journal of Neurochemistry*, *110*(2), 441–456. https://doi.org/10.1111/j.1471-4159.2009.06161.x

Shcherbakov, D., Knörzer, A., Espenhahn, S., Hilbig, R., Haas, U., & Blum, M. (2013). Sensitivity Differences in Fish Offer Near-Infrared Vision as an Adaptable Evolutionary Trait. *PLoS ONE*, *8*(5), e64429. https://doi.org/10.1371/journal.pone.0064429

Siegel, J. M. (2009, October). Sleep viewed as a state of adaptive inactivity. *Nature Reviews Neuroscience*. https://doi.org/10.1038/nrn2697

Spreafico, R., Frassoni, C., Arcelli, P., Battaglia, G., Wenthold, R. J., & De Biasi, S. (1994). Distribution of AMPA selective glutamate receptors in the thalamus of adult rats and during postnatal development. A light and ultrastructural immunocytochemical study. *Developmental Brain Research*, *82*(1–2), 231–244. https://doi.org/10.1016/0165-3806(94)90166-X

Stephan, F. K., & Zucker, I. (1972). Circadian rhythms in drinking behavior and locomotor activity of rats are eliminated by hypothalamic lesions. *Proceedings of the National Academy of Sciences of the United States of America*, *69*(6), 1583–1586. https://doi.org/10.1073/pnas.69.6.1583

Stephenson-Jones, M., Floros, O., Robertson, B., & Grillner, S. (2012). Evolutionary conservation of the habenular nuclei and their circuitry controlling the dopamine and 5-hydroxytryptophan (5-HT) systems. *Proceedings of the National Academy of Sciences of the United States of America*, *109*(3). https://doi.org/10.1073/pnas.1119348109

Stewart, A., Gaikwad, S., Kyzar, E., Green, J., Roth, A., & Kalueff, A. V. (2012). Modeling anxiety using adult zebrafish: A conceptual review. In *Neuropharmacology* (Vol. 62, pp. 135–143). https://doi.org/10.1016/j.neuropharm.2011.07.037

Stoop, R. (2012). Neuromodulation by Oxytocin and Vasopressin. *Neuron*, *76*(1), 142–159. https://doi.org/10.1016/J.NEURON.2012.09.025

Sutherland, R. J. (1982). The dorsal diencephalic conduction system: A review of the anatomy and functions of the habenular complex. *Neuroscience and Biobehavioral Reviews*, *6*(1), 1–13. https://doi.org/10.1016/0149-7634(82)90003-3

Svoboda, K., & Yasuda, R. (2006). Principles of two-photon excitation microscopy and its applications to neuroscience. *Neuron*, *50*(6), 823–839. https://doi.org/10.1016/j.neuron.2006.05.019

Tamai, T. K., Young, L. C., & Whitmore, D. (2007). Light signaling to the zebrafish circadian clock by Cryptochrome 1a. *Proceedings of the National Academy of Sciences of the United States of America*, *104*(37), 14712–14717. https://doi.org/10.1073/pnas.0704588104

Tavakoli-Nezhad, M., & Schwartz, W. J. (2006). Hamsters Running on Time: Is the Lateral Habenula a Part of the Clock? *Chronobiology International*, *23*(1–2), 217–224. https://doi.org/10.1080/07420520500521947

Tischkau, S. A., Mitchell, J. W., Tyan, S.-H., Buchanan, G. F., & Gillette, M. U. (2003). Ca2+/cAMP response element-binding protein (CREB)-dependent activation of Per1 is required for light-induced signaling in the suprachiasmatic nucleus circadian clock. *The Journal of Biological Chemistry*, *278*(2), 718–723. https://doi.org/10.1074/jbc.M209241200

Tosini, G., & Menaker, M. (1996). Circadian rhythms in cultured mammalian retina. *Science (New York, N.Y.)*, *272*(5260), 419–421. https://doi.org/10.1126/science.272.5260.419

Tosini, G., Pozdeyev, N., Sakamoto, K., & Iuvone, P. M. (2008, July). The circadian clock system in the mammalian retina. *BioEssays*. https://doi.org/10.1002/bies.20777

Trudel, E., & Bourque, C. W. (2010). Central clock excites vasopressin neurons by waking osmosensory afferents during late sleep. *Nature Neuroscience*, *13*(4), 467–474. https://doi.org/10.1038/nn.2503

Tsuji, T., Allchorne, A. J., Zhang, M., Tsuji, C., Tobin, V. A., Pineda, R., … Ludwig, M. (2017). Vasopressin casts light on the suprachiasmatic nucleus. *The Journal of Physiology*, *595*(11), 3497–3514. https://doi.org/10.1113/JP274025

Tunstall, B. J., Kirson, D., Zallar, L. J., McConnell, S. A., Vendruscolo, J. C. M., Ho, C. P., … Vendruscolo, L. F. (2019). Oxytocin blocks enhanced motivation for alcohol in alcohol dependence and blocks alcohol effects on GABAergic transmission in the central amygdala. *PLoS Biology*, *17*(4), e2006421. https://doi.org/10.1371/journal.pbio.2006421

Turner, K. J., Hawkins, T. A., Yáñez, J., Anadón, R., Wilson, S. W., & Folgueira, M. (2016). Afferent Connectivity of the Zebrafish Habenulae. *Frontiers in Neural Circuits*, *10*, 30. https://doi.org/10.3389/fncir.2016.00030

Vaccari, C., Lolait, S. J., & Ostrowski, N. L. (1998). Comparative Distribution of Vasopressin V1b and Oxytocin Receptor Messenger Ribonucleic Acids in Brain [1]. *Endocrinology*, *139*(12), 5015–5033. https://doi.org/10.1210/endo.139.12.6382

Valjakka, A., Vartiainen, J., Tuomisto, L., Tuomisto, J. T., Olkkonen, H., & Airaksinen, M. M. (1998). The fasciculus retroflexus controls the integrity of REM sleep by supporting the generation of hippocampal theta rhythm and rapid eye movements in rats. *Brain Research Bulletin*, *47*(2), 171–184. https://doi.org/10.1016/s0361-9230(98)00006-9

Van Der Horst, G. T. J., Muijtjens, M., Kobayashi, K., Takano, R., Kanno, S. I., Takao, M., … Yasui, A. (1999). Mammalian Cry1 and Cry2 are essential for maintenance of circadian rhythms. *Nature*, *398*(6728), 627–630. https://doi.org/10.1038/19323

Van Esseveldt, L. K. E., Lehman, M. N., & Boer, G. J. (2000). The suprachiasmatic nucleus and the circadian time-keeping system revisited. *Brain Research Reviews*. https://doi.org/10.1016/S0165-0173(00)00025-4

Vargas, R., Þorsteinsson, H., & Karlsson, K. Æ. (2012). Spontaneous neural activity of the anterodorsal lobe and entopeduncular nucleus in adult zebrafish: A putative homologue of hippocampal sharp waves. *Behavioural Brain Research*, *229*(1), 10–20. https://doi.org/10.1016/J.BBR.2011.12.025

Vatine, G., Vallone, D., Appelbaum, L., Mracek, P., Ben-Moshe, Z., Lahiri, K., … Foulkes, N. S. (2009). Light directs zebrafish period2 expression via conserved D and E boxes. *PLoS Biology*, *7*(10). https://doi.org/10.1371/journal.pbio.1000223

Vatine, G., Vallone, D., Gothilf, Y., & Foulkes, N. S. (2011). It's time to swim! Zebrafish and the circadian clock. *FEBS Letters*, *585*(10), 1485–1494. https://doi.org/10.1016/j.febslet.2011.04.007

Viswanath, H., Carter, A. Q., Baldwin, P. R., Molfese, D. L., & Salas, R. (2014, January 17). The medial habenula: Still neglected. *Frontiers in Human Neuroscience*. https://doi.org/10.3389/fnhum.2013.00931

Wada, S., Shen, B., Kawano-Yamashita, E., Nagata, T., Hibi, M., Tamotsu, S., … Terakita, A. (2018). Color opponency with a single kind of bistable opsin in the zebrafish pineal organ. *Proceedings of the National Academy of Sciences of the United States of America*, *115*(44), 11310–11315. https://doi.org/10.1073/pnas.1802592115

Wagner, F., French, L., & Veh, R. W. (2016). Transcriptomic-anatomic analysis of the mouse habenula uncovers a high molecular heterogeneity among neurons in the lateral complex, while gene expression in the medial complex largely obeys subnuclear boundaries. *Brain Structure & Function*, *221*(1), 39–58. https://doi.org/10.1007/s00429-014-0891-9

Wagner, F., Stroh, T., & Veh, R. W. (2014). Correlating habenular subnuclei in rat and mouse by using topographic, morphological, and cytochemical criteria. *Journal of Comparative Neurology*, *522*(11), 2650–2662. https://doi.org/10.1002/cne.23554

Wang, L. M. C., Dragich, J. M., Kudo, T., Odom, I. H., Welsh, D. K., O'Dell, T. J., & Colwell, C. S. (2009). Expression of the circadian clock gene Period2 in the hippocampus: Possible implications for synaptic plasticity and learned behaviour. *ASN Neuro*, *1*(3), 139–152. https://doi.org/10.1042/AN20090020

Wang, D. G., Gong, N., Luo, B., & Xu, T. L. (2006). Absence of gaba type a signaling in adult medial habenular neurons. *Neuroscience*, *141*(1), 133–141. https://doi.org/10.1016/j.neuroscience.2006.03.045

Watanabe, K., Vanecek, J., & Yamaoka, S. (2000). In vitro entrainment of the circadian rhythm of vasopressin-releasing cells in suprachiasmatic nucleus by vasoactive intestinal polypeptide. *Brain Research*, *877*(2), 361–366. https://doi.org/10.1016/S0006-8993(00)02724-4

Watson, A. G. (2018). *Integration of circadian clocks and metabolism in the hypothalamus*.

Webb, I. C., Baltazar, R. M., Wang, X., Pitchers, K. K., Coolen, L. M., & Lehman, M. N. (2009). Diurnal variations in natural and drug reward, mesolimbic tyrosine hydroxylase, and clock gene expression in the male rat. *Journal of Biological Rhythms*, *24*(6), 465–476. https://doi.org/10.1177/0748730409346657

Wee, C. L., Nikitchenko, M., Wang, W.-C., Luks-Morgan, S. J., Song, E., Gagnon, J. A., … Douglass, A. D. (2019). Zebrafish oxytocin neurons drive nocifensive behavior via brainstem premotor targets. *Nature Neuroscience*. https://doi.org/10.1038/s41593-019-0452-x

Weger, M., Weger, B. D., Diotel, N., Rastegar, S., Hirota, T., Kay, S. A., … Dickmeis, T. (2013). Real-time in vivo monitoring of circadian E-box enhancer activity: A robust and sensitive zebrafish reporter line for developmental, chemical and neural biology of the circadian clock. *Developmental Biology*, *380*(2), 259–273. https://doi.org/10.1016/J.YDBIO.2013.04.035

Whitmore, D., Foulkes, N. S., & Sassone-Corsi, P. (2000). Light acts directly on organs and cells in culture to set the vertebrate circadian clock. *Nature*, *404*(6773), 87–91. https://doi.org/10.1038/35003589

Whitmore, D., Foulkes, N. S., Strähle, U., & Sassone-Corsi, P. (1998). Zebrafish Clock rhythmic expression reveals independent peripheral circadian oscillators. *Nature Neuroscience*, *1*(8), 701–707. https://doi.org/10.1038/3703

Woods, I. G., Schoppik, D., Shi, V. J., Zimmerman, S., Coleman, H. A., Greenwood, J., … Schier, A. F. (2014). Neuropeptidergic signaling partitions arousal behaviors in zebrafish. *The Journal of Neuroscience: The Official Journal of the Society for Neuroscience*, *34*(9), 3142–3160. https://doi.org/10.1523/JNEUROSCI.3529-13.2014

Wrobel, L. J., Dupré, A., & Raggenbass, M. (2011). Excitatory action of vasopressin in the brain of the rat: role of cAMP signaling. *Neuroscience*, *172*, 177–186. https://doi.org/10.1016/J.NEUROSCIENCE.2010.10.006

Wulund, L., & Reddy, A. B. (2015). A brief history of circadian time: The emergence of redox oscillations as a novel component of biological rhythms. *Perspectives in Science*, *6*, 27–37. https://doi.org/10.1016/j.pisc.2015.08.002

Yamaguchi, Y. (2018). Arginine vasopressin signaling in the suprachiasmatic nucleus on the resilience of circadian clock to jet lag. *Neuroscience Research*, *129*, 57–61. https://doi.org/10.1016/j.neures.2017.10.007

Yamaguchi, Y., Suzuki, T., Mizoro, Y., Kori, H., Okada, K., Chen, Y., … Okamura, H. (2013). Mice genetically deficient in vasopressin V1a and V1b receptors are resistant to jet lag. *Science*, *342*(6154), 85–90. https://doi.org/10.1126/science.1238599

Yan, L., Smale, L., & Nunez, A. A. (2018). Circadian and photic modulation of daily rhythms in diurnal mammals. *European Journal of Neuroscience*. https://doi.org/10.1111/ejn.14172

Yañez, J., & Anadon, R. (1994). Afferent and efferent connections of the habenula in the larval sea lamprey (Petromyzon marinus L.): an experimental study. *The Journal of Comparative Neurology*, *345*(1), 148–160. https://doi.org/10.1002/cne.903450112

Yang, Y., Wang, H., Hu, J., & Hu, H. (2018). Lateral habenula in the pathophysiology of depression. *Current Opinion in Neurobiology*. Elsevier Ltd. https://doi.org/10.1016/j.conb.2017.10.024

Yang, Y., Liu, N., He, Y., Liu, Y., Ge, L., Zou, L., … Liu, X. (2018). Improved calcium sensor GCaMP-X overcomes the calcium channel perturbations induced by the calmodulin in GCaMP. *Nature Communications*, *9*(1), 1504. https://doi.org/10.1038/s41467-018-03719-6

Yokogawa, T., Hannan, M. C., & Burgess, H. A. (2012). The dorsal raphe modulates sensory responsiveness during arousal in zebrafish. *The Journal of Neuroscience: The Official Journal of the Society for Neuroscience*, *32*(43), 15205–15215. https://doi.org/10.1523/JNEUROSCI.1019-12.2012

Young, W. S., Li, J., Wersinger, S. R., & Palkovits, M. (2006). The Vasopressin 1b Receptor is Prominent in the Hippocampal Area CA2 Where It Is Unaffected by Restraint Stress or Adrenalectomy. *Neuroscience*, *143*(4), 1031. https://doi.org/10.1016/J.NEUROSCIENCE.2006.08.040

Yu, B., Mak, T., Li, X., Smith, L., Sun, Y., & Poon, C.-S. (2012). Stream-based Hebbian Eigenfilter for real-time neuronal spike discrimination. *BioMedical Engineering OnLine*, *11*(1), 18. https://doi.org/10.1186/1475-925X-11-18

Yu, E. Z., Hallenbeck, J. M., Cai, D., & McCarron, R. M. (2002). Elevated arylalkylamine-N-acetyltransferase (AA-NAT) gene expression in medial habenular and suprachiasmatic nuclei of hibernating ground squirrels. *Molecular Brain Research*, *102*(1–2), 9–17. https://doi.org/10.1016/S0169-328X(02)00138-9

Zhang, B., Yao, Y., Zhang, H., Kawakami, K., & Du, J. (2017). Left Habenula Mediates Light-Preference Behavior in Zebrafish via an Asymmetrical Visual Pathway. *Neuron*, *93*(4), 914-928.e4. https://doi.org/10.1016/J.NEURON.2017.01.011

Zhang, L., Hernández, V. S., Vázquez-Juárez, E., Chay, F. K., & Barrio, R. A. (2016). Thirst Is Associated with Suppression of Habenula Output and Active Stress Coping: Is there a Role for a Non-canonical Vasopressin-Glutamate Pathway? *Frontiers in Neural Circuits*, *10*, 13. https://doi.org/10.3389/FNCIR.2016.00013

Zhang, L., Hernández, V. S., Swinny, J. D., Verma, A. K., Giesecke, T., Emery, A. C., … Eiden, L. E. (2018). A GABAergic cell type in the lateral habenula links hypothalamic homeostatic and midbrain motivation circuits with sex steroid signaling. *Translational Psychiatry*, *8*(1), 50. https://doi.org/10.1038/s41398-018-0099-5

Zhao, H., & Rusak, B. (2005). Circadian firing-rate rhythms and light responses of rat habenular nucleus neurons in vivo and in vitro. *Neuroscience*, *132*(2), 519–528. https://doi.org/10.1016/J.NEUROSCIENCE.2005.01.012

Zhdanova, I. V, Wang, S. Y., Leclair, O. U., & Danilova, N. P. (2001). Melatonin promotes sleep-like state in zebrafish. *Brain Research*, *903*(1–2), 263–268. https://doi.org/10.1016/S0006-8993(01)02444-1

Zimmerman, C. A., Leib, D. E., & Knight, Z. A. (2017). Neural circuits underlying thirst and fluid homeostasis. *Nature Reviews. Neuroscience*, *18*(8), 459–469. https://doi.org/10.1038/nrn.2017.71

Zimmerman, N. H., & Menaker, M. (1979). The pineal gland: a pacemaker within the circadian system of the house sparrow. *Proceedings of the National Academy of Sciences*, *76*(2), 999–1003. https://doi.org/10.1073/pnas.76.2.999

Zoghbi, M. E., Bolaños, P., Villalba-Galea, C., Marcano, A., Hernández, E., Fill, M., & Escobar, A. L. (2000). Spatial Ca2+ Distribution in Contracting Skeletal and Cardiac Muscle Cells. *Biophysical Journal*, *78*(1), 164–173. https://doi.org/10.1016/S0006-3495(00)76582-9